

**SUPRAMOLECULAR ASSEMBLY WITH IONIC,  
REDOX-RESPONSIVE POLY(FERROCENYLSILANES):**

**ENGINEERING OF INTERFACES AND  
MOLECULAR RELEASE APPLICATIONS**

**PROEFSCHRIFT**

ter verkrijging van  
de graad van doctor aan de Universiteit Twente,  
op gezag van de rector magnificus,  
prof. dr. W. H. M. Zijm,  
volgens besluit van het College voor Promoties,  
in het openbaar te verdedigen  
op donderdag 10 januari 2008 om 16:45 uur

door

**Yujie Ma**

geboren op 18 april 1979  
te Wuhan, China

Dit proefschrift is goedgekeurd door:

Promotor: prof. dr. G. J. Vancso

Copromotor: dr. M. A. Hempenius

*The most beautiful thing we can experience is the mysterious.  
It is the source of all true art and science.*

Albert Einstein

This research has been financially supported by NanoNed (NanoImpuls, Project Number TCP. 6340), a National Nanotechnology Program coordinated by the Dutch Ministry of Economic Affairs, the Dutch Science Foundation for Chemical Research NWO-CW, the MESA<sup>+</sup> Institute for Nanotechnology of the University of Twente, and the University of Twente.



Supramolecular Assembly with Ionic, Redox-Responsive Poly(ferrocenylsilanes):  
Engineering of Interfaces and Molecular Release Applications

Y. Ma

Ph. D Thesis

University of Twente, MESA<sup>+</sup> Institute for Nanotechnology,  
Enschede, The Netherlands.

Cover illustration: Confocal laser scanning micrograph of organometallic microcapsules in water.

© Y. Ma 2008

ISBN: 978-90-365-2612-8

No part of this work may be reproduced by print, photocopy or any other means without the permission of the publisher.

Printed by PrintPartners Ipskamp, Enschede, The Netherlands.

# Contents

<b>Chapter 1</b>	<b>General Introduction</b>	<b>1</b>
<b>Chapter 2</b>	<b>Electrostatic Assembly with Polyelectrolytes</b>	<b>5</b>
2.1	Introduction	5
2.2	Polyelectrolytes in solution and at interfaces	6
2.3	Molecular interactions between polyelectrolytes	7
2.3.1	Ionic interactions	8
2.3.2	Hydrophobic interactions	8
2.4	Polyelectrolyte complexes	9
2.5	Layer-by-layer electrostatic assembly of polyelectrolytes	10
2.5.1	Planar multilayers	12
2.5.2	Multilayer capsules	17
2.5.3	Potential applications	21
2.5.4	Some frequently used characterization techniques	23
2.6	Concluding remarks	27
2.7	References and notes	27
<b>Chapter 3</b>	<b>Synthesis and Redox Properties of Water Soluble Poly(ferrocenylsilanes)</b>	<b>37</b>
3.1	Introduction	37
3.2	Synthesis and characterization of poly(ferrocenylsilane) polyelectrolytes with molar mass control	39
3.3	Fluorescence labelled poly(ferrocenylsilane) polycation	41
3.4	Redox chemistry of water soluble poly(ferrocenylsilanes)	43
3.4.1	Water-soluble oxidants	43
3.4.2	Viscosity behaviour of oxidized poly(ferrocenylsilane) polyions	45
3.4.3	Water-soluble reducing agents	45
3.5	Conclusions	46
3.6	Experimental	47
3.7	References	48
<b>Chapter 4</b>	<b>Substrate Supported Multilayers by Supramolecular Electrostatic Assembly of Poly(ferrocenylsilanes)</b>	<b>51</b>
4.1	Introduction	51
4.2	Multilayer fabrication and structure characterization	52
4.2.1	Multilayer deposition on planar interfaces	52
4.2.2	Film thickness dependence on solution salt concentration	54

4.2.3	Multilayer deposition on chemically patterned substrates	56
4.3	Redox properties of poly(ferrocenylsilane) planar multilayer films	59
4.3.1	Chemical oxidation	59
4.3.2	Patterned multilayers by “reactive” soft lithography	61
4.3.3	Multilayer electrochemistry	62
4.3.4	Controlled multilayer release by electrochemistry	63
4.4	Conclusions	67
4.5	Experimental	68
4.6	References and notes	70
<b>Chapter 5 Redox-Responsive Free-Standing Poly(ferrocenylsilane) Multilayer Microcapsules</b>		<b>73</b>
5.1	Introduction	73
5.2	Microcapsule fabrication	74
5.2.1	Core material and capsule formation	74
5.2.2	Capsule wall thickness	78
5.2.3	Capsule integrity and permeability	80
5.3	Redox-responsive permeability	81
5.3.1	Chemical oxidation	81
5.3.2	Chemical reduction	86
5.3.3	Composite-wall microcapsules	87
5.3.4	Electrochemistry	90
5.4	Discussion	91
5.4.1	(PSS <sup>-</sup> /PFS <sup>+</sup> ) <sub>5</sub> microcapsules	91
5.4.2	(PFS <sup>-</sup> /PAH <sup>+</sup> ) <sub>5</sub> microcapsules	92
5.4.3	Mechanism of redox-responsive permeability	93
5.5	Conclusions	96
5.6	Experimental	97
5.7	References and notes	99
<b>Chapter 6 Electrostatic Assembly of Poly(ferrocenylsilane) Polyelectrolytes with DNA</b>		<b>103</b>
6.1	Introduction	103
6.2	LBL assembly of poly(ferrocenylsilane) polycations and high molar mass ds-DNA	104
6.2.1	Macroporous multilayers	104
6.2.2	Redox properties	112
6.3	Molar mass effect	113
6.4	Conclusions	116

---

6.5	Experimental	116
6.6	References and notes	117
<b>Chapter 7</b>	<b>Applications of Poly(ferrocenylsilane) Polyelectrolytes</b>	<b>121</b>
7.1	Cationic poly(ferrocenylsilane) as DNA condensation and transfection agent	121
7.1.1	Introduction	121
7.1.2	Results and discussion	122
7.1.3	Conclusions	126
7.1.4	Experimental	126
7.2	Monodisperse polymer-virus hybrid nanoparticles	127
7.2.1	Introduction	127
7.2.2	Results and discussion	128
7.2.3	Conclusions and outlook	130
7.2.4	Experimental	131
7.3	Closing remarks	132
7.4	References	132
<b>Chapter 8</b>	<b>Outlook: Bringing New Shapes and Functions to Redox-Responsive Multilayer Structures</b>	<b>135</b>
8.1	Introduction	135
8.2	Multilayer nanotubes	135
8.2.1	Porous alumina as templates	136
8.2.2	Polycarbonate membrane as templates	138
8.2.3	Experimental	139
8.3	Separation membranes	140
8.3.1	Multilayer membranes	140
8.3.2	Responsive gating	140
8.4	Poly(ferrocenylsilane)/polysaccharide multilayers	141
8.5	Superhydrophobic coatings	142
8.6	Follow-up study on the redox-response of poly(ferrocenylsilane) multilayers and microcapsules	142
8.7	References and notes	143
<b>Summary</b>		<b>147</b>
<b>Samenvatting</b>		<b>151</b>
<b>Acknowledgements</b>		<b>155</b>
<b>Curriculum Vitae</b>		<b>157</b>





# Chapter 1

## General Introduction

As an on-going challenge in nanotechnology, miniaturization has been one of the key issues driving the fast technological advances in the electronics industry.<sup>1</sup> However, scientists have more or less agreed that continuous down-scaling of devices and components to the sub 50 nm scale can hardly be achieved by conventional “top-down” approaches due to some limitations, for example the resolution of photolithography.<sup>2</sup> As an alternative strategy, nanofabrication via the “bottom-up” approach in which functional nanostructures are formed by the self-assembly of molecular building blocks is considered to be a promising solution for the ultimate size reduction.<sup>3</sup> On the other hand, physical limits and processing requirements of traditional silicon-based technology will eventually prevent it from meeting the goal of making devices “smaller, faster, and cheaper”.<sup>4</sup> To solve this problem, material scientists have been constantly focusing on developing or utilizing new materials with improved properties and controlled architectures featuring some unique functions.

Inspired by nature, the study of self-assembly at different length scales has flourished in the past few decades. Biological systems often provide us with perfect examples of dividing complex structures and functions into different levels of building blocks, which are preferentially assembled through non-covalent (or supramolecular) chemistry.<sup>5</sup> Among the various secondary molecular interactions commonly used in self-assembly, electrostatic interactions possess the unique characteristics of a combination of relatively strong, long-range and non-selective nature.<sup>6</sup> An important “bottom-up” strategy making use of electrostatic interactions, is the layer-by-layer (LBL) sequential assembly technique.<sup>7</sup> One of the most attractive advantages of this method is that thin films can be tailor-made to display specific chemical and physical properties by the choice of polyelectrolyte material.<sup>7</sup>

Macromolecules including synthetic polymers and biomacromolecules are potentially ideal building blocks for the study of nanostructure formation by self-assembly because of their inherent nanosized length-scale, defined architectures, tuneable chemical functionalities, and ease of processing.<sup>8,9</sup> One of the most important classes of these materials are stimuli-responsive polymers. These “smart” polymeric materials can respond to specific external stimuli with drastic changes in their size and conformation.<sup>10</sup> In recent years, explorations on molecular structures based on stimuli-responsive polymers and their controlled properties in response to external *physical* stimuli, such as temperature, pH, ionic strength, solvent polarity variations, electric or magnetic fields and light have flourished. Nevertheless, structure-property manipulation using *chemical* stimuli still largely remains unexplored.<sup>11</sup> Among various types of stimuli, electrochemical stimuli are considered to be extremely promising in

the ultimate down-scaling of devices due to their unique possibility in realizing a localized trigger. Thus, material systems featuring redox-responsive components possess the important advantage in that they could be switched both chemically and electrochemically.

The electrostatic layer-by-layer assembly offers unique promises in making use of stimuli-responsive materials. This thesis will discuss the use of redox-responsive polymeric materials to build up supramolecular architectures through electrostatic assembly. The specific stimuli-responsive material used in our study are poly(ferrocenylsilanes) (PFSs) (Figure 1.1),<sup>12</sup> which belong to the class of redox-responsive organometallic polymers. The distinctive structural features of poly(ferrocenylsilanes) come from the silicon and iron atoms in the main chain, which make them valuable in the development of surface nano- and microstructuring strategies.<sup>13</sup> Due to the presence of redox-active ferrocene units in the polymer backbone, PFS can be reversibly oxidized and reduced by chemical<sup>14</sup> as well as electrochemical means.<sup>15</sup> Through the attachment or modification of substituents on silicon, water-soluble PFS featuring certain charges on the polymer side chains were obtained.<sup>16</sup> The charged nature and redox-responsiveness of these organometallic polyelectrolytes makes them particularly useful in the electrostatic self-assembly process for the fabrication of novel functional supramolecular nanostructures.

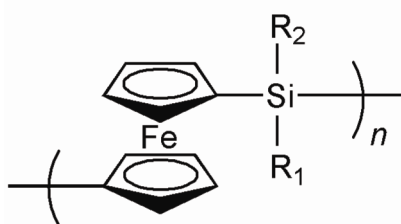


**Figure 1.1** Molecular structure of poly(ferrocenylsilanes). R<sub>1</sub> = R<sub>2</sub> = alkyl, aryl.

In Chapter 2 a literature overview will be given on the features and development of the electrostatic assembly technique. Apart from discussions on the substrate-assisted layer-by-layer assembly, examples on closely related issues of polyelectrolyte complex formation will also be covered.

The first part of the thesis (Chapter 3) deals with the synthesis and redox properties of PFS strong polyelectrolytes used throughout the study. Poly(ferrocenylsilane) polyions and fluorescence labelled polycations were synthesized with controlled molar mass. Fully reversible redox chemistry of these polyelectrolytes was demonstrated following the discovery of several water soluble redox agents.

The layer-by-layer electrostatic assembly of PFS polyions into planar multilayer films and free-standing microcapsules is presented in the second part of the thesis (Chapter 4 and 5). The dependence of multilayer structural characteristics on fabrication parameters was studied in detail. The chemical and electrochemical redox properties of PFS multilayers as well as the responsive molecular permeability of the microcapsules are established and described in these Chapters.

Chapter 6 describes the hybrid electrostatic assembly of poly(ferrocenylsilane) polycations with the natural anionic polyelectrolyte DNA. Multilayer assembly using double-stranded, high molar mass DNA resulted in unique redox-responsive macroporous thin films and free-standing microcapsules with excellent molecular permeability. The formation mechanism of the peculiar macroporous architectures was proposed and confirmed by the electrostatic assembly using PFS and DNA with varying molar masses.

Going beyond the above fundamental studies, Chapter 7 describes various applications of organometallic poly(ferrocenylsilane) polyelectrolytes. For example, cationic poly(ferrocenylsilane) polyelectrolytes were used in plasmid DNA condensation to form polymer-DNA complexes displaying promising gene transfer properties. When poly(ferrocenylsilane) polyanions were self-assembled with positively charged cowpea chlorotic mottle virus (CCMV) proteins, monodisperse polymer-virus nanoparticles that may be used as nanometer-sized compartments were obtained.

In the final part (Chapter 8), the fabrication of various other forms of multilayer structures based on poly(ferrocenylsilane) polyelectrolytes, for example multilayer nanotubes and free-standing planar films are discussed. Many new functions are envisaged by a combination of the unique redox-responsive properties of poly(ferrocenylsilane) and these new shapes.

## References

1. Tseng, G. Y.; Ellenbogen, J. C. *Science* **2001**, *294*, 1293.
2. (a) Ito, T.; Okazaki, S. *Nature* **2000**, *406*, 1027; (b) Niemeyer, C. M. *Science* **2002**, *297*, 62.
3. Whitesides, G. M.; Mathias, J. P.; Seto, C. T. *Science* **1991**, *254*, 1312.
4. (a) Schulz, M. *Nature* **1999**, *399*, 729; (b) Mathur, N. *Nature* **2002**, *419*, 573.
5. Whitesides, G. M.; Crzybowski, B. *Science* **2002**, *295*, 2418.
6. Faul, C. F. J.; Antonietti, M. *Adv. Mater.* **2003**, *15*, 673.
7. Decher, G.; Schlenoff, J. B. (Eds.) *Multilayer Thin Films, Sequential Assembly of Nanocomposite Materials*, Wiley-VCH, Weinheim, Germany, **2003**.
8. Li, H.; Huck, W. T. S. *Curr. Opin. Solid State Mat. Sci.* **2002**, *6*, 3.
9. Barlow, S.; O'Hare, D. *Chem. Rev.* **1997**, *97*, 637.
10. Kwon, I. C.; Bae, Y. H.; Kim, S. W. *Nature* **1991**, *354*, 291.
11. J. Liu, Y. Lu, *Adv. Mater.* **2006**, *18*, 1667.
12. (a) Manners, I. *Synthetic Metal-Containing Polymers*, Wiley-VCH, Weinheim, **2004**; (b) Kulbaba, K.; Manners, I. *Macromol. Rapid Commun.* **2001**, *22*, 711; (c) Whittell, G. R.; Manners, I. *Adv. Mater.* **2007**, *19*, 3439.
13. Korczagin, I.; Lammertink, R. G. H.; Hempenius, M. A.; Golze, S.; Vancso, G. J. *Adv. Polym. Sci.* **2006**, *200*, 91.

14. (a) Nguyen, M. T.; Diaz, A. F.; Dement'ev, V. V.; Pannell, K. H. *Chem. Mater.* **1993**, *5*, 1389; (b) Pudelski, J. K.; Foucher, D. A.; Honeyman, C. H.; Macdonald, P. M.; Manners, I.; Barlow, S.; O'Hare, D. *Macromolecules* **1996**, *29*, 1894; (c) Giannotti, M. I.; Lv, H.; Ma, Y.; Steenvoorden, M. P.; Overweg, A. R.; Roerdink, M.; Hempenius, M. A.; Vancso, G. J. *J. Inorg. Organomet. Polym. Mater.* **2005**, *15*, 527.
15. Rulkens, R.; Lough, A. J.; Manners, I.; Lovelace, S. R.; Grant, C.; Geiger, W. E. *J. Am. Chem. Soc.* **1996**, *118*, 12683.
16. (a) Power-Billard, K. N.; Manners, I. *Macromolecules* **2000**, *33*, 26; (b) Hempenius, M. A.; Robins, N. S.; Lammertink, R. G. H.; Vancso, G. J. *Macromol. Rapid Commun.* **2001**, *22*, 30; (c) Hempenius, M. A.; Vancso, G. J. *Macromolecules* **2002**, *35*, 2445; (d) Hempenius, M. A.; Brito, F. F.; Vancso, G. J. *Macromolecules* **2003**, *36*, 6683.

# Chapter 2

## Electrostatic Assembly with Polyelectrolytes

*In this Chapter, fundamentals in the electrostatic assembly of polyelectrolytes are reviewed. Broadly speaking, the electrostatic assembly encompasses the construction of supramolecular nanostructures by coupling different building blocks through ionic interactions. Here, after introductions on some of the important molecular interactions between polyelectrolytes, basics on polyelectrolyte complex formation are addressed. As a special case of polyelectrolyte complexation, discussions are mainly focused on the “template-assisted” layer-by-layer sequential assembly of polyelectrolytes.*

### 2.1 Introduction

As an important and promising strategy in nanotechnology, self-assembly aims at gaining precise control over material structures down to the atomic level.<sup>1</sup> While continuous efforts are directed at the creation of low-dimensional nanostructures, materials science is experiencing an unprecedented evolution. With the rapid development and multi-disciplinary broadening of materials science, many structural platforms that feature unprecedented and characteristic functions have been introduced. New functional structures could be fabricated, on one hand, by the incorporation of classical materials using contemporary techniques. However, the real breakthrough may lie in the design and advance of novel functional materials.<sup>2</sup>

Making use of Coulombic interactions, the electrostatic self-assembly constitutes a versatile tool for nano- and microscale fabrication of devices and synthesis of novel supramolecular material structures.<sup>3, 5-15</sup> In materials science, the templated electrostatic “layer-by-layer (LBL)” sequential deposition is a simple method for the synthesis of multilayer thin films with controlled thickness and composition. One of the most attractive advantages of this assembly technique is that thin films can be tailor-made to display desired chemical and physical properties by the choice of specific polyelectrolyte material.<sup>5-15</sup> Aqueous processing enables synthetic as well as natural polyelectrolytes to be assembled for a variety of applications, from electroluminescent devices to biosensor arrays.<sup>5, 6, 14, 16</sup> Moreover, the development of various free-standing multilayer structures provides a new dimension for material design.<sup>13</sup> Here, an overview is given on the various aspects of electrostatic layer-by-layer assembly using polyelectrolytes. The following discussions start from introducing the physical backgrounds of polyelectrolytes and the dominating molecular interactions between

polyelectrolytes. Later on, the issue of polyelectrolyte complex formation that is closely related to the stability and reversibility of layer-by-layer assembled polyelectrolyte multilayers is discussed with famous examples of DNA condensation.<sup>17, 18</sup> Polyelectrolyte multilayer thin films can be viewed as a special case of polyelectrolyte complexes. In the final part, great attention is focused on various aspects of planar substrate-supported as well as spherical free-standing multilayer thin film structures fabricated by the electrostatic layer-by-layer assembly technique.

## 2.2 Polyelectrolytes in solution and at interfaces

Polyelectrolytes (or polyions) encompass a large group of polymeric materials ranging from natural to synthetic that are charged or chargeable in nature. With their significant industrial and commercial value in bio- and medical related applications, polyelectrolytes are becoming increasingly important in recent years.<sup>5</sup>

Most of the properties of polyelectrolytes originate from their distinctive charged molecular characteristics.<sup>19</sup> When the charge density is not very low, polyelectrolyte solution behaviour strongly depends on added salt because of the electrostatic interactions between charges (*vide infra*). In the absence of added salt, the interactions between charges are simple Coulombic interactions. In this condition, polyion chains are expected to adopt a more expanded or stretched conformation than neutral polymers. Thus macroscopically, the osmotic pressure of salt-free polyelectrolyte solutions often exceeds that of neutral polymers at similar concentrations by several orders of magnitude.<sup>19</sup> Furthermore, the viscosity of dilute salt-free polyelectrolyte solutions is proportional to the square root of polymer concentration according to the Fuoss' law:<sup>20, 21</sup>

$$\eta \sim c^{1/2} \quad (2.1)$$

while for neutral polymer the relation is linear.

In the presence of added salt with a concentration of  $n$ , the Coulombic interaction between two charges at a distance  $r$  is given by the Debye-Hückel potential as:

$$v(r) = \frac{kTl_B}{r} \exp - \kappa r \quad (2.2)$$

where  $l_B = \frac{q^2}{4\pi\epsilon kT}$  is the so called Bjerrum length, with  $q$  and  $\epsilon$  denoting the elementary charge and the dielectric constant of water, respectively; and  $\kappa^{-1} = (8\pi nl_B)^{-1/2}$  is the Debye screening length.<sup>5b, 22</sup> At very high ionic strength, the charges are screened and the solution behaviour bears similar characteristic as that of uncharged polymer.

When a polyelectrolyte solution is brought into contact with a charged surface, the electrostatic forces between the charges on the polyions and the surface take into action. In

the close proximity of the charged surface, the tightly bound surface charges constitute the Stern layer, which is covered by a diffuse layer composed of mobile ions. The surface potential created, in this case, decreases with the distance from the surface (Figure 2.1). Similar to polyelectrolyte solutions, the decay of the surface electrical potential also depends on solution ionic strength according to the Debye-Hückel approximation. Adsorption of polyelectrolytes will happen as long as the screening length  $\kappa^{-1}$  is smaller than the chain thickness.<sup>5b</sup>

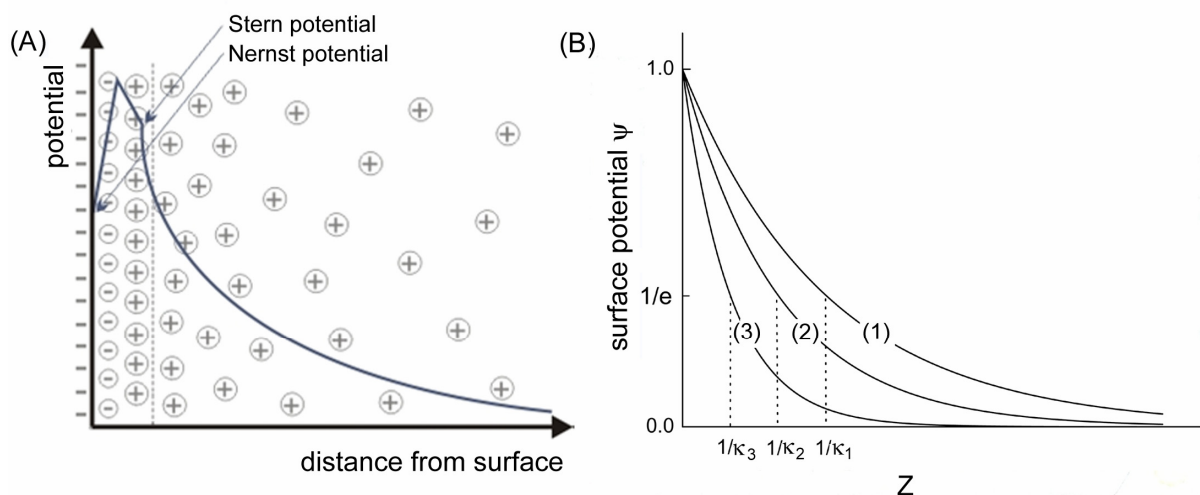


**Figure 2.1** (A) Schematic representation of the electrical double layer of a charged surface in contact with an electrolyte solution. The tightly bound surface charges constitute the Stern layer, which is covered by the diffuse layer composed of mobile ions. The electrical potential decreases exponentially in the diffuse layer. (B) Schematic representation of the surface electrical potential dependence on solution ionic strength. The solution ionic strength increases in the sequence of 1-2-3. The Debye screening length  $\kappa^{-1}$  denotes the double layer thickness, which decreases with increasing solution ionic strength.

### 2.3 Molecular interactions between polyelectrolytes

Self-assembly or supramolecular chemistry makes use of secondary interactions, among which van der Waals interactions, hydrogen-bonding, hydrophobic interactions, coordination bonding and ionic interactions are the most known ones.<sup>3,4</sup> In order to achieve a certain degree of molecular order, the type of interactions utilized in self-assembly should comply with the following criteria: interactions should be strong enough to provide *stability*; but not too strong that first contacts are *irreversibly* trapped.<sup>3</sup> In the following section, the two dominating molecular interactions between (oppositely) charged polyelectrolyte species will be discussed.

### 2.3.1 Ionic interactions

The electrostatic assembly described in this thesis is closely related to ionic interactions between charges. When two charges  $Q_1$  and  $Q_2$  are separated by a distance  $r$ , the potential energy  $V$  of their interaction and the Coulomb force  $F$  are given by:

$$V = \frac{Q_1 Q_2}{4\pi\epsilon_0\epsilon r}; F = \frac{Q_1 Q_2}{4\pi\epsilon_0\epsilon r^2} \quad (2.3)$$

where  $\epsilon_0$  is the dielectric permeability of free space and  $\epsilon$  is the relative permeability or dielectric constant of the medium. For like charge interaction, both  $V$  and  $F$  are positive so the force is repulsive, while for opposite charge interactions they are negative so the force is attractive.<sup>4</sup>

It could be calculated that for two point charges at a sub nm molecular distance, the Coulombic interaction at room temperature is in the order of several hundred  $kT$  (Boltzman constant  $k = 1.38 \times 10^{-23}$  J/K;  $T$  is the temperature) and comparable to that of covalent bonds. Considering the general expression of the distance dependence of potential energy  $V \propto \frac{1}{r^{n+m-1}}$  for the interaction of an  $n$ -pole with an  $m$ -pole (where  $m, n$  always  $\geq 1$ ),<sup>23</sup> it is obvious from equation (2.1) that Coulombic interaction is long-range in nature since  $V$  scales with  $1/r$ .

### 2.3.2 Hydrophobic interactions

Synthetic polyelectrolytes are often composed of a hydrophobic backbone, in many cases a hydrocarbon main chain. In aqueous solutions of such polyelectrolytes, an interaction mediated by water – the hydrophobic interaction – will take place, which is closely related to the so-called “hydrophobic effect”.<sup>4</sup>

The hydrophobic effect originates from the strong inclination of water molecules to form hydrogen bonds with each other. When water molecules come in contact with non-polar molecules that are unable to form hydrogen bonds, water molecules will tend to pack around the hydrophobic molecules in order not to give up any hydrogen bonding sites. This is an unfavourable entropic effect, thus will result in the unusually strong attraction between hydrophobic molecules and surfaces in water.<sup>4, 24</sup> To give an example, the strength of hydrophobic interactions between two methane molecules has been reported to be about - 8.5 kJ/mol.<sup>4</sup>

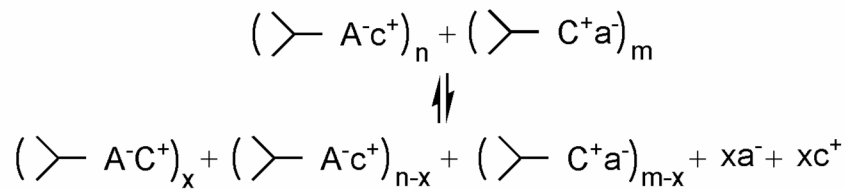
Apart from electrostatic forces, hydrophobic interactions play an important role in bringing two oppositely charged polyelectrolytes together (see Chapter 2.4). In the case of polyelectrolyte adsorption onto a solid substrate, the driving force for the adsorbate onto the solid-water interface is also related to the entropy gain expected by the release of water molecules from the interface.<sup>25</sup> However, a direct measurement of hydrophobic interactions is



not so straightforward. Kotov has carried out a thermodynamic analysis on the layer-by-layer (LBL) assembled polyelectrolyte multilayer systems (see Chapter 2.5), which indicates an indispensable contribution of hydrophobic interactions to the overall Gibbs free energy of film formation.<sup>25a</sup> It was even shown that proteins could adsorb irreversibly on a negatively charged surface with the hydrophobic interactions overcoming Coulombic repulsion.<sup>25d</sup>

## 2.4 Polyelectrolyte complexes

When polycation and polyanion solutions are mixed, a spontaneous formation of interpolymer complexes accompanied by the release of counterions is expected. The reaction of the polyelectrolyte complex formation can be described by the following scheme:



**Scheme 2.1** Polyelectrolyte complex formation in solution.

where  $\text{A}^-$ ,  $\text{C}^+$  are the charged groups of the polyelectrolytes;  $\text{a}^-$ ,  $\text{c}^+$  are the counterions;  $m$ ,  $n$  are the number of the anionic and cationic groups in solution;  $m/n = x$  determines the molar mixing ratio. The degree of conversion of the reaction illustrated in Scheme 2.1 determines the binding efficiency of the two components and whether some small counterions still remain in the complex. Another important feature of polyelectrolyte complexes is that even when the ionic bonding reaches the 1:1 stoichiometry, an overcharging of the complex particles is still expected.<sup>26</sup>

Since two oppositely charged species are involved, polyelectrolyte complexation appears to be “electrostatically driven”. As a matter of fact hydrophobic interactions have been established to play a very important role in polyelectrolyte complex formation.<sup>25, 27</sup> The driving force for the shifting of the equilibrium in Scheme 2.1 is mainly the gain in entropy caused by release of counterions originally localized in the vicinity of the polyelectrolyte coils. Many of the polyelectrolyte complexes are insoluble in water, which forms the basic criteria for a successful electrostatic layer-by-layer deposition. However, in special conditions water-soluble polyelectrolyte complexes can also be formed with the participation of weak polyelectrolytes or non-stoichiometric systems.<sup>5b, 26</sup> As a result, the stability of these water-soluble systems can be strongly influenced by solution pH or ionic strength.

It has been pointed out that the study of polyelectrolyte complexes is very helpful in understanding the criteria for a successful layer-by-layer deposition (see Chapter 2.5), as well as some of the stimuli-responsive behaviour of polyelectrolyte multilayer systems.<sup>5, 7</sup> In

general, polyelectrolyte complexes formed between strong polyelectrolytes display highly aggregated features. However, polyelectrolyte complex particle dispersions could be obtained when the aggregation stops on a colloidal level in extremely diluted solutions. Electron and X-ray absorption microscopy showed that complexation led to polydisperse systems of nearly spherical particles.<sup>26</sup> A practical application of these complex particle systems is to use them as material carriers in for example DNA delivery vehicles.<sup>28</sup>

DNA can be compacted to toroids, rods, or spheroids that are tens to hundreds of nanometers in diameter in the presence of multivalent cations, including cationic polymers (Figure 2.2).<sup>28, 29</sup> In the extreme cases, condensed DNA only occupies  $10^{-3} - 10^{-4}$  of the volume of naked DNA coils.<sup>30</sup> The polyplexes formed from DNA and polycations often lack any periodic order. This typical polyelectrolyte complex formation is different from lipid-DNA complexation, where lamellar structures are often observed resulting from some supramolecular assembly process.<sup>31</sup>

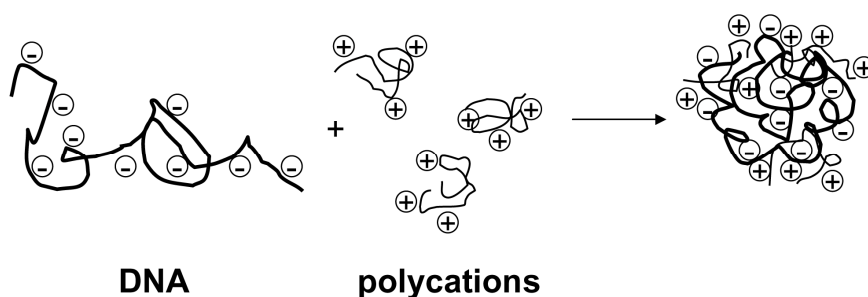


**Figure 2.2** Schematic of DNA condensation by cationic polyelectrolytes.

Since DNA condensation has very practical applications in gene therapy, it has attracted a lot of scientific attention. First DNA is packed for its smooth transfer through the cell membrane, after which a release of the genetic information is desired. Thus, the formation, transfection efficiency, degradation or dissociation, as well as the interaction of DNA/polycation polyplexes with biomacromolecules all constitute important aspects for improved performance.<sup>29</sup>

## 2.5 Layer-by-layer electrostatic assembly of polyelectrolytes

The electrostatic layer-by-layer (LBL) technique is based on the sequential adsorption of cationic and anionic species onto charged surfaces, which was first introduced by the group of Decher in the early 1990s.<sup>32</sup> A great advantage of LBL is its versatility: A wide range of materials from polyelectrolytes to colloidal particles could be assembled in this way onto substrates of any type and any shape.<sup>5</sup> Here, discussions are mainly confined in thin film structures assembled from polyelectrolytes with ionic and hydrophobic interactions as the main driving force.

The typical LBL multilayer fabrication procedure involves a dipping and a rinsing step to remove the excess, non-adsorbed material between each layer deposition (Figure 2.3).<sup>5</sup> This process could be repeated as many times as desired to create multilayer thin films comprised of semi-interpenetrated alternating polyelectrolyte layers.<sup>33</sup> The typical layer thickness ranges from 0.5 to 10 nm, depending on the polymer molar mass and adsorption conditions.<sup>34</sup>

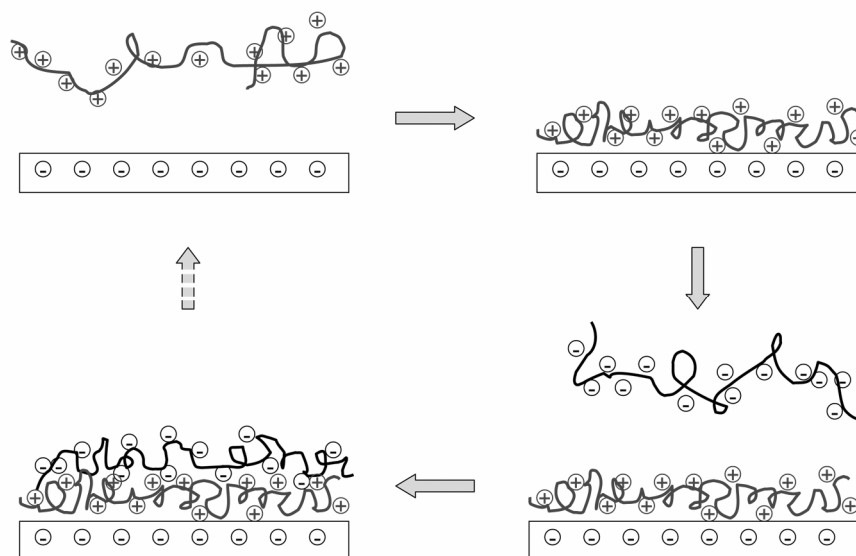


**Figure 2.3** Schematic representation of the LBL electrostatic assembly with polyelectrolytes.

Various synthetic organic polyelectrolytes, such as poly(styrene sulfonate) (PSS), poly(acrylic acid) (PAA) and poly(allylamine hydrochloride) (PAH) have been extensively studied in the LBL technique.<sup>7</sup> In the mean time, constant efforts have also been made to utilize biological polyelectrolytes, such as DNA and proteins to fabricate functional thin film structures.<sup>35-45</sup> With synthetic developments, organometallic polyelectrolytes with inorganic elements and transition metals in the main chain gave access to multilayer structures that may possess some unprecedented functions.<sup>46, 47</sup>

Due to the versatility of material selection and the simplicity of the LBL technique, tremendous success has been achieved in the LBL electrostatic deposition of polyelectrolytes. However, not every arbitrary chosen polyanion/polycation pair can be successfully assembled. The possibility of alternating polyion adsorption onto surfaces has been considered to depend on the phase behaviour of polyelectrolyte complexes in solution. Polyelectrolyte multilayers result from a higher affinity of the complexes to surfaces than to solvents.<sup>48</sup>

Although glass, silicon wafers, quartz, gold substrates and colloidal particles are the most commonly studied substrates, there are almost no limitations in the type of substrates that could be employed in the LBL process.<sup>49, 50</sup> But in order for the electrostatic adsorption to take place, in the case of planar substrates most of the time an additional surface treatment step to render a pre-charged substrate is necessary.<sup>51-53</sup> The choice of substrates mainly

depends on the convenience for particular analytical methods and application purposes. In the following sections, planar substrate-supported multilayers and free-standing microcapsules will be addressed separately, followed by discussions on the important application potentials of this technique.

### 2.5.1 Planar multilayers

#### 2.5.1.1 Formation and characterization

The exploration of the LBL technique starts with depositing multilayers onto flat-shaped substrates. In order to confirm successful multilayer formation, different characterization techniques have been introduced. Generally, the multilayer deposition will be interrupted with defined intervals and will be resumed after an ex-situ or in-situ characterization.

The simplest way to monitor the multilayer build-up is by UV/Vis spectroscopy. As long as coloured materials are incorporated during the LBL deposition process, changes in its characteristic absorbance with increasing the number of deposited layers could be easily followed. For example, poly(ferrocenylsilane) (PFS) has two characteristic absorbance bands in the reduced state: an intense ligand-to-metal charge transfer transition (LMCT) at  $\sim 220$  nm and a weak *d-d* band centered at  $\sim 450$  nm.<sup>54</sup> When multilayers were deposited from PFS polyelectrolytes onto quartz substrates, a linear increase of absorbance at both bands has been observed.<sup>47d</sup>

Information on film thickness increase with increasing the number of bilayers is normally obtained from ellipsometry measurements of multilayers deposited on silicon wafers. Unlike UV/Vis spectroscopy that relies on the molar extinction coefficient of deposited absorbing materials, ellipsometry is a more universal physical method in determining thin film thickness of any material based on refractive index contrast (see also Chapter 2.5.4). Moreover, ellipsometry measures the change in polarization of light upon reflection, while UV/Vis spectroscopy studies the light absorbance. Thus multilayers deposited on optically non-transparent substrates can be characterized by ellipsometry but not by transmission UV/Vis spectroscopy. Ellipsometry is routinely used to determine the optical constants and thin film thickness with sub-nanometer accuracy.<sup>55</sup> Often a direct measurement of the contribution of each individual layer is necessary, especially when the dipping conditions (such as ionic strength and pH) can strongly affect the film growth.<sup>56</sup>

Other methods to determine film thickness include X-ray reflectometry<sup>57</sup> and atomic force microscopy (AFM).<sup>58</sup> When AFM was used to measure the film thickness, a depression was first made on the film surface using the AFM tip. The depth of the depression after it becomes constant was treated as the film thickness.<sup>58, 59</sup> However, in many cases material accumulation was observed along the edges of the depression, making the whole procedure difficult to control.

The surface elemental composition of a multilayer thin film can be characterized using X-ray photoelectron spectroscopy (XPS).<sup>60</sup> Different peak positions in an XPS spectrum correspond to the electron kinetic energy of different elements ( $E_k$ ), which is related to their binding energy ( $E_b$ ).<sup>61</sup> XPS spectra of multilayers composed of different numbers of polyelectrolyte bilayers in the LBL process can provide complementary evidence for a successful LBL deposition and some insight on the structural interpenetration of the thin films.<sup>62</sup>

A general way to obtain multilayer surface coverage, *i.e.* the adsorbed amount of material, is by quartz crystal microbalance (QCM).<sup>63</sup> Multilayers are prepared on special electrodes (often gold or silver) and frequency changes are monitored for each deposited (bi)layer. The frequency decrease ( $\Delta F$ ) upon material adsorption is linearly related to the adsorbed mass ( $M$ ) by the Sauerbrey equation.<sup>64</sup> In such a way, a linear frequency decrease implies a linear film growth profile. However, slight non-linearity was often observed in the deposition of the first several layers in a multilayer system that has overall linear growth behaviour.<sup>49a, 65</sup>

Another way to quantify the surface coverage of multilayers makes good use of certain functionalities in the multilayer system. For example, poly(ferrocenylsilanes) (PFS) are well-known for their redox-responsive property.<sup>66, 67</sup> PFS can be reversibly oxidized electrochemically, which could be easily monitored by cyclic voltammetry (see Chapter 2.5.4).<sup>67</sup> A typical cyclic voltammogram of PFS shows two oxidation waves (Figure 2.4), indicating intermetallic coupling between neighbouring iron centers in the polymer chain.<sup>67a</sup>

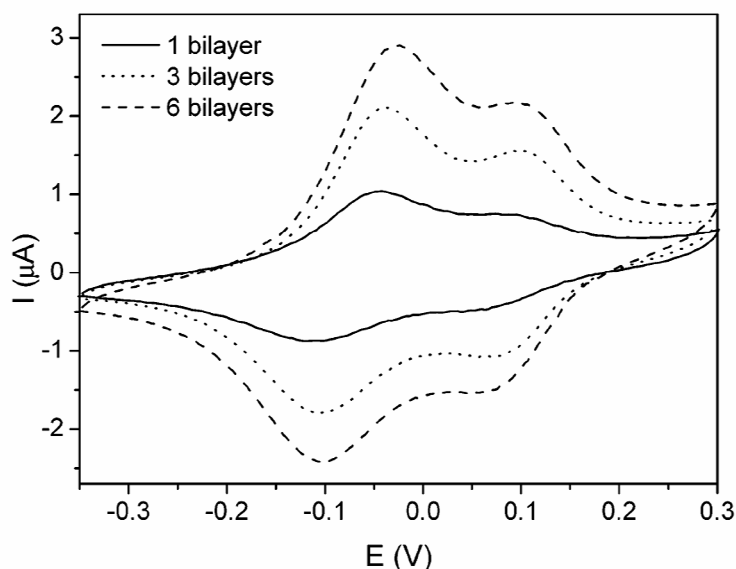


**Figure 2.4** Cyclic voltammograms of one, three and six bilayers of PFS weak polyelectrolytes on gold electrodes featuring a monolayer of sodium 3-mercapto-1-propanesulfonate. Scan rate was 30 mV/s. The electrolyte was 0.1 M aqueous NaClO<sub>4</sub> solutions and the potential was referenced to an Hg/HgSO<sub>4</sub> reference electrode. Reproduced with permission from [46b]. Copyright 2002 American Chemical Society.

When CVs were recorded on multilayers composed of PFS polyelectrolytes, the ferrocene surface coverage  $\Gamma$  of each sample could be calculated. The plot of  $\Gamma$  as a function of the bilayer number will provide quantitative information on the multilayer growth.<sup>46b</sup>

Like in other thin film studies, the surface morphology of the obtained multilayers is often characterized by AFM,<sup>68, 69-71</sup> scanning electron microscopy (SEM)<sup>72-74</sup> and transmission electron microscopy (TEM).<sup>47d</sup>

Although some of the above-mentioned measurements could be carried out in-situ (such as QCM<sup>75, 76</sup> and ellipsometry<sup>72a</sup>), most of the other techniques are ex-situ methods. Many other in-situ characterization approaches have also been developed in order to obtain kinetic information on multilayer deposition, such as surface plasmon resonance spectroscopy (SPR),<sup>77, 78</sup> optical waveguide lightmode spectroscopy (OWLS),<sup>79-81</sup> X-ray and neutron reflectometry.<sup>57, 82, 83</sup> In Figure 2.5, an example is given on the deposition kinetics of the poly(L-lysine) (PLL)/heparin (HEP) multilayer system characterized by electrochemical OWLS (EC-OWLS). It is observed that the adsorption of each polyelectrolyte layer is rather fast, as the adsorbed mass  $\Gamma$  reaches an equilibrium value within one minute of the injection of a new polyelectrolyte solution. The relatively flat plateau regions in the curve also indicate the absence of apparent desorption after rinsing.<sup>81</sup> It is worth noting that the adsorbed mass upon each layer deposition is not really constant, demonstrating a not so regular multilayer growth profile.

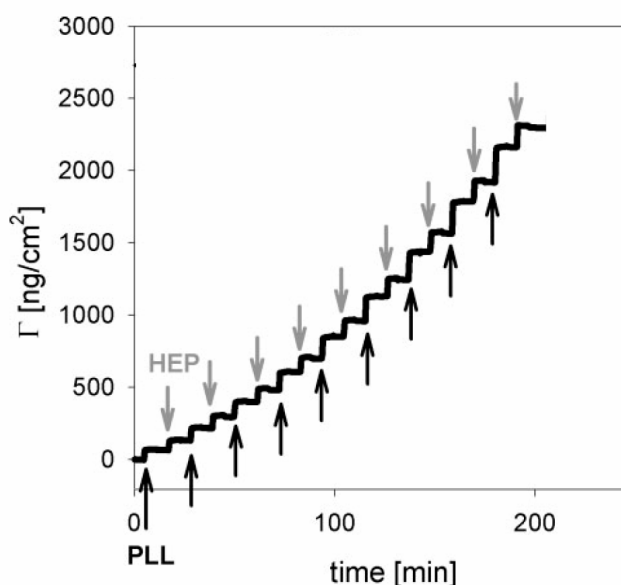


**Figure 2.5** Evolution of the adsorbed mass  $\Gamma$  [ $\text{ng}/\text{cm}^2$ ] on an ITO substrate measured in situ by EC-OWLS as a function of time during the alternating deposition of PLL and HEP layers from HEPES150 buffer. Black and grey arrows correspond to the injection of PLL and HEP, respectively. Reproduced with permission from [81]. Copyright 2006 Wiley-VCH Verlag GmbH.

### 2.5.1.2 Structure and properties

It is not so straightforward to get a clear picture of the internal structure of polyelectrolyte multilayers. Insight into the in-depth structure of multilayer thin films was obtained when the results from different characterization methods were compared.<sup>5</sup>

Generally, the structure of polyelectrolyte multilayers has been regarded as consisting of stratified layers with strong interdigitation of the polyanion and polycation species.<sup>82, 83</sup> In a typical zone model describing the basic structure of a film, three distinctive zones were illustrated (Figure 2.6).<sup>5, 82, 84</sup> The first layers are those in close proximity with the substrate (zone I), followed by an intermediate zone with relative constant properties (zone II), finally terminated by the third one (zone III) in close contact with the outside environment (air or water). The division between these zones originates from their distinctive properties, which are determined by their distances from the interfaces. The existence of zone I was indicated by the fact that most of the time a regular film growth was only observed after the deposition of several bilayers (it has been reported that this number is around six<sup>84</sup>). Zone II was considered to be a charge-compensated neutral zone, while the outermost zone III determines many of the multilayer surface properties.<sup>56, 84, 85</sup>

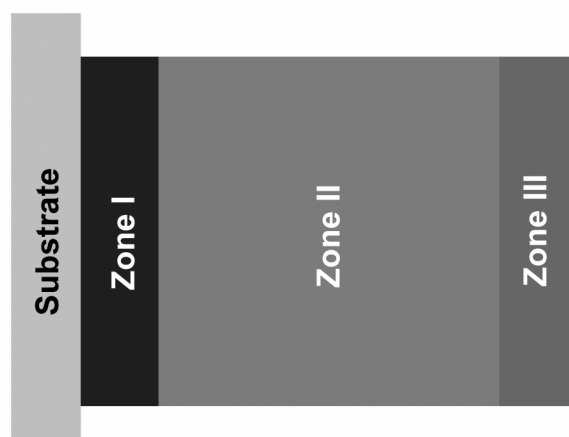


**Figure 2.6** The zone model for polyelectrolyte multilayers. Zone I consists of the first several bilayers that are close to the multilayer/substrate interface. Similarly, the bilayers in Zone III are in close contact with the multilayer/air or multilayer/water interface. Zone II is considered to be a charge-compensated neutral zone.

It has been reported that the surface wettability of sequentially adsorbed polyelectrolyte layers is controlled primarily by the outmost surface layer.<sup>56, 85</sup> Thus, it is possible to create surfaces with molecularly tuneable wetting properties by simply changing the nature of the outmost adsorbed polyelectrolyte layer. This can be accomplished via the use of surface layers with different chemical structures or by controlling the surface composition of a single layer combination.<sup>84</sup> The contact angle of a multilayer thin film can not only provide wettability information, but also serve as a parameter to describe the level of multilayer interlayer interpenetration.<sup>56</sup> Figure 2.7 shows an example of the measured

advancing contact angle values on an organic-organometallic hybrid multilayer composed of PFS and PSS. The results demonstrate the systematic and consistent alternation of the advancing contact angle value between  $75 \pm 2^\circ$  for PSS-terminated surfaces and  $67 \pm 5^\circ$  for PFS terminated surfaces. This gives the evidence that PFS-terminated surfaces are slightly more hydrophilic than PSS-terminated multilayer surfaces.<sup>47b</sup>

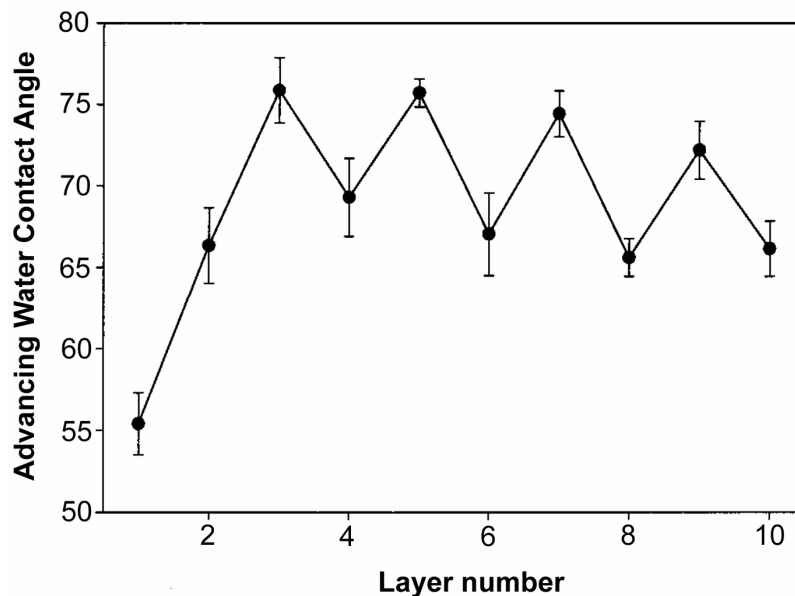


**Figure 2.7** Advancing water contact angles on PSS polyanion (odd number layers) and PFS polycation (even number layers) terminated multilayer films on gold substrates. Reproduced with permission from [47b]. Copyright 2000 American Chemical Society.

Apart from surface hydrophobicity, the  $\zeta$ -potential of a multilayer has also been observed to largely depend on the outmost layer.<sup>84</sup> The surface morphology of a multilayer film as examined by AFM measurements shows that polyelectrolyte multilayer growth will gradually smoothen the roughness of a substrate.<sup>51</sup> This can be explained if the uniform thin film deposition follows the surface morphology.<sup>58</sup>

A more complicated multilayer property is the film/bilayer thickness. In the case of strong polyelectrolytes, an almost universal behaviour of bilayer thickness increase with increasing the polyelectrolyte solution salt concentration has been observed.<sup>82, 84, 86-88</sup> However, rather different power laws of bilayer thickness dependence on solution salt concentration have been reported. Controversy exists between a linear dependence<sup>82, 86</sup> and a square root dependence.<sup>87, 88</sup> For weak polyelectrolytes whose charge density strongly depends on solution pH, pH dependent thickness is often expected and also experimentally verified.<sup>56, 89</sup> Figure 2.8 shows an example of the layer thickness dependence on solution pH of a multilayer fabricated from poly(acrylic acid) (PAA) and poly(allylamine hydrochloride) (PAH). The charge densities of both PAA and PAH are dependent on solution pH, which caused their strongly pH-dependent adsorption behaviour.<sup>89</sup> In order to fully understand polyelectrolyte multilayer pH dependence, attempts were also made to obtain the internal  $pK_a$  value of the multilayers.<sup>90</sup>



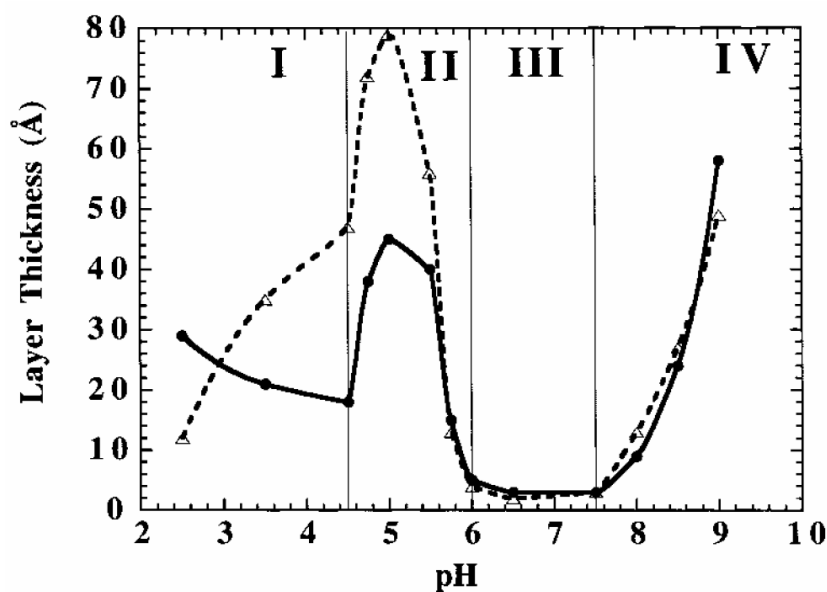


**Figure 2.8** Average thickness increment contributed by a PAA (solid line) and PAH (dashed line) layer as a function of solution pH. Both PAA and PAH were deposited from dipping solutions of the same pH. Reproduced with permission from [89]. Copyright 2000 American Chemical Society.

It is more or less accepted that polyelectrolyte LBL deposition is a kinetically-controlled process, since most of the existing examples display irreversibility.<sup>7</sup> However, reports have shown that in weak polyelectrolyte systems it is possible to reverse the multilayer deposition at sufficiently high ionic strength (*vide infra*).<sup>91, 92</sup> The study of multilayer thermal behaviour revealed the internal dynamics of multilayer systems. It has been shown that polyelectrolyte multilayers undergo very slow rearrangements at elevated temperature. Experimental evidences include the dependence of lipid diffusion coefficient into multilayers<sup>93</sup> and the shrinkage of multilayer microcapsules (see Chapter 2.5.2) upon heating.<sup>94</sup> Temperature induced reorganization of the polyelectrolyte multilayers has been attributed to an entropy-driven conformational change of the polymer chains.

## 2.5.2 Multilayer capsules

A further exploration of the electrostatic LBL technique was pioneered by the group of Möhwald in 1998, when fabrication, structure and properties of polyelectrolyte multilayer capsules were first reported.<sup>95</sup> The method involves colloidal-templated consecutive polyelectrolyte adsorption followed by the decomposition of the templating core. This template-assisted assembly and template removal for the fabrication of free-standing thin film structures was soon extended for the production of other functional LBL structures,<sup>13</sup> such as free-standing mechanical thin films<sup>96-98</sup> and polyelectrolyte nanotubes.<sup>99-101</sup> The most fascinating aspect of hollow micro- or nano-capsule systems lies in the fact that due to the LBL preparation, the assembled stable capsules normally display permeability to small molecules but not to big or macromolecules.<sup>102</sup> The selective permeability of multilayer

capsules provides a unique micro- or nanometer sized confinement, which also forms the foundation of controlled-release related applications.<sup>103-107</sup>

The method of constructing hollow polyelectrolyte containers by the LBL method is illustrated in Figure 2.9. As shown in the figure, the stepwise film deposition onto curved substrates imitates that of planar film fabrication. All aqueous processing necessitates the development of efficient methods to separate carrier particles from the polyelectrolyte and washing solutions. There are normally two ways to achieve this. One is by removing the excess polyelectrolyte through centrifugation/washing cycles before the next layer is deposited.<sup>95</sup> An alternative method is by using a membrane filter system in which the polyelectrolyte and washing solutions can be added and eluted continuously.<sup>108</sup>

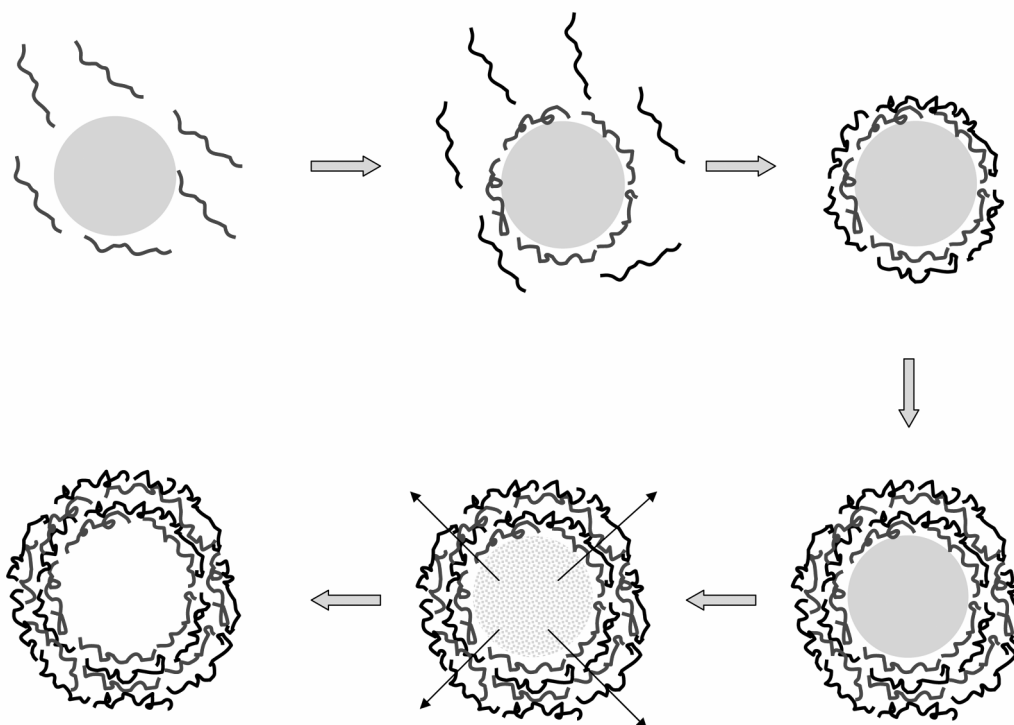


**Figure 2.9** Schematic representation of polyelectrolyte multilayer capsule fabrication. Polyelectrolytes are deposited onto charged colloidal particles in a LBL fashion followed by template dissolution.

Different types of colloids from organic,<sup>109, 110</sup> inorganic<sup>111-113</sup> to metal<sup>114</sup> particles may all serve as the templating material. Most of the capsule shell properties depend on the fabrication procedure involved. One of the most important steps in capsule fabrication, which may affect the multilayer properties, is the core removing process. For each type of template material there are corresponding dissolution procedures. Some colloidal particles such as melamine formaldehyde (MF), polystyrene sulfonate (PSS) and silica microspheres often require rather harsh dissolution conditions involving strong acid or solvent treatment.<sup>109, 110, 113</sup> In recent years, growing attention has been paid to metal carbonate crystals that could be removed by pH-neutral ethylenediaminetetraacetic acid (EDTA) solutions.<sup>111, 112</sup> The size of the capsules can vary from tens of microns down to nanometer-size, and is well-defined by

the size of the template. Multilayer deposition becomes more difficult upon decreasing the size of the colloidal templates to nanoparticles.<sup>114</sup> However, Decher *et al.* have demonstrated the successful polyelectrolyte LBL deposition onto gold nanoparticles as small as 13.5 nm and subsequent core removal to yield nanocapsules.<sup>114</sup>

Due to the novel shape introduced here, different characterization techniques are utilized to characterize coated colloids and multilayer capsules. A successful LBL assembly can usually be followed and confirmed by light scattering<sup>108, 115, 116</sup> and electrophoretic mobility (zeta potential)<sup>117</sup> measurements upon each (bi) layer deposition. The polyelectrolyte covered core/shell particles, as well as the morphology of the formed capsules can be visualized by scanning electron microscopy (SEM) or transmission electron microscopy (TEM).<sup>95, 118, 119</sup> An optimal capsule system requires a complete removal of the templating material, which can be characterized by SEM equipped with energy dispersive X-ray spectroscopy (EDX),<sup>111a</sup> or confocal Raman microscopy (CRM).<sup>120</sup> CRM is a rather powerful tool in that it can not only collect the chemical spectra of a polyelectrolyte capsule system, but also combine it with an imaging technique to provide direct visual information on material distribution.<sup>121</sup> Capsule wall thickness is often measured by atomic force microscopy (AFM).<sup>122</sup> Images of the capsule shell are collected using tapping or contact mode AFM, after which sectional analysis will be carried out to get statistical values on the multilayer thickness. Apart from acquiring surface morphology information,<sup>123</sup> another important application of AFM is force measurement. Fery *et al.* has reported the successful determination of the Young's modulus of PSS/PAH microcapsules by micromechanical tests using AFM.<sup>124</sup>

A very important technique to in-situ visualize and obtain permeability and mechanical information about multilayer capsules is confocal laser scanning microscopy (CLSM, see also Chapter 2.5.4). Multilayer capsules are considered to be semipermeable, excluding higher molar mass species but allowing diffusion of low molar mass polar species.<sup>120, 125, 126</sup> CLSM studies on fluorescence labelled multilayer capsules or a capsule sample mixed with a certain fluorescence probe could provide qualitative information on the size, integrity and permeability of a capsule system.<sup>107, 120, 126</sup> More sophisticated, quantitative measurements could also be performed based on CLSM imaging. For example, using fluorescence recovery after photobleaching (FRAP), the permeability coefficient of a capsule wall could be calculated.<sup>127, 128</sup> By recording the deformation of capsules under introduced osmotic pressure from polyelectrolyte solutions with varying concentrations, the mechanical properties such as capsule wall elasticity have also been acquired.<sup>129</sup>

Among various interesting properties displayed by multilayer capsules, application-driven issues such as active capsule permeability control have drawn growing attention during the past decade. In this respect, stimuli-responsive multilayer systems are becoming particularly important for permeability manipulation of the capsules.<sup>11</sup> Many polyelectrolyte multilayer capsule systems display general responsive behaviour under environmental changes in temperature,<sup>94c, 130, 131</sup> solvent,<sup>132</sup> and ionic strength.<sup>131, 133</sup> More interesting capsule

systems that could respond to specific stimuli are often based on functional wall materials. For example, incorporating polyelectrolytes whose charge density can vary depending on external pH constitutes one of the ways to render stimuli-responsiveness to multilayer capsules.<sup>134</sup> Figure 2.10 demonstrates an example of capsules made of poly(styrene sulfonate) (PSS) and poly(allylamine hydrochloride) (PAH) based on melamine formaldehyde (MF) colloidal particles. These capsules were prepared and kept at pH  $\sim$  8. CLSM imaging showed that these capsules, as prepared, were essentially impermeable to fluorescein (FITC) labelled dextran molecules ( $M_w = 7.0 \times 10^4$  g/mol). On reducing the pH value to lower than 6, the capsule walls displayed complete permeability to the same fluorescent probe molecules. Moreover, a reversal of the pH to a higher value would keep the FITC-dextran molecules trapped inside the capsules, indicating the reversibility of the pH induced permeability response. This type of structural response has been considered to originate in the charge density alterations of the pH sensitive PAH polyelectrolytes.<sup>134</sup>

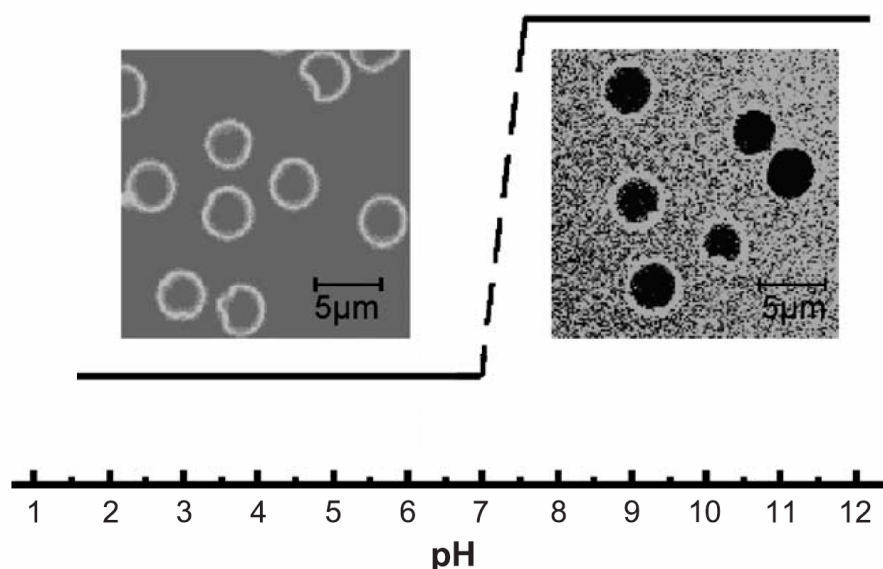


**Figure 2.10** pH dependent permeability of poly(styrene sulfonate) (PSS)/poly(allylamine hydrochloride) (PAH) microcapsules based on melamine formaldehyde (MF) cores. The fluorescence-labelled probe molecule is dextran-FITC ( $M_w = 7.0 \times 10^4$  g/mol). Reproduced with permission from [134d]. Copyright 2004 Elsevier.

Similar principles to regulate intermolecular interactions in the originally charge compensated multilayer structures have also been proved in a multilayer capsule system containing redox-responsive polymers.<sup>135</sup> Various other types of stimuli, including light,<sup>136</sup> magnetic-field<sup>137</sup>, ultrasound<sup>138</sup> and specific interactions<sup>11</sup> have also been employed to stimulate multilayer capsule permeability response.

### 2.5.3 Potential applications

Since LBL electrostatic self-assembly has proven to be such a versatile tool for the design and construction of complex polymeric architectures, numerous potential applications are envisaged.<sup>6</sup> Interesting applications range from sensors,<sup>139</sup> functional coatings,<sup>72b, 140</sup> enzyme immobilization,<sup>38a</sup> electrochromic thin films,<sup>141</sup> nanomechanical films,<sup>142</sup> modified electrodes,<sup>143</sup> to some biomedical related areas.<sup>14</sup> Polyelectrolyte multilayer micro- and nanocapsules, on the other hand, may be applied in areas such as medicine, delivery systems, self-repairing coatings<sup>144</sup> and micro or nano-sized reactors.<sup>107</sup> Several examples of the interesting application potentials of multilayer deposition are given below.

With the development of nanoscience and nanotechnology, many of the micro-or nano-devices require the placement of functional objects onto substrates in a pre-determined arrangement.<sup>6b</sup> When polyelectrolyte multilayers are to be incorporated into these devices, the ability to pattern these thin films becomes a crucial factor. Patterned multilayers may have potential applications for producing complex optical or electro-optical devices, such as waveguides and display materials.<sup>6b, 34</sup> Early attempts for selective multilayer assembly on specific areas involved microcontact printing ( $\mu$ CP) through the use of self-assembled monolayers (SAM) as molecular templates.<sup>145, 146</sup> Figure 2.11 illustrates the common procedure for the preparation of multilayer patterns using  $\mu$ CP. Alternating acid (COOH) and oligoethylene glycol (EG) functional surfaces are most commonly used as the template surfaces. Areas covered with oligomers of PEO were found to prevent adsorption of polyions due to enthalpic and entropic interfacial effects.<sup>146</sup> Area-selective LBL deposition of polyelectrolytes can lead to two-dimensionally patterned multilayer thin films.

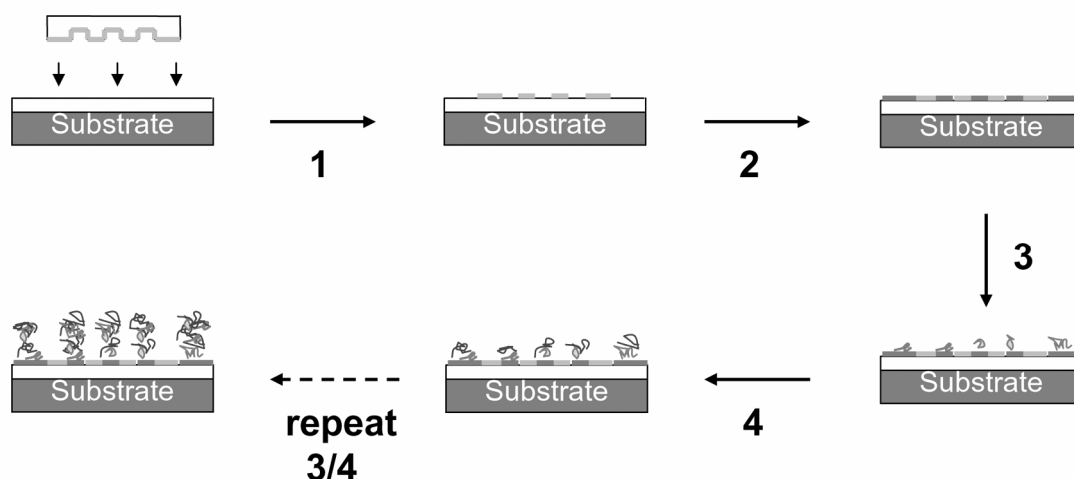


**Figure 2.11** Schematic illustration of multilayer patterns formed by selective deposition onto hydrophilic/hydrophobically patterned self-assembled monolayers on gold using  $\mu$ CP. A thiol resist (e.g. EG terminated) is first printed by a polydimethylsiloxane (PDMS) stamp onto the Au substrate followed by backfilling the substrate with a second thiol (e.g. COOH terminated). Polyelectrolyte multilayers will preferentially adsorb onto the backfilled areas of the chemically patterned template.

Later, nonlithographical methods such as inkjet printing were introduced.<sup>147</sup> The development of new techniques, such as the “lift-off” approach,<sup>148</sup> “polymer on polymer” stamping<sup>149</sup> and nanoimprint lithography (NIL) assisted LBL assembly<sup>150</sup> has also been reported.

Responsive polyelectrolyte multilayers are promising in some specific application areas. Recently, LBL assembled multilayer thin films have been used to build planar defects into self-assembled colloidal photonic crystals (CPCs), allowing for chemically active defects responsive to various environmental stimuli.<sup>149, 151</sup> One of the examples involves making use of the redox-responsive properties of the organometallic polymer poly(ferrocenylsilane) (PFS).<sup>47e</sup> The idea is to achieve precise and reversible tuning of the intergap transmitting state of the CPC, by simple redox cycling. As illustrated in Figure 2.12A, the PFS multilayer planar defect was prepared by their LBL deposition onto a flat polydimethylsiloxane (PDMS) sheet. Following the “polymer-transfer printing”, the PFS multilayers were then transfer-printed onto the surface of a planar CPC consisting of silica spheres. The desired heterostructure was completed by the growth of a second CPC on top of the defect and clearly visualized by SEM (Figure 2.12B).

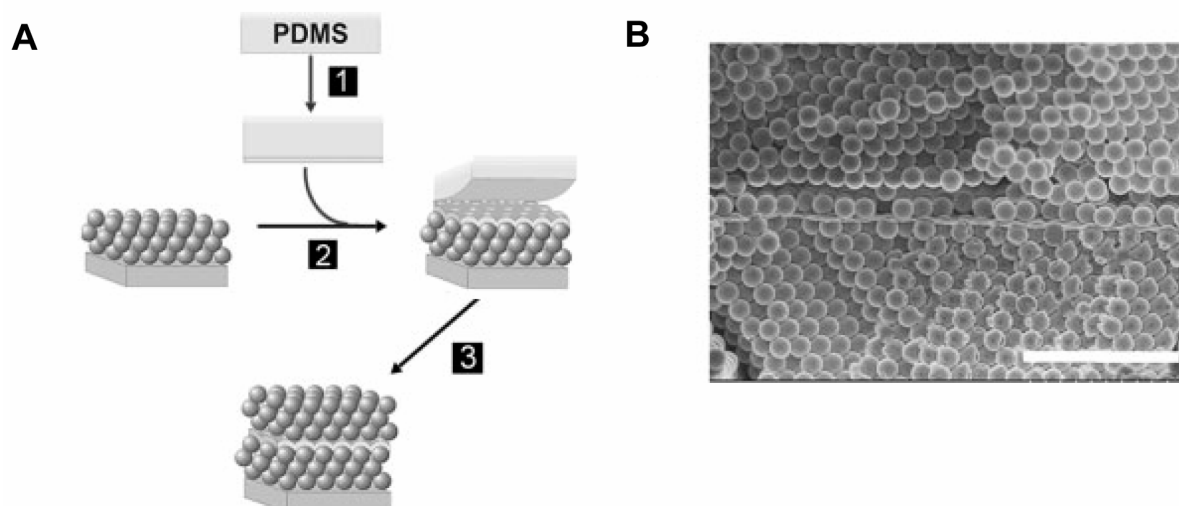


**Figure 2.12** Illustration of the incorporation of PFS PEMs into colloidal photonic crystals: (A) Schematic illustration of sample preparation: 1) Growth of a PEM onto a flat PDMS stamp; 2) Transfer printing of the PEM onto the bottom CPC; 3) Crystallization of the top CPC. (B) Cross-sectional scanning electron microscopy image of a silica CPC with embedded PFS defect layer composed of PFS polyelectrolyte multilayers. Scale bar is 2  $\mu\text{m}$ . Reproduced with permission from [47e]. Copyright 2005 Wiley-VCH Verlag GmbH.

The defect wavelength was subsequently tuned by chemical oxidation and reduction cycles. A hexane solution of iodine and a THF solution of decamethylferrocene were used, respectively, as the oxidant and reducing agent. After the first conditioning cycle, an almost completely reversible and reproducible tuning of the defect states was achieved, as demonstrated in Figure 2.13B. Complemented by ellipsometry experiments, oxidation of the PFS defect multilayer was reported to lead to a 4 nm red-shift of the defect position due to a

14% increase in thickness and a 6.5% increase of the refractive index of the PFS multilayers. Moreover, the defect wavelength can also be switched between intermediate oxidized states by controlling the fraction of oxidized ferrocene units. These unique properties also imply potential applications such as optical sensors or PC-based laser sources.<sup>47e</sup>

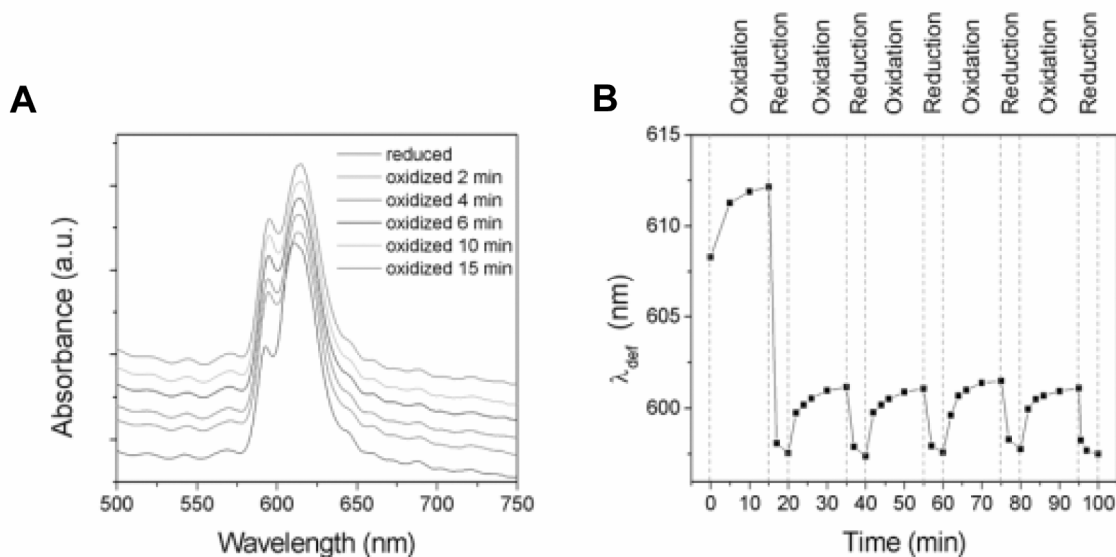


**Figure 2.13** (A) Transmission spectra of a PFS-defect CPC in the reduced and oxidized states; (B) Changes of the wavelength position of the defect state during redox cycles. The polyelectrolyte species used here are PFS polyelectrolyte multilayers. Reproduced with permission from [47e]. Copyright 2005 Wiley-VCH Verlag GmbH.

Another interesting and important application of responsive and degradable polyelectrolyte multilayers is for controlled release purposes. Lynn *et al.* have reported the delivery and sustained release of DNA from multilayers with a hydrolytically degradable synthetic polycation.<sup>152</sup> Multilayer capsules as vehicles for the encapsulation and release of functional species have also been addressed.<sup>153, 154</sup>

## 2.5.4 Some frequently used characterization techniques

### 2.5.4.1 Spectroscopic ellipsometry (SE)

Ellipsometry is a versatile tool for the investigation of the dielectric properties of thin films. The working principle of ellipsometry is based on the reflection of elliptically polarized light from a planar sample surface or parallel interfaces.<sup>155</sup> By measuring the changes in phase and amplitude of the polarization of the light upon reflection, thickness, refractive index and extinction coefficient of thin film samples can be determined. Figure 2.14 shows the schematic drawing of the working principle of a rotating analyzer ellipsometer.<sup>155</sup>

The ellipsometric parameters  $\Psi$  and  $\Delta$  are defined by the two components of the polarization state of the light in the plane of the reflection (the “*p*” plane) and perpendicular to this plane (the “*s*” plane). The amplitude ratio  $\tan\Psi$  is related to the amplitude (*A*) difference between the incident (*i*) and the reflected (*r*) polarized light as:

$$\tan \Psi = \frac{A_p^r / A_s^r}{A_p^i / A_s^i} \quad (2.4)$$

while the phase shift  $\Delta$  represents the change in the phase ( $\delta$ ) difference:

$$\Delta = (\delta_p^r - \delta_s^r) - (\delta_p^i - \delta_s^i) \quad (2.5)$$

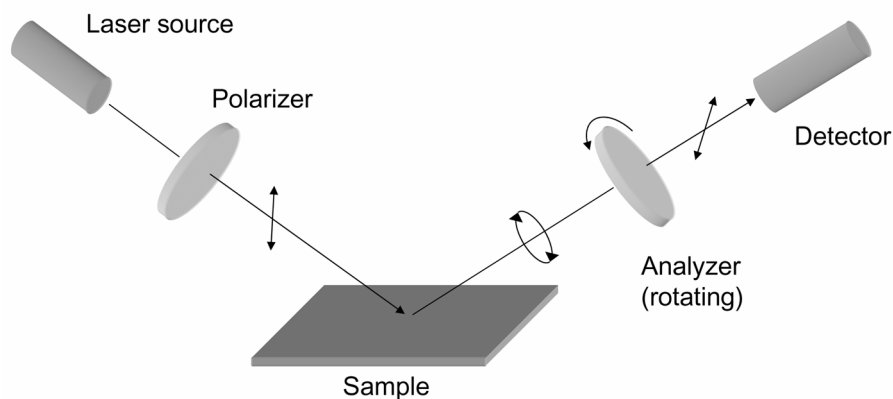


**Figure 2.14** Schematic principle of a rotating analyzer ellipsometer.

Ellipsometry measures the ratio of the total reflection coefficients,  $r_p$  and  $r_s$ , which is described by the fundamental equation of ellipsometry:

$$\rho = \frac{r_p}{r_s} = \tan \Psi e^{i\Delta} \quad (2.6)$$

According to the Fresnel equation, the total reflection coefficients are dependent on the phase change ( $\beta$ ) in the light wave, which is a function of the thin film thickness  $d$ , the wavelength of the light  $\lambda$ , the refractive index  $n_2$  and the extinction coefficient  $k_2$  of the thin film material, and the angle of reflection  $\theta_2$  as:

$$\beta = 2\pi\left(\frac{d}{\lambda}\right)(n_2 - jk_2) \cos \theta_2 \quad (2.7)$$

Thus  $\Psi$  and  $\Delta$  are linked to the thickness and optical constants of the thin film.

From equation 2.7 it is easily noticed that  $\Psi$  and  $\Delta$  also depend on the wavelength of the incident light. Spectroscopic ellipsometry (SE) employs broad band light sources that cover a certain spectral range. By measuring ellipsometric parameters at various  $\lambda$  values and at different incident angles, both the thickness  $d$  and refractive index  $n_2$  of the thin film can be determined based on fitting procedures using computer models.

#### 2.5.4.2 Cyclic voltammetry (CV)

Cyclic voltammetry (CV) is the most widely used electrochemical technique for acquiring qualitative and quantitative information about electrochemical reactions. It offers rapid location of the redox potentials of electroactive species.<sup>156</sup> In a typical CV experiment, a linear potential scanning with a triangular waveform is acting as the excitation signal, which sweeps the potential of the electrode between two switching potentials (Figure 2.15A). In this



process, the current is recorded as a function of the potential and shown in a cyclic voltammogram. In Figure 2.15B showing an example of a typical cyclic voltammogram, the most important parameters are labelled, *i. e.* the anodic and cathodic peak current ( $i_{pa}$ ,  $i_{pc}$ ), and the anodic and cathodic peak potential ( $E_{pa}$ ,  $E_{pc}$ ). The number of electrons transferred in a reversible electrochemical process  $n$  is thus determined by:

$$\Delta E_p = E_{pa} - E_{pc} = \frac{59}{n} \quad (2.8)$$

Scan rates ( $v$ ) can be varied. In a diffusion controlled charge transfer system the voltammetric peak current is proportional to  $v^{1/2}$ . The amount of charge involved in the electron transfer process ( $Q$ ) can be determined by integration of the area under the  $i$ - $E$  curves of the cyclic voltammograms, which does not depend on the scan rate. Then the surface coverage of electroactive species  $\Gamma$  can be determined by the following equation:

$$\Gamma = Q/nFA \quad (2.9)$$

where  $F$  is the Faraday constant (96,485 C/mol) and  $A$  is the geometric surface area of the electrode.<sup>157</sup>

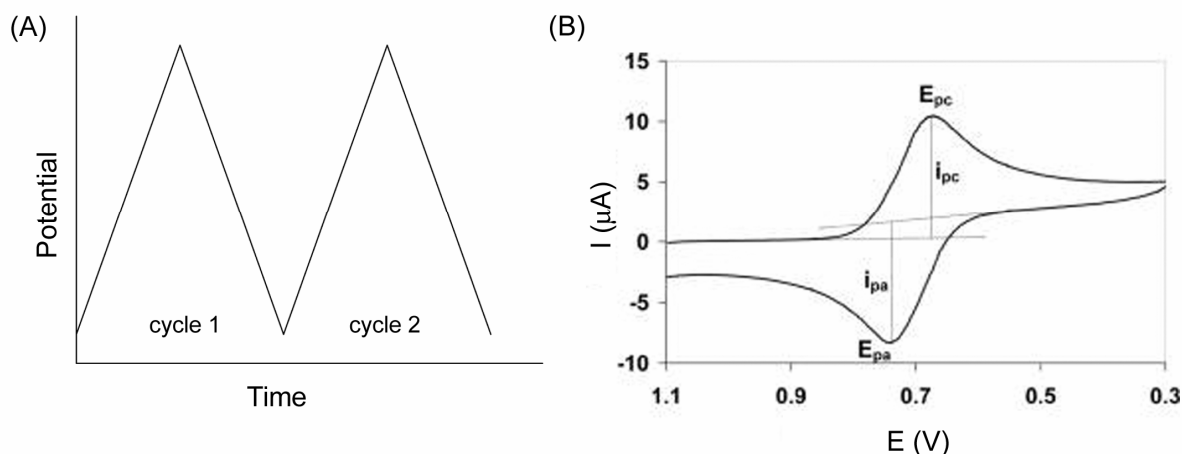


**Figure 2.15** (A) Typical excitation signal used in cyclic voltammetry. (B) An example of a cyclic voltammogram recorded for a reversible one-electron transfer electrochemical process. The characteristic parameters including the anodic and cathodic peak current ( $i_{pa}$ ,  $i_{pc}$ ), the anodic and cathodic peak potential ( $E_{pa}$ ,  $E_{pc}$ ) are labelled in the graph.

#### 2.5.4.3 Atomic force microscopy (AFM)

Atomic force microscopy (AFM) is a powerful technique that can perform surface topography imaging as well as force measurements down to the single molecular level.<sup>157</sup> AFM images are recorded by raster scanning a very sharp tip over the sample surface with a feedback control monitoring the tip-sample interactions. Depending on the characteristics of the sample, different operating modes are employed in AFM imaging. In contact mode AFM, the tip and sample are in continuous contact during scanning. Alternatively, tapping mode AFM works when the tip is in intermittent contact with the sample at certain oscillating amplitude. Tapping mode AFM is particularly useful for imaging the surface of soft materials,

where sample movement or damage can hardly be avoided from contact mode AFM. Based on differences in energy dissipation, tapping mode AFM can also detect material contrast based on their distinctive mechanical properties. Thus, tapping mode AFM is more often applied in studying the surface morphology of polyelectrolyte multilayers and microcapsules.

#### 2.5.4.4 Confocal laser scanning microscopy (CLSM)

The introduction of confocal detection originates from the necessity of improving the contrast and spatial resolution of the conventional microscope. In a confocal system, the signal-to-background ratio is maximized by minimizing the detection volume. As shown in Figure 2.16 of the schematic of a CLSM, a laser beam is coupled into a microscopy objective with a high numerical aperture, which focuses the beam into a diffraction limited spot within the sample. The fluorescence emission from the sample is collected by the same objective and separated from the excitation beam by a dichroic mirror. Finally the collected fluorescence light will be filtered, focused onto a detector pinhole and collected into the photodetector.<sup>158</sup>

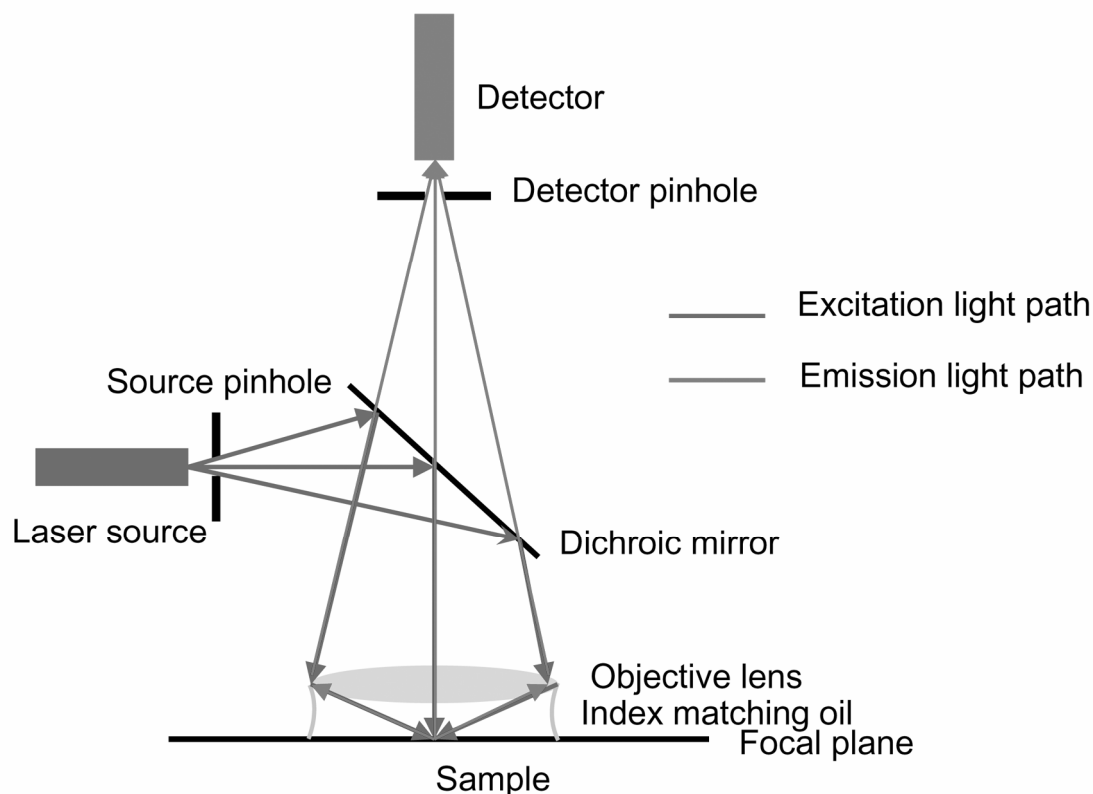


**Figure 2.16** Schematic representation of a confocal laser scanning microscope (CLSM).

Apart from basic fluorescence and transmittance imaging, CLSM can also perform in more complicated applications such as fluorescence recovery after photobleaching (FRAP) and Förster resonance energy transfer (FRET). In FRAP, a laser pulse with a high intensity will locally photobleach the fluorophore, resulting in a dark area within the sample. The still fluorescing species will diffuse throughout the sample and replace the non-fluorescent materials. The rate of this fluorescent recovery will be recorded and correlated to the diffusion

coefficient of the fluorescent molecules. FRET is based on the electromagnetic dipole-dipole interaction between an optically excited donor molecule and an acceptor molecule that is able to efficiently absorb light at wavelengths of the donor emission. Upon changing the distance between the donor and acceptor, both the fluorescence intensities as well as the donor fluorescence life time will be changed. Thus FRET constitutes an important technique to study molecular interactions.<sup>158, 159</sup>

## 2.6 Concluding remarks

The charged nature of polyelectrolytes enables the use of electrostatic interactions to direct their assembly into a large variety of functional structures. On the one hand, the non-selective characteristic of electrostatic forces ensures the incorporation of different functional materials without loss of their specific functions. On the other hand, the dependence of the intrinsic physical properties of polyelectrolytes on solution and environmental conditions provides a broad scope for manipulating the fabrication process.

Polyelectrolyte multilayer thin films can be prepared by the electrostatic layer-by-layer self-assembly technique with controlled thickness and molecular architectures. Applying the same principle of film growth onto colloidal templates, micron- or nano-sized polymeric containers featuring controlled molecular permeability could also be obtained. Numerous application potentials ranging from nanotechnology to biomedical science are envisaged from polyelectrolyte multilayers with various shapes containing different polyelectrolyte species.

Constituting a fundamental broad topic by itself, the formation of polyelectrolyte complexes is closely related to the fabrication and stability of polyelectrolyte multilayers. Unlike self-assembled material systems, polyelectrolyte complexes often lack any particular structural order. However, many complexes containing biomacromolecules such as DNA present special importance in some significant fields of applications.

## 2.7 References and notes

1. (a) Whitesides, G. M.; Mathias, J. P.; Seto, C. T. *Science* **1991**, *254*, 1312; (b) Whitesides, G. M.; Crzybowski, B. *Science* **2002**, *295*, 2418; (c) Barth, J. V.; Costantini, G.; Kern, K. *Nature* **2005**, *437*, 671; (d) Lehn, J. –M. *Perspectives in Supramolecular Chemistry*, Wiley & Sons, **1994**.
2. Kwon, I. C.; Bae, Y. H.; Kim, S. W. *Nature* **1991**, *354*, 291.
3. Faul, C. F. J.; Antonietti, M. *Adv. Mater.* **2003**, *15*, 673.

4. Israelachvili, J. N. *Intermolecular and Surface Forces (2<sup>nd</sup> Ed.)*, Academic Press Limited, London, **1992**.
5. (a) Decher, G. *Science* **1997**, *277*, 1232; (b) Decher, G.; Schlenoff, J. B. (Eds.) *Multilayer Thin Films, Sequential Assembly of Nanocomposite Materials*, Wiley-VCH, Weinheim, Germany, **2003**.
6. (a) Hammond, P. T. *Curr. Opin. Colloid Interface Sci.* **1999**, *4*, 430; (b) Hammond, P. T. *Adv. Mater.* **2004**, *16*, 1271.
7. Bertrand, P.; Jonas, A.; Laschewsky, A.; Legras, R. *Macromol. Rapid Commun.* **2000**, *21*, 319.
8. (a) Schönhoff, M. *Curr. Opin. Colloid Interface Sci.* **2003**, *8*, 86; (b) Schönhoff, M. *J. Phys. Condens. Matter* **2003**, *15*, R1781.
9. Shi, X.; Shen, M. Möhwald, H. *Prog. Polym. Sci.* **2004**, *29*, 987.
10. Cooper, C. L.; Dubin, P. L.; Kayitmazer, A. B.; Turksen, S. *Curr. Opin. Colloid Interface Sci.* **2005**, *10*, 52.
11. Sukhishvili, S. A. *Curr. Opin. Colloid Interface Sci.* **2005**, *10*, 37.
12. Johnston, A. P. R.; Cortez, C.; Angelatos, A. S.; Caruso, F. *Curr. Opin. Colloid Interface Sci.* **2006**, *11*, 203.
13. Jiang, C. Tsukruk, V. V. *Adv. Mater.* **2006**, *18*, 829.
14. Tang, Z.; Wang, Y.; Podsiadlo, P.; Kotov, N. A. *Adv. Mater.* **2006**, *18*, 3203.
15. Ma, Y.; Hempenius, M. A.; Vancso, G. J. *J. Inorg. Organomet. Polym. Mater.* **2007**, *17*, 3.
16. (a) Ferreira, M.; Rubner, M. F. *Macromolecules* **1995**, *28*, 7107; (b) Cheng, J. H.; Fou, A. F.; Rubner, M. F. *Thin Solid Films* **1994**, *244*, 985; (c) Ladam, G.; Gergely C.; Senger, B.; Decher, G.; Voegel, J. C.; Schaaf, P.; Cuisinier, F. J. G. *Biomacromolecules* **2000**, *1*, 674.
17. Hamley, I. W.; Castelletto, V. *Angew. Chem. Int. Ed.* **2007**, *46*, 4442.
18. Putnam, D. *Nat. Mater.* **2006**, *5*, 439.
19. Gray, F. M. *Polymer Electrolytes*, Royal Society of Chemistry, Cambridge, **1997**.
20. Fuoss, R. M. *J. Polym. Sci.* **1948**, *3*, 603.
21. Tanford, C. *Physical Chemistry of Macromolecules*, John Wiley & Sons, Inc. **1967**.
22. (a) Hunter, R. J. *Introduction to Modern Colloid Science*, Oxford University Press, **1993**; (b) Jones, R. A. L. *Soft Condensed Matter*, Oxford University Press, **2002**.
23. Atkins, P.; de Paula, J. *Atkin's Physical Chemistry*, Oxford University Press Inc., New York, **2002**.
24. Chandler, D. *Nature* **2005**, *437*, 640.
25. (a) Kotov, N. A. *NanoStructured Mater.* **1999**, *12*, 789; (b) Dubas, S. T.; Schlenoff, J. B. *Macromolecules* **1999**, *32*, 8153; (c) Lojou, É.; Bianco, P. *Langmuir* **2004**, *20*, 748; (d) K. J.; Hsu, S. L.; McCarthy, T. J. *Langmuir* **2007**, *23*, 3260.

26. Thünemann, A. F.; Müller, M.; Dautzenberg, H.; Joanny, J. -F.; Löwen, H. *Adv. Polym. Sci.* **2004**, *166*, 113.
27. Philipp, B.; Dautzenberg, H.; Linow, K.-J.; Kötz, J.; Dawydoff, W. *Prog. Polym. Sci.* **1989**, *14*, 91.
28. Vijayanathan, V.; Thomas, T.; Thomas, T. J. *Biochemistry* **2002**, *41*, 14085.
29. De Smedt, S. C.; Demeester, J.; Hennink, W. E. *Pharm. Res.* **2000**, *17*, 113.
30. Bloomfield, V. A. *Curr. Opin. Struc. Biol.* **1996**, *6*, 334.
31. Safinya, C. R. *Curr. Opin. Struc. Biol.* **2001**, *11*, 440.
32. (a) Decher, G.; Hong, J.-D. *Macromol. Chem. Macromol. Symp.* **1992**, *46*, 321; (b) Decher, G.; Hong, J.-D.; Schmitt, J. *Thin Solid Films* **1992**, *210-211*, 831.
33. Cheung, J. H.; Stockton, N. B.; Rubner, M. F. *Macromolecules* **1997**, *30*, 2712.
34. Clark, S. L.; Hammond, P. T. *Adv. Mater.* **1998**, *10*, 1515.
35. Lvov, Y.; Decher, G.; Sukhorukov, G. *Macromolecules* **1993**, *26*, 5396.
36. Decher, G.; Lehr, B.; Lowack, K.; Lvov, Y.; Schmitt, J. *Biosens. Bioelectron.* **1994**, *9*, 677.
37. Lvov, Y.; Haas, H.; Decher, G.; Möwald, H.; Michailov, A. *Langmuir* **1994**, *10*, 4232.
38. (a) Lvov, Y.; Ariga, K.; Ichinose, I.; Kunitake, T. *J. Am. Chem. Soc.* **1995**, *117*, 6117; (b) Onda, M.; Lvov, Y.; Ariga, K.; Kunitake, T. *Jpn. J. Appl. Phys.* **1997**, *36*, L1608.
39. Caruso, F.; Niikura, K.; Furlong, D. N.; Okahata, Y. *Langmuir* **1997**, *13*, 3422.
40. Calvo, E. J.; Battaglini, F.; Danilowicz, C.; Wolosiuk, A.; Otero, M. *Faraday Discuss.* **2000**, *116*, 47.
41. Zhu, H.; Ji, J.; Shen, J. *Biomacromolecules* **2004**, *5*, 1933.
42. Johnston, A. P. R.; Read, E. S.; Caruso, F. *Nano Lett.* **2005**, *5*, 953.
43. Kujawa, P.; Moraille, P.; Sanchez, J.; Badia, A.; Winnik, F. M. *J. Am. Chem. Soc.* **2005**, *127*, 9224.
44. (a) Vinogradova, O. I.; Lebedeva, O. V.; Vasilev, K.; Gong, H.; Garcia-Turiel, J.; Kim, B.-S. *Biomacromolecules* **2005**, *6*, 1495; (b) Gong, H.; Garcia-Turiel, J.; Vasilev, K.; Vinogradova, O. I. *Langmuir* **2005**, *21*, 7545.
45. Wang, B.; Anzai, J.-I. *Langmuir* **2007**, *23*, 7378.
46. (a) Hempenius, M. A.; Robins, N. S.; Lammertink, R. G. H.; Vancso, G. J. *Macromol. Rapid Commun.* **2001**, *22*, 30; (b) Hempenius, M. A.; Robins, N. S.; Péter, M.; Kooij, E. S.; Vancso, G. J. *Langmuir* **2002**, *18*, 7629; (c) Hempenius, M. A.; Brito, F. F.; Vancso, G. J. *Macromolecules* **2003**, *36*, 6683; (d) Hempenius, M. A.; Vancso, G. J. *Macromolecules* **2002**, *35*, 2445.
47. (a) Power-Billard, K. N.; Manners, I. *Macromolecules* **2000**, *33*, 26; (b) Ginzburg, M.; Galloro, J.; Jäkle, F.; Power-Billard, K. N.; Yang, S.; Sokolov, I.; Lam, C. N.; Neumann, C. A. W.; Manners, I.; Ozin, G. A. *Langmuir* **2000**, *16*, 9609; (c) Wang, Z.; Lough A.; Manners, I. *Macromolecules* **2002**, *35*, 7669; (d) Halfyard, J.; Galloro, J.; Ginzburg, M.; Wang, Z.; Coombs, N.; Manners, I.; Ozin, G. A. *Chem. Commun.* **2002**, 1746; (e)

- Fleischhaker, F.; Arsenault, A. C.; Wang, Z.; Kitaev, V.; Peiris, F. C.; von Freymann, G.; Manners, I.; Zentel, R.; Ozin, G. A. *Adv. Mater.* **2005**, *17*, 2455.
48. Sukhishvili, S. A.; Kharlampieva, E.; Izumrudov, V. *Macromolecules* **2006**, *39*, 8873.
49. (a) Hsieh, M. C.; Farris, R. J.; McCarthy, T. J. *Macromolecules* **1997**, *30*, 8453; (b) Leväsalmi, J. –M.; McCarthy, T. J. *Macromolecules* **1997**, *30*, 1752; (c) Phuvanartnuruks, V.; McCarthy, T. J. *Macromolecules* **1998**, *31*, 1906.
50. Kotov, N. A.; Magonov, S.; Tropsha, E. *Chem. Mater.* **1998**, *10*, 886.
51. Lvov, Y.; Decher, G.; Möhwald, H. *Langmuir* **1993**, *9*, 481.
52. Saremi, F.; Maassen, E.; Tieke, B. *Langmuir* **1995**, *11*, 1068.
53. Other driving forces, such as hydrogen bonding and hydrophobic interactions have also been successfully utilized to give layer-by-layer thin film structures, in which the application of a charged surface is not necessary.
54. Manners, I. *Adv. Organomet. Chem.* **1995**, *37*, 131.
55. Porter, M. D.; Bright, T. B.; Allara, D. L.; Chidsey, C. E. D. *J. Am. Chem. Soc.* **1987**, *109*, 3559.
56. Yoo, D.; Shiratori, S. S.; Rubner, M. F. *Macromolecules* **1998**, *31*, 4309.
57. Plech, A.; Salditt, T.; Münster, C.; Peisl, J. *J. Colloid Interface Sci.* **2000**, *223*, 74.
58. Yang, H. C.; Aoki, K.; Hong, H.-G.; Sackett, D. D.; Arendt, M. F.; Yau, S.-L.; Bell, C. M.; Mallouk, T. E. *J. Am. Chem. Soc.* **1993**, *115*, 11855.
59. McAloney, R. A.; Sinyor, M.; Dudnik, V.; Goh, M. C. *Langmuir* **2001**, *17*, 6655.
60. Briggs, D.; Seah, M. P. *Practical Surface Analysis*, John Wiley & Sons, New York, **1986**.
61. Andrade, J. D. *Surface and Interfacial Aspects of Biomedical Polymers volume 1: Surface Chemistry and Physics*, Plenum Press, New York, **1985**.
62. Lee, H.; Kepley, L. J.; Hong, H. –G.; Akhter, S.; Mallouk, T. E. *J. Phys. Chem.* **1988**, *92*, 2597.
63. Caruso, F.; Serizawa, T.; Furlong, D. N.; Okahata, Y. *Langmuir* **1995**, *11*, 1546.
64. Sauerbrey, G. *Z. Phys.* **1959**, *155*, 206.
65. Laurent, D.; Schlenoff, J. B. *Langmuir* **1997**, *13*, 1552.
66. (a) Nguyen, M. T.; Diaz, A. F.; Dement'ev, V. V.; Pannell, K. H. *Chem. Mater.* **1993**, *5*, 1389; (b) Pudelski, J. K.; Foucher, D. A.; Honeyman, C. H.; Macdonald, P. M.; Manners, I.; Barlow, S.; O'Hare, D. *Macromolecules* **1996**, *29*, 1894; (c) Arsenault, A. C.; Miguez, H.; Kitaev, V.; Ozin, G. A.; Manners, I. *Adv. Mater.* **2003**, *15*, 503.
67. (a) Foucher, D.; Ziembinski, R.; Petersen, R.; Pudelski, J.; Edwards, M.; Ni, Y.; Massey, J.; Jaeger, C. R.; Vancso, G. J.; Manners, I. *Macromolecules* **1994**, *27*, 3992; (b) Rulkens, R.; Lough, A. J.; Manners, I.; Lovelace, S. R.; Grant, C.; Geiger, W. E. *J. Am. Chem. Soc.* **1996**, *118*, 12683; (c) Péter, M.; Hempenius, M. A.; Kooij, E. S.; Jenkins, T. A.; Roser, S. J.; Knoll, W.; Vancso, G. J. *Langmuir* **2004**, *20*, 891.
68. Lvov, Y.; Decher, G.; Möhwald, H. *Langmuir* **1993**, *9*, 481.

69. Caruso, F.; Furlong, D. N.; Ariga, K.; Ichinose, I.; Kunitake, T. *Langmuir* **1998**, *14*, 4559.
70. Kim, D. K.; Han, S. W.; Kim, C. H.; Hong, J. D.; Kim, K. *Thin Solid Films* **1999**, *350*, 153.
71. Lobo, R. F. M.; Pereira-da-Silva, M. A.; Raposo, M.; Faria, R. M.; Oliveira Jr. O. N. *Nanotechnology* **2003**, *14*, 101.
72. (a) Mendelsohn, J. D.; Barrett, C. J.; Chan, V. V.; Pal, A. J.; Mayes, P. A. M.; Rubner, M. F. *Langmuir* **2000**, *16*, 5017; (b) Zhai, L.; Cebeci, F. Ç.; Cohen, R. E.; Rubner, M. F. *Nano Lett.* **2004**, *4*, 1349.
73. Zhang, X.; Shi, F.; Yu, X.; Liu, H.; Fu, Y.; Wang, Z.; Jiang, L.; Li, X. *J. Am. Chem. Soc.* **2004**, *126*, 3064.
74. Zhang, L.; Chen, H.; Sun, J.; Shen, J. *Chem. Mater.* **2007**, *19*, 948.
75. Dante, S.; Advincula, R.; Frank, C. W.; Stroeve, P. *Langmuir* **1999**, *15*, 193.
76. Pardo-Yissar, V.; Katz, E.; Lioubashevski, O.; Willner, I. *Langmuir* **2001**, *17*, 1110.
77. (a) Advincula, R.; Aust, E.; Meyer, W.; Knoll, W. *Langmuir* **1996**, *12*, 3536; (b) Knoll, W. *Annu. Rev. Phys. Chem.* **1998**, *49*, 569.
78. Kurth, D. G.; Osterhout, R. *Langmuir* **1999**, *15*, 4842.
79. Picart, C.; Lavallo, Ph.; Hubert, P.; Cuisinier, F. J. G.; Decher, G.; Schaaf, P.; Voegel, J.-C. *Langmuir* **2001**, *17*, 7414.
80. Heuberger, R.; Sukhorukov, G. B.; Vörös, J. Textor, M.; Möhwald, H. *Adv. Funct. Mater.* **2005**, *15*, 357.
81. Boulmedais, F.; Tang, C. S.; Keller, B.; Vörös, J. *Adv. Funct. Mater.* **2006**, *16*, 63.
82. Lösche, M.; Schmitt, J.; Decher, G.; Bouwman, W.; Kjaer, K. *Macromolecules* **1998**, *31*, 8893.
83. Schlenoff, J. B.; Dubas, S. T. *Macromolecules* **2001**, *34*, 592.
84. Ladam, G.; Schaad, P.; Voegel, J. C.; Schaaf, P.; Decher, G.; Cuisinier, F. *Langmuir* **2000**, *16*, 1249.
85. Chen, W.; McCarthy, T. J. *Macromolecules* **1997**, *30*, 78.
86. Dubas, S. T.; Schlenoff, J. B. *Macromolecules* **1999**, *32*, 8153.
87. (a) Steitz, R.; Leiner, V.; Siebrecht, R.; v. Klitzing, R. *Colloid Surf. A-Physicochem. Eng. Asp.* **2000**, *163*, 63, (b) Steitz, R.; Jaeger, W.; v. Klitzing, R. *Langmuir* **2001**, *17*, 4471.
88. Ruths, J.; Essler, F.; Decher, G.; Riegler, H. *Langmuir* **2000**, *16*, 8871.
89. Shiratori, S. S.; Rubner, M. F. *Macromolecules* **2000**, *33*, 4213.
90. Rmaile, H. H.; Schlenoff, J. B. *Langmuir* **2002**, *18*, 8263.
91. Dubas, S. T.; Schlenoff, J. B. *Macromolecules* **2001**, *34*, 3736.
92. Kovacevic, D.; van der Burgh, S.; de Keizer, A.; Cohen Stuart, M. A. *Langmuir* **2002**, *18*, 5607.
93. Wang, L.; Schönhoff, M.; Möhwald, H. *J. Phys. Chem. B* **2002**, *106*, 9135.

94. (a) Ibarz, G.; Dähne, L.; Donath, E.; Möhwald, H. *Chem. Mater.* **2002**, *14*, 4059; (b) Köhler, K.; Shchukin, D. G.; Möhwald, H.; Sukhorukov, G. B. *J. Phys. Chem. B* **2005**, *109*, 18250; (c) Leporatti, S.; Gao, C.; Voigt, A.; Donath, E.; Möhwald, H. *Eur. Phys. J. E* **2001**, *5*, 13;
95. (a) Donath, E.; Sukhorukov, G. B.; Caruso, F.; Davis, S. A.; Möhwald, H. *Angew. Chem. Int. Ed.* **1998**, *37*, 2201; (b) Peyratout, C. S.; Dähne, L. *Angew. Chem. Int. Ed.* **2004**, *43*, 3762.
96. Mamedov, A. A.; Kotov, N. A. *Langmuir* **2000**, *16*, 5530.
97. Lutkenhaus, J. L.; Hrabak, K. D.; McEnnis, K.; Hammond, P. T. *J. Am. Chem. Soc.* **2005**, *127*, 17228.
98. Podsiadlo, P.; Liu, Z.; Paterson, D.; Messersmith, P. B.; Kotov, N. A. *Adv. Mater.* **2007**, *19*, 949.
99. (a) Liang, Z.; Susha, A. S.; Yu, A.; Caruso, F. *Adv. Mater.* **2003**, *15*, 1849; (b) Ai, S.; He, Q.; Tao, C.; Zheng, S. Li, J. *Macromol. Rapid Commun.* **2005**, *26*, 1965; (c) Tian, Y.; He, Q.; Cui, Y.; Tao, C.; Li, J. *Chem. Eur. J.* **2006**, *12*, 4808.
100. Ding, B.; Gong, J.; Kim, J.; Shiratori, S. *Nanotechnology* **2005**, *16*, 785.
101. Artyukhin, A. B.; Bakajin, O.; Stroeve, P.; Noy, A. *Langmuir* **2004**, *20*, 1442.
102. Sukhorukov, G. B.; Donath, E.; Moya, S.; Susha, A. S.; Voigt, A.; Hartmann, J.; Möhwald, H. *J. Microencapsul.* **2000**, *17*, 177.
103. Douglas, T.; Young, M. *Nature* **1998**, *393*, 152.
104. Rebek, J. J. *Chem. Soc. Rev.* **1996**, *25*, 255.
105. Discher, D. E.; Eisenberg, A. *Science* **2002**, *297*, 967.
106. Jansen, J. F. G. A.; de Brabander-van den Berg, E. M. M.; Meijer, E. W. *Science* **1994**, *266*, 1226.
107. Dähne, L.; Leporatti, S.; Donath, E.; Möhwald, H. *J. Am. Chem. Soc.* **2001**, *123*, 5431.
108. Voigt, A.; Lichtenfeld, H.; Sukhorukov, G. B.; Zastrow, H.; Donath, E.; Bäumlner, H.; Möhwald, H. *Ind. Eng. Chem. Res.* **1999**, *38*, 4037.
109. Gao, C.; Moya, S.; Donath, E.; Möhwald, H. *Macromol. Chem. Phys.* **2002**, *203*, 953.
110. (a) Caruso, F.; Lichtenfeld, H.; Giersig, M.; Möhwald, H. *J. Am. Chem. Soc.* **1998**, *120*, 8523; (b) Caruso, F.; Caruso, R. A.; Möhwald, H. *Chem. Mater.* **1999**, *11*, 3309; (c) Pastoriza-Santos, I.; Schöler, B.; Caruso, F. *Adv. Funct. Mater.* **2001**, *11*, 122.
111. (a) Antipov, A. A.; Shchukin, D.; Fedutik, Y.; Petrov, A. I.; Sukhorukov, G. B.; Möhwald, H. *Colloid Surf. A-Physicochem. Eng. Asp.* **2003**, *224*, 175; (b) Sukhorukov, G. B.; Volodkin, D. V.; Günther, A. M.; Petrov, A. I.; Shenoy, D. B.; Möhwald, H. *J. Mater. Chem.* **2004**, *14*, 2073.
112. Zhu, H.; Stein, E. W.; Lu, Z.; Lvov, Y. M. McShane, M. J. *Chem. Mater.* **2005**, *17*, 2323.
113. Such, G. K.; Tjijto, E.; Postma, A.; Johnston, A. P. R.; Caruso, F. *Nano Lett.* **2007**, *7*, 1706.



114. Schneider, G.; Decher, G. *Nano Lett.* **2004**, *4*, 1833.
115. Lichtenfeld, H.; Knapschinsky, L.; Sonntag, H.; Shilov, V. *Colloid Surf. A-Physicochem. Eng. Asp.* **1995**, *104*, 313.
116. Dai, Z.; Dähne, L.; Möhwald, H.; Tiersch, B.; *Angew. Chem. Int. Ed.* **2002**, *41*, 4019.
117. Caruso, F.; Lichtenfeld, H.; Donath, E.; Möhwald, H. *Macromolecules* **1999**, *32*, 2317.
118. Caruso, F.; Caruso, R. A.; Möhwald, H. *Science* **1998**, *282*, 1111.
119. Donath, E.; Moya, S.; Neu, B.; Sukhorukov, G. B.; Georgieva, R.; Voigt, A.; Bäuml, H.; Kiesewetter, H.; Möhwald, H. *Chem. Eur. J.* **2002**, *8*, 5481.
120. Dong, W.-F.; Ferri, J. K.; Adalsteinsson, T.; Schönhoff, M.; Sukhorukov, G. B.; Möhwald, H. *Chem. Mater.* **2005**, *17*, 2603.
121. Dong, W.-F.; Sukhorukov, G. B.; Möhwald, H. *Phys. Chem. Chem. Phys.* **2003**, *5*, 3003.
122. Dai, Z.; Dähne, L.; Donath, E.; Möhwald, H. *Langmuir* **2002**, *18*, 4553.
123. (a) Leporatti, S.; Voigt, A.; Mitlöhner, R.; Sukhorukov, G. B.; Donath, E.; Möhwald, H. *Langmuir* **2000**, *16*, 4059; (b) Gao, C.; Leporatti, S.; Donath, E.; Möhwald, H. *J. Phys. Chem. B* **2000**, *104*, 7144.
124. (a) Dubreuil, F.; Elsner, N.; Fery, A. *Eur. Phys. J. E.* **2003**, *12*, 215; (b) Fery, A.; Dubreuil, F.; Möhwald, H. *New J. Phys.* **2004**, *6*, 18.
125. Sukhorukov, G. B.; Brumen, M.; Donath, E.; Möhwald, H. *J. Phys. Chem. B* **1999**, *103*, 6434.
126. Georgieva, R.; Moya, S.; Hin, M.; Mitlöhner, R.; Donath, E.; Kiesewetter, H.; Möhwald, H.; Bäuml, H. *Biomacromolecules* **2002**, *3*, 517.
127. Ibarz, G.; Dähne, L.; Donath, E.; Möhwald, H. *Chem. Mater.* **2002**, *14*, 4059.
128. Glinel, K.; Sukhorukov, G. B.; Möhwald, H.; Khrenov, V.; Tauer, K. *Macromol. Chem. Phys.* **2003**, *204*, 1784.
129. (a) Gao, C.; Leporatti, S.; Moya, S.; Donath, E.; Möhwald, H. *Langmuir* **2001**, *17*, 3491; (b) Gao, C.; Donath, E.; Moya, S.; Dudnik, V.; Möhwald, H. *Eur. Phys. J. E* **2001**, *5*, 21.
130. Köhler, K.; Shchukin, D. G.; Sukhorukov, G. B.; Möhwald, H. *Macromolecules* **2004**, *37*, 9546.
131. Gao, C.; Leporatti, S.; Moya, S.; Donath, E.; Möhwald, H. *Chem. Eur. J.* **2003**, *9*, 915.
132. Dong, W.-F.; Liu, S.; Wan, L.; Mao, G.; Kurth, D. G.; Möhwald, H. *Chem. Mater.* **2005**, *17*, 4992.
133. (a) Gao, C.; Möhwald, H.; Shen, J. *ChemPhysChem* **2004**, *5*, 116; (b) Tong, W.; Dong, W.-F.; Gao, C.; Möhwald, H. *J. Phys. Chem. B* **2005**, *109*, 13159; (c) Köhler, K.; Biesheuvel, P. M.; Weinkamer, R.; Möhwald, H.; Sukhorukov, G. B. *Phys. Rev. Lett.* **2006**, *97*, 188301.
134. (a) Sukhorukov, G. B.; Antipov, A. A.; Voigt, A.; Donath, E.; Möhwald, H. *Macromol. Rapid Commun.* **2001**, *22*, 44; (b) Déjugnat, C.; Sukhorukov, G. B. *Langmuir* **2004**, *20*, 7265; (c) Mauser, T.; Déjugnat, C.; Sukhorukov, G. B. *Macromol. Rapid Commun.* **2004**, *25*, 1781; (d) Antipov, A. A.; Sukhorukov, G. B. *Adv. Colloid Interface Sci.* **2004**,

- 111, 49; (e) Mauser, T.; Déjугnat, C.; Möhwald, H.; Sukhorukov, G. B. *Langmuir* **2006**, *22*, 5888.
135. Ma, Y.; Dong, W.-F.; Hempenius, M. A.; Möhwald, H.; Vancso, G. J. *Nat. Mater.* **2006**, *5*, 724.
136. (a) Radt, B.; Smith, T. A.; Caruso, F. *Adv. Mater.* **2004**, *16*, 2184; (b) Skirtach, A. G.; Déjuginat, C.; Braun, D.; Susha, A. S.; Rogach, A. L.; Parak, W. J.; Möhwald, H.; Sukhorukov, G. B. *Nano Lett.* **2005**, *5*, 1371.
137. Lu, Z.; Prouty, M. D.; Guo, Z.; Golub, V. O.; Kumar, C. S. S. R.; Lvov, Y. M. *Langmuir* **2005**, *21*, 2042.
138. (a) De Geest, B. G.; Skirtach, A. G.; Mamedov, A. A.; Antipov, A. A.; Kotov, N. A.; De Smedt, S. C.; Sukhorukov, G. B. *Small* **2007**, *3*, 804. (b) Skirtach, A. G.; De Geest, B. G.; Mamedov, A.; Antipov, A. A.; Kotov, N. A.; Sukhorukov, G. B. *J. Mater. Chem.* **2007**, *17*, 1050.
139. Constantine, C. A.; Gattás-Asfura, K. M.; Mello, S. V.; Crespo, G.; Rastogi, V.; Cheng, T.-C.; DeFrank, J. J.; Leblanc, R. M. *Langmuir* **2003**, *19*, 9863.
140. Bravo, J.; Zhai, L.; Wu, Z.; Cohen, R. E.; Rubner, M. F. *Langmuir* **2007**, *23*, 7293.
141. (a) DeLongchamp, D. M.; Kastantin, M.; Hammond, P. T. *Chem. Mater.* **2003**, *15*, 1575; (b) DeLongchamp, D. M.; Hammond, P. T. *Adv. Funct. Mater.* **2004**, *14*, 224.
142. Mamedov, A. A.; Kotov, N. A.; Prato, M.; Guldi, D. M.; Wicksted, J. P.; Hirsch, A. *Nat. Mater.* **2002**, *1*, 190.
143. Sun, J.; Sun, Y.; Zou, S.; Zhang, X.; Sun, C.; Wang, Y.; Shen, J. *Macromol. Chem. Phys.* **1999**, *200*, 840.
144. Shchukin, D. G.; Möhwald, H. *Small* **2007**, *3*, 926.
145. Xia, Y.; Whitesides, G. M. *Angew. Chem. Int. Ed.* **1998**, *37*, 550.
146. Hammond, P. T.; Whitesides, G. M. *Macromolecules* **1995**, *28*, 7569.
147. Yang, S. Y.; Rubner, M. F. *J. Am. Chem. Soc.* **2002**, *124*, 2100.
148. Hua, F.; Shi, J.; Lvov, Y.; Cui, T. *Nano Lett.* **2002**, *2*, 1219.
149. Park, J.; Hammond, P. T. *Adv. Mater.* **2004**, *16*, 520.
150. Crespo-Biel, O.; Ravoo, B. J.; Reinhoudt, D. N.; Huskens, J. *J. Mater. Chem.* **2006**, *16*, 3997.
151. (a) Tétreault, N.; Arsenault, A. C.; Mihi, A.; Wong, S.; Kitaev, V.; Manners, I.; Miguez, H.; Ozin, G. A. *Adv. Mater.* **2005**, *17*, 1912. (b) Fleischhaker, F.; Arsenault, A. C.; Kitaev, V.; Peiris, F. C.; von Freymann, G.; Manners, I.; Zentel, R.; Ozin, G. A. *J. Am. Chem. Soc.* **2005**, *127*, 9318.
152. (a) Zhang, J.; Chua, L. S.; Lynn, D. M. *Langmuir* **2004**, *20*, 8015; (b) Jewell, C. M.; Zhang, J.; Fredin, N. J.; Lynn, D. M. *J. Control. Release* **2005**, *106*, 214; (c) Jewell, C. M.; Zhang, J.; Fredin, N. J.; Wolff, M. R.; Hacker, T. A.; Lynn, D. M. *Biomacromolecules* **2006**, *7*, 2483; (d) Wood, K. C.; Chuang, H. F.; Batten, R. D.; Lynn, D. M.; Hammond, P. T. *Proc. Natl. Acad. Sci.* **2006**, *103*, 10207.

153. Shchukin, D. G.; Patel, A. A.; Sukhorukov, G. B.; Lvov, Y. M. *J. Am. Chem. Soc.* **2004**, *126*, 3374.
154. Parganonkar, N.; Lvov, Y. M.; Li, N.; Steenekamp, J. H.; de Villier, M. M. *Pharm. Res.* **2005**, *22*, 826.
155. (a) Tompkins, H. G.; McGahan, W. A. *Spectroscopic Ellipsometry and Reflectometry: A User's Guide*, Wiley, New York, **1999**; (b) Vos, J. G.; Forster, R. J.; Keyes, T. E. *Interfacial Supramolecular Assemblies*, Wiley, England, **2003**.
156. (a) Finklea, H. O. *Electroanalytical chemistry*; Bard, A. J.; Rubinstein, I. (Ed.) Marcel Dekker, Inc. New York, **1996**; (b) Monk, P. *Fundamentals of Electroanalytical Chemistry*, John Wiley & Sons Ltd, **2001**; (c) Wang, J. *Analytical Electrochemistry (3<sup>rd</sup> Ed.)*, Wiley-VCH, New Jersey, **2007**.
157. (a) Binning, G.; Quate, C. F. Gerber, C. *Phys. Rev. Lett.* **1986**, *56*, 930; (b) Hugel, T.; Seitz, M. *Macromol. Rapid Commun.* **2001**, *22*, 989.
158. Böhmer, M.; Enderlein, J. *ChemPhysChem* **2003**, *4*, 792.
159. Caruso, F.; Donath, E.; Möhwald, H. *J. Phys. Chem. B.* **1998**, *102*, 2011.



# Chapter 3

## Synthesis and Redox Properties of Water Soluble Poly(ferrocenylsilanes)\*

*In this chapter the synthesis and redox chemistry of water soluble poly(ferrocenylsilane) strong polyelectrolytes are described. Poly(ferrocenylsilane) polyions and fluorescence labelled polycations were obtained from side group modifications on the precursor polymer poly(ferrocenyl(3-chloropropyl)methylsilane) synthesized with controlled molar mass in the presence of  $\text{Et}_3\text{SiH}$ . UV/Vis spectroscopy confirmed that poly(ferrocenylsilane) polyelectrolytes could be effectively oxidized by ferric chloride ( $\text{FeCl}_3$ ) and potassium ferricyanide ( $\text{K}_3\text{Fe}(\text{CN})_6$ ). Subsequent complete reduction of the oxidized water-soluble polymers was achieved using ascorbic acid (vitamin C) or dithiothreitol (DTT).*

### 3.1 Introduction

The multidisciplinary broadening of materials science could greatly benefit from the design and synthesis of new functional materials. Macromolecules containing inorganic elements or organometallic units have attracted growing attention since they may combine novel optical, electrical, magnetic and chemical characteristics with the processability of polymers.<sup>1, 2</sup> Poly(ferrocenylsilanes) (PFS), composed of alternating ferrocene and silane units in the polymer main chain, belong to this class of materials. Oligomers of PFS with degrees of polymerization up to 10 were first obtained by Rosenberg in a condensation polymerization.<sup>3</sup> The real breakthrough in the synthetic chemistry of PFS has been realized by the group of Manners in the early 1990s, when PFS was first synthesized in a true polymeric form through the thermal ring-opening polymerization (ROP) of silicon bridged ferrocenophanes.<sup>4</sup> Later on, living anionic and transition metal-catalyzed polymerization methodologies have also been established, giving access to well defined, monodisperse poly(ferrocenylsilane) homo- and block copolymers.<sup>5, 6</sup>

The distinctive structural features of poly(ferrocenylsilanes) come from the silicon and iron atoms in the main chain, which make them valuable in the development of surface nano- and microstructuring strategies.<sup>7</sup> PFS were found to be effective resists in reactive ion etching

---

\* Part of the work described in this Chapter has been published: Giannotti, M. I.; Lv, H.; Ma, Y.; Steenvoorden, M. P.; Overweg, A. R.; Roerdink, M.; Hempenius, M. A.; Vancso, G. J. *J. Inorg. Organom. Polym. Mater.* **2005**, *15*, 527.

processes due to the formation of an etch resistant iron/silicon oxide layer.<sup>8</sup> This resulted in the surface patterning applications of PFS using soft lithographic techniques as well as block copolymer lithography.<sup>9, 10</sup> Phase separated PFS block copolymer thin films were also reported to be catalytically active for the synthesis of carbon nanotubes.<sup>11</sup> One particularly important property of PFS is their unique redox-activity. Oxidation and reduction of PFS can be performed by chemical reactions,<sup>12</sup> where the extent and reversibility of oxidation were only reported recently.<sup>13</sup> Alternatively, the oxidation and reduction process of PFS is more precisely controlled using electrochemistry.<sup>14</sup> Oxidation of iron centers in PFS changes its electrical, optical and physical properties. Previous studies on self-assembled end-functionalized PFS monolayers on gold revealed electrochemically induced morphology and volume/thickness changes.<sup>15</sup> Atomic force microscopy (AFM) based single molecule force spectroscopy (SMFS) measurements on poly(ferrocenylsilane) single chains showed a significantly increased Kuhn length and segment elasticity after oxidation, demonstrating a redox-induced changes of the torsional potential energy landscape.<sup>16</sup>

With their significant industrial and commercial value in bio-related and medical applications, water-soluble polymers are becoming increasingly important in recent years. Although water-soluble organic macromolecules have been widely studied, their inorganic and organometallic counterparts are largely unexplored.<sup>2</sup> The macromolecular properties of poly(ferrocenylsilane) depend, to a large extent, on the substituents on silicon. Along with other characteristics, such as the crystallinity<sup>17</sup> and glass transition temperature<sup>6</sup>, the solubility of PFS<sup>18-23</sup> can be tuned by varying the size and type of the substituents. Modification of the polymer side groups has been shown to give access to water-soluble PFS.<sup>19-23</sup> Homopolymers of water-soluble PFS have potential uses as electrode modifiers and redox-active polymeric electrolytes. These materials may also be useful in redox-controlled drug delivery applications since various water-soluble ferrocenium salts have been shown to display anti-cancer activity.<sup>24</sup> The most interesting aspect of the processabilities of PFS polyelectrolytes is the use of ionic interactions to deposit these polymers onto substrates by the so-called electrostatic layer-by-layer technique.<sup>25</sup> Water-soluble block copolymers with a poly(ferrocenylsilane) polyelectrolyte block, on the other hand, can self-assemble in aqueous media and the resulting micellar and vesicular aggregates may demonstrate redox-tunable encapsulation properties and emulsifying abilities for heterogeneous catalysis.<sup>26</sup>

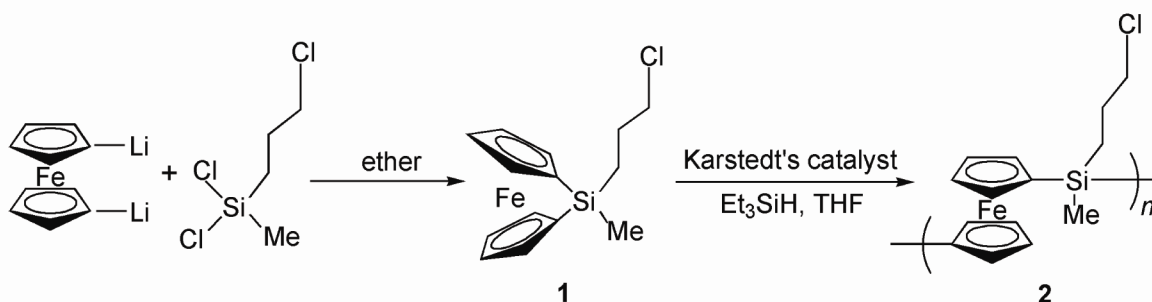
In this Chapter, the synthesis and redox chemistry of water soluble poly(ferrocenylsilane) strong polyelectrolytes are described. PFS polyions are often synthesized through the ring-opening polymerization (ROP) of a silicon-bridged ferrocenophane followed by side-group modifications. A recent development in transition metal catalyzed ring-opening polymerization (ROP) of silicon bridged ferrocenophane offers facile polymer molar mass control by the use of Et<sub>3</sub>SiH in the polymerization process.<sup>27</sup> Applying the same methodology to polymerize the precursor polymer followed by side group modification, poly(ferrocenylsilane) polyelectrolytes and rhodamine labelled polycations with

controlled molar masses are synthesized. The water solubility of these poly(ferrocenylsilane) polyelectrolytes necessitates the use of water soluble oxidants and reducing agents. In the second part of this Chapter the discovery of several effective water soluble poly(ferrocenylsilane) redox agents is described. Moreover, the solubility and stability of oxidized poly(ferrocenylsilane) polyions are also discussed.

### 3.2 Synthesis and characterization of poly(ferrocenylsilane) polyelectrolytes with molar mass control

Water soluble poly(ferrocenylsilane) polyelectrolytes were synthesized by side-group modification of a precursor polymer.<sup>19-23</sup> The starting silaferrocenophane monomers (Scheme 3.1)<sup>19, 20</sup> are obtained from the reaction of 1,1'-dilithioferrocene with a dichloroorganosilane ( $RR'SiCl_2$ ), in the presence of the complexing agent tetramethylethylenediamine, TMEDA, which promotes the formation of 1,1'-dilithioferrocene.<sup>2</sup> The corresponding high molar mass polymers are readily accessible by thermal<sup>4</sup> and transition metal catalyzed ROP.<sup>5</sup> Transition metal catalyzed ROP is a relatively mild method since it occurs in solution and at ambient temperature. Many functionalities (such as polar or ionic moieties) do not tolerate the highly basic dilithioferrocene or the reactive chlorosilanes, are incompatible with the reactive strained monomer itself, or hinder monomer purification. Thus, the synthetic route leading to poly(ferrocenylsilane) polyelectrolytes often necessitates a side-group modification step after polymerization.<sup>22</sup>

The precursor polymer poly(ferrocenyl(3-chloropropyl)methylsilane) **2** was prepared through the transition metal catalyzed ROP (Scheme 3.1) in the presence of triethylsilane ( $Et_3SiH$ ). It has been reported that varying amounts of  $Et_3SiH$  allow the polymerization of [1]dimethylsilaferrocenophane with molecular weight control over a range of  $2.0 \times 10^3 < M_n < 4.5 \times 10^4$  g/mol with PDI values in the range of 1.1–2.3.<sup>27</sup> A mechanistic consideration suggested that oxidative addition of the Si-H group of the silane at the catalytic center competes with that of the strained Si-C bond in the ferrocenophane monomer.<sup>27</sup>



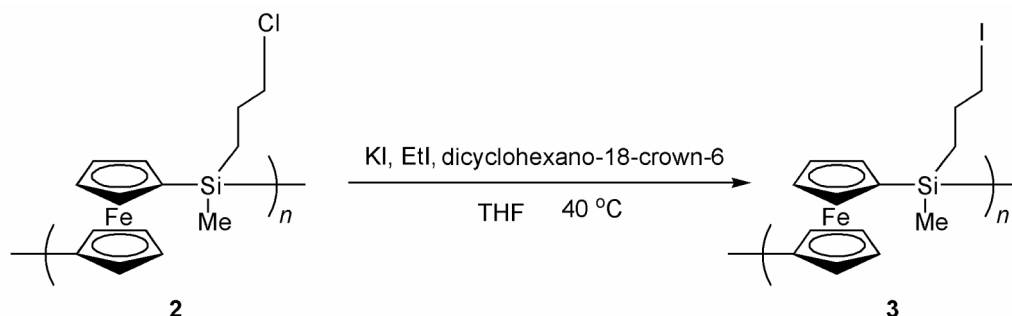
**Scheme 3.1** Synthesis of poly(ferrocenyl(3-chloropropyl)methylsilane) with molar mass control.

The molecular characteristics of precursor polymers obtained with varying molar ratios of silane : monomer measured by gel permeation chromatography (GPC) are summarized in Table 3.1. The molar mass of **2** prepared in the presence of  $\text{Et}_3\text{SiH}$  does show a difference from that of the same polymer synthesized in the absence of silane ( $M_w \sim 3.11 \times 10^5$ ).<sup>23</sup> But the degree of molar mass control is very limited since similar results were obtained with varying the molar ratio of  $\text{Et}_3\text{SiH}$  : monomer from 1:50 to 1:150. This can be explained by the difference in reactivity of the Si-C bond of the ferrocenophane monomer with varying substituents on silicon when reacting with the Si-H group of the silane.<sup>28</sup>

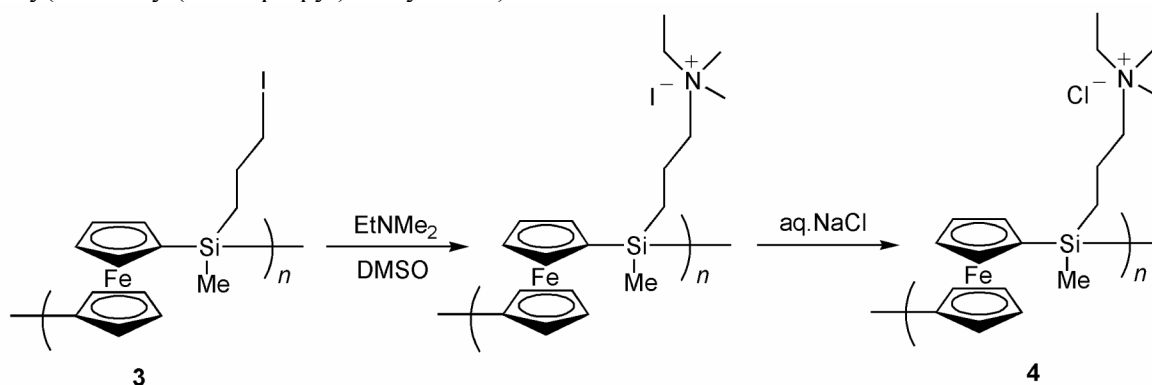
**Table 3.1** Molecular characteristics (by GPC) of poly(ferrocenyl(3-chloropropyl)methylsilane) synthesized in the presence of  $\text{Et}_3\text{SiH}$ .

$\text{Et}_3\text{SiH}$ : monomer (molar ratio)	$M_n$ (g/mol)	$M_w$ (g/mol)	$M_w/M_n$
1:50	$1.36 \times 10^4$	$3.13 \times 10^4$	2.30
1:100	$1.43 \times 10^4$	$3.53 \times 10^4$	2.48
1:150	$1.65 \times 10^4$	$3.84 \times 10^4$	2.33

Poly(ferrocenyl(3-chloropropyl)methylsilane) **2** was quantitatively transferred in a halogen exchange reaction to poly(ferrocenyl(3-iodopropyl)methylsilane) **3** (Scheme 3.2). Subsequent nucleophilic substitution reactions give access to poly(ferrocenylsilane) polycation **4** (Scheme 3.3) and polyanion **5** (Scheme 3.4).<sup>23</sup>

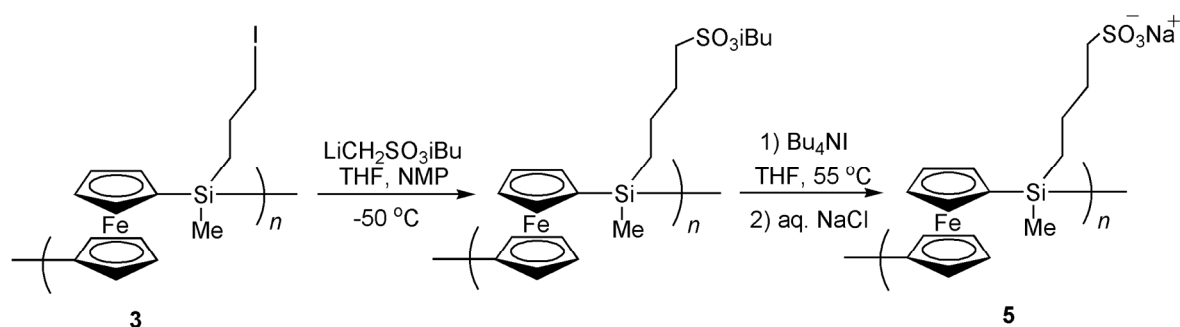


**Scheme 3.2** Halogen exchange to transform poly(ferrocenyl(3-chloropropyl)methylsilane) into poly(ferrocenyl(3-iodopropyl)methylsilane).



**Scheme 3.3** Synthesis of poly(ferrocenylsilane) polycation **4**.





**Scheme 3.4** Synthesis of poly(ferrocenylsilane) polyanion **5**.

Viscometry measurements on PFS polycation **4** were performed in water, with the ionic strength tuned by NaCl (0.02 M). A starting solution of the polymer with a concentration of 3 mg/mL was diluted several times and the viscosity of the solution was recorded. In Figure 3.1 the reduced viscosity,  $\eta_{sp}/c$  (specific viscosity over concentration), is plotted against polymer concentration  $c$ , showing the typical behaviour of polyelectrolyte solutions, *i.e.* a strong increase of the reduced viscosity with decreasing polymer concentration.<sup>29</sup>

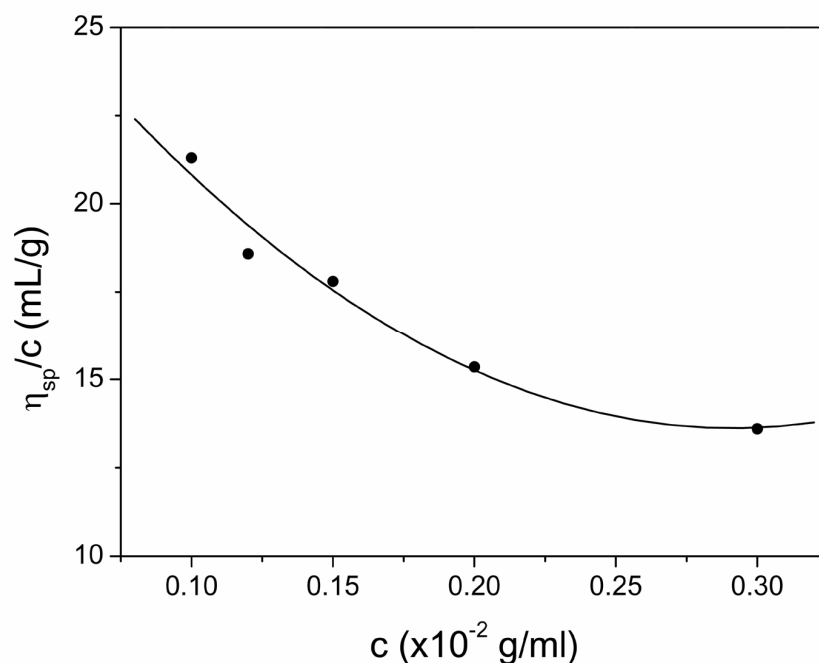
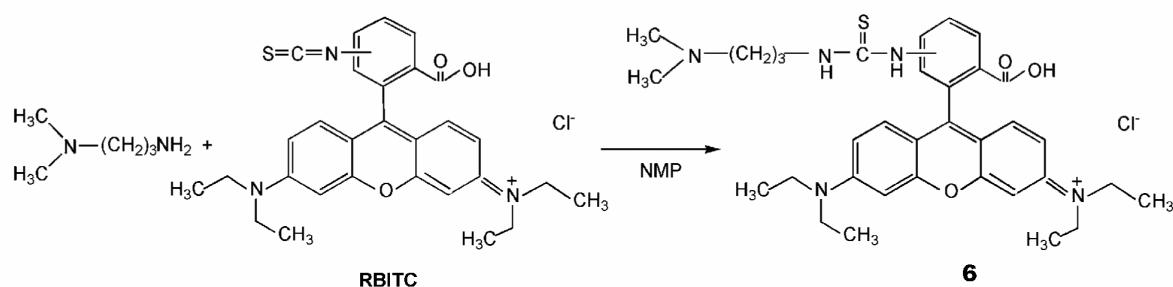


**Figure 3.1** Reduced viscosity ( $\eta_{sp}/c$ ) as a function of the concentration ( $c$ ) of PFS polycation **4** in 0.02 M NaCl solution.

### 3.3 Fluorescence labelled poly(ferrocenylsilane) polycation

In order to facilitate the characterization of poly(ferrocenylsilane) assemblies at later stages, fluorescence labelled poly(ferrocenylsilane) polycations were synthesized. Commercially available rhodamine B isothiocyanate (RBITC) was chosen as the fluorescence

tag. RBITC was first linked to 3-(dimethylamino)-1-propylamine to yield fluorescence labelled amine **6** according to the reaction described in Scheme 3.5. Following the procedure as shown in Scheme 3.3 but adding amine **6** to the Me<sub>2</sub>NEt, rhodamine-labelled poly(ferrocenylsilane) polycation (RBITC-PFS) was obtained.



UV/Vis spectroscopy provided evidence of RBITC incorporation. In addition to typical PFS absorption bands, the UV/Vis spectrum (Figure 3.2) of RBITC-PFS in water (2 mg/mL) showed a new absorption shoulder at 554 nm. This new band has been ascribed to the rhodamine fluorescence tag on the polymer, which was lightly shifted from the original absorption of RBITC (540 nm). From the spectrum, the rhodamine labelled PFS repeating units were estimated to be 1-2%.

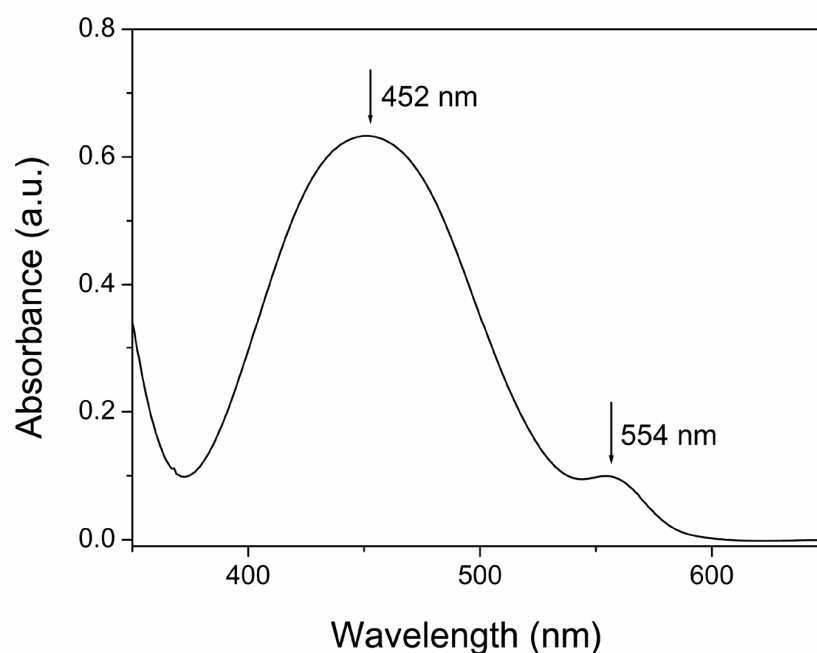


**Figure 3.2** UV/Vis spectrum of PFS-RBITC. The characteristic band at 452 nm belongs to PFS, while the shoulder at 554 nm is ascribed to the rhodamine fluorescence tag on the polymer.

The fluorescent excitation and emission spectra of RBITC-PFS was recorded by a spectrofluorometer (Figure 3.3).

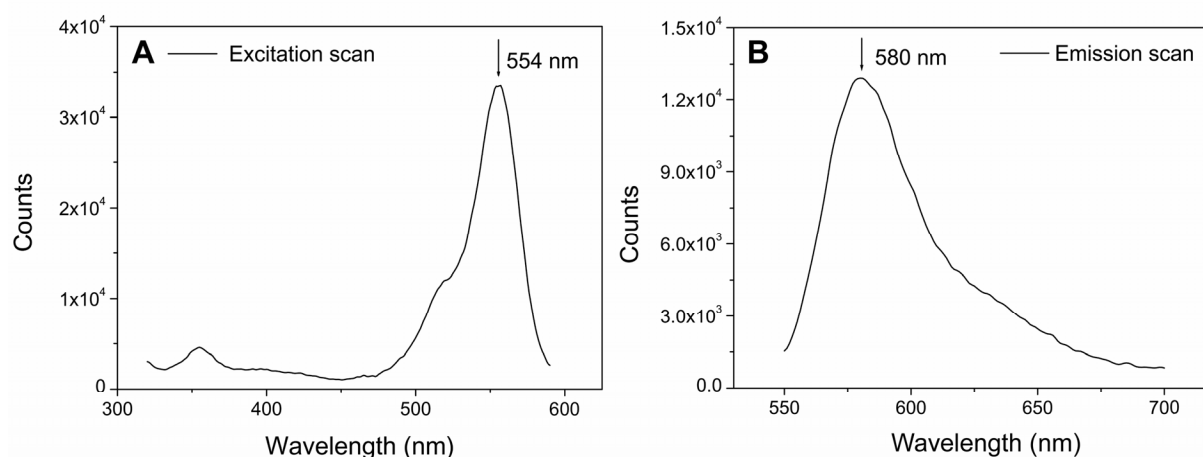


**Figure 3.3** (A) Fluorescence excitation scan of RBITC-PFS aqueous solution. (B) Fluorescence emission scan of RBITC-PFS aqueous solution.

The emission scan showed an emission peak at 580 nm. Comparing to the original RBITC emission wavelength of 573 nm, there was a slight change in the fluorescent characteristics of the dye molecules after coupling to PFS. An additional synchronous scan confirmed RBITC to be the only fluorescent active component of the compound (data not shown).

### 3.4 Redox chemistry of water soluble poly(ferrocenylsilanes)

Ferrocene (Fc) groups are redox-active. Due to the ferrocene containing backbone, PFS belongs to the class of stimuli-responsive polymers.<sup>30</sup> Many attempts to reversibly oxidize and reduce PFS by chemical<sup>12, 13</sup> as well as electrochemical<sup>14, 15</sup> methods have already been reported. PFS polyelectrolytes have potential applications as electrode materials and redox-active polymeric electrolytes for which the ionic conductivity could be tuned by oxidation and reduction of the ferrocene units.<sup>24</sup> Although effective chemical oxidation and reducing agents for PFS in organic solvents (such as hexane, dichloromethane, THF, and toluene) have been relatively well-recognized, the identification of good water-soluble oxidizing and reducing agents is still to be explored.

#### 3.4.1 Water-soluble oxidants

In our first attempt, FeCl<sub>3</sub> was chosen due to its effectiveness in oxidizing PFS in organic solvents. However, it easily hydrolyzes in aqueous medium when the pH value is higher than 7. The oxidation tests were carried out by dissolving FeCl<sub>3</sub> in MilliQ water containing a low concentration of hydrochloric acid (10<sup>-5</sup> - 10<sup>-4</sup> M). When mixed with the FeCl<sub>3</sub> solution, the clear PFS polycation solution showed an almost instantaneous colour

change from yellow–orange to green–blue, indicating oxidation. This process was followed by UV/Vis spectroscopy. As can be seen in Figure 3.4A, the PFS polycation has a characteristic visible *d-d* band absorbance at  $\lambda = 447$  nm.<sup>31</sup> After oxidation, a new peak at  $\lambda = 637$  nm (Figure 3.4A) appeared due to the ferrocenium centers developed.<sup>32</sup>

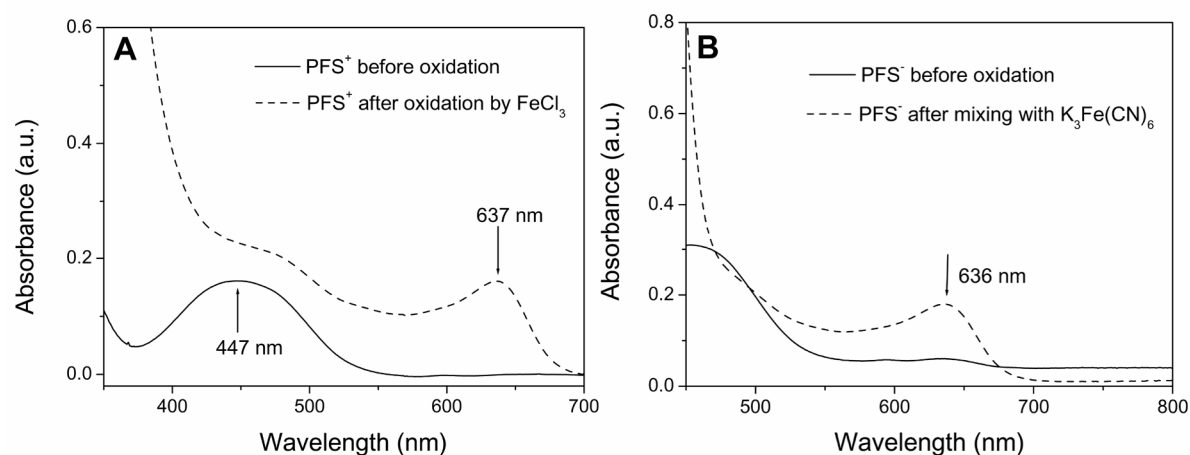


**Figure 3.4** UV/Vis spectra of aqueous solutions of (A) PFS polycation **4** before and after oxidation with  $\text{FeCl}_3$  and (B) PFS polyanion **5** before and after oxidation with  $\text{K}_3\text{Fe}(\text{CN})_6$ .

Polyions **4** and **5** studied here are both strong polyelectrolytes, *i.e.* their charge densities do not depend on solution pH. However, the linear charge density does depend on the oxidation state of the PFS polymer. The same degree of change in the oxidation state of the polymer backbone is expected to have exactly opposite effects on the solubility of the polycation and polyanion. In the case of a PFS polycation, oxidation will introduce additional positive charges on the polymer main chain, thus increasing the overall positive charge density of the polycation species. This will most probably result in a better water solubility of the cationic PFS polyelectrolytes. On the contrary, decreased overall charge density and solubility in water are expected for oxidized PFS polyanions. Moreover, experimental observations show that the solubility of PFS polyelectrolytes in the neutral state does also depend on the size and nature of the counter ions presented in the aqueous media. Large or multi-valent counter ions tend to induce decreased water solubility of the polyions. When the same  $\text{FeCl}_3$  solutions were used to oxidize PFS polyanion, some green precipitants immediately appeared in the reaction mixture, indicating a combination of oxidation and counter-ion induced solubility change of the polymer.

In order to further test the counter ion effects, potassium hexacyanoferrate ( $\text{K}_3\text{Fe}(\text{CN})_6$ ) was used to oxidize the PFS polycation **4** and polyanion **5**, respectively. As expected, the addition of the multi-valent counter anion  $\text{Fe}(\text{CN})_6^{3-}$  induced an immediate precipitation of the polycations, with a slight colour change from yellow to light-green. When the polyanions were oxidized by  $\text{K}_3\text{Fe}(\text{CN})_6$ , the solution remained transparent even after the colour change to green. The effective oxidation was again confirmed by UV/Vis spectra (Figure 3.4B). The absence of an apparent solubility decrease of the oxidized polyanion even after storage also

indicates that potassium ferricyanide is a rather mild oxidant for PFS. This implies incomplete oxidation of PFS polyelectrolytes could be achieved using  $K_3Fe(CN)_6$ .

Based on previous studies, iodine ( $I_2$ ) is also an oxidant for PFS.<sup>12, 13, 33</sup> It was not possible to follow the reaction by UV/Vis spectroscopy because of the rather broad absorbance band of  $I_2$  in the region of  $\lambda = 420\text{--}600$  nm. However,  $^{57}Fe$  Mössbauer spectroscopy has demonstrated  $I_2$ -doped poly(ferrocenylmethylphenylsilane) to be a mixed valence compound with an extent of oxidation  $\leq 86\%$ .<sup>13</sup>

### 3.4.2 Viscosity behaviour of oxidized poly(ferrocenylsilane) polyions

Viscometry measurements on oxidized PFS polycation **4** were again performed in water containing 0.02 M NaCl to test for possible chain scission. A starting aqueous solution of polycation **4** (1 mg/mL) was mixed with  $FeCl_3$  in an eq  $FeCl_3$ /eq ferrocene (FC) ratio equal to 1. Then the viscosity of the aqueous solution of the partially oxidized PFS studied here was monitored with time. As shown in Figure 3.5, the viscosity of the solution slowly decreases with time. This is probably due to a slow polymer chain cleavage process by the nucleophilic attack at the ferrocenium sites following the initial rapid (partial) oxidation.<sup>34</sup>

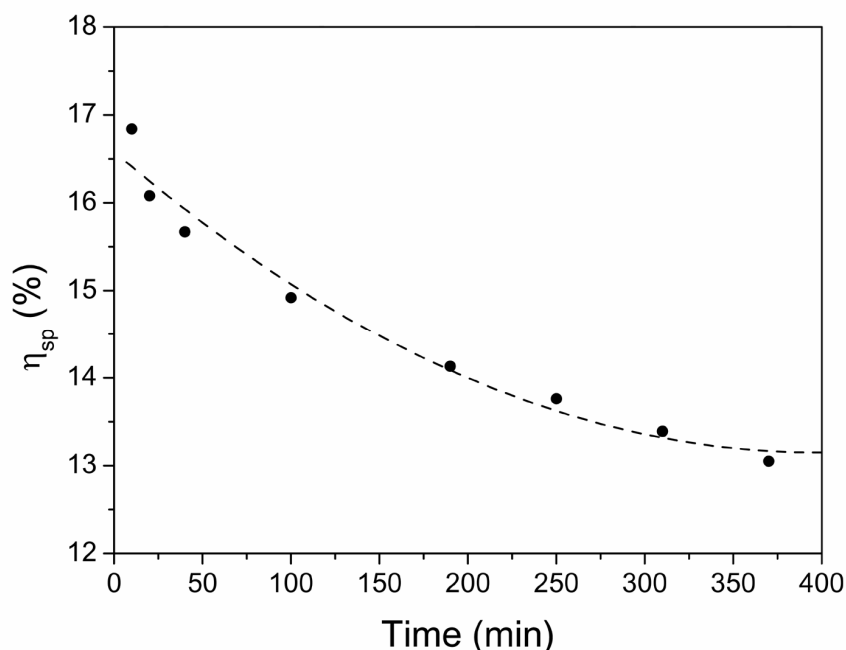


**Figure 3.5** Specific viscosity ( $\eta_{sp}$ ) of  $FeCl_3$ -oxidized PFS polycation **4** dependence on time.

### 3.4.3 Water-soluble reducing agents

In order to convert the oxidized water-soluble species back to their original neutral form, various reducing agents were examined. The  $FeCl_3$  oxidized PFS polycation **4** was found to be successfully reduced with water-soluble ascorbic acid (vitamin C). Colour change from green-blue to yellow–orange took place immediately upon introducing the reducing

agent solution, as shown in Figure 3.6, giving evidence of the high speed of the reduction reaction. The PFS polycation showed redox-reversibility with the re-appearance of the characteristic ferrocene absorption at  $\lambda = 447$  nm. Dithiothreitol (DTT) and hydrazine ( $\text{N}_2\text{H}_2$ ) were also tested as reducing agents for this water-soluble oxidized PFS. While DTT induced also a similar characteristic colour change from green–blue to yellow–orange, the commonly used ferrocenium reducing agent hydrazine led to the formation of some orange precipitate in the aqueous medium.

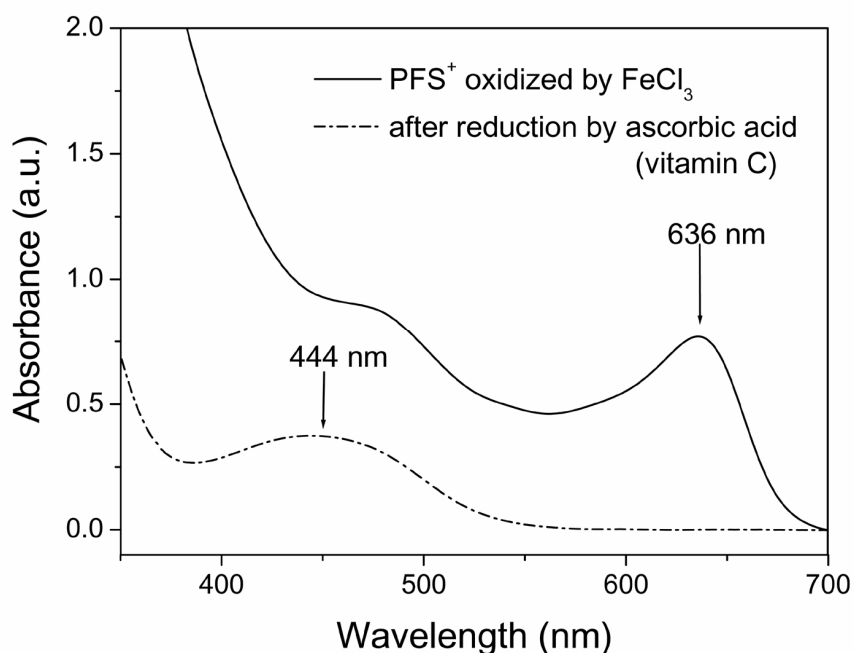


**Figure 3.6** UV/Vis spectra of oxidized PFS polycation aqueous solutions before and after reduction using ascorbic acid (vitamin C).

### 3.5 Conclusions

Water-soluble poly(ferrocenylsilane) strong polyelectrolytes were obtained through side group modifications of poly(ferrocenyl(3-halopropyl)methylsilanes) with controlled molar mass. In a similar way, rhodamine labelled poly(ferrocenylsilane) polycations containing 1-2% fluorescence labelled repeating units were also successfully synthesized. The redox chemistry of these organometallic polyelectrolytes showed full reversibility. Viscosity measurements on oxidized poly(ferrocenylsilane) polyelectrolytes demonstrated a slow polymer degradation with time.

### 3.6 Experimental

**(3-Chloropropyl)methylsilaferrrocenophane 1** A mixture of ferrocene (20.0 g, 0.108 mol), TMEDA (15.0 g, 0.129 mol) and BuLi (148 mL, 0.24 mol) in heptane (250 mL) was stirred under argon for 48 h. The heptane was removed and after several heptane washing/removal steps, dilithioferrocene was stirred in dry diethyl ether (300 mL) and cooled to  $-60\text{ }^{\circ}\text{C}$ . Dichloro(3-chloropropyl)methylsilane (22.65 g, 0.118 mol) was added with dry ether (30 mL) and the mixture was stirred for 16~18 h. The product (as an orange-red solid) was vacuum sublimed and further purified by recrystallization and transferred into the glovebox. Yield 16.3 g (0.054 mol, 50%).

**Poly(ferrocenyl(3-chloropropyl)methylsilane) 2** In a glovebox under purified  $\text{N}_2$ , Karstedt's catalyst ( $\text{C}_8\text{H}_{18}\text{OPtSi}_2$ , 0.1 mL,  $\sim 1$  mol%) was added to a solution of (3-chloropropyl)methylsilaferrrocenophane (300 mg, 1 mmol) and  $\text{Et}_3\text{SiH}$  ( $\sim 3\text{ }\mu\text{L}$ , molar ratio of monomer :  $\text{Et}_3\text{SiH} = 1 : 50$ ) in dry THF (3 mL), and stirring was continued for 24 h. Precipitation in methanol afforded poly(ferrocenyl(3-chloropropyl)methylsilane) as an orange solid. Yield 0.274 g (92 %).

**Poly(ferrocenyl(3-iodopropyl)methylsilane) 3** A solution of poly(ferrocenyl(3-chloropropyl)methylsilane) (2.83 g, 9.29 mmol repeat units), dicyclohexano-18-crown-6 (0.92 g, 2.40 mmol), KI (1.16 g, 7.07 mmol), and iodoethane (15 mL, 190 mmol) was stirred at  $40^{\circ}\text{C}$  for a week. The polymer was precipitated in MeOH, dried, and stirred with the same reagents for another few days at  $40^{\circ}\text{C}$ . Iodoethane was added during the reaction every few days to complete the halogen exchange. Precipitation in MeOH gave poly(ferrocenyl(3-iodopropyl)methylsilane) as an orange solid. Yield 3.45 g (93 %).  $^1\text{H NMR}$  ( $\text{CDCl}_3$ ):  $\delta$ 0.46 ( $\text{SiCH}_3$ , s, 3H); 1.00 (1- $\text{CH}_2$ , m, 2H); 1.87 (2- $\text{CH}_2$ , m, 2H); 3.22 (3- $\text{CH}_2$ , m, 2H); 3.99 + 4.23 (Cp, m, 8H).  $M_n = 2.68 \times 10^4$  g/mol,  $M_w = 5.59 \times 10^4$  g/mol,  $M_w/M_n = 2.09$ .

**Poly(ferrocenylsilane) polycation 4** Poly(ferrocenyl(3-iodopropyl)methylsilane) (1.0 g, 2.6 mmol r.u.) was dissolved in THF (18 mL), and  $\text{Me}_2\text{NEt}$  (5 mL, 46 mmol) and DMSO (9 mL) were added. The polymer had precipitated within 18 h. THF was evaporated; DMSO (6 mL) and  $\text{Me}_2\text{NEt}$  (4 mL, 36 mmol) were added. The product in DMSO (15 mL) was transferred to a Spectra/Por 4 dialysis hose and dialyzed against MilliQ water (1.6 L), 0.1 M NaCl (3 x 1.6 L), and then against MilliQ. Concentration of the salt-free polyelectrolyte solution by a flow of  $\text{N}_2$  produced polycation 4 as orange-brown flakes. Yield 0.87 g (91%). Based on the molar mass of 3 and excluding any chain scission or cross-linking reactions, the molar mass of polycation 4 was calculated as  $M_w = 5.3 \times 10^4$  g/mol.

**Poly(ferrocenylsilane) polyanion 5** A solution of isobutyl methanesulfonate (1.75 g, 11.5 mmol) in dry THF (12.5 mL) was cooled under argon to  $-80\text{ }^{\circ}\text{C}$ , and *n*-BuLi (5.0 mL, 8 mmol) was added dropwise. After stirring for 20 min, a solution of poly(ferrocenyl(3-iodopropyl)methylsilane) (1 g, 2.5 mmol r.u.) in a solvent mixture of THF (9 mL) and NMP (4 mL) was added dropwise. Stirring was continued at  $-50\text{ }^{\circ}\text{C}$  for 5 h. The reaction was

terminated at  $-50\text{ }^{\circ}\text{C}$  by adding MeOH (0.5 mL). Precipitation in MeOH (150 mL) gave PFS-SO<sub>3</sub>R as an orange solid. PFS-SO<sub>3</sub>R (0.80 g, 1.83 mmol) was stirred with NBu<sub>4</sub>I (2.15 g, 5.85 mmol) in THF (60 mL) at  $55\text{ }^{\circ}\text{C}$  for overnight. By then, the polymer was precipitated. THF was evaporated, MeOH (60 mL) and NBu<sub>4</sub>I (2.15 g, 5.85 mmol) were added, and stirring was continued for 2 weeks. The solution was dialyzed using a Spectra/Por 4 dialysis hose ( $M_w$  cut-off 3000 g/mol) against MeOH/MilliQ (2 x 500/1000 mL) to remove NBu<sub>4</sub>I. Further dialysis was performed against 0.1 M NaCl (3 x 1.6 L) and MilliQ (3 x 1.6 L). Evaporation of MilliQ with a flow of N<sub>2</sub> gave polyanion **3** as amber flakes. Yield 0.726 g (98%). Based on the molar mass of **3** and excluding any chain scission or cross-linking reactions, the molar mass of polyanion **5** was calculated as  $M_w = 5.2 \times 10^4$  g/mol.

**Rhodamine labelled poly(ferrocenylsilane) polycations RBITC-PFS** A solution of RBITC (100 mg, 0.19 mmol) and 3-(dimethylamino)-1-propylamine (0.3 mL, 2.4 mmol) in NMP (2.5 mL) was stirred in the dark in the glovebox for a week. Precipitation and washing in diethyl ether and heptane gave a quantitative yield of RBITC-amine compound **6** as purple powder. Polymer **3** (300 mg, 0.87 mmol r.u.) was dissolved in THF (6 mL), and Me<sub>2</sub>NEt (2 mL, 18.4 mmol) and DMSO (3 mL) were added. The polymer had precipitated within 18h. THF was evaporated; DMSO (2 mL), Me<sub>2</sub>NEt (1.2 mL, 10 mmol) and RBITC-amine compound **6** (50 mg, 0.08 mmol) were added. Stirring was continued for a week. The polycation product in DMSO (5 mL) was transferred to a Spectra/Por 4 dialysis hose and dialyzed against MilliQ water (1.5 L, 0.1 M NaCl), until the disappearance of observable red color from the water. Dialysis was then continued against pure MilliQ. Concentration of the salt-free polyelectrolyte solution by a mild flow of nitrogen gave polycation **4** with quantitative yield as orange-red flakes. Based on UV/Vis measurements, the RBITC coupled repeating units were estimated to be 1-2%.

**Characterization** Gel permeation chromatography (GPC) was carried out in tetrahydrofuran (THF), using polystyrene standards. UV/Vis spectra were recorded on a Varian Cary 300 Bio UV/Visible spectrophotometer in the wavelength region between 200 to 800 nm. Fluorescence excitation and emission spectra were recorded on an Edinburgh FS 900 fluorospectrophotometer. Viscosity measurements were performed on an Ubbelohde viscometer.

### 3.7 References

1. Barlow, S.; O'Hare, D. *Chem. Rev.* **1997**, *97*, 637.
2. (a) Manners, I. *Synthetic Metal-Containing Polymers*, Wiley-VCH, Weinheim, **2004**; (b) Kulbaba, K.; Manners, I. *Macromol. Rapid Commun.* **2001**, *22*, 711; (c) Whittell, G. R.; Manners, I. *Adv. Mater.* **2007**, *19*, 3439.



3. (a) Rosenberg, H.; Rausch, M. D.; US Patent 3,060,215, **1962**; (b) Neuse, E. W.; Rosenberg, H. *J. Macromol. Sci.* **1970**, *C4*, 1.
4. Foucher, D. A.; Tang, B. Z.; Manners, I. *J. Am. Chem. Soc.* **1992**, *114*, 6246.
5. (a) Rulkens, R.; Lough, A. J.; Manners, I. *J. Am. Chem. Soc.* **1994**, *116*, 797; (b) Ni, Y. Z.; Rulkens, R.; Pudelski, J. K.; Manners, I. *Macromol. Rapid. Commun.* **1995**, *16*, 637; (c) Reddy, N. P.; Yamashita, H.; Tanaka, M. *J. Chem. Soc. Chem. Commun.* **1995**, 2263.
6. Manners, I. *Chem. Commun.* **1999**, 857.
7. Korczagin, I.; Lammertink, R. G. H.; Hempenius, M. A.; Golze, S.; Vancso, G. J. *Adv. Polym. Sci.* **2006**, *200*, 91.
8. Lammertink, R. G. H.; Hempenius, M. A.; Chan, V. Z.-H.; Thomas, E. L.; Vancso, G. J. *Chem. Mater.* **2001**, *13*, 429.
9. Korczagin, I.; Golze, S.; Hempenius, M. A.; Vancso, G. J. *Chem. Mater.* **2003**, *15*, 3663.
10. Cheng, J. Y.; Ross, C. A.; Chan, V. Z.-H.; Thomas, E. L.; Lammertink, R. G. H.; Vancso, G. J. *Adv. Mater.* **2001**, *13*, 1174.
11. (a) Hinderling, C.; Keles, Y.; Stöckli, T.; Knapp, H. F.; de los Arcos, T.; Oelhafen, P.; Korczagin, I.; Hempenius, M. A.; Vancso, G. J.; Pugin, R.; Heinzelmann, H. *Adv. Mater.* **2004**, *16*, 876; (b) Lastella, S.; Jung, Y. J.; Yang, H. C.; Vajtai, R.; Ajayan, P. M.; Ryu, C. Y.; Rider, D. A.; Manners, I. *J. Mater. Chem.* **2004**, *14*, 1791.
12. (a) Nguyen, M. T.; Diaz, A. F.; Dement'ev, V. V.; Pannell, K. H. *Chem. Mater.* **1993**, *5*, 1389; (b) Pudelski, J. K.; Foucher, D. A.; Honeyman, C. H.; Macdonald, P. M.; Manners, I.; Barlow, S.; O'Hare, D. *Macromolecules* **1996**, *29*, 1894; (c) Arsenault, A. C.; Miguez, H.; Kitaev, V.; Ozin, G. A.; Manners, I. *Adv. Mater.* **2003**, *15*, 503.
13. Giannotti, M. I.; Lv, H.; Ma, Y.; Steenvoorden, M. P.; Overweg, A. R.; Roerdink, M.; Hempenius, M. A.; Vancso, G. J. *J. Inorg. Organom. Polym. Mater.* **2005**, *15*, 527.
14. (a) Foucher, D.; Ziembinski, R.; Petersen, R.; Pudelski, J.; Edwards, M.; Ni, Y.; Massey, J.; Jaeger, C. R.; Vancso, G. J.; Manners, I. *Macromolecules* **1994**, *27*, 3992; (b) Rulkens, R.; Lough, A. J.; Manners, I.; Lovelace, S. R.; Grant, C.; Geiger, W. E. *J. Am. Chem. Soc.* **1996**, *118*, 12683.
15. (a) Péter, M.; Hempenius, M. A.; Kooij, E. S.; Jenkins, T. A.; Roser, S. J.; Knoll, W.; Vancso, G. J. *Langmuir* **2004**, *20*, 891; (b) Péter, M.; Lammertink, R. G. H.; Hempenius, M. A.; Vancso, G. J. *Langmuir* **2005**, *21*, 5115.
16. (a) Zou, S.; Ma, Y.; Hempenius, M. A.; Schönherr, H.; Vancso, G. J. *Langmuir* **2004**, *20*, 6278; (b) Zou, S.; Hempenius, M. A.; Schönherr, H.; Vancso, G. J. *Macromol. Rapid Commun.* **2006**, *27*, 103; (c) Zou, S.; Hempenius, M. A.; Schönherr, H.; Vancso, G. J. *Polymer* **2006**, *47*, 2483.
17. Foucher, D. A.; Ziembinski, R.; Tang, B. Z.; Macdonald, P. M.; Massey, J.; Jaeger, C. R.; Vancso, G. J.; Manners, I. *Macromolecules* **1993**, *26*, 2878.
18. Nguyen, M. T.; Diaz, A. F.; Dement'ev, V. V.; Pannell, K. H. *Chem. Mater.* **1993**, *5*, 1389.

19. Power-Billard, K. N.; Manners, I. *Macromolecules* **2000**, *33*, 26.
20. Hempenius, M. A.; Robins, N. S.; Lammertink, R. G. H.; Vancso, G. J. *Macromol. Rapid Commun.* **2001**, *22*, 30.
21. Hempenius, M. A.; Vancso, G. J. *Macromolecules* **2002**, *35*, 2445.
22. Wang, Z.; Lough, A.; Manners, I. *Macromolecules* **2002**, *35*, 7669.
23. Hempenius, M. A.; Brito, F. F.; Vancso, G. J. *Macromolecules* **2003**, *36*, 6683.
24. Köpf-Maier, P.; Köpf, H.; Neuse, E. W. *Angew. Chem. Int. Ed.* **1984**, *23*, 456.
25. (a) Decher, G.; Hong, J.-D.; *Macromol. Chem. Macromol. Symp.* **1992**, *46*, 321; (b) Decher, G.; Hong, J.-D. *Thin Solid Films* **1992**, *210-211*, 831.
26. (a) Resendes, R.; Massey, J.; Dorn, H.; Winnik, M. A.; Manners, I. *Macromolecules* **2000**, *33*, 8; (b) Power-Billard, K. N.; Manners, I. *Macromol. Rapid Commun.* **2002**, *23*, 607; (c) Power-Billard, K. N.; Spontak, R. J.; Manners, I. *Angew. Chem. Int. Ed.* **2004**, *43*, 1260; (d) Wang, X. S.; Winnik, M. A.; Manners, I. *Macromol. Rapid Commun.* **2002**, *23*, 210.
27. (a) Gómez-Elipse, P.; Macdonald, P. M.; Manners, I. *Angew. Chem. Int. Ed. Engl.* **1997**, *36*, 762; (b) Gómez-Elipse, P.; Resendes, R.; Macdonald, P. M.; Manners, I. *J. Am. Chem. Soc.* **1998**, *120*, 8348; (c) Bartole-Scott, A.; Resendes, R.; Manners, I. *Macromol. Chem. Phys.* **2003**, *204*, 1259.
28. Fuoss, R. M. *J. Polym. Sci.* **1948**, *3*, 603.
29. Temple, K.; Jäkle, F.; Sheridan, J. B.; Manners, I. *J. Am. Chem. Soc.* **2001**, *123*, 1355.
30. (a) Kwon, I. C.; Bae, S. Y. H.; Kim, W. *Nature* **1991**, *354*, 291; (b) Yerushalmi, R.; Scherz, A.; van der Boom, M. E.; Kraatz, H. B. *J. Mater. Chem.* **2005**, *15*, 4480.
31. Manners, I. *Adv. Organomet. Chem.* **1995**, *37*, 131.
32. Prins, R. *Chem. Commun.* **1970**, 280.
33. Espada, L.; Pannell, K. H.; Papkov, V.; Leites, L.; Bukalov, S.; Suzdalev, I.; Tanaka, M.; Hayashi, T. *Organometallics* **2002**, *21*, 3758.
34. Cyr, P. W.; Tzolov, M.; Manners, I.; Sargent, E. H. *Macromol. Chem. Phys.* **2003**, *204*, 915.

## Chapter 4

### Substrate Supported Multilayers by Supramolecular Electrostatic Assembly of Poly(ferrocenylsilanes)\*

*Water-soluble poly(ferrocenylsilane) strong polyelectrolytes have been employed in the electrostatic layer-by-layer supramolecular assembly process to give full organometallic polyion multilayer structures on various planar supports. The multilayer film growth was found to follow a linear profile, monitored by UV/Vis spectroscopy, spectroscopic ellipsometry and quartz crystal microgravimetry. Additional ellipsometric studies showed a square root dependence of the film thickness on polyelectrolyte solution salt (NaCl) concentration. The redox-responsive nature of the ferrocene-containing polymer backbone renders the multilayers removable by chemical oxidation. UV/Vis spectroscopy and ellipsometry measurements showed a fast and complete PFS multilayer removal by exposure to FeCl<sub>3</sub> solutions. This oxidation induced dissolution was used to create PFS multilayer patterns by a “reactive” soft lithography procedure using hydrophilic PDMS stamps and FeCl<sub>3</sub> solutions as ink. PFS multilayers can also be reversibly oxidized and reduced electrochemically. When left for a prolonged time under an oxidation potential, the release of PFS polyelectrolytes from their multilayers can be realized. The quantity and rate of material release can be conveniently controlled by the on-off switching of the potential and the application of different oxidation potentials. The possibility of area-selective deposition of multilayers onto chemically patterned substrates was also explored.*

#### 4.1 Introduction

Water-soluble poly(ferrocenylsilanes) (PFSs) constitute a unique group of functional polyelectrolytes that can be incorporated into the electrostatic layer-by-layer supramolecular assembly process.<sup>1, 2</sup> The redox characteristics of the organometallic main chain have great promise to bring new functions to polyelectrolyte multilayer thin films and microcapsules.<sup>3</sup> In order to study the redox related properties of poly(ferrocenylsilane) multilayer structures, it is essential to first establish the deposition conditions for their well-defined layer-by-layer assembly. In our previous studies on multilayers built from weak PFS polyelectrolytes, very

---

\* Part of the work described in this Chapter has been published: Ma, Y.; Dong, W.-F.; Kooij, E. S.; Hempenius, M. A.; Möhwald, H.; Vancso, G. J. *Soft Matt.* **2007**, *3*, 889.

thin films were obtained when depositing from salt-free solutions.<sup>4</sup> Recently the successful preparation of much thicker films by using polyelectrolyte solutions containing sodium chloride (NaCl) has been established. In the following sections, discussions are focused on the preparation, characterization and film thickness manipulation of PFS multilayers on various planar substrates. As a follow-up on the reversible redox chemistry of poly(ferrocenylsilane) bulk solutions described earlier in Chapter 3, studies on the redox properties of PFS multilayers on flat interfaces are also described in this Chapter.

Apart from their redox responsive properties, PFS can act as effective resists in reactive ion etching processes due to the formation of an etch resistant iron/silicon oxide layer.<sup>5</sup> As an extension of studying PFS multilayers with full coverages, attempts were made to create two-dimensionally patterned full organometallic multilayers on silicon substrates. These patterns may have potential applications as electrochemically modulated diffraction gratings<sup>6</sup> and as etch barriers in reactive ion etch processes.

## 4.2 Multilayer fabrication and structure characterization

### 4.2.1 Multilayer deposition on planar interfaces

The electrostatic layer-by-layer assembly process of organometallic polyions **4** and **5** (see molecular structures in Chapter 3) on quartz slides was first monitored by UV/Vis spectroscopy. Multilayers were built up from 2 mg/mL polyelectrolyte aqueous solutions containing 0.5 M NaCl. Figure 4.1 shows the increase of the characteristic absorbance of PFS as an intense ligand-to-metal charge transfer transition (LMCT) at  $\lambda = 216 \text{ nm}$ <sup>7</sup> as a function of the number of bilayers.

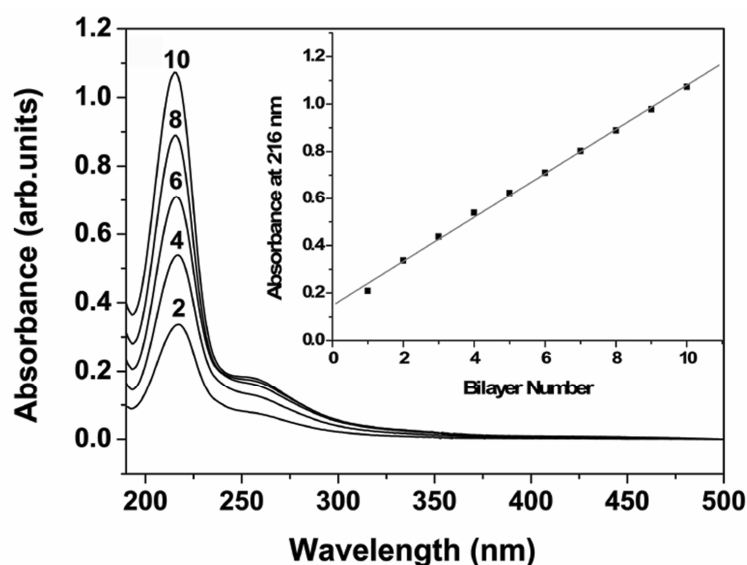


**Figure 4.1** UV/Vis absorption spectra of sequentially adsorbed layers of PFS polyions from aqueous solutions (2 mg/mL, 0.5 M NaCl) on quartz.

A linear growth of the absorbance as a function of the number of bilayers was observed until at least 12 bilayers, giving evidence for a well-defined deposition process.<sup>1,2</sup>

The linearity in film growth was further proved by the results from quartz crystal microbalance (QCM) measurements after each bilayer deposition (Figure 4.2). The QCM frequency shift ( $\Delta F$ ) is related linearly to the mass change on the electrode as defined by the Sauerbrey equation:<sup>8</sup>

$$\Delta F = -1.832 \times 10^8 M / A \quad (4.1)$$

where  $M$  is the mass added to the resonator, and  $A$  is the surface area of the resonator. According to equation (4.1), a 1 Hz change in  $\Delta F$  corresponds to a 0.9 ng mass increase when the actual electrode area is  $A = 0.16 \pm 0.01 \text{ cm}^2$ . The linear fit of the QCM data gave a mass value of 695.6 ng/cm<sup>2</sup> for each adsorbed bilayer of PFS under the previously mentioned adsorption conditions.

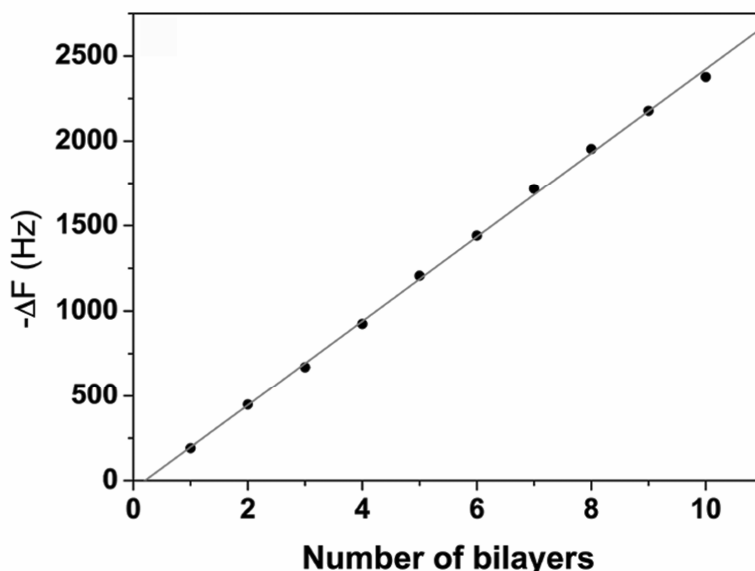


**Figure 4.2** QCM frequency change as a function of bilayer number.

Figure 4.3 shows the surface morphology of these organometallic multilayers deposited on silicon substrates (with predeposited PEI + (PSS/PAH)<sub>2</sub> layers) under the same experimental conditions by tapping mode AFM. When the adsorbed (PFS<sup>-</sup>/PFS<sup>+</sup>) bilayer numbers increased from one to ten, the root mean square (rms) roughness of the multilayer covered silicon substrate decreased from 0.9 to 0.7 nm over a scan area of 1 x 1 μm<sup>2</sup>, indicating that the uniform film growth followed the substrate surface morphology.<sup>9</sup>

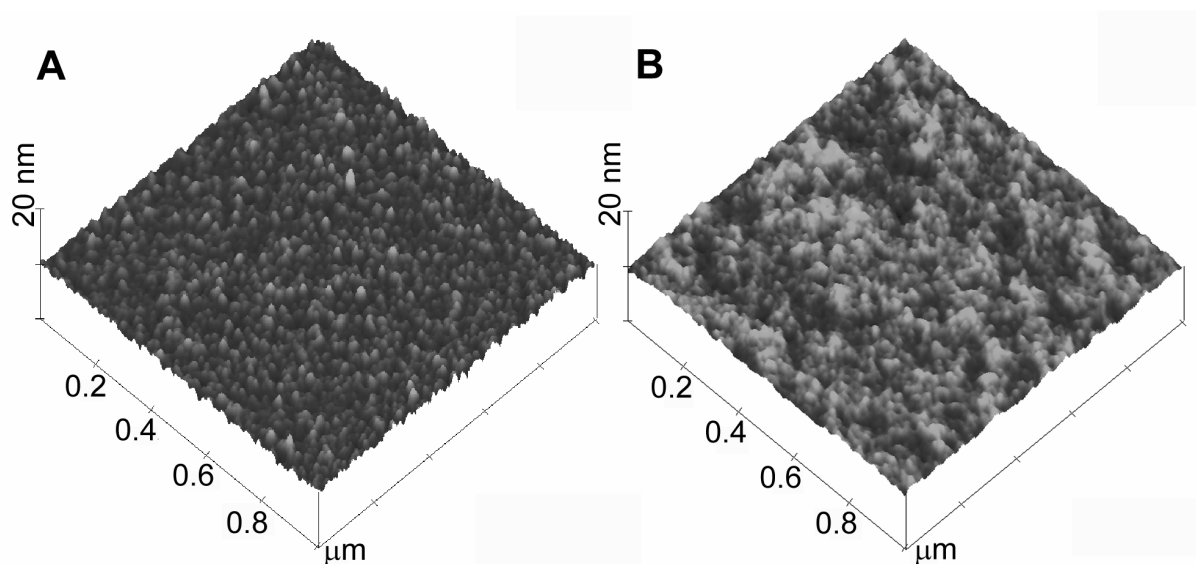


**Figure 4.3** Tapping mode AFM height images of (A) one bilayer and (B) ten bilayers of (PFS<sup>-</sup>/PFS<sup>+</sup>) on a silicon substrate with predeposited PEI+(PSS/PAH)<sub>2</sub> layer.

The thickness of PFS multilayers deposited on silicon wafers was measured by spectroscopic ellipsometry. The thickness values were obtained based on fitting the ellipsometry spectra recorded after each dipping cycle. From the slope of the linear increase of film thickness, a bilayer thickness of 4.5 nm under the above deposition conditions was calculated. This value is much larger than the value obtained before on similar multilayer systems prepared from the same polyelectrolyte solutions but without additional salt (0.61 nm, see also Figure 4.4A). A similar increase of film thickness with increasing salt concentrations of the polyelectrolyte solutions used for surface deposition has been shown for many other polyelectrolyte multilayer systems, which was attributed to the combination of the “salting-out” effect and screening of long-range electrostatic interactions.<sup>10</sup>

#### 4.2.2 Film thickness dependence on solution salt concentration

A systematic study was carried out to determine the multilayer thickness dependence on polyelectrolyte solution salt (NaCl) concentrations. For this purpose, thin films were prepared in a layer-by-layer fashion on silicon substrates from PFS polyelectrolyte aqueous solutions maintaining the polymer concentration (2 mg/mL) but varying the NaCl concentration. The thickness of the samples was measured by a Woollam VASE ellipsometer by high accuracy spectroscopic scans between 0.8 ~ 4.5 eV at 65°, 70° and 75°, respectively. The bilayer thickness for each NaCl concentration can be deduced from the fitted film thickness and the corresponding bilayer numbers. In Figure 4.4A, the thickness values (of a 5 and 10 bilayer sample for each concentration, respectively) as a function of the salt concentration are presented. The normalized thickness data (with respect to the thickness of multilayers prepared from salt-free polyelectrolyte solutions) can be fitted with a straight line,

as a function of the square root of the corresponding salt concentration. A similar square root dependence of thin film thickness on solution salt concentration has been observed before for other polyelectrolyte multilayer systems.<sup>11</sup> Theoretically, with increasing ionic strength ( $I$ ), the Debye screening length ( $1/\kappa$ ), which describes the extent of repulsive interactions between like-charged segments, decreases. This leads to a decrease in effective bilayer thickness. According to the relationship  $1/\kappa \sim I^{-1/2}$ , a square-root dependence of Debye length on ionic strength is expected. Therefore, the increase of bilayer thickness with increasing solution ionic strength is expected to also follow a square-root dependence, which explains the observed trend in our case.<sup>10c, 12</sup>

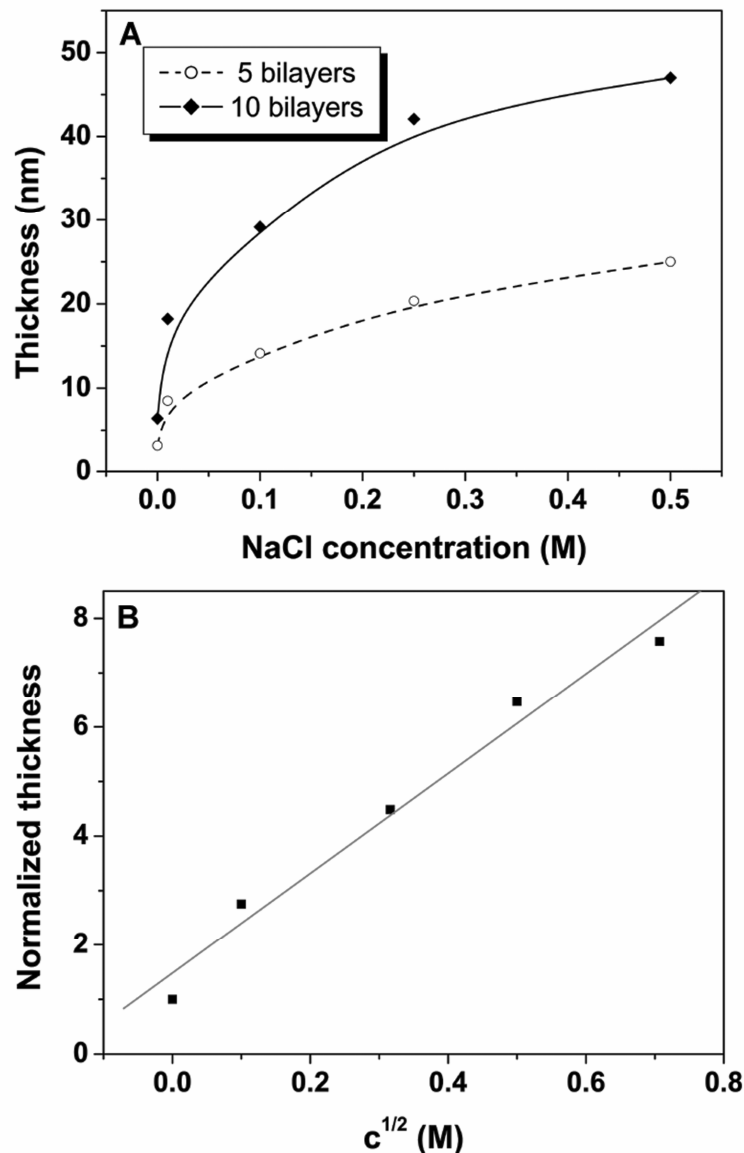


**Figure 4.4** (A) PFS polyelectrolyte multilayer film thickness dependence on salt concentration; lines were drawn as a guide for the eye. (B) Normalized bilayer thickness dependence on the square root of salt concentration. The bilayer thickness is normalized by dividing the corresponding film thickness by the film thickness of multilayers containing the same number of bilayers prepared from polyion solutions without salt.

### 4.2.3 Multilayer deposition on chemically patterned substrates

Patterned multilayers may have potential applications for producing complex optical or electro-optical devices, such as waveguides and display materials.<sup>13, 14</sup> Early attempts at selective multilayer assembly on specific areas involved microcontact printing through the use of self-assembled monolayers (SAM) as molecular templates (see Chapter 2.5.3).<sup>15, 16</sup> Later, nonlithographical means such as inkjet printing were introduced.<sup>17</sup> The development of new techniques, such as the “lift-off” approach,<sup>18</sup> and the “polymer on polymer” stamping<sup>19</sup> followed.

In the first attempt, PFS polyions were deposited onto hydrophilic/hydrophobically patterned gold substrates. Patterned self-assembled monolayers (SAMs) consisting of methyl-terminated (1-octadecanethiol, ODT) and hydroxyl-terminated (11-mercapto-1-undecanol, C11OH) alkanethiols were introduced on gold substrates, using the microcontact printing ( $\mu$ CP) method, followed by the adsorption of PFS polyelectrolytes with different numbers of bilayers. Contact mode AFM was used to characterize the patterned surface before and after polyion deposition. As demonstrated in Figure 4.5, the chemically patterned gold substrates showed minimal height contrast, but a relatively high contrast in friction force, with the hydroxyl-terminated lines corresponding to the high friction areas. After coating with PFS polyion multilayers, even after one single bilayer deposition, an obvious height contrast was observed (similar to the example shown in Figure 4.5, which was taken from a three bilayer sample). Moreover, the contrast in the friction force was reversed, showing a very selective deposition on the hydrophobic methyl-terminated stripes.



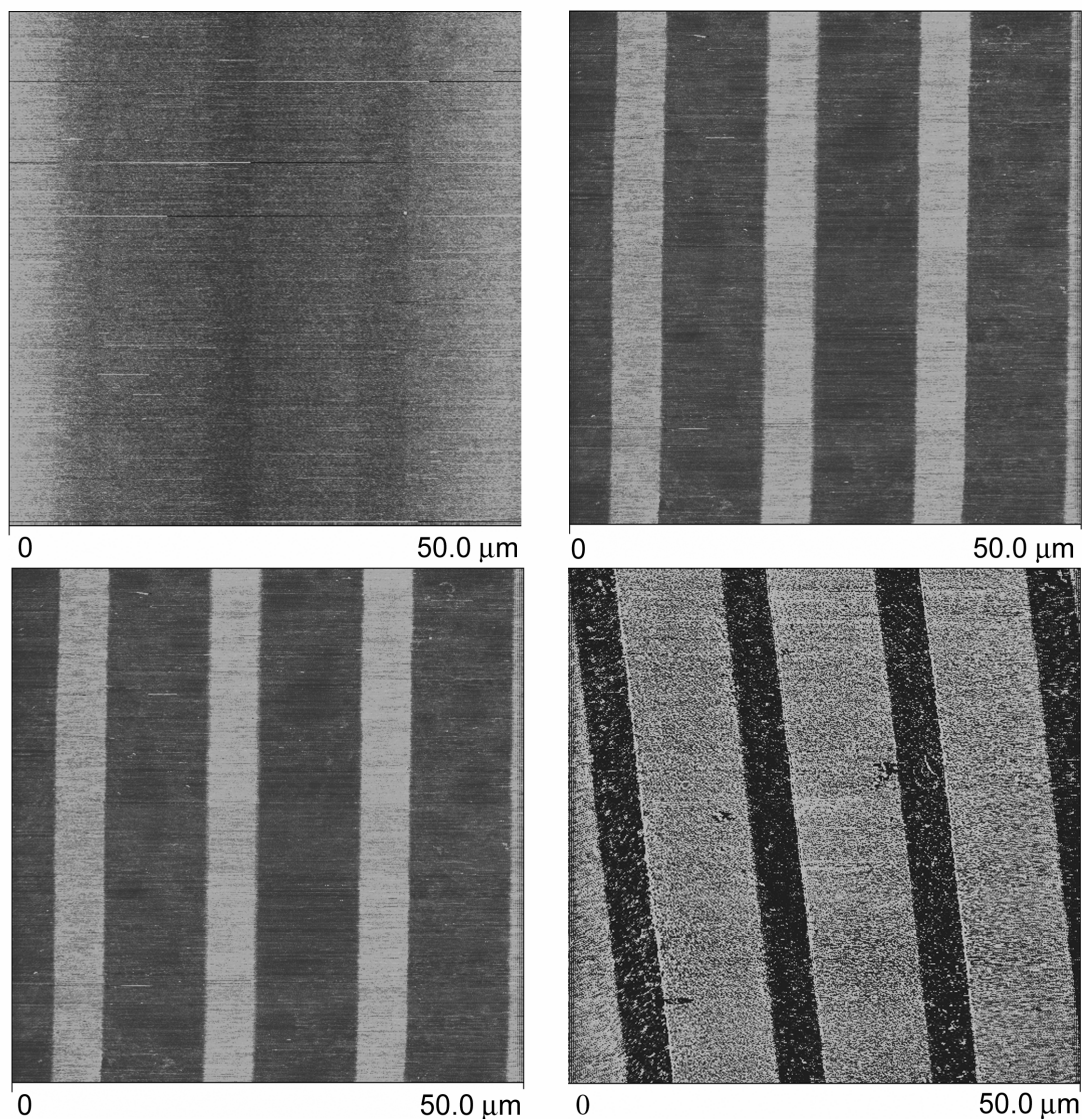


**Figure 4.5** Contact mode AFM height (z range is 30 nm) and friction force (z range is 0.2 V) images of patterned methyl- (broader lines) and hydroxyl- (narrower lines) alkanethiol self-assembled monolayers on gold (top) and of three (PFS<sup>-</sup>/PFS<sup>+</sup>) bilayers adsorbed on this prepatterned substrate (bottom). The feature sizes of the PDMS stamps were 5 μm x 10 μm.

The AFM height and friction images clearly show that the trench areas (narrower lines) on the patterns were essentially free of polymer in the unpatterned, hydrophilic regions, up to 5 bilayers of polyion deposition. It was observed however that when the number of deposited bilayers was  $\geq 6$ , some polymer was actually adsorbed on the resist regions of the patterned surface (Figure 4.6). From the AFM images of the patterned multilayers, film thickness was measured as the height difference between the brighter and darker stripes. In this way, a non-linear film growth was observed (Figure 4.7), which was similar to other patterned polyelectrolyte multilayer systems reported before when thin films were deposited from salt solutions.<sup>20</sup> Before the apparent transition point at six bilayers, the average bilayer thickness is 3-4 nm, still consistent with the former ellipsometry results on a continuous film ( $\sim 4.5$  nm).

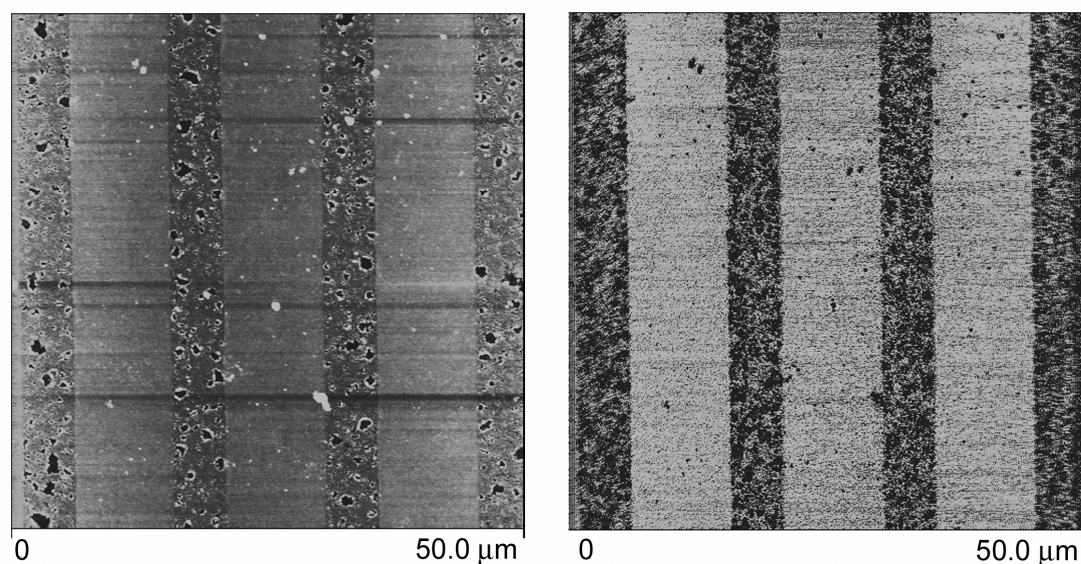


**Figure 4.6** Contact mode AFM height ( $z$  range is 30 nm) and friction force ( $z$  range is 0.5 V) images recorded for a hydrophilic/hydrophobically patterned gold substrate after the deposition of six (PFS<sup>-</sup>/PFS<sup>+</sup>) bilayers on the hydrophobic stripes.

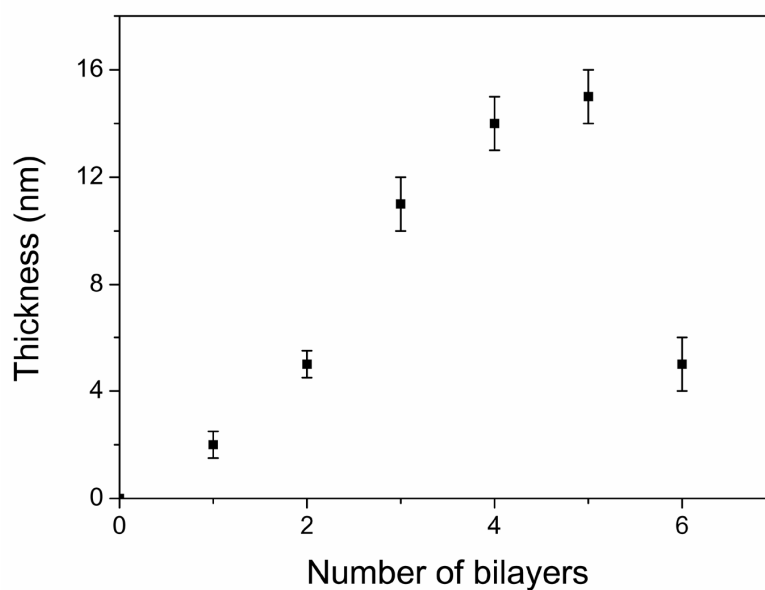
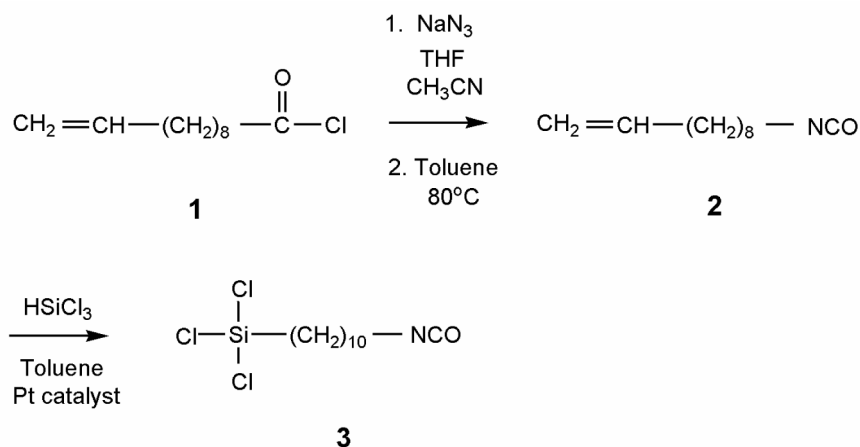


**Figure 4.7** Film thicknesses measured from AFM images of patterned PFS multilayers versus the number of deposited bilayers from polyelectrolyte aqueous solutions containing 0.5 M NaCl.

The same idea could be extended to create chemically patterned silicon substrates for the same purpose. Silane-based compounds can form stable monolayers on hydrated silicon dioxide surfaces.<sup>21</sup> However, the preparation of hydrophilic/hydrophobic patterned silane monolayers still largely remains a challenge due to the fact that the highly reactive functional silane molecules are not tolerant of any hydroxyl-containing compound.<sup>22, 23</sup> Here, a procedure is proposed to prepare chemically patterned silicon substrates by a two-step silanization/deprotection reaction. An isocyanate-terminated trichlorosilane compound **3** was first synthesized according to Scheme 4.1. After patterning the silicon substrates with this compound following a simple  $\mu$ CP procedure, the substrates were immersed into dried

tetraethylene glycol (EG, 1 mM) NMP solutions at 50°C for a surface reaction to render the patterned area adsorption resistant.<sup>24</sup> Figure 4.8 shows the AFM height and friction images of a silicon substrate after microcontact printing with trichlorosilane compound **3** using a PDMS stamp with feature size of 5 μm x 10 μm followed by reaction with hydroxyl-terminated EG. A patterned surface was successfully obtained, but the accumulation of materials on the edges of the patterns could not be ignored for subsequent layer-by-layer multilayer deposition.



**Scheme 4.1** Synthesis of an isocyanate terminated chlorosilane **3**

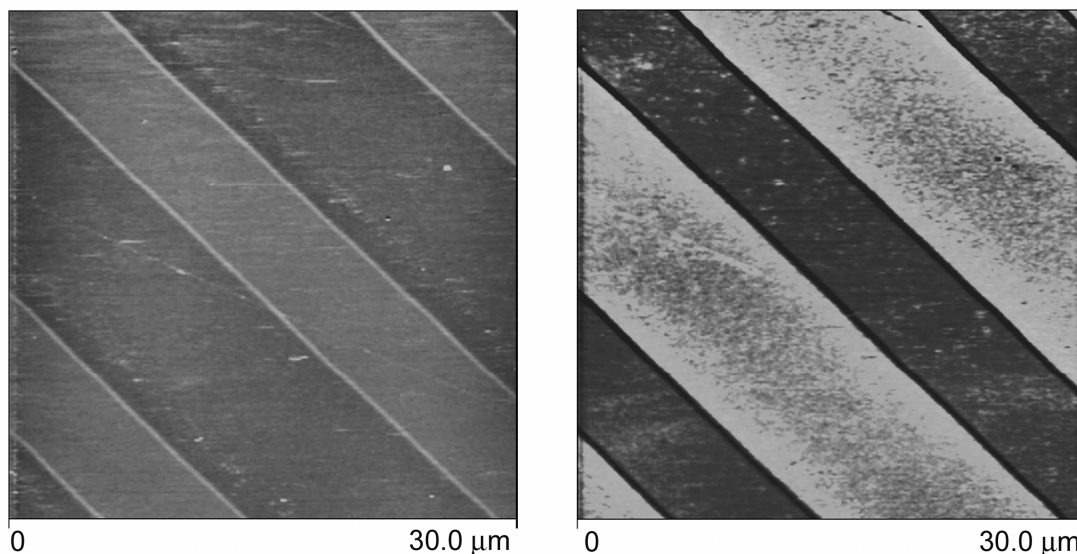


**Figure 4.8** Contact-mode AFM height (z range is 10 nm) and friction force (z range is 1.5 V) images of a silicon substrate patterned by a μCP procedure using PDMS stamps (feature size 5 μm x 10 μm) with EG-coupled isocyanate-terminated trichlorosilane **3**.

### 4.3 Redox properties of poly(ferrocenylsilane) planar multilayer films

#### 4.3.1 Chemical oxidation

As discussed in Chapter 3, an easy way to tune the redox state of PFS is by chemical methods. In order to study the chemical redox behaviour of poly(ferrocenylsilane) planar

films, full organometallic multilayers containing  $\text{PFS}^-/\text{PFS}^+$  polyelectrolytes were first assembled onto silicon wafers followed by subsequent oxidation using  $\text{FeCl}_3$ . UV/Vis spectroscopy was first applied to follow the PFS characteristic absorbance before and after chemical oxidation. As demonstrated in Figure 4.9, after immersing a ten bilayer  $\text{PFS}^-/\text{PFS}^+$  multilayer sample (deposited from 2 mg/mL polyelectrolyte solutions containing 0.5 M NaCl) on a quartz substrate into a  $\text{FeCl}_3$  aqueous solution (0.5 mM) for only two minutes, the characteristic strong absorbance of PFS at 216 nm became completely invisible. This indicated a fast redox response of the multilayers to chemical oxidation by  $\text{FeCl}_3$ , accompanied by an instantaneous and almost complete material loss from the as-assembled multilayers.

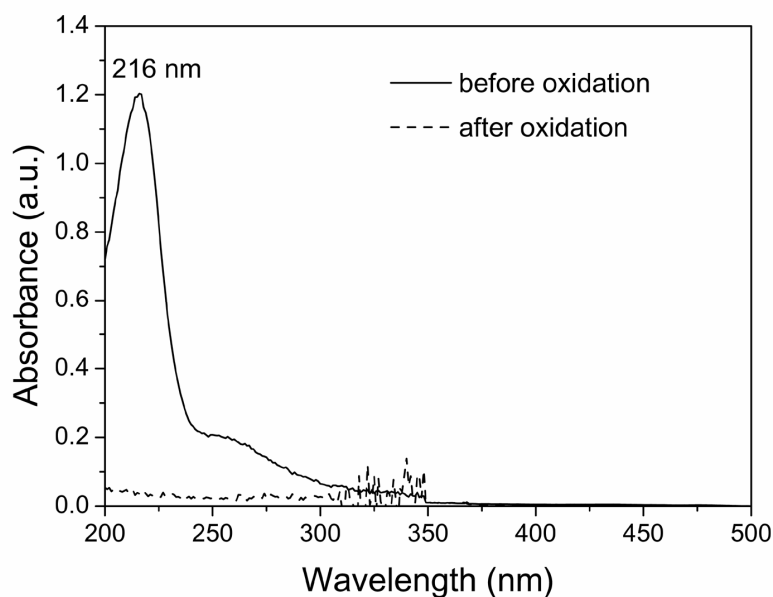


**Figure 4.9** UV/Vis spectra of a  $(\text{PFS}^-/\text{PFS}^+)_{10}$  film on quartz before and after oxidation (2 min in 0.5 mM  $\text{FeCl}_3$  aqueous solution). The PFS characteristic peak at 216 nm was not visible after oxidation.

The oxidation induced multilayer removal was further investigated by ellipsometry measurements on multilayer thickness upon chemical oxidation. Figure 4.10 summarizes the ellipsometric spectra for a bare silicon substrate, the same substrate after deposition of a ten bilayer film (deposited from 2 mg/mL polyelectrolyte solutions containing 0.25 M NaCl), and after subsequent oxidation by  $\text{FeCl}_3$ . The spectra were recorded at three different incident angles of  $65^\circ$ ,  $70^\circ$  and  $75^\circ$ . The substantial changes in the shape of spectra as well as  $\Delta$  values upon completion of the layer-by-layer assembly indicated the existence of a thin film. When fitted, the spectra gave a thickness value of 42 nm, in agreement with thicknesses obtained earlier under the same deposition conditions (2 mg/mL PFS polyions, 0.25 M NaCl). The sample was then immersed into  $\text{FeCl}_3$  aqueous solution (3 mM) for five minutes followed by thorough rinsing and drying. As shown in Figure 4.10, the spectrum of the oxidized PFS multilayer sample (Figure 4.10C) is almost identical to that of the bare silicon (Figure 4.10A). From fittings on Figure 4.10C, a film thickness of only 3 nm was obtained, indicating close to

complete material loss by chemical oxidation. Further experiments on silicon wafers bearing PFS multilayers with varying thicknesses confirmed similar fast removal of the films. As control experiments, ellipsometric spectra of multilayer films treated with the hydrochloric acid (HCl) solutions used to dissolve the  $\text{FeCl}_3$  were recorded, which showed no observable changes after immersion for a relatively long period (more than 30 minutes).

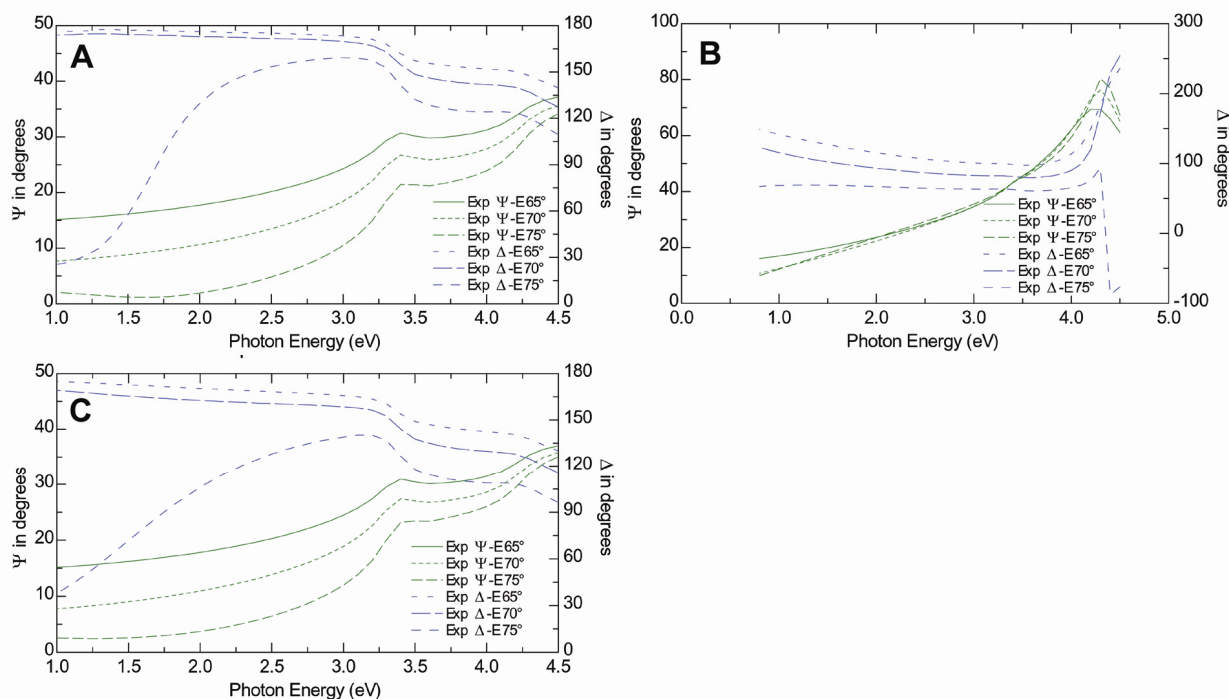


**Figure 4.10** Ellipsometry spectra recorded for (A) bare silicon, (B) the same silicon with a  $(\text{PFS}^-/\text{PFS}^+)_{10}$  film and (C) the same multilayer sample after oxidation (5 min in 3 mM  $\text{FeCl}_3$  aqueous solution). The thickness deduced from (B) was 42 nm, while after oxidation it had decreased to 3 nm (C).

The mechanism of multilayer removal by chemical oxidation was considered to result from the disruption of the originally charge compensated layer-by-layer structure due to the introduction of additional positive charges on the polymer main chain. Moreover, the solubility variations on the multilayer components also contributed to the multilayer dissolution from the substrates. A more detailed discussion will follow in Chapter 5.

### 4.3.2 Patterned multilayers by “reactive” soft lithography

The peculiar removable properties of the poly(ferrocenylsilane) multilayers could be utilized to create patterned multilayers. Here, starting from continuous PFS multilayers, a micromolding in capillaries (MIMIC)<sup>15</sup> procedure was followed using PFS oxidant ( $\text{FeCl}_3$  aqueous solutions) as ink. PDMS stamps were first treated with UV/ozone for 1 h in order to render their surfaces hydrophilic.<sup>25</sup> In the patterning procedure as demonstrated in Figure 4.11, after drying under a  $\text{N}_2$  stream the stamps were put in immediate contact with the multilayers on the silicon substrate. A drop of oxidant solution was then placed in front of the stamp and a

rapid filling of the channels was observed. After a certain time (2-5 minutes), the stamps were removed to reveal patterns formed as a result of partial selective removal of PFS in the oxidant-filled microchannels, as demonstrated by tapping mode AFM imaging (Figure 4.11B). Multilayers with different thicknesses were patterned in a similar procedure and a constant height decrease of around 2-3 nm was observed in the ink-filled trench area, indicating only partial removal of these multilayers. This can be partly explained by the very restricted diffusion volume for the dissociated macromolecules due to the small dimensions of the microchannels.

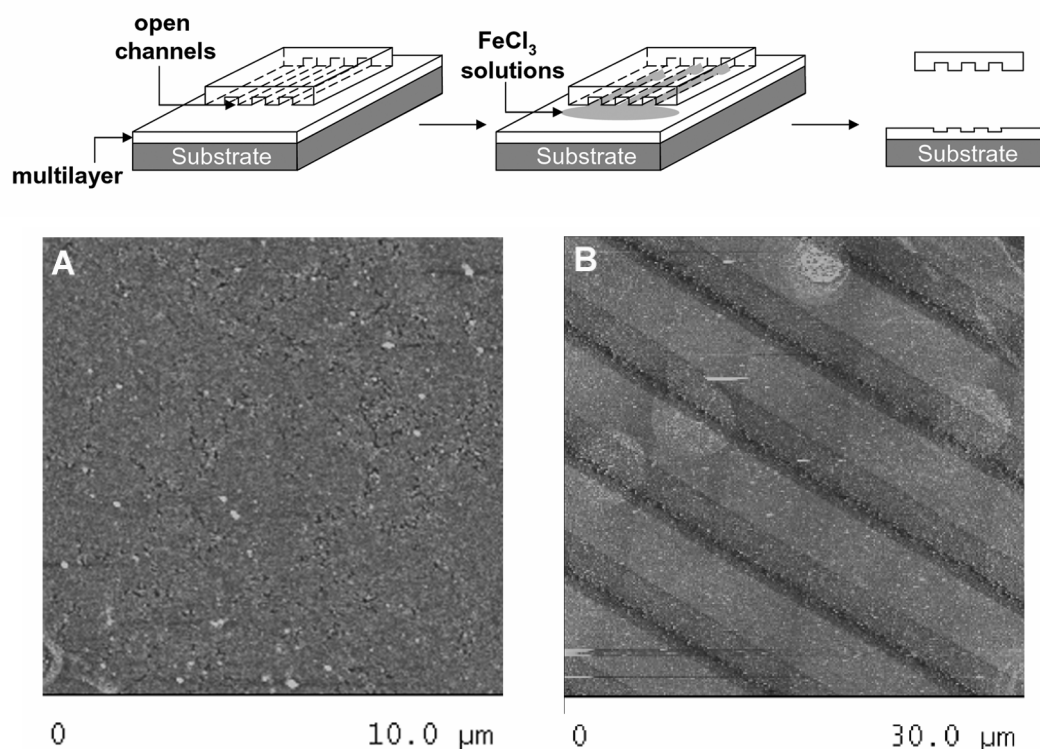


**Figure 4.11** Top: schematic of the reactive MIMIC procedure; Bottom: Tapping mode AFM height images recorded for a continuous  $(\text{PFS}^-/\text{PFS}^+)_3$  multilayer sample (A) before MIMIC (z range is 15 nm) and (B) after MIMIC for two minutes using  $\text{FeCl}_3$  (1 mM) as ink (z range is 25 nm). Line patterns with partial selectively removed trenches (3  $\mu\text{m}$ , darker stripes) separated by fully covered multilayers (4  $\mu\text{m}$ , brighter stripes) were obtained.

### 4.3.3 Multilayer electrochemistry

Alternatively, PFS can be reversibly oxidized and reduced electrochemically.<sup>26</sup> A typical voltammogram shows two oxidation waves, indicating intermetallic coupling between neighbouring iron centers in the polymer chain.<sup>26a</sup> The first oxidation wave has been attributed to the oxidation of ferrocene centers having neutral neighbouring units. The remaining ferrocene units, predominantly those in positions next to the oxidized ones, will be oxidized in the second wave and at higher potentials. In order to study the electrochemical properties of PFS multilayers by cyclic voltammetry (CV), thin films were prepared on gold electrodes. Figure 4.12 shows the variation of current versus time as the potential is cycled

between  $-0.4$  and  $0.4$  V on a  $(\text{PFS}^+/\text{PFS}^-)_8$  bilayer sample, relative to a mercury/mercury sulphate electrode ( $\text{Hg}/\text{Hg}_2\text{SO}_4$ , MSE). The electrochemically triggered oxidation and reduction could be repeated for many times, with very good superposition of the recorded cyclic voltammograms.<sup>27</sup>

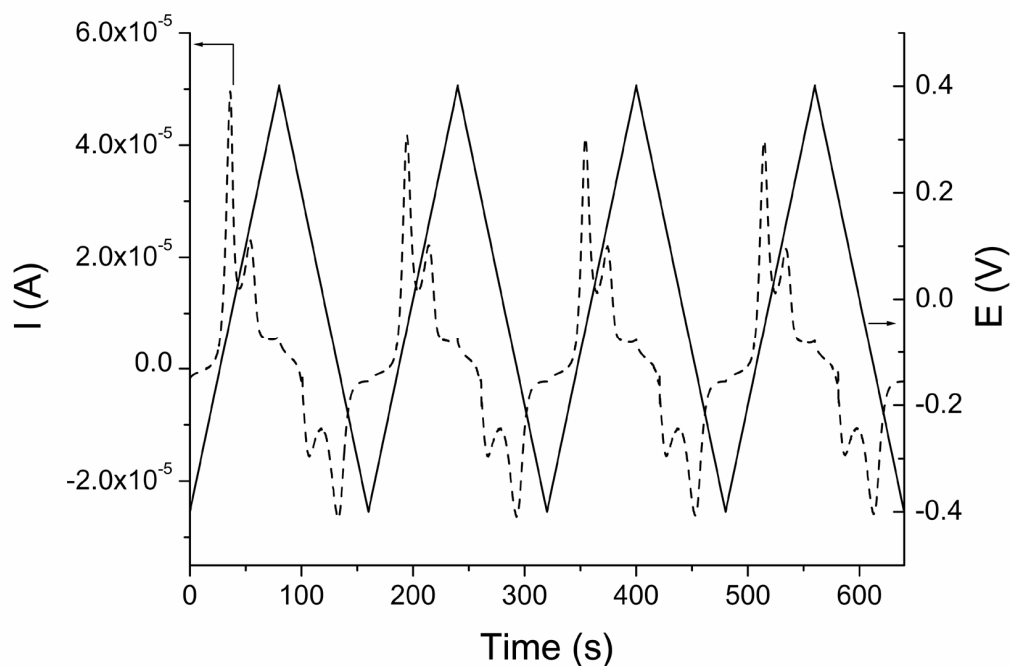


**Figure 4.12** Excitation signal and cyclic voltammograms as a function of time for an 8-bilayer PFS film on gold. Experiments were carried out in  $0.1$  M  $\text{NaClO}_4$  aqueous solution using a  $\text{Hg}/\text{Hg}_2\text{SO}_4$  reference electrode and a Pt counter electrode.

#### 4.3.4 Controlled multilayer release by electrochemistry<sup>†</sup>

Layer-by-layer constructed thin film structures can serve as platforms for controlled, active material release applications. As a typical scenario, deconstruction of multilayer structures by a certain trigger will simply result in a release of the embedded materials (*e.g.* drugs or DNA).<sup>28</sup> In many cases, precise control over the release of the embedded materials is highly desirable. In Chapter 4.3.1 a peculiar PFS multilayer removal phenomenon was observed when applying a chemical redox trigger. However, chemical oxidation of PFS multilayers resulted in a fast, almost instantaneous release of the PFS polyelectrolytes that was difficult to control.

In Chapter 4.3.3 the reversible electrochemical redox behaviour of PFS multilayers has been demonstrated. In a series of continuous electrochemical events, the cyclic voltammograms recorded on the same multilayers could be superimposed very well. The application of a constant oxidative potential on the PFS multilayers should lead to charge imbalance within the thin film. In order to maintain a charge-balanced multilayer structure,

<sup>†</sup> This section will be published in a separate article.

multilayer re-arrangements and/or material release should take place, just similar to the multilayer removal in the presence of an oxidation agent.

For electrochemical release experiments,  $(\text{PFS}^-/\text{PFS}^+)_5$  multilayers were prepared on 3-aminopropyltrimethoxysilane treated ITO substrates. In the first attempt, a series of cyclic voltammograms were recorded when the voltage was held at a constant oxidation potential of 0.4 V, where full oxidation of PFS was expected, for different time intervals. As demonstrated in Figure 4.13A, the peak currents of recorded cyclic voltammograms after holding for 5, 10, 20, 30, 45, 60, 80, 100, 120, 150 and 180 min gradually decreased. The slow reduction of the peak currents implied a decreased amount of electroactive material on the surface. In the mean time, the oxidation/reduction peak potential remained at the same position throughout the experiment. The almost identical electron-transfer behaviour as reflected from the shape of the CV curves indicates that there was no significant change in the material properties at the surface. In addition, during the electrochemical process only a relatively small potential (0.4 V) was applied, under which undesired electrochemical processes such as the electrolysis of water are unlikely to take place.<sup>28</sup> Thus, the mechanism of material release was considered to originate from the oxidation of the polymers.

As mentioned, the actual amount of electroactive material scales linearly with the charge  $Q$  involved in the electrochemical oxidation/reduction process (Chapter 2.5.4.2), which could be obtained from the integration of the area under the recorded cyclic voltammograms. In this way, the decrease in the amount of PFS on the ITO electrode surface was quantified and plotted as a function of the accumulated holding time at 0.4 V. Starting from the original film before maintaining the oxidation potential (*i.e.* at time 0, where  $Q\%$  is taken as 100%), Figure 4.13B illustrates the remaining percentage of integrated charge  $Q$  involved in the oxidation process relative to the amount at time 0 as a function of time. The slow decrease of  $Q\%$  with time represented the same degree of decrease in the amount of ferrocene/ferrocenium units on the surface. In other words, PFS polyelectrolytes that were originally incorporated in the multilayer thin film structure on the ITO surface were gradually released into the electrolyte solution. The material release stops when the potential is not maintained at 0.4 V since completely superimposable cyclic voltammograms (similar to those shown in Figure 4.12) were recorded during each intermission of the whole electrochemical oxidation process. From the Figure it is observed that finally when the accumulated holding time reached three hours, over 95% of the original material had been lost. This can be correlated with the full oxidation case in the above chemical oxidation experiments on the same type of multilayers on quartz and silicon substrates (Chapter 4.3.1). Compared with chemical oxidation, the speed of electrochemical-induced material release is much slower.



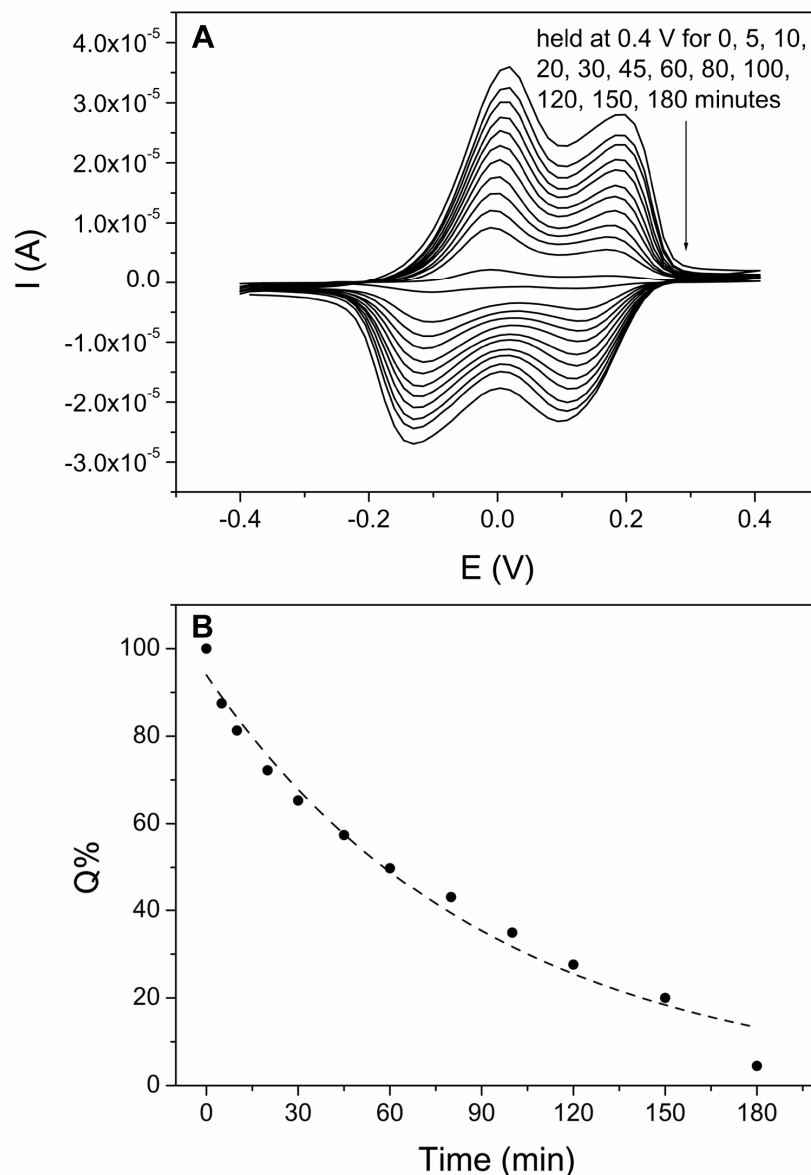


**Figure 4.13** (A) Cyclic voltammograms recorded on a  $(\text{PFS}^-/\text{PFS}^+)_5$  multilayer on a 3-aminopropyltrimethoxysilane treated ITO substrate after different holding time intervals at 0.4 V for up to 3 hours. Experiments were carried out in 0.1 M  $\text{NaClO}_4$  aqueous solution using a  $\text{Hg}/\text{Hg}_2\text{SO}_4$  reference electrode and a Pt counter electrode, at a constant scan rate of 50 mV/s. (B) Remaining percentage of integrated charge  $Q$  involved in the oxidation process relative to that from time 0 as a function of accumulated holding time at the potential of 0.4 V.

As briefly discussed earlier, previous studies have revealed that the double waves in a typical cyclic voltammogram of a PFS sample correspond to the stepwise oxidation of the polymer. In order to control the speed of material release and the amount of material ultimately released, a second set of experiments were carried out by holding the potential at 0.1 V, which is the location of the valley between the first and the second oxidation wave. At this potential, only partial oxidation of the polymer is expected. Again, the cyclic voltammograms recorded for the same type of  $(\text{PFS}^-/\text{PFS}^+)_5$  multilayer sample on ITO substrates after holding at 0.1 V for prolonged time intervals are presented in Figure 4.14A. A

similar trend of decrease in the oxidation/reduction peak currents was observed, but at a lower speed. After maintaining the potential at 0.1 V for five hours, the highest peak current was still close to  $2.5 \times 10^{-5}$  A, while in the above case, holding the potential at 0.4 V for only 30 minutes had resulted in the same degree of current decrease. As we discuss in the next paragraph, oxidation at this lower voltage also allows the controlled release of residual PFS remaining on the electrode.

The original cyclic voltammograms was translated to the quantitative value of  $Q$  and the corresponding release profile at 0.1 V is presented in Figure 4.14B.

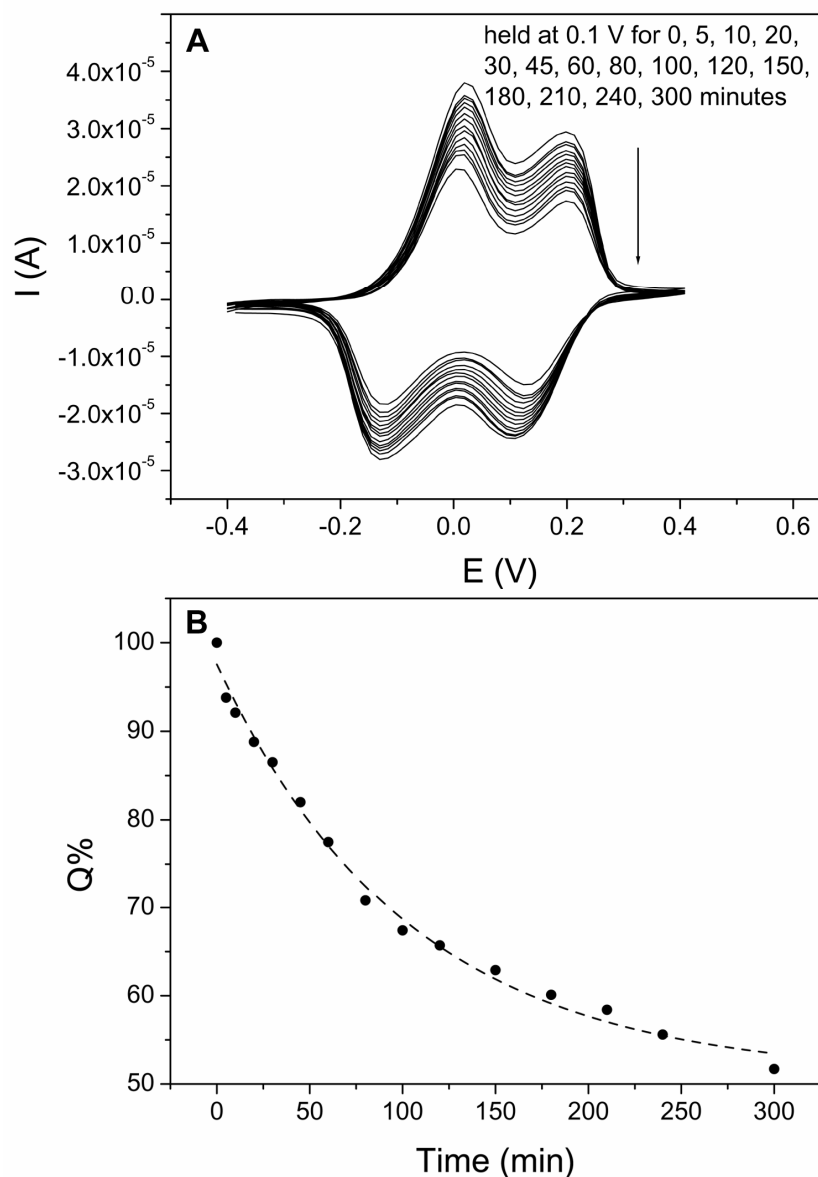


**Figure 4.14** (A) Cyclic voltammograms recorded on a  $(\text{PFS}^-/\text{PFS}^+)_5$  multilayer on a 3-aminopropyltrimethoxysilane treated ITO substrate after different holding time intervals at 0.1 V up to 5 hours. Experiments were carried out in 0.1 M  $\text{NaClO}_4$  aqueous solution using a  $\text{Hg}/\text{Hg}_2\text{SO}_4$  reference electrode and a Pt counter electrode, at a constant scan rate of 50 mV/s. (B) Remaining percentage of integrated charge  $Q$  involved in the oxidation process relative to that from time 0 as a function of accumulated holding time at the potential of 0.1 V.

Comparing Figure 4.13B with 4.14B, after oxidation for three hours material loss was 95% when the potential was held at 0.4 V but only 33% in the case of 0.1 V. It is clear from the Figure that material loss only reached  $\sim 50\%$  even after oxidation for 5 hours when the potential was held at a partial oxidation voltage. Assuming only half of the ferrocene units were oxidized during the first oxidation wave, an expected material loss of 33% was calculated based on complete partial oxidation at 0.1 V.

The deviation of the actual experimental result of close to 50% from the expected value of 33% can be explained as follows. In fact, the relative ratio between the two oxidation peak areas in the CVs as shown in Figure 4.12-4.14 is larger than 1:1, indicating that more than half of the ferrocene units are oxidized in the first oxidation peak. This is in accordance with former results from the electrochemistry experiments on multilayers made from weak PFS polyelectrolytes. The deviation of the electrochemical behaviour of water soluble PFS from other types of PFS was explained by the fact that the free penetration of the solvent and counterions into the polyelectrolyte multilayers ensured a better screening and solvation of the ferrocenium sites.<sup>29</sup>

In summary, the release of PFS polyelectrolytes from PFS multilayers can be realized by electrochemistry. The quantity of material release can be precisely manipulated by a simple on-off switching of the electrical potential. The rate of release can be further varied by applying different oxidation potentials. The controlled release of electroactive components from polyelectrolyte multilayers provides great opportunities in exploring their potential in controlled delivery applications.

## **4.4 Conclusions**

Water-soluble poly(ferrocenylsilanes) were successfully employed in electrostatic layer-by-layer supramolecular assembly to give fully organometallic polyelectrolyte multilayers. PFS multilayer growth follows a linear profile and film thickness can be easily tuned by varying salt concentrations of the polyion solutions. The stimuli-responsive characteristics of PFS multilayers were demonstrated by their removal upon chemical oxidation and by their reversible oxidation and reduction activities under an electrochemical stimulus. This phenomenon was used to create PFS multilayer patterns by a MIMIC procedure, using PFS oxidant  $\text{FeCl}_3$  as ink. The release of PFS polyelectrolytes from PFS multilayers can also be realized electrochemically by prolonged exposure to a small potential ( $\leq 0.4$  V). In contrast to chemical oxidation where PFS loss is instantaneous, the quantity and rate of material release can be precisely manipulated by the on-off switching of the electrical potential and the application of different oxidation potentials. We demonstrate that both burst release and controlled release of PFS polyelectrolytes from their multilayer thin film structures are possible by the choice of stimuli. PFS multilayers provide great opportunities in

smart, stimuli-responsive delivery applications. Some successful attempts were made to selectively deposit poly(ferrocenylsilane) multilayers on patterned gold and silicon substrates.

## 4.5 Experimental

**Materials** Polyethyleneimine (PEI,  $M_w \sim 2.5 \times 10^4$  g/mol), poly(styrene sulfonate) (PSS,  $M_w \sim 7.0 \times 10^4$  g/mol), poly(allylamine hydrochloride) (PAH,  $M_w \sim 7.0 \times 10^4$  g/mol), sodium 3-mercapto-1-propanesulfonate, 3-aminopropyltrimethoxysilane, ferric chloride ( $\text{FeCl}_3$ ) were obtained from Aldrich and used as received.

**Synthesis of isocyanate-terminated trichlorosilane 3** 10-undecenoyl chloride **1** ( $\text{C}_{11}\text{H}_{19}\text{OCl}$ , 25.0 g, 0.123 mol) were added dropwise to 1:1 solution mixture of  $\text{CH}_3\text{CN}$ -THF (100 mL) containing sodium azide ( $\text{NaN}_3$ , 10.0 g, 0.154 mol). NMR showed complete conversion of the acyl chloride after 24 h. NMR and FTIR suggested a Curtius rearrangement reaction at room temperature to isocyanate compound **2** at 50% conversion from the corresponding acyl azide. After removing the solvent, the acyl azide and isocyanate mixture was heated at  $80^\circ\text{C}$  in 30 mL dry toluene for 4 days to complete the Curtius rearrangement.<sup>30</sup> After distillation, isocyanate compound **2** (4.28 g, 0.024 mol) was silanized using trichlorosilane (9.44 mL, 12.7 g, 0.094 mol) in the presence of a Pt catalyst in dry toluene (10 mL) at room temperature for five weeks. NMR showed over 93% conversion and the product **3** (6.69 g, 89.6% yield) was purified by removing all the unreacted trichlorosilane and solvent through a vacuum condensation procedure. All the reactions were conducted under argon atmosphere using a Schlenk line.

**Multilayer fabrication** Multilayers were deposited on quartz slides, silicon wafers, quartz crystal microbalance (QCM) electrodes, Indium Tin Oxide (ITO) substrates, gold electrodes and gold substrates with microcontact printed hydrophobic/hydrophilic patterns. Quartz slides, silicon wafers and ITO substrates were cleaned by immersing them into a mixture of  $\text{H}_2\text{O}$ ,  $\text{H}_2\text{O}_2$  and  $\text{NH}_4\text{OH}$  with a volume ratio of 5:1:1 for 20 minutes followed by extensive rinsing with MilliQ and drying under a nitrogen stream. Gold and QCM electrodes were cleaned with Piranha solution ( $\text{H}_2\text{SO}_4$  and  $\text{H}_2\text{O}_2$  with a volume ratio of 7:3), washed with MilliQ, and dried by nitrogen. *Caution! Piranha is highly corrosive, reacts violently with organic materials, and should be handled with utmost care!* Except for the gold electrodes and ITO substrates, the cleaned substrates were first dipped into a PEI solution ( $\sim 10$  mM) for 30 minutes to impart positive charges onto the substrates. The cleaned gold electrodes were first immersed in an aqueous solution of sodium 3-mercapto-1-propanesulfonate ( $\sim 0.1$  mM) to impart negative charges onto the substrates. The cleaned ITO substrates were first immersed in a toluene solution of 3-aminopropyltrimethoxysilane (10 mM) to impart positive charges onto the substrates. Patterned gold and silicon substrates were obtained by microcontact printing using PDMS stamps. In a typical printing procedure, the stamps were inked with a thiol (in

ethanol) or silane (in dry toluene) solution (1 ~ 10 mM) before brought into contact with the cleaned substrates. After removal of the stamps, the substrates were immersed into a backfilling or an ethylene glycol solution (1 mM) for further reactions. The (modified) substrates were alternatively immersed in the polycation and polyanion aqueous solutions (2 mg/mL, 0-0.5 M NaCl) for 10 minutes, with rinsing, dipping into pure MilliQ (2 minutes), secondary rinsing and drying with a stream of nitrogen between each deposition step.

**Multilayer oxidation** Multilayers prepared on quartz slides and silicon substrates were exposed to FeCl<sub>3</sub> solution with varying periods. After oxidation the substrates were rinsed with, dipped into (2 minutes) and rinsed again with MilliQ before drying with a N<sub>2</sub> stream.

**Micromolding in capillaries (MIMIC)** PDMS stamps were treated with UV/ozone for 1 h in order to render hydrophilic surfaces. After oxidation, the stamps were stored in water in order to maintain their hydrophilicity.<sup>31</sup> In the patterning procedure, the stamps were dried under a N<sub>2</sub> stream before they were put in immediate contact with a continuous poly(ferrocenylsilane) multilayer prepared on silicon substrate. A drop of FeCl<sub>3</sub> solution (1 mM) was then placed in front of the stamp and a rapid filling of the channels was observed. After a few minutes, the stamps were removed and patterns were formed as a result of partial selective removal of PFS in the oxidant-filled microchannels.

**Characterization** UV/Vis spectra were recorded using a Varian Cary 300 Bio UV/Visible spectrophotometer. QCM measurements were performed with a HP-53131 frequency counter, a HP-4194A impedance analyzer, and a custom-made resonator circuit operated by a HP-E3620A power supply. Double sides of the QCM electrode were covered with polyelectrolyte multilayers. Mass changes were calculated from the Sauerbrey equation. Multilayer film thickness was obtained using spectroscopic ellipsometry. Multilayer films were deposited on silicon substrates containing a thin oxide layer plus the predeposited PEI layer and analyzed on a Woollam VASE ellipsometer (rotating analyzer configuration). Spectra were obtained in the wavelength region between 270 and 1550 nm at three different incident angles of 65°, 70° and 75°. The thickness of the bilayer assemblies was obtained by fitting the spectra to a five-layer model consisting of a substrate, a silicon oxide layer with thickness of 1.70 nm, a predeposited layer with thickness of 0.63 nm, and a PFS layer with thickness  $d_{PFS}$  in contact with air. The thickness data were obtained by evaluating the optical constants at every energy/wavelength with the film thickness as a fit parameter. Atomic force microscopy (AFM) experiments were performed by using a NanoScope IIIa multimode AFM (Veeco-Digital Instruments, Santa Barbara, CA) in tapping mode using silicon cantilevers (Nanosensors, Wetzlar, Germany) at room temperature, in air. Cyclic voltammetry (CV) measurements were carried out on an Autolab PGSTAT10 (Ecochemie, Utrecht, The Netherlands) potentiostat in a three-electrode configuration. The gold or ITO substrates acted as the working electrode, Hg/Hg<sub>2</sub>SO<sub>4</sub> (MSE) as the reference electrode (+ 0.61 V<sub>NHE</sub>), and Pt as the counter electrode. NaClO<sub>4</sub> aqueous solution (0.1 M) was used as the electrolyte. Prior to the measurements, the electrochemical cell was degassed by passing nitrogen through the electrolyte solution for five

minutes. Cyclic voltammograms were recorded between  $-0.4 V_{MSE}$  and  $+0.4 V_{MSE}$  at scan rates ranging from 10 to 50 mV/s. For electrochemical controlled release experiments, the cyclic voltammograms were recorded at a constant scan rate of 50 mV/s. A series of cyclic voltammograms were recorded after holding the oxidation potentials at different values for different time intervals. The amount of transferred charge  $Q$  was calculated based on the integration of the area under each cyclic voltammogram.

## 4.6 References and notes

1. Decher, G. *Science* **1997**, *277*, 1232.
2. Decher, G.; Schlenoff, J. B. (Eds.) *Multilayer Thin Films, Sequential Assembly of Nanocomposite Materials*, Wiley-VCH, Weinheim, Germany, **2003**.
3. Donath, E.; Sukhorukov, G. B.; Caruso, F.; Davis, S. A.; Möhwald, H. *Angew. Chem. Int. Ed.* **1998**, *37*, 2201.
4. Hempenius, M. A.; Robins, N. S.; Peter, M.; Kooij, E. S.; Vancso, G. J. *Langmuir* **2002**, *18*, 7629.
5. Lammertink, R. G. H.; Hempenius, M. A.; Chan, V. Z.-H.; Thomas, E. L.; Vancso, G. J. *Chem. Mater.* **2001**, *13*, 429.
6. Schanze, K. S.; Bergstedt, T. S.; Hauser, B. T.; Cavalaheiro, C. S. P. *Langmuir* **2000**, *16*, 795.
7. Manners, I. *Adv. Organomet. Chem.* **1995**, *37*, 131.
8. Sauerbrey, G. *Z. Phys.* **1959**, *155*, 206.
9. (a) Lvov, Y.; Decher, G.; Möhwald, H. *Langmuir* **1993**, *9*, 481; (b) Yang, H. C.; Aoki, K.; Hong, H. -G.; Sackett, D. D.; Arendt, M. F.; Yau, S.-L.; Bell, C. M.; Mallouk, T. E. *J. Am. Chem. Soc.* **1993**, *115*, 11855.
10. (a) Zhang, Y.; Tirrell, M.; Mays, J. W. *Macromolecules* **1996**, *29*, 7299; (b) Lösche, M.; Schmitt, J.; Decher, G.; Bouwman, W. G.; Kjaer, K. *Macromolecules* **1998**, *31*, 8893; (c) Dubas, S. T.; Schlenoff, J. B. *Macromolecules* **1999**, *32*, 8153.
11. (a) Ruths, J.; Essler, F.; Decher, G.; Riegler, H. *Langmuir* **2000**, *16*, 8871; (b) Steitz, R.; Leiner, V.; Siebrecht, R.; v. Klitzing, R. *Coll. Surf. A Physicochem. Eng. Aspects* **2000**, *163*, 63; (c) Steitz, R.; Jaeger, W.; v. Klitzing, R. *Langmuir* **2001**, *17*, 4471.
12. Kooij, E. S.; Wormeester, H.; Brouwer, E. A. M.; van Vroonhoven, E.; van Silfhout, A.; Poelsema, B. *Langmuir* **2002**, *18*, 4401.
13. Clark, S. L.; Hammond, P. T. *Adv. Mater.* **1998**, *10*, 1515.
14. Hammond, P. T. *Adv. Mater.* **2004**, *16*, 1271.
15. Xia, Y.; Whitesides, G. M. *Angew. Chem. Int. Ed.* **1998**, *37*, 550.
16. Hammond, P. T.; Whitesides, G. M. *Macromolecules* **1995**, *28*, 7569.
17. Yang, S. Y.; Rubner, M. F. *J. Am. Chem. Soc.* **2002**, *124*, 2100.

18. Hua, F.; Shi, J.; Lvov, Y.; Cui, T. *Nano Lett.* **2002**, *2*, 1219.
19. Park, J.; Hammond, P. T. *Adv. Mater.* **2004**, *16*, 520.
20. (a) Clark, S. L.; Montague, M.; Hammond, P. T. *Supramolecular Science* **1997**, *4*, 141; (b) Clark, S. L.; Montague, M. F.; Hammond, P. T. *Macromolecules* **1997**, *30*, 7237.
21. Pomerantz, M.; Segmüller, A.; Netzer, L.; Sagiv, J. *Thin Solid Films* **1985**, *132*, 153.
22. Pallandre, A.; Glinel, K.; Jonas, A. M.; Nysten, B. *Nano Lett.* **2004**, *4*, 365.
23. (a) Xia, Y.; Mrksich, M.; Kim, E.; Whitesides, G. M. *J. Am. Chem. Soc.* **1995**, *117*, 9576; (b) Wang, D.; Thomas, S. G.; Wang, K. L.; Xia, Y.; Whitesides, G. M. *Appl. Phys. Lett.* **1997**, *70*, 1593; (c) Pompe, T.; Fery, A.; Herminghaus, S.; Kriele, A.; Lorenz, H.; Kotthaus, J. P. *Langmuir* **1999**, *15*, 2398.
24. (a) Wang, R. L. C.; Kreuzer, H. J.; Grunze, M. *J. Phys. Chem. B* **1997**, *101*, 9767; (b) Harder, P.; Grunze, M.; Dahint, R.; Whitesides, G. M.; Laibinis, P. E. *J. Phys. Chem. B* **1998**, *102*, 426.
25. Kumar, A.; Whitesides, G. M. *Appl. Phys. Lett.* **1993**, *63*, 2002.
26. (a) Foucher, D.; Ziembinski, R.; Petersen, R.; Pudelski, J.; Edwards, M.; Ni, Y.; Massey, J.; Jaeger, C. R.; Vancso, G. J.; Manners, I. *Macromolecules* **1994**, *27*, 3992; (b) Rulkens, R.; Lough, A. J.; Manners, I.; Lovelace, S. R.; Grant, C.; Geiger, W. E. *J. Am. Chem. Soc.* **1996**, *118*, 12683; (c) Péter, M.; Hempenius, M. A.; Kooij, E. S.; Jenkins, T. A.; Roser, S. J.; Knoll, W.; Vancso, G. J. *Langmuir* **2004**, *20*, 891.
27. It has been observed that for each PFS multilayer sample, except for the first CV scan, all the rest of a series of continuous scans could be superimposed very well. The oxidation and reduction waves of the first cyclic voltammogram was not symmetric, and the area under the oxidation wave is larger compared to the other scans. Ellipsometry and UV/Vis spectroscopy have detected a multilayer “thinning” phenomenon after electrochemical oxidation. Yet the exact mechanism, whether this is related to certain material loss or simply a multilayer re-organization, has not been clarified.
28. Boulmedais, F.; Tang, C. S.; Keller, B.; Vörös, J. *Adv. Funct. Mater.* **2006**, *16*, 63.
29. Péter, M. *Engineering of Surfaces with Organometallic Poly(ferrocenylsilanes)*, PhD Thesis, University of Twente, **2002**, ISBN 90 3651715x.
30. Brady, A. C.; Hodder, B.; Martin, A. S.; Sambles, J. R.; Ewels, C. P.; Jones, R.; Briddon, P. R.; Musa, A. M.; Panetta, C. A.; Mattern, D. L. *J. Mater. Chem.* **1999**, *9*, 2271.
31. Li, X.-M.; Péter, M.; Huskens, J.; Reinhoudt, D. N. *Nano Lett.* **2003**, *3*, 1449.





# Chapter 5

## Redox-Responsive Free-Standing Poly(ferrocenylsilane) Multilayer Microcapsules\*

*Free-standing microcapsules were fabricated from the electrostatic layer-by-layer self-assembly of poly(ferrocenylsilane) polyelectrolytes onto curved substrates followed by core dissolution. Optimal preparation conditions were established in order to obtain microcapsules with desired properties. The responsive molecular permeability of these full organometallic as well as organometallic/organic hybrid microcapsules under a redox stimulus was studied in detail. A combination of electrostatic forces and polymer solubility variations was found to be responsible for the peculiar permeability response of the poly(ferrocenylsilane) microcapsules.*

### 5.1 Introduction

Apart from substrate-supported planar films, various forms of free-standing flexible nanostructures prepared by the layer-by-layer electrostatic self-assembly have shown promising application potentials, such as in sensing, nanofabrication, controlled release, biomimics and tissue engineering.<sup>1,2</sup> Incorporating “smart” polymers, *i.e.* polymers that can respond to external stimuli, such as changes in temperature, light and chemical environment with strong and non-linear changes in size and conformation,<sup>3</sup> into free-standing polyelectrolyte multilayers presents significant promise in broadening their potential applications.<sup>4</sup> Since its introduction in 1998, polyelectrolyte multilayer microcapsules have constituted the most studied free-standing multilayer structures. Many stimuli-responsive polymeric microcapsule systems have been proposed in the past decade. Nevertheless, conventional organic polyelectrolyte based microcapsules have shown their limitations in some significant applications due to their slow response to trace amounts of trigger or restricted freedom of choice of stimuli.<sup>5</sup> Among various stimuli, electrochemical stimuli

---

\* Part of the work described in this Chapter has been or will be published: Ma, Y.; Dong, W.-F.; Hempenius, M. A.; Möhwald, H.; Vancso, G. J. *Nat. Mater.* **2006**, *5*, 724; Ma, Y.; Dong, W.-F.; Kooij, E. S.; Hempenius, M. A.; Möhwald, H.; Vancso, G. J. *Soft Matt.* **2007**, *3*, 889; Ma, Y.; Hempenius, M. A.; Kooij, E. S.; Dong, W.-F.; Möhwald, H.; Vancso, G. J. in Förch, Schönherr, Jenkins (Eds.) *Surface Design: Applications in Bioscience and Nanotechnology*, Wiley-VCH, Weinheim, Germany, **2008**, submitted.

possess the unique promise of realizing a localized trigger. Recently, Shchukin *et al.* have demonstrated an application of polyelectrolyte microcapsules as microcontainers with electrochemically reversible flux of redox-active materials.<sup>6,7</sup> However, constructing capsules featuring redox-responsive compounds in the wall has still rarely been discussed.

In the previous Chapters, the reversible redox properties of water-soluble poly(ferrocenylsilane) (PFS) bulk solutions and substrate-supported multilayer assemblies have been demonstrated. In this Chapter, discussions will be focused on a new form of multilayer structure, *i.e.* free-standing microcapsules. Microcapsules made from PFS polyelectrolytes may serve as a unique polymeric microcontainer system that could specifically respond to redox-stimuli. In order to obtain microcapsules with desired properties leading toward their “smart” applications, one of the prerequisites is to understand their structure-permeability relationship. Thus, the quality, *i.e.* integrity, yield and stability of these capsules was first studied by varying the fabrication procedure (*e.g.* choice of core material and corresponding dissolution protocols) as well as the multilayer wall thickness (number of bilayers). Furthermore, the dependence of capsule permeability to a certain molecular probe, *i.e.* tetramethylrhodamine isothiocyanate (TRITC) labelled dextran ( $4.4 \times 10^3$  g/mol), on capsule wall thickness was also studied by confocal laser scanning microscopy (CLSM). In this way, the optimal conditions for the fabrication of intact PFS microcapsules as well as essential elements of structure-property relationship of these capsules were established.

Later on, studies on the stimuli-responsive properties of PFS multilayer microcapsules were carried out by exposing them to chemical oxidants (*e.g.* iodine and ferric chloride,  $\text{FeCl}_3$ ) and reducing agents. Moreover, composite-wall multilayer capsules featuring PFS components in the inner-wall and organic redox-inert polyelectrolyte species poly(styrene sulfonate) ( $\text{PSS}^-$ ) and poly(allylamine hydrochloride) ( $\text{PAH}^+$ ) on the outer-wall were fabricated as a means to manipulate the size-controlled responsive permeability of polyelectrolyte microcapsules on a molecular level. Since a redox trigger can also be realized electrochemically, the electrochemical redox-responsive behaviour of PFS-containing microcapsules was also studied. Finally, the permeability responses of hybrid microcapsules of  $(\text{PSS}^-/\text{PFS}^+)_5$  and  $(\text{PFS}^-/\text{PAH}^+)_5$  were investigated in order to fully understand the mechanism of redox-triggered capsule permeability variations.

## 5.2 Microcapsule fabrication

### 5.2.1 Core material and capsule formation

Using water-soluble poly(ferrocenylsilane) polycation **4** and polyanion **5** (see molecular structures in Chapter 3), the same conditions that allowed us to deposit thick multilayers from polyelectrolyte solutions containing relatively high NaCl concentrations (0.5

M) were used to fabricate PFS<sup>-</sup>/PFS<sup>+</sup> multilayers onto colloidal templates.<sup>8</sup> The first attempt in fabricating hollow PFS capsules was to use melamine formaldehyde (MF) colloidal particles as templates followed by core removal with hydrochloric acid (HCl).<sup>9</sup> The electrostatic layer-by-layer assembly process was monitored by electrophoretic mobility measurements. Figure 5.1 summarizes the changes in zeta( $\zeta$ )-potential recorded upon layer deposition for polyanion/polycation pairs (in the sequence of (PSS<sup>-</sup>/PAH<sup>+</sup>)<sub>2</sub>(PFS<sup>-</sup>/PFS<sup>+</sup>)<sub>3</sub>) on MF cores. The alternation of the  $\zeta$ -potential between positive and negative values indicated the successful charge reversal of the particle surface during the layer-by-layer sequential deposition.<sup>10</sup>

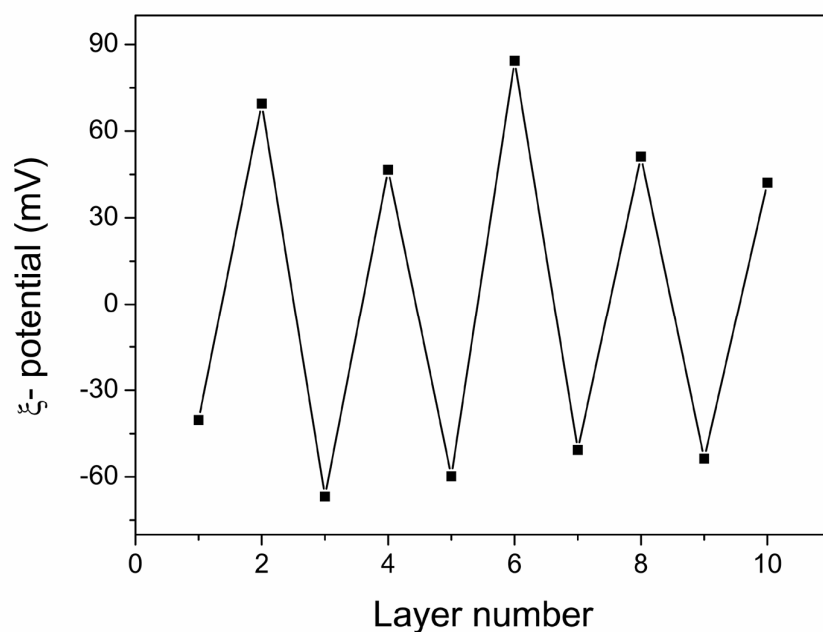


**Figure 5.1**  $\zeta$ -potential measurements following the LBL deposition of polyions (in the sequence of (PSS<sup>-</sup>/PAH<sup>+</sup>)<sub>2</sub>(PFS<sup>-</sup>/PFS<sup>+</sup>)<sub>3</sub>) on MF cores.

After removing the MF cores by HCl (pH = 1.0) and subsequently performing several rinsing steps, UV/Vis measurements were carried out on the aqueous dispersion of the obtained capsules ((PSS<sup>-</sup>/PAH<sup>+</sup>)<sub>2</sub>(PFS<sup>-</sup>/PFS<sup>+</sup>)<sub>3</sub> capsule wall structure). As shown in Figure 5.2, the absorbance characteristic of PFS was observed as an intense ligand-to-metal charge-transfer transition at  $\lambda = 216$  nm, in accordance with former results on planar PFS polyelectrolyte multilayer films.<sup>11, 12</sup> In addition, the slowly precipitated capsules showed a yellow colour, indicating the presence of ferrocene-containing material in the capsule wall.

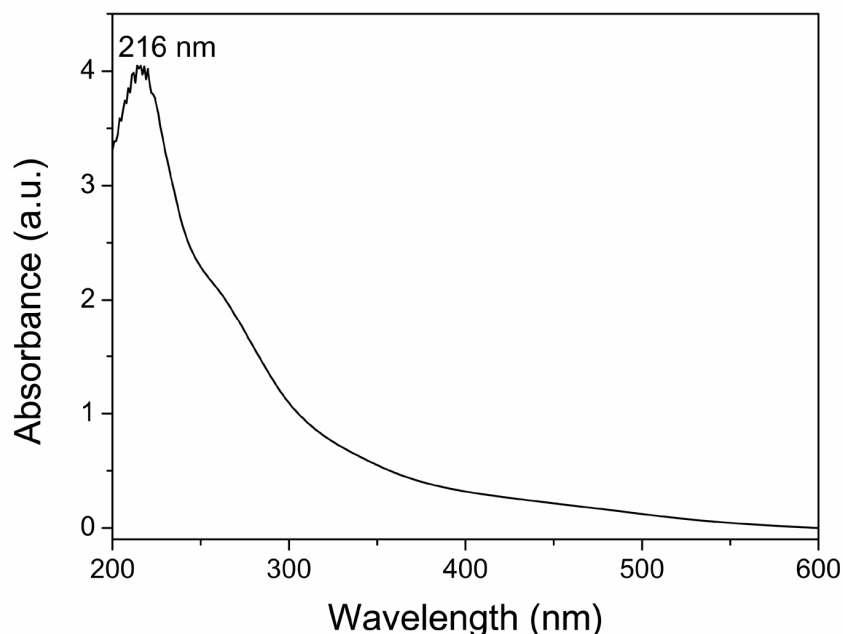


**Figure 5.2** UV/Vis spectrum of the aqueous dispersion of  $(\text{PSS}^-/\text{PAH}^+)_2(\text{PFS}^-/\text{PFS}^+)_3$  capsules. The strong absorbance at  $\lambda = 216$  nm is characteristic for PFS.

However, a drawback in using MF templates is that the strong acid treatment (pH = 1),<sup>13</sup> required to remove the core material, may have some influence on the macromolecular structure of PFS.<sup>14</sup> Although hollow capsules have been successfully obtained by using MF particles as the template, the fast core dissolution process tends to disrupt the multilayer wall structure due to the abrupt rising of osmotic pressure from the microcapsule interior.<sup>15</sup> This is demonstrated by confocal laser scanning microscope (CLSM) studies on the capsule dispersions in the presence of different fluorescence labelled probe molecules. In Figure 5.3, representative CLSM images of  $(\text{PSS}^-/\text{PAH}^+)_2(\text{PFS}^-/\text{PFS}^+)_3$  capsule dispersion mixed with tetramethylrhodamine isothiocyanate (TRITC) and fluorescein isothiocyanate (FITC) labelled dextran ( $M_w = 6.6 \times 10^4$  g/mol) are shown. Although intact capsules could be identified from the population, most of the capsules were found deformed or broken. The non-broken capsules display complete permeability to small TRITC molecules (Figure 5.3A) but were essentially non-permeable to the  $6.6 \times 10^4$  g/mol dextran molecules (Figure 5.3B). This is in accordance with the common semi-permeable characteristics of polyelectrolyte multilayer capsules (see also Chapter 2).<sup>16</sup>

The broken capsules in the dry state can also be visualized by AFM as shown in Figure 5.4. Obviously the openings present in the wall of both  $(\text{PSS}^-/\text{PAH}^+)_2(\text{PFS}^-/\text{PFS}^+)_3$  and  $(\text{PSS}^-/\text{PAH}^+)_5(\text{PFS}^-/\text{PFS}^+)_3$  microcapsules contributed to their deformation and permeability when characterized by CLSM (Figure 5.3B).

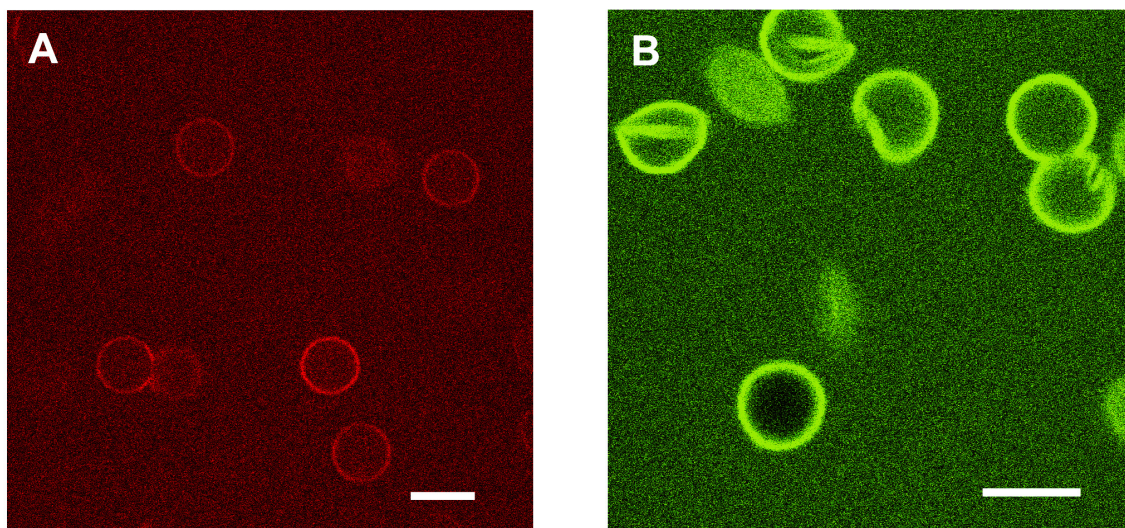


**Figure 5.3** CLSM images of  $(\text{PSS}^-/\text{PAH}^+)_2(\text{PFS}^-/\text{PFS}^+)_3$  microcapsules based on MF cores in the presence of (A) TRITC and (B) FITC-dextran ( $6.6 \times 10^4$  g/mol). Scale bar is  $5 \mu\text{m}$  for both images.

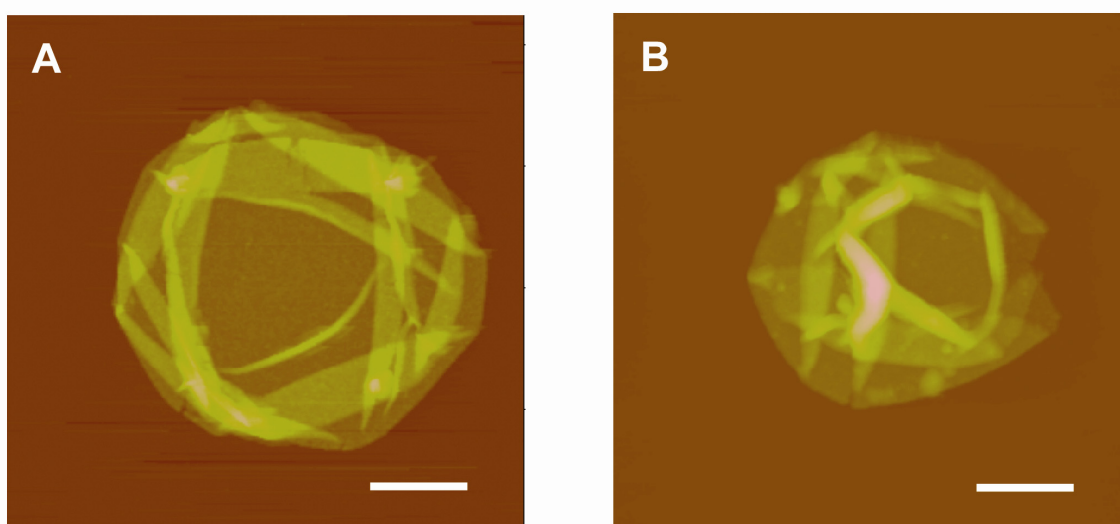


**Figure 5.4** Representative tapping mode AFM height images of (A)  $(\text{PSS}^-/\text{PAH}^+)_2(\text{PFS}^-/\text{PFS}^+)_3$  (z range is 600 nm) and (B)  $(\text{PSS}^-/\text{PAH}^+)_5(\text{PFS}^-/\text{PFS}^+)_3$  (z range is  $1.2 \mu\text{m}$ ) microcapsules fabricated from MF particles on a freshly cleaved mica surface. Scale bar is  $1 \mu\text{m}$  for both images.

Complementary to the MF cores, more stable microcapsules of better quality, solely composed of PFS polyanions and polycations, were fabricated in high yield using manganese carbonate ( $\text{MnCO}_3$ ) templates (average diameter,  $5\text{-}10 \mu\text{m}$ ). Metal carbonate crystals that can be removed by ethylenediaminetetraacetic acid (EDTA) solutions have been extensively employed in recent years due to their relative ease of synthesis, dissolution in mild conditions and suitability in the fabrication of clean capsules.<sup>17, 18</sup> These  $\text{MnCO}_3$  microparticles were prepared by the so-called colloidal aggregation method, using ethanol as the poor solvent in the precipitation process.<sup>17</sup> It has been reported that ethanol can provide effective control over

the crystallization process, leading to  $\text{MnCO}_3$  crystals with desired size and size distribution.<sup>17</sup> Figure 5.5A shows an example of a typical scanning electron micrograph (SEM) of the  $\text{MnCO}_3$  templates used in this study. The stability and spherical shape of these colloidal particles make them good candidates for the preparation of microcapsules. Upon completion of the layer-by-layer deposition, the templates were dissolved in a pH-neutral aqueous environment using 0.2 M EDTA solutions. After thorough cleaning, intact (non-broken) capsules were obtained in high yield. In Figure 5.5B, a typical CLSM image of PFS capsules made of five bilayers of PFS polyanions and rhodamine-labelled PFS polycations (Chapter 3) is displayed. The spherical shape of the  $\text{MnCO}_3$  cores has been preserved, and the average size of a typical batch of capsules ( $8.9 \pm 1.0 \mu\text{m}$ ) matches that of the templates ( $8.5 \pm 1.3 \mu\text{m}$ ), within the experimental error.

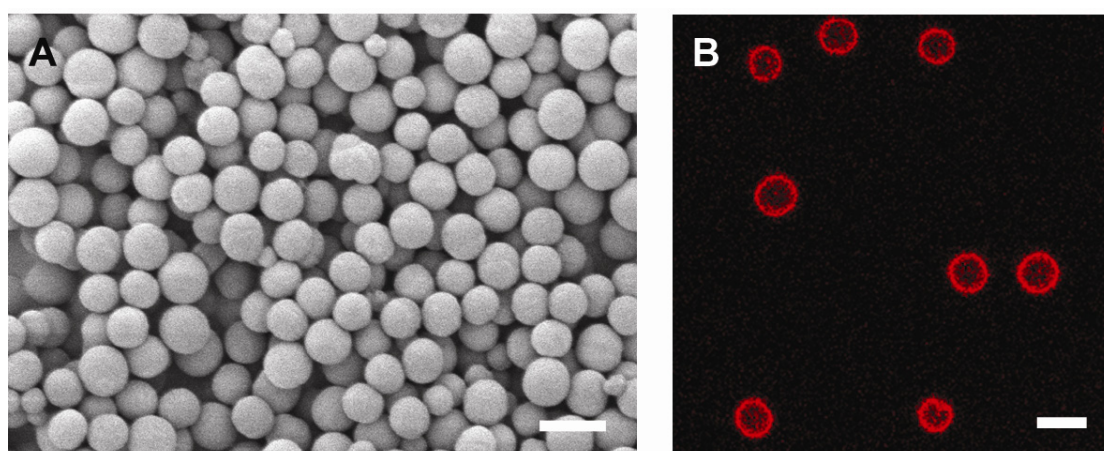


**Figure 5.5** (A) A scanning electron micrograph (SEM) of manganese carbonate ( $\text{MnCO}_3$ ) microparticles prepared by the colloidal aggregation method. (B) A confocal laser scanning micrograph (CLSM) of  $(\text{PFS}^-/\text{PFS}^+)_5$  microcapsules using  $\text{MnCO}_3$  particles as the core material followed by template removal using EDTA. Rhodamine-labelled  $\text{PFS}^+$  was used to directly visualize the capsules. Scale bar =  $10 \mu\text{m}$  for both images.

### 5.2.2 Capsule wall thickness

In order to study capsule permeability response, it is a prerequisite to establish the multilayer growth regime where the permeability of capsules (to a certain probe) can be predicted. It is reported that the wall thickness and permeability of hollow capsules are a function of the deposited number of polyelectrolyte bilayers and solution salt concentration. The mechanical strength of the capsules originates from the ionically crosslinked polymer chains in the wall. The integrity of the capsules depends on whether the mechanical strength of the capsule wall can withstand the osmotic stress accompanying core dissolution.<sup>19</sup> The influence of capsule wall thickness on the integrity and permeability behaviour of microcapsules is clearly demonstrated in Chapter 5.2.3 (*vide infra*).

In this work, PFS capsules with different wall thickness (varying numbers of deposited polyelectrolyte bilayers) were fabricated and the shell thickness in the dry state was

measured by tapping mode AFM, using a method described in detail elsewhere.<sup>20</sup> Briefly, a drop of capsule dispersion was first dried on freshly-cleaved mica, then the minimum height in the fold-free region was measured and taken as twice the wall thickness. Figure 5.6 displays an example of a dried capsule with four bilayers of PFS polyanion/polycation. An average bilayer (PFS<sup>-</sup>/PFS<sup>+</sup>) thickness of  $6.0 \pm 0.3$  nm for assembly from 0.5 M NaCl was calculated. This value was larger than the typical bilayer thickness ( $\sim 4.5$  nm) obtained on planar (silicon or gold) substrates under similar adsorption conditions. A possible explanation for this variation in film thickness may be related to the dependence of multilayer film growth on the characteristics of the templating materials, *e.g.* on surface charge density.<sup>21</sup> The surface of the collapsed capsules, as shown in AFM images, exhibited a roughness (rms, in an area of  $3 \times 3 \mu\text{m}^2$ ) of  $\sim 5$  nm, which was significantly larger than the respective rms values obtained for multilayer films on planar substrates, which were in the sub nm range (see Chapter 4).

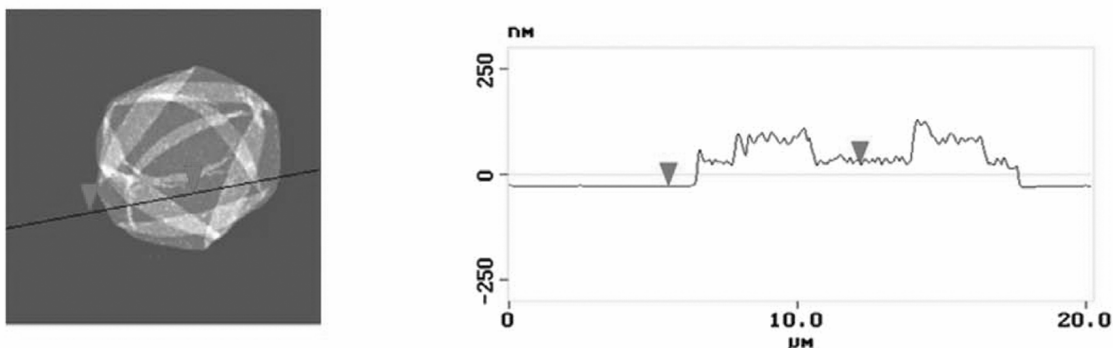


**Figure 5.6** PFS capsule wall thickness measured by TM-AFM (four bilayers of (PFS<sup>-</sup>/PFS<sup>+</sup>)), the AFM thickness of the capsules is measured by the difference in the heights labelled by the arrows in the Figure.

In Figure 5.7, the increase of capsule wall thickness and corresponding bilayer thickness as a function of the number of bilayers are presented. Due to the instability of capsules with less than three polyelectrolyte bilayers (*vide infra*), film thickness data corresponding to bilayer numbers of one and two were not available. As shown in Figure 5.7B, the calculated corresponding PFS<sup>-</sup>/PFS<sup>+</sup> bilayer thickness is not constant when the capsule wall is composed of different numbers ( $n = 3-6$ ) of bilayers. If the film growth is linear, a constant value of thickness/bilayer would be expected. However, the plot of bilayer thickness versus the number of deposited bilayers (Figure 5.7B) does show a trend towards a linear growth regime when the number of adsorbed bilayers ( $n$ ) is larger than four. A similar trend has also been reported before for capsules made from the commonly-used polyion pair PSS/PAH,<sup>19</sup> where a transition from a loosely packed to a more condensed film upon increasing the wall thickness was observed.

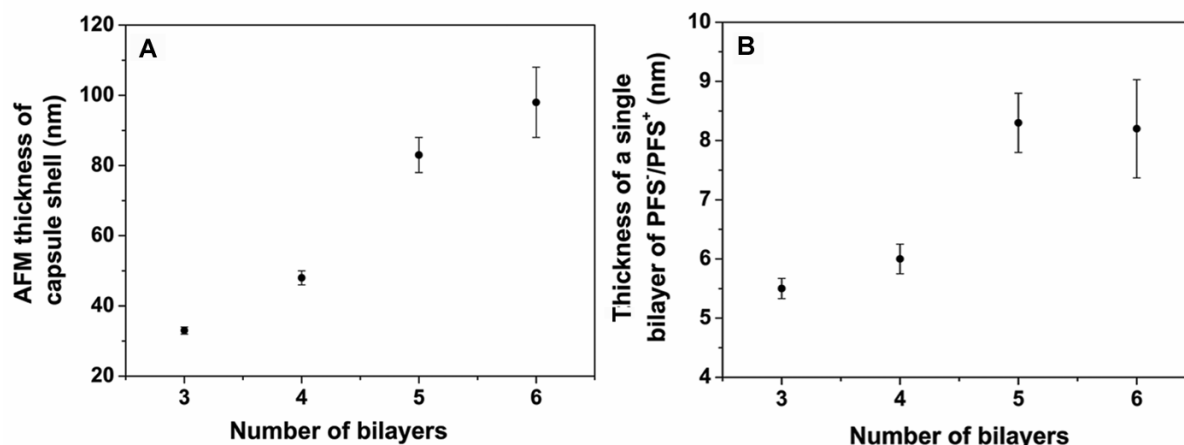


**Figure 5.7** (A) PFS capsule wall thickness and (B) average bilayer thickness dependence on the number of bilayers.

### 5.2.3 Capsule integrity and permeability

Permeability of multilayer microcapsules is governed by a combination of hydrodynamic sieving, electrostatic interactions, and Donnan effects in the polymeric shell.<sup>13</sup> A direct visualization of capsule permeability is often realized by measuring the equilibrium distribution of fluorescence-labelled probe molecules of varying sizes across the intact capsule wall. The molecular probe chosen for this study is TRITC-labelled dextran ( $M_w \sim 4.4 \times 10^3$  g/mol), which has a hydrodynamic radius of 2.1 nm and a diffusion coefficient of  $1.1 \times 10^{-10}$  m<sup>2</sup>/s in water.<sup>19</sup> Dextran was chosen due to its charge-neutral nature and stable spherical shape in water.<sup>22</sup>

The dependence of capsule integrity and permeability on the number of deposited polyelectrolyte bilayers is shown in Figure 5.8. Capsules with the same average size (around 10  $\mu$ m) but different wall thickness values show different degrees of integrity and permeability to the same molecular probe. Most of the capsules containing less than four bilayers of PFS polyions are permeable to the dextran probe molecules (Figure 5.8A and B), with the number of broken capsules decreasing with increasing the total bilayer numbers. Again, stable and impermeable capsules were obtained when the bilayer number is higher than four (see example of Figure 5.8C). Since the hydrodynamic radius of the probe molecules is 2.1 nm, the effective mesh size of impermeable PFS microcapsules must be smaller than this value. Compared to the capsules with the same number of bilayers prepared from MF cores (Figure 5.3), the yield of intact capsules is much higher for these wall thickness values. The impermeable quality of PFS microcapsules made of more than four bilayers of PFS polyion pairs obtained in the multilayer linear growth regime is one of the crucial prerequisites for their detailed stimuli-responsive permeability studies.



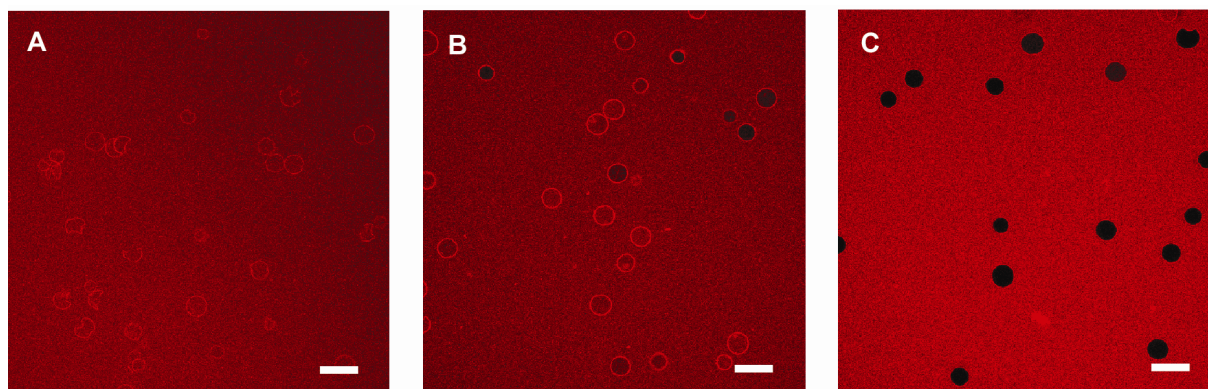


**Figure 5.8**  $(\text{PFS}^-/\text{PFS}^+)_n$  capsules visualized by CLSM: (A)  $n = 1$  ; (B)  $n = 3$ ; and (C)  $n = 6$ . The fluorescence probe was TRITC-dextran ( $M_w \sim 4.4 \times 10^3$  g/mol), and samples were all measured in fresh MilliQ water. With an increasing number of bilayers, capsules of the same mean size showed different permeability to dextran molecules. Stable and impermeable capsules were obtained when  $n > 4$ . All the capsules were prepared by the same procedure from 1 mg/mL PFS polyelectrolyte solutions containing 0.5 M NaCl. Scale bar = 20  $\mu\text{m}$  for all images.

### 5.3 Redox-responsive permeability

#### 5.3.1 Chemical oxidation

The unique chemical constitution of  $\text{PFS}^-/\text{PFS}^+$  capsules ensures their peculiar redox-responsive permeability. Two types of oxidants were used for the study of redox-responsive permeability of PFS microcapsules that are originally impermeable to the reference molecular probe (TRITC labelled dextran,  $4.4 \times 10^3$  g/mol). In the presence of the same probe molecules, CLSM was used to visualize the relative fluorescent intensity change in the capsule interior before and after mixing the capsule suspension with the aqueous oxidant solutions.

The first studied oxidant was iodine. In practice, an equal volume (10  $\mu\text{L}$ ) of PFS capsules (containing five or six bilayers of  $\text{PFS}^-/\text{PFS}^+$ ) aqueous dispersion was mixed with saturated iodine ( $\text{I}_2$ ) aqueous solution (with a small amount of KI to increase solubility) for overnight. TRITC-dextran was then mixed with these capsules before observation. Figure 5.9 shows the representative CLSM images of  $(\text{PFS}^-/\text{PFS}^+)_5$  capsules with and without iodine treatment. In the left image the unoxidized PFS capsules still preserve their impermeable nature three days after storage in water, with close to 90 percent of the capsules having no penetration of  $4.4 \times 10^3$  g/mol dextran molecules. The statistics also hold for the PFS capsules containing six bilayers of  $\text{PFS}^-/\text{PFS}^+$  in the wall. The percentage of impermeable capsules remained the same even when we mixed the fluorescence dye with the capsule dispersion for overnight. This also shows that these PFS capsules, with a relatively thick wall (over 40 nm), are very stable upon storage. The right image displays that after  $\text{I}_2$  treatment for a certain period, more capsules became permeable to the probe molecules. By counting the number of

impermeable capsules in at least 10 locations of the same scan area ( $240 \times 240 \mu\text{m}^2$ ), the statistics of the impermeable capsules were collected and depicted in the histogram in Figure 5.10. After different durations of treatment, the fractions of impermeable capsules made of five and six bilayers of PFS polyion pairs had decreased to 45% and 65%, respectively. Compared to the original percentage of impermeable capsules (90%), a significant fraction of the original impermeable capsules increased their permeability towards the same molecules after iodine treatment. This is an indication that iodine is capable of oxidizing PFS capsules. From the CLSM images there is no measurable size and shape difference of the capsules before and after iodine treatment.

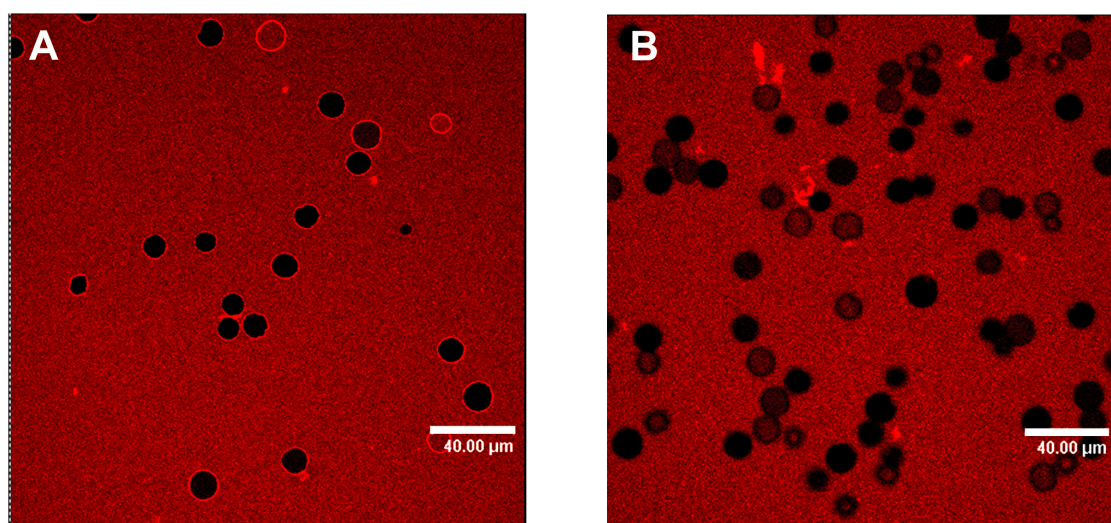


**Figure 5.9**  $(\text{PFS}^-/\text{PFS}^+)_5$  capsules that were (A) impermeable to TRITC-dextran ( $4.4 \times 10^3 \text{ g/mol}$ ) molecules became (B) partially permeable after iodine oxidation. Scale bar =  $40 \mu\text{m}$ .

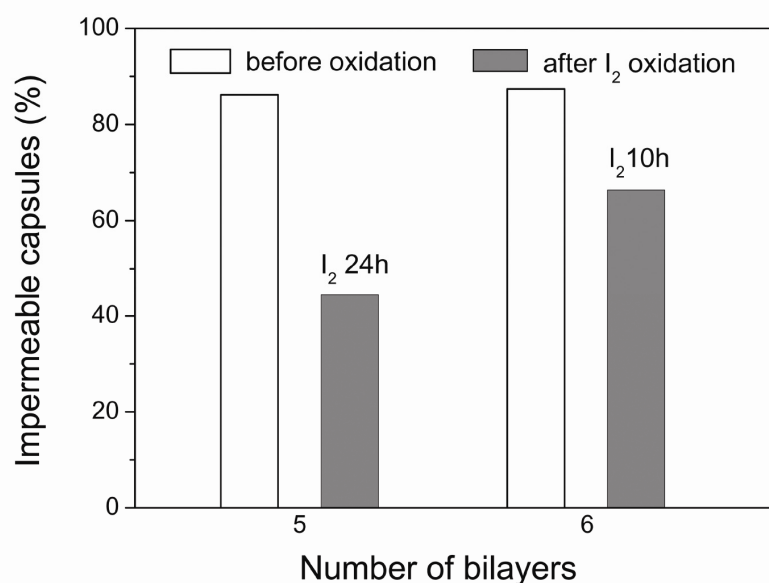


**Figure 5.10** Comparison of the percentage of impermeable capsules before and after oxidation. The statistics were collected by counting the numbers of permeable and impermeable capsules in at least 10 different locations of the same imaging area of different samples, respectively.

Although iodine is capable of oxidizing PFS and of tuning the permeability of PFS capsules, it appears to be not so efficient and the process is simply too slow. This is in accordance with previous bulk oxidation studies, where it is reported to be difficult to fully oxidize PFS by the use of  $I_2$ .<sup>23</sup> It was also observed that during the iodine treatment, some brown precipitants (possibly undissolved iodine) appeared in the capsule-oxidant mixture, and this could probably slow down the oxidation reaction even more.

Since ferric chloride ( $FeCl_3$ ) has been reported to be more effective in oxidizing PFS than iodine, the chemical oxidation study of PFS microcapsules was continued by using  $FeCl_3$  as the oxidant. In this way, a much more effective oxidation of the capsules was observed. Instead of incubation for overnight,  $FeCl_3$  aqueous solution (1 mM) was on-site added to the capsule-dye mixture during CLSM imaging. With the diffusion of the  $Fe^{3+}$  ions originating from the  $FeCl_3$  added, PFS capsules were observed to display a fast and continuous expansion. Figure 5.11 shows a series of CLSM micrographs of  $(PFS^-/PFS^+)_5$  capsules following the different stages of  $FeCl_3$  oxidation with time. The originally impermeable capsules started to expand and became permeable after mixing with  $FeCl_3$  for seven minutes. The swelling continued for the majority of the capsules (over 90%) for approximately another five minutes, until their final disintegration. Before their disintegration, the oxidized capsules also became completely permeable to  $4.4 \times 10^3$  g/mol TRITC-dextran molecules, as the fluorescence intensity from outside and inside the capsules could no longer be differentiated. It should be noted that permeability was statistically defined and the overall permeability was referred to a situation where  $\geq 90\%$  capsules displayed the same quality. Control experiments showed that the permeability and integrity of the capsules remain unchanged when mixed with hydrochloric acid solutions of similar pH value (pH  $\sim 4$ ) for at least several hours.

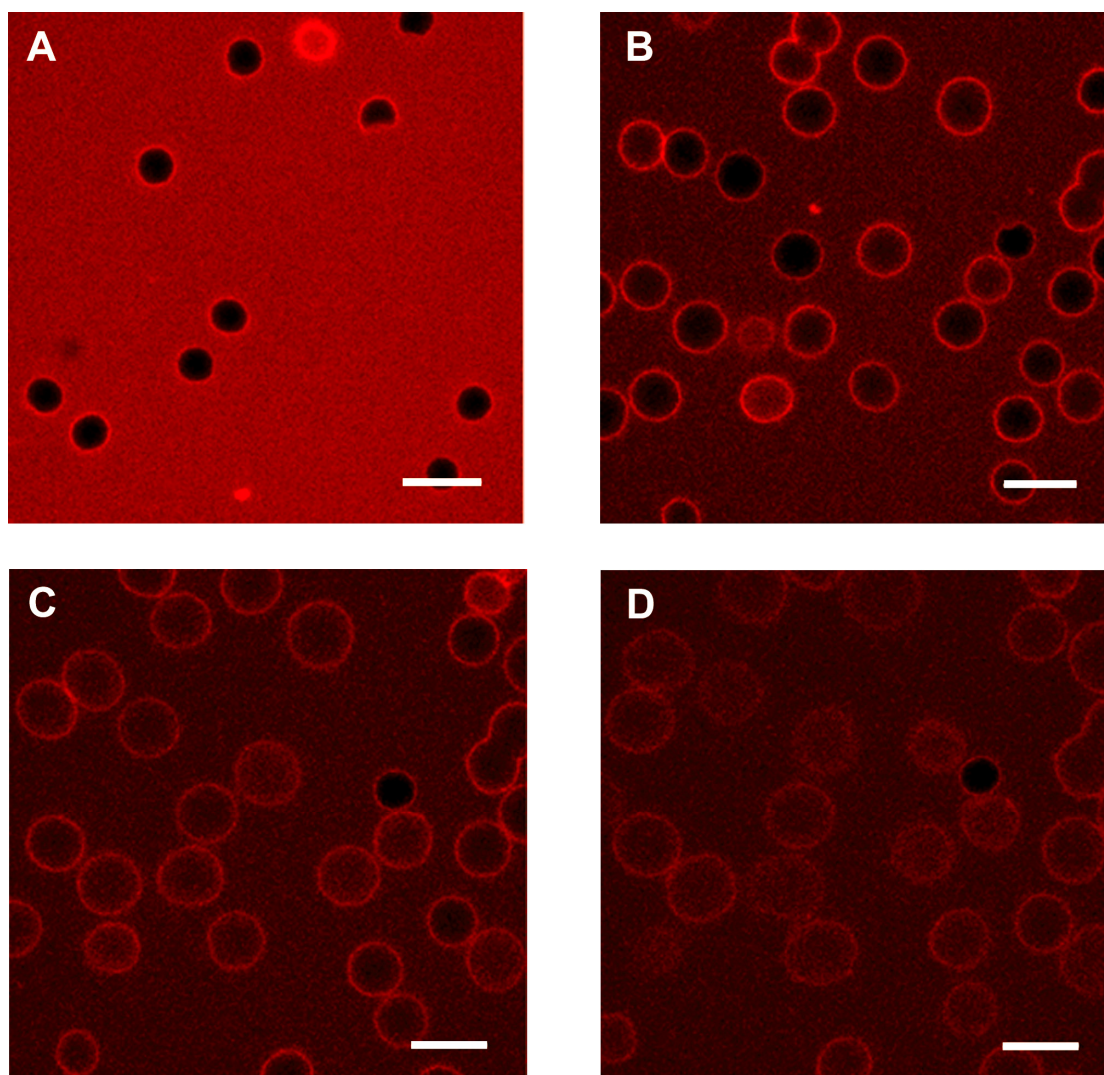


**Figure 5.11** Examples of representative confocal laser scanning micrographs of (PFS<sup>-</sup>/PFS<sup>+</sup>)<sub>5</sub> microcapsules in the presence of TRITC-dextran ( $4.4 \times 10^3$  g/mol) at (A) 0 min; (B) 7 min; (C) 8 min; (D) 9 min after the addition of FeCl<sub>3</sub> (1 mM) aqueous solutions. Capsules show increasing permeability to TRITC-dextran ( $4.4 \times 10^3$  g/mol) molecules with time and increase their size as the oxidation proceeds. Scale bar = 15  $\mu$ m.

The remarkable swelling and disintegration of these capsules turned out to be independent on capsule wall thickness, since a similar redox-response was also observed when the number of absorbed PFS bilayers was increased to six. For example, the expansion and disintegration process of a microcapsule sample featuring a six bilayer PFS<sup>-</sup>/PFS<sup>+</sup> capsule wall was monitored as a function of time to describe the kinetics of the capsule swelling under these conditions. The oxidation-induced expansion sets in following a certain induction period<sup>24</sup> at room temperature (see also the above example). Since the redox switching of PFS has been observed to occur within seconds, the induction period was considered to be a result of a slow diffusion of the Fe<sup>3+</sup> ions to the location of the capsules and to the capsule interior. After the induction period, data were collected on the mean diameter values of the capsules from the onset of adding FeCl<sub>3</sub> until the final disappearance of the capsules. The degree of capsule expansion was calculated (averaged over a population of *ca.* 20 capsules) as:

$$\text{capsule expansion (\%)} = \frac{\overline{d_t - d_0}}{d_0} \times 100\%$$

where  $d$  is the diameter of the capsules observed by CLSM, with subscripts  $0$  and  $t$  denoting values prior to and at “ $t$ ”, respectively. Figure 5.12 summarizes the expansion data as a function of time.

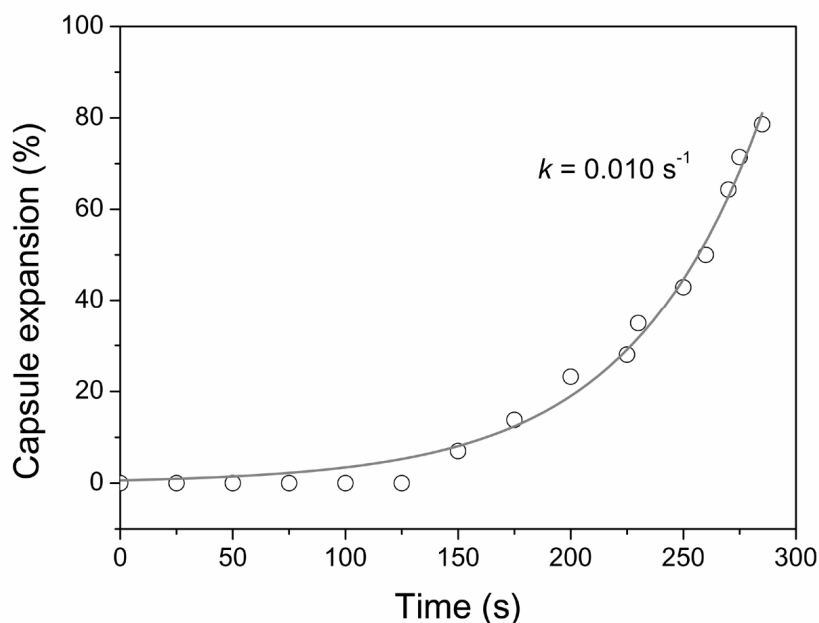


**Figure 5.12** (PFS<sup>-</sup>/PFS<sup>+</sup>)<sub>6</sub> capsule expansion with time in the final FeCl<sub>3</sub>-oxidized states. The circles represent the experimental data and the line is an exponential fit, which gives a first-order expansion rate constant  $k = 0.01 \text{ s}^{-1}$  for the example shown.

The open circles in Fig. 5.12 represent the experimental data that were fitted by a simple exponential growth curve as depicted by the black line. The data indicate that the capsules expand in an accelerated manner towards the final disintegration, following kinetics similar to a first-order process, and the rate law can be described as:

$$\frac{A}{A_0} \sim e^{kt}$$

with  $k$  as the rate constant. A fit of the data resulted in a typical  $k$ -value of  $0.010 \text{ s}^{-1}$  in the present case, and this value was found to strongly depend on the concentration of the oxidant. Our study on the local oxidation of (PFS<sup>-</sup>/PFS<sup>+</sup>)<sub>5</sub> capsules showed that when the concentration of the FeCl<sub>3</sub> solutions decreased from 3 to 1 mM, the duration of complete capsule disintegration increased from 2 to 15 minutes (*vide infra*). These times are more than one order of magnitude shorter than those measured for main chain scission (see Chapter 3).

### 5.3.2 Chemical reduction

The fully reversible redox chemistry of PFS provides the possibility to control microcapsule permeability response by the use of PFS reducing agents. The stoichiometry of oxidant ( $\text{FeCl}_3$ ) and reducing agents is assumed to be 2:1 since the oxidation of vitamin C and dithiothreitol (DTT) both involve a two-electron transfer process.

In a reduction experiment, DTT was mixed at a certain point with the aqueous PFS microcapsule suspension during the  $\text{FeCl}_3$  oxidation. Figure 5.13 shows a series of representative CLSM micrographs recorded during the sequential oxidation-reduction process of  $(\text{PFS}^-/\text{PFS}^+)_5$  microcapsules. As discussed, the whole process of oxidation-induced  $(\text{PFS}^-/\text{PFS}^+)_5$  microcapsule permeability change and expansion until its final disintegration will last for no more than 15 minutes under the afore-mentioned oxidation conditions ( $\text{FeCl}_3$ , 1 mM). In the experiment associated with Figure 5.13, the onset of capsule permeability change and expansion occurred after mixing with  $\text{FeCl}_3$  solutions for 8 minutes.

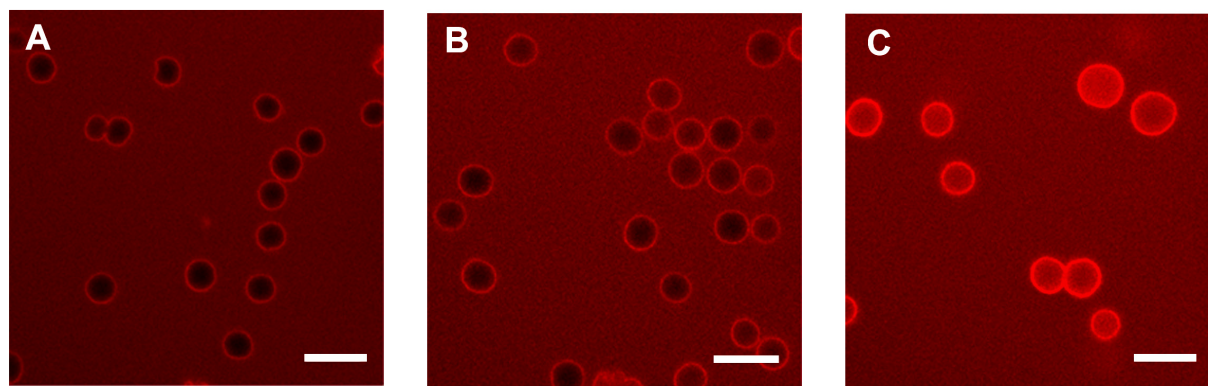


**Figure 5.13** Representative confocal laser scanning micrographs of  $(\text{PFS}^-/\text{PFS}^+)_5$  microcapsules (A) before oxidation; (B) 10 min after adding oxidation agents  $\text{FeCl}_3$  (1 mM); and (C) another 10 min after adding reducing agents DTT (0.5 mM) to (B). The oxidation induced continuous expansion of capsules can be stopped by adding PFS reducing agents. Scale bar = 15  $\mu\text{m}$ .

Figure 5.13B shows that when the reducing agent was added 10 minutes after the oxidation agent, many of the capsules had already become completely permeable to the probe TRITC-dextran molecules (Figure 5.13C) and the mean diameter of the microcapsules increased to  $\sim 1.5$  times its original value (averaged on *ca.* 20 capsules). As observed in Figure 5.13C, instead of an accelerated expansion and final disintegration if only oxidants were added, these reducing agent treated oxidized capsules still retained their spherical shape. The DTT treatment was continuously monitored for 30 minutes. Only a very small portion of capsules ( $< 5\%$ , based on *ca.* 200 capsules) were observed to have disintegrated. However, many capsules beared an increased capsule diameter of close to two times the original value (averaged on *ca.* 30 capsules with increasing the duration of reducing agent treatments). This was considered to most likely result from a relatively slow response to reduction mainly due to diffusion of the reducing agent molecules into the capsule wall. The majority of the

capsules (~ 95%) that had undergone the whole oxidation-reduction treatment were essentially stable and showed excellent permeability to the probe molecules. Thus, chemical oxidation and reduction allows one to manipulate the permeability of the organometallic polyelectrolyte multilayer capsules.

### 5.3.3 Composite-wall microcapsules

In order to maintain the spherical shape and integrity of the capsules, and in the mean time effectively change the capsule permeability, capsules with PFS polyion pairs in the inner layers and redox-insensitive organic polyelectrolyte pairs PSS<sup>-</sup>/PAH<sup>+</sup> in the outer layers were fabricated. After depositing five bilayers of PFS<sup>-</sup>/PFS<sup>+</sup>, different numbers of (PSS<sup>-</sup>/PAH<sup>+</sup>) “capping” bilayers were coated onto the templates before core dissolution.

The as-prepared “composite-wall” capsules were visualized by CLSM. As examples of (PFS<sup>-</sup>/PFS<sup>+</sup>)<sub>5</sub>(PSS<sup>-</sup>/PAH<sup>+</sup>)<sub>1</sub> capsules demonstrated in Figure 5.14, these composite-wall capsules were robust and essentially impermeable to  $4.4 \times 10^3$  g/mol TRITC-dextran molecules (with a population of  $\geq 90\%$ ). After being mixed with FeCl<sub>3</sub> aqueous solution (2 mM), the capsules started to become permeable, as was evident from the rise in the fluorescent intensity in the capsule interior. Figure 5.14B shows one of the representative CLSM images of (PFS<sup>-</sup>/PFS<sup>+</sup>)<sub>5</sub>(PSS<sup>-</sup>/PAH<sup>+</sup>)<sub>1</sub> microcapsules after mixing with FeCl<sub>3</sub> solutions for 20 minutes. At this stage, the majority (more than 70%) of the capsules were completely permeable to the same probe molecules, as a result of oxidation of the redox-responsive PFS in the capsule wall.

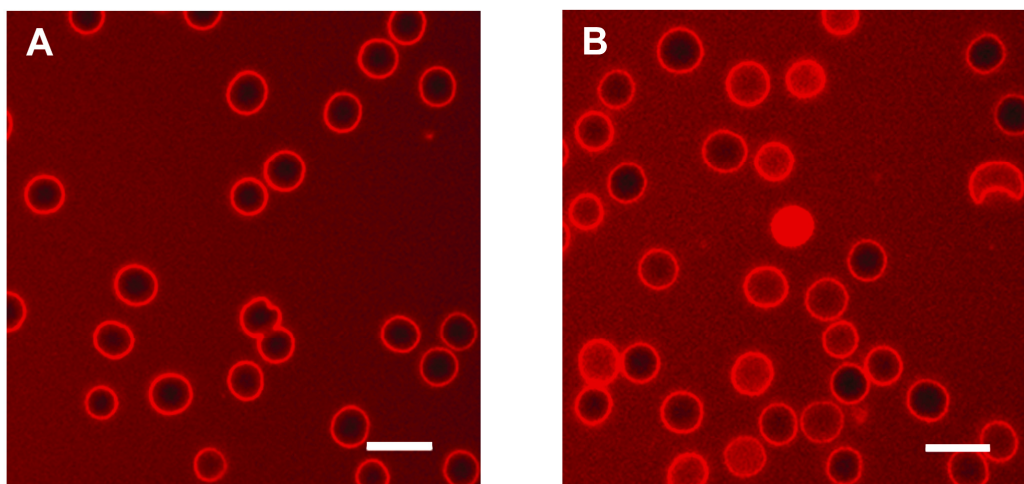


**Figure 5.14** Local oxidation of (PFS<sup>-</sup>/PFS<sup>+</sup>)<sub>5</sub>(PSS<sup>-</sup>/PAH<sup>+</sup>)<sub>1</sub> microcapsules by FeCl<sub>3</sub> (2 mM) monitored by CLSM. The majority (> 70%) of capsules that are originally impermeable (A) to  $4.4 \times 10^3$  g/mol dextran molecules show permeability (B) after oxidation for 20 minutes. Scale bar = 10  $\mu$ m.

Compared to the above studied (PFS<sup>-</sup>/PFS<sup>+</sup>)<sub>5</sub> microcapsules, (PFS<sup>-</sup>/PFS<sup>+</sup>)<sub>5</sub>(PSS<sup>-</sup>/PAH<sup>+</sup>)<sub>1</sub> composite-wall microcapsules exhibited a slower response to the same concentration of chemical redox-stimuli. By applying oxidants with the same concentration (FeCl<sub>3</sub>, 1 mM),

it took more than half an hour for the impermeable  $(\text{PFS}^-/\text{PFS}^+)_5(\text{PSS}^-/\text{PAH}^+)_1$  capsules to show the same degree of permeability as the full organometallic  $(\text{PFS}^-/\text{PFS}^+)_5$  microcapsules. In addition to varying the oxidant concentrations, the rate of permeability increase can be tuned by changing the number of capping  $(\text{PSS}^-/\text{PAH}^+)$  bilayers on the capsule wall. Oxidation experiments were performed on composite microcapsules containing different numbers of  $(\text{PSS}^-/\text{PAH}^+)$  bilayers. Increasing the number of “capping” layers slows down the permeability change of the capsules. Obviously these redox-insensitive polyelectrolyte bilayers are acting as “blocking” layers on the capsule surface. When increasing the number of capping  $\text{PSS}^-/\text{PAH}^+$  bilayers  $n$  from 1 to 3 on the same  $(\text{PFS}^-/\text{PFS}^+)_5$  inner-layer structure and using oxidant solutions with the same concentration ( $\text{FeCl}_3$ , 2 mM), the recorded time scale for more than 80% of impermeable capsules to become permeable increased from 1 to 6 hours.

“Composite-wall” PFS microcapsules were further characterized by AFM to check the integrity and wall thickness in the dry state. Examples of TM-AFM images of  $(\text{PFS}^-/\text{PFS}^+)_5(\text{PSS}^-/\text{PAH}^+)_2$  capsules before and after oxidation are shown in Figure 5.15.

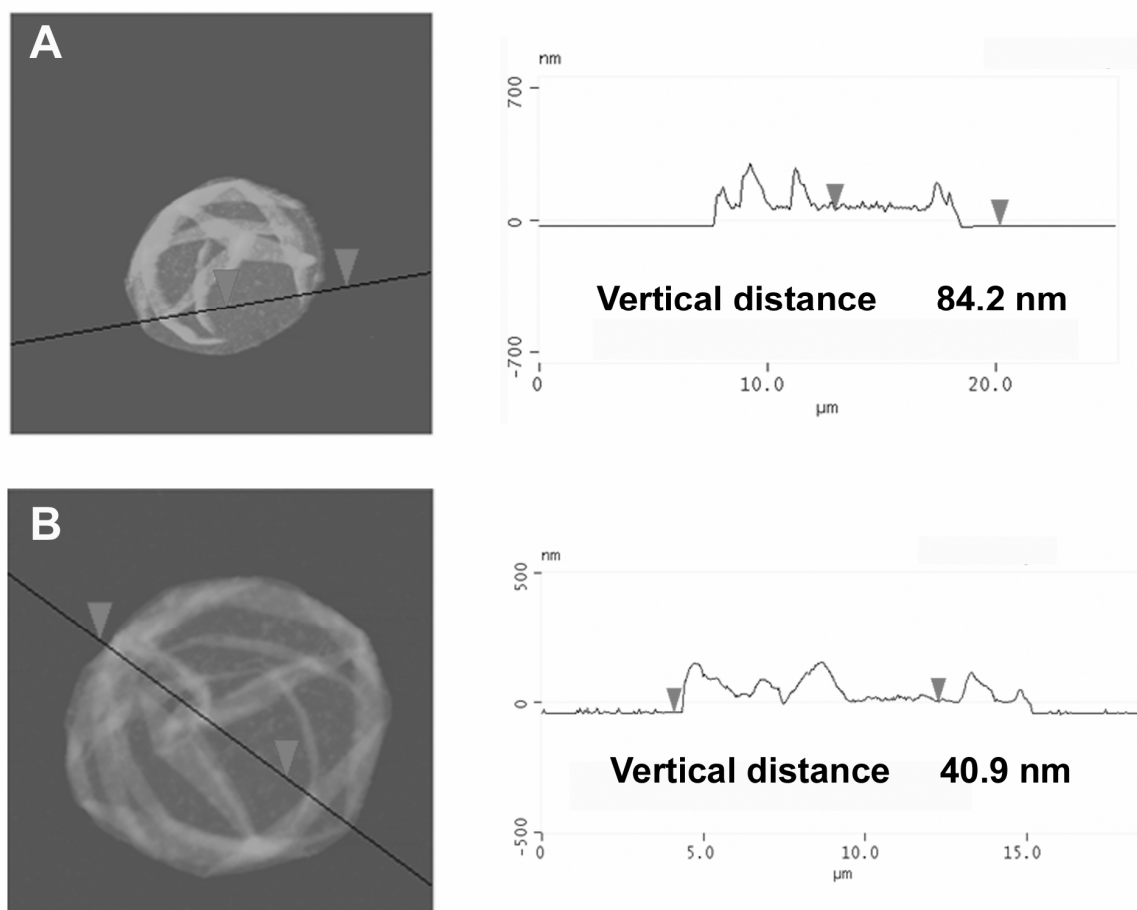


**Figure 5.15** Representative TM-AFM height images of  $(\text{PFS}^-/\text{PFS}^+)_5(\text{PSS}^-/\text{PAH}^+)_2$  capsules before and after oxidation for overnight (8 h) by  $\text{FeCl}_3$  (1 mM). The integrity of the capsules has been preserved.



Both of the capsules show their integrity and characteristic hollow spherical structure. It is worth noting that even with only one capping bilayer of PSS<sup>-</sup>/PAH<sup>+</sup>, many of the capsules still preserved their shape and integrity after oxidation for over two hours. When nine randomly chosen (PFS<sup>-</sup>/PFS<sup>+</sup>)<sub>5</sub>(PSS<sup>-</sup>/PAH<sup>+</sup>)<sub>1</sub> capsules with varying oxidation periods from two hours to overnight were studied by AFM, none of them were found broken. At the same time, the capsule wall thickness had undergone a dramatic change. The double wall thickness values of the capsules with (PFS<sup>-</sup>/PFS<sup>+</sup>)<sub>5</sub>(PSS<sup>-</sup>/PAH<sup>+</sup>)<sub>n</sub> wall structures measured by AFM before and after chemical oxidation are presented in Table 5.1. The consistency of the capsule wall thickness after oxidation indicates that the oxidation had completed within the treatment periods and that the capsules had reached a more or less “stable” oxidized state. Considering the wall thickness of capsules solely composed of PFS polyelectrolytes (Chapter 5.2.2) and experimental errors in AFM, it is clearly shown from Table 5.1 that the wall thickness values of composite wall capsules cannot be viewed as a simple linear addition of the contributions from the PFS<sup>-</sup>/PFS<sup>+</sup> and PSS<sup>-</sup>/PAH<sup>+</sup> bilayers.

The decrease in capsule wall thickness as illustrated in Table 5.1 shows that some material loss from the capsule wall happened during the chemical oxidation process. The PSS<sup>-</sup>/PAH<sup>+</sup> bilayer thickness under the experimental conditions (2 mg/mL, 0.5 M NaCl) is normally below 5 nm.<sup>19, 25, 26</sup> This value corresponds to a double wall thickness below 10 nm for one PSS<sup>-</sup>/PAH<sup>+</sup> bilayer. Taking this into consideration, the oxidized-capsule wall thickness values as summarized in Table 5.1 are apparently higher than the expected capsule wall thickness if only PSS<sup>-</sup>/PAH<sup>+</sup> were present in the capsule wall. This suggests that although material loss occurred during the oxidation process, not all the PFS polyelectrolytes were released from the capsule shell. Moreover, increasing the number of “capping” layers seemed to decrease the degree of material loss. When the number of PSS<sup>-</sup>/PAH<sup>+</sup> bilayers increased from 1 to 3, the decrease in capsule wall thickness upon oxidation dropped from ~ 70% to only ~ 30%. In addition, there was no substantial change in the root-mean-square (rms) roughness (5-6 nm) of the capsule wall in the fold-free regions after chemical oxidation. Both CLSM and AFM measurements showed no measurable capsule diameter difference before and after oxidation.

**Table 5.1** (PFS<sup>-</sup>/PFS<sup>+</sup>)<sub>5</sub>(PSS<sup>-</sup>/PAH<sup>+</sup>)<sub>n</sub> capsule wall thicknesses as measured by TM-AFM before and after oxidation for overnight (8 h) by FeCl<sub>3</sub> (1 mM).

No. of Capping bilayers	before oxidation (nm)	after oxidation (nm)
1	69 ± 3	22 ± 3
2	83 ± 3	38 ± 3
3	98 ± 2	70 ± 10

### 5.3.4 Electrochemistry

Poly(ferrocenylsilanes) can be fully and reversibly oxidized and reduced by electrochemical methods (see also Chapter 4).<sup>27</sup> Depending on the electrostatic characteristics of the last-deposited polyelectrolyte layer, multilayer capsules bear positive or negative charges on their outer-wall. This makes it possible to immobilize multilayer microcapsules onto charged surfaces through electrostatic interactions. In order to study the electrochemical responsiveness of PFS microcapsules, microcapsules with  $(\text{PFS}^-/\text{PFS}^+)_5(\text{PSS}^-/\text{PAH}^+)_1$  wall structures were deposited onto gold substrates featuring a sodium 3-mercaptopropionate monolayer. The negatively charged surface is ideal for the adsorption of positively charged microcapsules.<sup>28</sup> Cyclic voltammograms (CV) were recorded for the organometallic-organic composite-wall polyelectrolyte microcapsules at different scan rates, as demonstrated in Figure 5.16. The CVs of adsorbed PFS microcapsules show the two reduction waves characteristic for PFS. Interestingly, the two oxidation waves could not be resolved when the scan rate was higher than 10 mV/s. This contrasts with former results on PFS multilayer films adsorbed on flat substrates, where the two oxidation and reduction waves always showed up in the same range of scan rates.<sup>11</sup> It is likely that the capping  $\text{PSS}^-/\text{PAH}^+$  may slow down the electron transfer process.<sup>29</sup> The CV scans can be repeated for many times, showing the full reversibility of the electrochemical redox process.

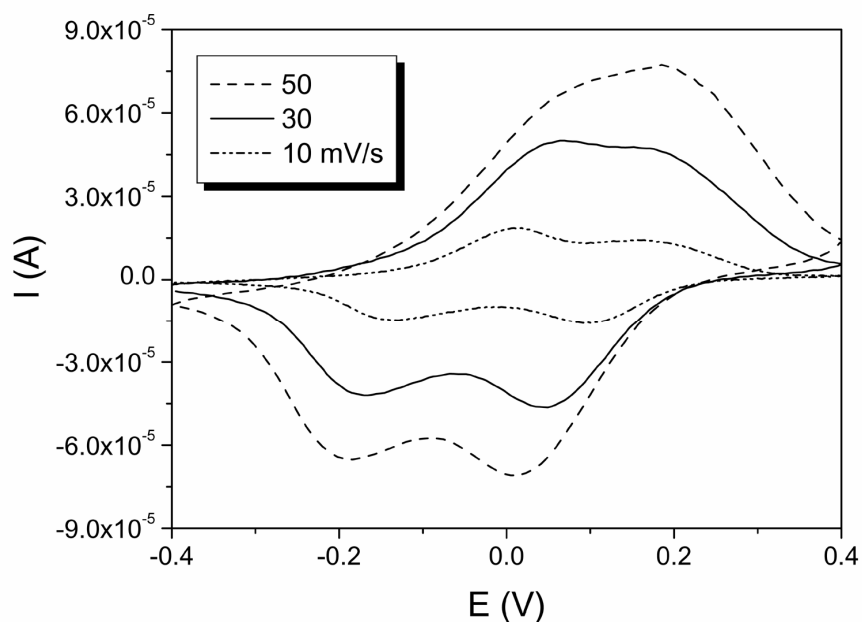


**Figure 5.16** Cyclic voltammograms recorded on one layer of  $(\text{PFS}^-/\text{PFS}^+)_5(\text{PSS}^-/\text{PAH}^+)_1$  capsules deposited on a gold electrode featuring a monolayer of sodium 3-mercaptopropionate. Scan rate 10-50 mV/s, 0.1 M  $\text{NaClO}_4$  aqueous electrolyte solution,  $\text{Hg}/\text{Hg}_2\text{SO}_4$  reference and Pt counter electrodes.

## 5.4 Discussion

### 5.4.1 (PSS<sup>-</sup>/PFS<sup>+</sup>)<sub>5</sub> microcapsules

In order to further investigate the influence of multilayer composition on the redox-controlled permeability of layer-by-layer constructed microcapsules, microcapsules made from redox-sensitive PFS polycations and redox-insensitive polyanionic species poly(styrene sulfonate) (PSS) were fabricated. The PSS used here has a molar mass of  $7.0 \times 10^4$  g/mol, similar to that of the PFS polyelectrolytes.<sup>30</sup> The fabrication and characterization of (PSS<sup>-</sup>/PFS<sup>+</sup>)<sub>5</sub> microcapsules follows the same procedure as that of the (PFS<sup>-</sup>/PFS<sup>+</sup>)<sub>5</sub> system. Like the above-studied fully organometallic PFS microcapsules, these organic-organometallic microcapsules also showed a redox-responsive permeability increase under the same chemical redox-trigger (FeCl<sub>3</sub>). The originally impermeable capsules (towards  $4.4 \times 10^3$  g/mol TRITC-dextran) enlarged, became permeable to the probe, and finally disintegrated when exposed to the oxidants. However, the typical accompanying capsule expansion and disintegration proceeded at a lower speed compared to the (PFS<sup>-</sup>/PFS<sup>+</sup>)<sub>5</sub> microcapsules at the same oxidant concentration.

The maximum duration from the onset of oxidation induced capsule expansion until the complete disintegration of the capsules increased with decreasing the oxidant concentration. A similar trend of capsule expansion rate dependence on oxidant concentration was also observed in the above (PFS<sup>-</sup>/PFS<sup>+</sup>)<sub>5</sub> capsule system. For a clear comparison, the recorded times until disintegration of these two capsule systems are summarized in the following table (Table 5.2).

**Table 5.2** Duration (in minutes) of oxidation induced capsule expansion until final disintegration for (PSS<sup>-</sup>/PFS<sup>+</sup>)<sub>5</sub> and (PFS<sup>-</sup>/PFS<sup>+</sup>)<sub>5</sub> systems, with varying oxidant concentrations.

Concentration (FeCl <sub>3</sub> , mM)	1	2	3	6
(PSS <sup>-</sup> /PFS <sup>+</sup> ) <sub>5</sub>	35		15	6
(PFS <sup>-</sup> /PFS <sup>+</sup> ) <sub>5</sub>	15	3	2	

The redox-responsive properties of these organic-organometallic microcapsules support the basic conclusion that PFS polycations alone are sufficient to provide characteristic redox-activity to layer-by-layer constructed multilayer microcapsules. Moreover, replacing one of the redox-responsive PFS polyion components with another redox-inert polyelectrolyte species could serve as an alternative method for tuning the speed of the permeability response under a redox-trigger of the corresponding microcapsules.

### 5.4.2 (PFS<sup>-</sup>/PAH<sup>+</sup>)<sub>5</sub> microcapsules

Cationic and anionic PFS polyelectrolytes undergo different solution solubility changes upon chemical oxidation. Upon oxidation, PFS picks up additional positive charges on the polymer main chain. The oxidation-induced positive charges will have exactly opposite effects on the overall charge density of the PFS polycations and polyanions. With increasing the positive charge density, PFS polycations will become more soluble. On the contrary, the negative charges in the side groups of the PFS polyanions are compensated by the positive charges induced in their main chain. This may decrease the solubility of the anionic PFS polyelectrolyte species. Moreover, it may be expected that the negatively charged sulfonate groups (SO<sub>3</sub><sup>-</sup>) on PFS polyanions will contribute to their precipitation in aqueous media in the presence of Fe<sup>3+</sup> due to ionic “cross-linking”. Based on their solubility changes in exactly opposite directions, we expect accordingly different capsule volume variations upon chemical oxidation by FeCl<sub>3</sub>. To verify this, planar multilayers and microcapsules based on PFS<sup>-</sup>/PAH<sup>+</sup> were also fabricated followed by studies on their chemical redox-responsive behaviour.

Multilayers of PAH<sup>+</sup>/PFS<sup>-</sup> were first adsorbed onto quartz substrates featuring a pre-deposited PEI layer from 2 mg/mL aqueous solutions containing 0.5 M NaCl. The pH of the PAH<sup>+</sup> solutions was tuned to 6.3 using 0.1 M NaOH solutions.<sup>31</sup> UV/Vis spectra recorded after each bilayer deposition confirmed a well-defined linear growth profile of the PAH<sup>+</sup>/PFS<sup>-</sup> multilayer system under current experimental conditions. Upon completion of the layer-by-layer deposition, a ten bilayer sample of (PAH<sup>+</sup>/PFS<sup>-</sup>) on quartz was immersed into FeCl<sub>3</sub> solution (1 mM) for different time intervals followed by UV/Vis characterization. Unlike the fast and complete desorption of PFS<sup>+</sup>/PFS<sup>-</sup> multilayers from planar substrates, the change in the absorbance at 216 nm was minimal after oxidation for more than one hour. This shows that it is difficult to remove PAH<sup>+</sup>/PFS<sup>-</sup> multilayers by a similar chemical oxidation reaction.

In a second approach, (PAH<sup>+</sup>/PFS<sup>-</sup>)<sub>5</sub> microcapsules were fabricated from polyelectrolyte solutions with the same concentration (2 mg/mL containing 0.5 M NaCl) onto colloidal templates (MnCO<sub>3</sub>) followed by core removal. CLSM studies showed that the obtained capsules were also impermeable to the same molecular probe (4.4 x 10<sup>3</sup> g/mol TRITC-dextran, Figure 5.17A). Similarly, (PAH<sup>+</sup>/PFS<sup>-</sup>)<sub>5</sub> microcapsules were then mixed with FeCl<sub>3</sub> solutions (6 mM) to evaluate their permeability response. All of the originally impermeable capsules became completely permeable to the same probe molecules after oxidation for 15 to 20 minutes. In the mean time, the capsules underwent a continuous shrinkage in their size, which is clearly demonstrated in the CLSM images shown in Figure 5.17. Subsequent addition of PFS reducing agent DTT to the reaction mixture could not reverse the capsule shrinkage.

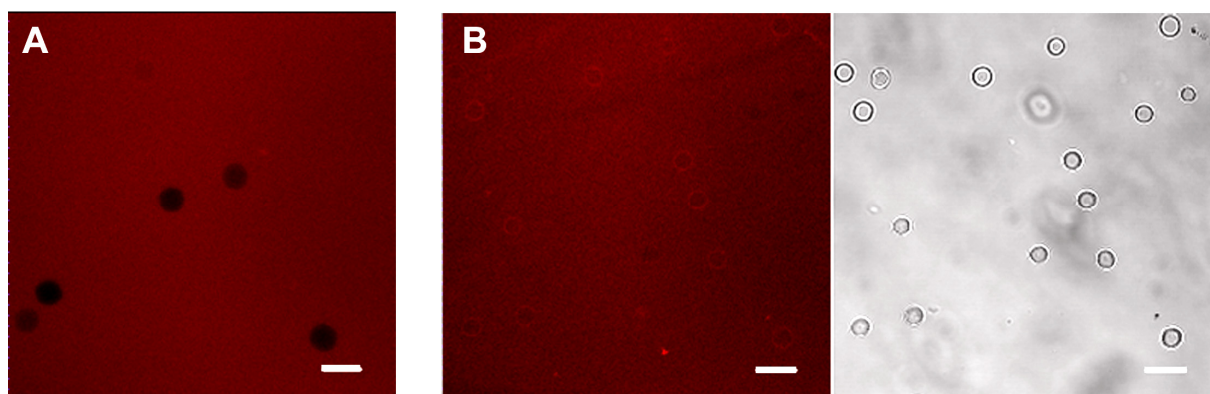


**Figure 5.17** CLSM images of  $(\text{PAH}^+/\text{PFS}^-)_5$  microcapsules oxidized by  $\text{FeCl}_3$  (6 mM) for (A) 4 minutes and (B) 20 minutes (right Figure is the transmittance image). Fluorescence probe is TRITC-dextran ( $4.4 \times 10^3$  g/mol). Scale bar = 10  $\mu\text{m}$  for all the images.

The oxidized  $(\text{PAH}^+/\text{PFS}^-)_5$  microcapsules were also studied by atomic force microscopy (AFM) in tapping mode in the dry state. As a comparison, TM-AFM images of typical examples of  $(\text{PAH}^+/\text{PFS}^-)_5$  microcapsules before and after chemical oxidation by  $\text{FeCl}_3$  are shown in Figure 5.18. After oxidation, the original hollow structure of the microcapsules as prepared was lost. Instead, a collapsed and filled “pancake”-like shape was adopted after oxidation, accompanied by a decrease in the capsule diameter. The  $(\text{PAH}^+/\text{PFS}^-)_5$  capsule shrinking phenomenon is just contrary to the previously studied swelling behaviour of  $(\text{PFS}^+/\text{PFS}^-)_5$  and  $(\text{PFS}^+/\text{PSS}^-)_5$  microcapsules.

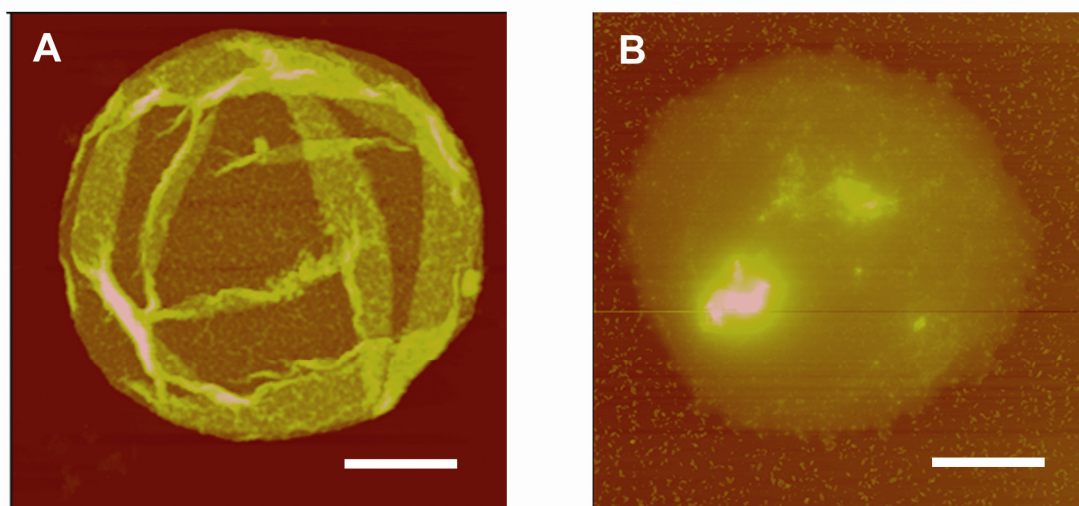


**Figure 5.18** TM-AFM images of  $(\text{PAH}^+/\text{PFS}^-)_5$  microcapsules in the dry state before (A) and after (B) chemical oxidation by  $\text{FeCl}_3$  (6 mM). Scale bar is 2  $\mu\text{m}$  for both images and z range is 600 nm for (A) and 400 nm for (B).

### 5.4.3 Mechanism of redox-responsive permeability

The observed permeability changes can be explained as follows. When mixed with oxidants, the PFS macromolecules in the capsule wall are slowly oxidized. During oxidation,

the ferrocene (Fc) groups in the polymer main chain will become positively charged. The rising positive charges in the polymer main chain can bring coulomb repulsion within the chains, actually stretching the chain and making it stiffer.<sup>32,33</sup>

Moreover, since all the polyelectrolyte species in the capsule wall bear the same main chain structure, electrostatic repulsion will occur both intra- and inter-chain. With increasing repulsive forces along the chain as well as in the multilayer growth direction, a more loosened multilayer structure will be favoured. Thus, one would accordingly expect increased pore sizes and enhanced permeability of the multilayer capsules. As experimental evidence, enhanced permeability was demonstrated in the I<sub>2</sub> oxidation case and in the early stages of FeCl<sub>3</sub> oxidation.

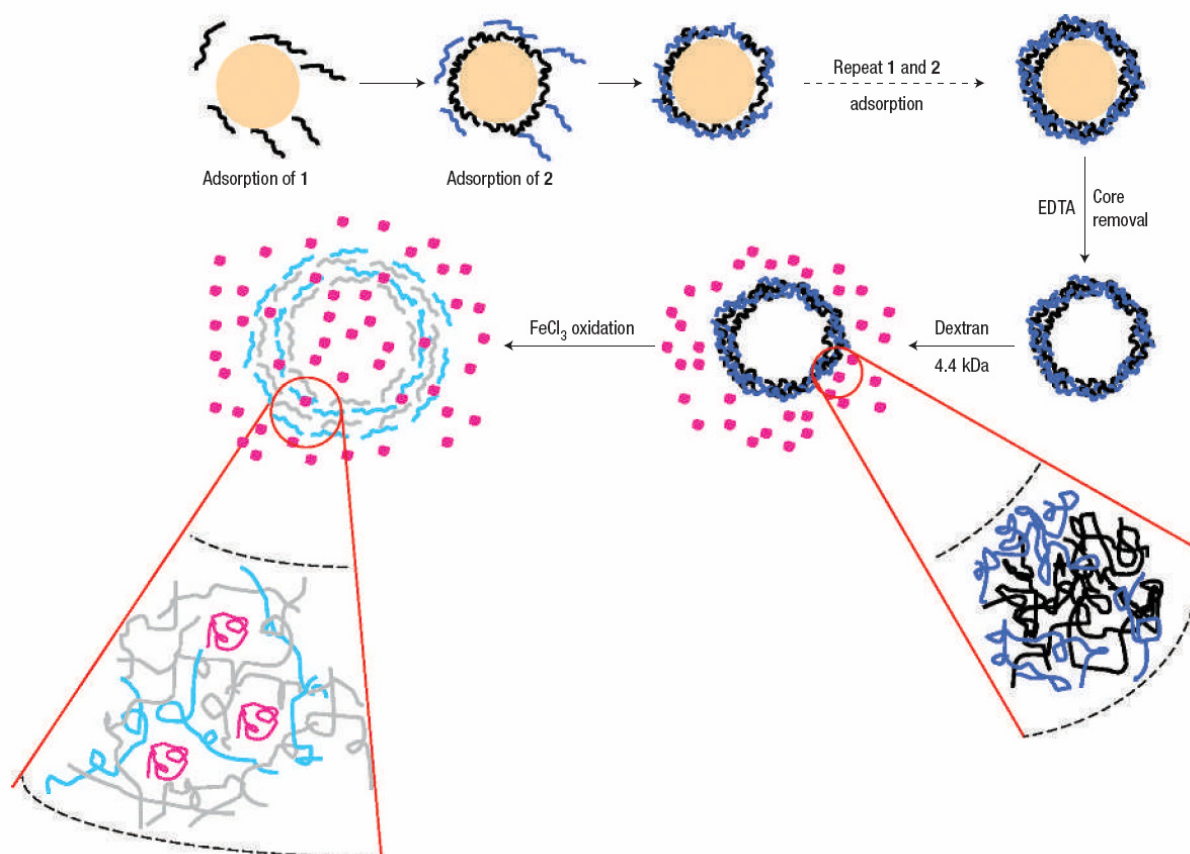
In the later stages of oxidation when FeCl<sub>3</sub> was used as the oxidant, peculiar capsule expansion and final disintegration phenomena were observed. The reason for this is as follows. Since it is well-accepted that FeCl<sub>3</sub> is a more effective and stronger oxidant for PFS, it will cause a more rapid rising of positive charges in the polymer main chain. As a consequence, a faster increase of the electrostatic repulsion between the positive charges on the polyelectrolyte backbones would be expected, both intra- and inter-molecular. In the meantime, the overall charge density of the oppositely charged PFS<sup>-</sup> and PFS<sup>+</sup> polyelectrolytes species changes. The induced positive charges on the polymer main chain will increase the positive charge density of the PFS polycations and compensate the negative charges in the PFS polyanions. When fully oxidized, cationic PFS will double its positive charges but anionic PFS will become charge neutral. Thus increasing the degree of oxidation will finally lead to the ultimate disintegration of the original charge compensated layer-by-layer structure.

It is worth noting that a very small trigger (FeCl<sub>3</sub> with concentrations in the sub-mM range) is already sufficient to cause a fast and drastic permeability change and capsule disintegration. In addition to the electrostatic arguments presented above, PFS chains might undergo chain scission by nucleophilic attack at the ferrocenium sites in the oxidized PFS chains, which could cause the multilayer capsules to decompose. In Chapter 3, viscosity studies on oxidized PFS polycation aqueous solutions were discussed. The FeCl<sub>3</sub> oxidized PFS showed a slow decrease in solution viscosity with time, which indicated a slow chain-scission. But the rate of chain-scission (in the time scale of hours) is much slower when compared to the time scale of the capsule oxidation experiments. In other words, within an experimental time scale of 15 minutes up to one hour, there is no substantial viscosity change of the oxidized PFS polycation solution. This makes it very unlikely that polymer chain scission caused the capsule disintegration. The fast PFS polyelectrolyte multilayer removal on flat substrates by oxidation, requiring less than five minutes, further supports the idea that variation in the electrostatic interactions within the multilayers is most likely the major driving force for the capsule expansion-disintegration phenomenon.

The study on the oxidation of organic-organometallic microcapsules composed of PSS<sup>-</sup>/PFS<sup>+</sup> and PFS<sup>-</sup>/PAH<sup>+</sup> provided more insight into the mechanism of redox-induced permeability response. During the oxidation process, another contributing effect to the final capsule disintegration is the polyelectrolyte solubility variations. Cationic and anionic PFS polyelectrolytes underwent different solution solubility changes upon chemical oxidation. Cationic PFS retained its water solubility due to the increase of its positive charge density. On the contrary, the decrease of overall charge density and possible cross-linking effects induced by the Fe<sup>3+</sup> ions will decrease the solubility of the anionic PFS polyelectrolyte species (see also Chapter 3). Based on their solubility changes in exactly opposite directions, we expect accordingly different capsule volume variation upon chemical oxidation by FeCl<sub>3</sub>. Indeed, PSS<sup>-</sup>/PFS<sup>+</sup> and PFS<sup>-</sup>/PAH<sup>+</sup> behaved differently upon chemical oxidation. Experiments showed that similar to the (PFS<sup>-</sup>/PFS<sup>+</sup>)<sub>5</sub> capsules, (PSS<sup>-</sup>/PFS<sup>+</sup>)<sub>5</sub> capsules underwent expansion and permeability changes, while (PAH<sup>+</sup>/PFS<sup>-</sup>)<sub>5</sub> capsules experienced a shrinkage in size. TM-AFM showed collapsed (PAH<sup>+</sup>/PFS<sup>-</sup>)<sub>5</sub> capsules whose original “hollow” structures appeared to be lost after oxidation, giving further indication of the formation of more compact water-insoluble complexes. It is worth noting that the charge densities of the strong polyelectrolyte PSS and the weak polyelectrolyte PAH would not be dramatically altered under the weakly acidic conditions introduced by the oxidant FeCl<sub>3</sub>. The shrinkage of (PAH<sup>+</sup>/PFS<sup>-</sup>)<sub>5</sub> capsules was driven by minimization of interfacial free energy through decreasing the surface area in contact with the aqueous medium. Similar capsule shrinking phenomena have been observed before in other polyelectrolyte systems, when calcium (Ca<sup>2+</sup>) ion was shown to effectively complex the carboxylic acid groups of poly(methylacrylic acid) (PMA) in the basic pH region.<sup>34</sup>

The whole process is illustrated in Scheme 5.1.

In summary, before oxidation, the polyelectrolyte multilayer is stable due to the compensated charges on the polymer side chains. With the rising intra- and inter-chain electrostatic repulsion following oxidation, the PFS polyelectrolytes will adopt a more extended macromolecular conformation and the inter-layer spacing within the multilayer structure will increase accordingly. This results in a macroscopic permeability increase of the microcapsules. With increasing the extent of polymer oxidation, the overall charge density and solubility of oppositely charged PFS polyelectrolytes change in different directions as well. The rising positive charges on the PFS polyelectrolytes start to modify the originally charge-compensated structure.<sup>2, 35, 36</sup> When the charge density along one of the polyelectrolyte backbone decreases to below the minimum needed to form a stable multilayer structure, the original layer-by-layer structure will be destroyed.



**Scheme 5.1** Representation of poly(ferrocenylsilane) multilayer microcapsule formation and permeability control by redox-stimulus. Polyelectrolyte multilayer microcapsules were fabricated through their electrostatic layer-by-layer self-assembly onto spherical substrates ( $\text{MnCO}_3$ ) followed by core removal using EDTA. The permeability of these capsules could be tuned by the introduction of a chemical oxidizing or reducing agent. Red bundles represent probe dextran molecules. The varying colours of the polymer chains represent their different oxidation states and conformations.

## 5.5 Conclusions

Water-soluble poly(ferrocenylsilane) polyelectrolytes were successfully employed in the electrostatic layer-by-layer self-assembly process onto colloidal particles ( $\text{MF}$ ,  $\text{MnCO}_3$ ) followed by template removal to give full organometallic multilayer microcapsules. Manganese carbonate microparticles were chosen as the optimum core material due to its effectiveness in fabricating intact capsules with high yield. AFM and CLSM imaging showed that the stability and integrity of the capsules obtained depend mainly on the wall thickness, which is tuned by varying the number of deposited polyelectrolyte bilayers. We demonstrated that by using fluorescence-labelled  $4.4 \times 10^3$  g/mol dextran as the reference probe molecule, stable and impermeable PFS capsules with an average size of around  $10 \mu\text{m}$  were obtained when the bilayer number is higher than four.

The permeability of these stable PFS capsules could be tuned via chemical oxidation. Two oxidation agents, iodine ( $\text{I}_2$ ) and iron chloride ( $\text{FeCl}_3$ ) are both effective in oxidizing



water-soluble PFS based multilayer capsules.  $\text{FeCl}_3$  has been proven to be more effective in the fact that a very dilute solution (in the sub-mM range) is sufficient to cause a fast increase in the capsule permeability. Permeability change is believed to result from increased pore size due to the multilayer expansion along the chain direction and in the multilayer growth direction, which was caused by oxidation-introduced additional positive charges along the polymeric backbone. Capsules made solely from PFS oxidized by  $\text{FeCl}_3$  show continuous expansion behaviour towards their final disintegration. The rate of expansion could be easily tuned by varying the number of deposited polyelectrolyte bilayers and the concentration of the oxidants used. The capsule disintegration is mainly caused by the rising of positive charges along the polymer main chain and final disruption of the original charge-compensated multilayer structure. A comparison of the responsive behaviour of fully PFS capsules and PFS/organic polyelectrolyte hybrid capsules revealed that oxidation-induced solubility change of the polyions also contributed to capsule redox-response.

Composite-wall microcapsules, fabricated by the additional adsorption of the redox-insensitive polyelectrolyte species  $\text{PSS}^-/\text{PAH}^+$  as the capsule capping layers, were introduced to ensure the shape and integrity of redox-responsive PFS capsules. As demonstrated by CLSM, the permeability changing rate can be further manipulated by varying the number of  $\text{PSS}^-/\text{PAH}^+$  bilayers. AFM studies on collapsed capsules also show decreased capsule wall thicknesses upon chemical oxidation, indicating some material loss.

Finally, the electrochemical oxidation of these composite-wall microcapsules featuring PFS polyelectrolytes was studied by immobilizing them onto gold substrates. Cyclic voltammograms exhibited oxidation and reduction waves typical for PFS, verifying the reversible electrochemical addressability of these redox-responsive microcapsules.

The novel organometallic multilayer system introduced here has great potential to open up a new pathway to include redox-stimulus responsive materials into controlled release applications. These we envisage above all in diverse areas as pharmacy and nanomaterials science.

## 5.6 Experimental

**Materials** Poly(styrene sulfonate) sodium salt (PSS,  $M_w \sim 7.0 \times 10^4$  g/mol), poly(allylamine hydrochloride) (PAH,  $M_w \sim 7.0 \times 10^4$  g/mol), polyethyleneimine (PEI,  $M_w \sim 2.5 \times 10^4$  g/mol), manganese sulphate ( $\text{MnSO}_4$ ), ammonium bicarbonate ( $\text{NH}_4\text{HCO}_3$ ), ethylenediaminetetraacetic acid trisodium salt (EDTA), tetramethylrhodamine isothiocyanate (TRITC), TRITC labelled dextran (TRITC-dextran,  $M_w \sim 4.4 \times 10^3$  g/mol), fluorescein isothiocyanate labelled dextran (FITC-dextran,  $M_w \sim 6.6 \times 10^4$  g/mol), sodium 3-mercaptopropanesulfonate, ferric chloride ( $\text{FeCl}_3$ ), dithiothreitol (DTT) were obtained from Aldrich and used as received. Melamine formaldehyde (MF, average diameter 3.8  $\mu\text{m}$ ) particles were

obtained from Microparticles GmbH (Berlin, Germany). Manganese carbonate ( $\text{MnCO}_3$ ) particles were prepared according to the reported method,<sup>17</sup> by using ethanol (concentration 2.5% v/v in the final mixture) as the poor solvent in the crystallization process.

**Polyelectrolyte multilayer capsule preparation** Alternating adsorption of polyelectrolytes (PFS, 1 mg/mL; PSS/PAH, 2 mg/mL) onto the  $\text{MnCO}_3$  microparticles ( $\sim 10\%$  w/w in aqueous suspension) was carried out in 0.5 M NaCl solution for 10 min followed by centrifugation (1500 rpm, 2 min) and three MilliQ washing/centrifugation steps. Since the  $\text{MnCO}_3$  particles possess positively charged surfaces, negatively charged polyelectrolyte species ( $\text{PSS}^-$  or  $\text{PFS}^-$ ) were chosen as the first layer. After the deposition of a desired number of polyelectrolyte bilayers, the coated particles were subjected to core dissolution in 0.2 M EDTA (pH = 7) solution. After 60 minutes of agitation, the suspension was centrifuged (1500 rpm, 10 min), the supernatant was removed, and the capsules were re-suspended in fresh EDTA. This washing procedure was repeated three times. The resultant capsules were washed thoroughly with MilliQ for three times and finally re-dispersed and stored in MilliQ.

**Multilayer capsule deposition onto gold substrates** Gold substrates were cleaned with Piranha solution ( $\text{H}_2\text{SO}_4$  and  $\text{H}_2\text{O}_2$  with a volume ratio of 7:3), washed with MilliQ, and dried with a stream of nitrogen. *Caution! Piranha is highly corrosive, reacts violently with organic materials, and should be handled with utmost care!* For microcapsule deposition, the cleaned gold electrodes were first immersed in an aqueous solution of sodium 3-mercaptopropanesulfonate ( $\sim 0.1$  mM) to impart negative charges onto the substrates. The modified gold electrodes were subsequently immersed into a microcapsule suspension for 20 minutes, followed by rinsing, dip-rinsing with MilliQ (2 minutes), and finally stored in pure MilliQ.

**Characterization** UV/Vis spectra were recorded using a Varian Cary 300 Bio UV/Visible spectrophotometer. Zeta-potential of the microcapsules were measured in water using a Zetasizer Nanoinstrument Nano Z setup. Each value was averaged from five parallel measurements. Confocal laser scanning microscopy (CLSM) images were taken with either a Leica TCS NT (100 x or 40 x oil immersion objective) or Zeiss LSM 510 (63 x oil immersion objective) confocal scanning system. Equal volumes of capsule suspension and TRITC-dextran (2 mg/mL) aqueous solution were mixed before observation. On-site oxidized/reduced samples were monitored by adding another equal volume of oxidant or reducing agent solution and making a continuous scan under the same spot in focus. Atomic force microscopy (AFM) experiments were performed by using a NanoScope IIIa multimode AFM (Veeco-Digital Instruments, Santa Barbara, CA) in tapping mode using silicon cantilevers (Nanosensors, Wetzlar, Germany) at room temperature, in air. Samples for AFM imaging were prepared by drying a droplet of capsule suspension on top of a freshly cleaved mica surface. Scanning Electron Microscopy (SEM) samples were prepared by applying a drop of particle suspension (concentration  $\sim 10^7$  particles/mL) onto a steel grid with carbon black glue followed by vacuum drying overnight. After sputtering with gold, the sample was measured using SEM (JSM 5600 LV, Jeol, Tokyo, Japan) at an operation voltage of 1.5 keV.

Cyclic voltammetry (CV) measurements were carried out on an Autolab PGSTAT10 (Ecochemie, Utrecht, The Netherlands) potentiostat in a three-electrode configuration. The gold substrates acted as the working electrode, Hg/Hg<sub>2</sub>SO<sub>4</sub> (MSE) as the reference electrode (+ 0.61 V<sub>NHE</sub>), and Pt as the counter electrode. NaClO<sub>4</sub> aqueous solution (0.1 M) was used as the electrolyte. Prior to the measurements, the electrochemical cell was degassed by passing nitrogen through the electrolyte solution for five minutes. Cyclic voltammograms were recorded between - 0.4 V<sub>MSE</sub> and + 0.4 V<sub>MSE</sub> at scan rates ranging from 10 to 50 mV/s.

## 5.7 References and notes

1. Decher, G.; Schlenoff, J. B. (Eds.) *Multilayer Thin Films, Sequential Assembly of Nanocomposite Materials*, Wiley-VCH, Weinheim, Germany, **2003**.
2. (a) Shi, X.; Shen, M.; Möhwald, H. *Prog. Polym. Sci.* **2004**, *29*, 987; (b) Hammond, P. T. *Adv. Mater.* **2004**, *16*, 1271; (c) Jiang, C.; Tsukruk, V. V. *Adv. Mater.* **2006**, *18*, 829; (d) Tang, Z.; Wang, Y.; Podsiadlo, P.; Kotov, N. A. *Adv. Mater.* **2006**, *18*, 3203.
3. (a) Ryan, A. J.; Crook, C. J.; Howse, J. R.; Topham, P.; Jones, R. A. L.; Geoghegan, M.; Parnell, A. J.; Ruiz-Pérez, L.; Martin, S. J.; Cadby, A.; Menelle, A.; Webster, J. R. P.; Gleeson, A. J.; Bras, W. *Faraday Discuss.* **2005**, *128*, 55; (b) Hugel, T.; Holland, N. B.; Cattani, A.; Moroder, L.; Seitz, M.; Gaub, H. E. *Science* **2002**, *296*, 1103; (c) Kwon, I. C.; Bae, Y. H.; Kim, S. W. *Nature* **1991**, *354*, 291.
4. Sukhishvili, S. A. *Curr. Opin. Colloid Interface Sci.* **2005**, *10*, 37.
5. Liu, J.; Lu, Y. *Adv. Mater.* **2006**, *18*, 1667.
6. Shchukin, D. G.; Möhwald, H. *Small* **2007**, *3*, 926.
7. Shchukin, D. G.; Köhler, K.; Möhwald, H. *J. Am. Chem. Soc.* **2006**, *128*, 4560.
8. Donath, E.; Sukhorukov, G. B.; Caruso, F.; Davis, S. A.; Möhwald, H. *Angew. Chem. Int. Ed.* **1998**, *37*, 2201.
9. Gao, C.; Möhwald, H.; Shen, J. *Adv. Mater.* **2003**, *15*, 930.
10. Caruso, F.; Lichtenfeld, H.; Donath, E.; Möhwald, H. *Macromolecules* **1999**, *32*, 2317.
11. Hempenius, M. A.; Robins, N. S.; Péter, M.; Kooij, E. S.; Vancso, G. J. *Langmuir* **2002**, *18*, 7629.
12. Ginzburg, M.; Galloro, J.; Jäkle, F.; Power-Billard, K. N.; Yang, S.; Sokolov, I.; Lam, C. N. C.; Neumann, A. W.; Manners, I.; Ozin, G. A. *Langmuir* **2000**, *16*, 9609.
13. (a) Sukhorukov, G. B.; Brumen, M.; Donath, E.; Möhwald, H. *J. Phys. Chem. B* **1999**, *103*, 6434; (b) Georgieva, R.; Moya, S.; Hin, M.; Mitlöhner, R.; Donath, E.; Kiesewetter, H.; Möhwald, H.; Bäumer, H. *Biomacromolecules* **2002**, *3*, 517.
14. As control, acid treatment of PFS polyelectrolytes under the same experimental conditions as the MF core dissolution has been carried out. PFS polycations with M<sub>w</sub> of around 3.0 x 10<sup>4</sup> g/mol was treated with HCl (pH = 1) for 30 min. Afterwards NaOH solution was

added until a neutral pH value was obtained. The acid-treated polycations were characterized by GPC, which showed a nearly unchanged polymer molar mass. This indicated that a short strong acid treatment will most likely not influence the integrity of the PFS polyelectrolytes.

15. Dubreuil, F.; Elsner, N.; Fery, A. *Eur. Phys. J. E.* **2003**, *12*, 215.
16. Hempenius, M. A.; Brito, F. F.; Vancso, G. J. *Macromolecules* **2003**, *36*, 6683.
17. Antipov, A. A.; Shchukin, D.; Fedutik, Y.; Petrov, A. I.; Sukhorukov, G. B.; Möhwald, H. *Coll. Surf. A: Physicochem. Eng. Asp.* **2003**, *224*, 175.
18. Zhu, H.; Stein, E. W.; Lu, Z.; Lvov, Y. M.; McShane, M. J. *Chem. Mater.* **2005**, *17*, 2323.
19. Dong, W.-F.; Ferri, J. K.; Adalsteinsson, T.; Schönhoff, M.; Sukhorukov, G. B.; Möhwald, H. *Chem. Mater.* **2005**, *17*, 2603.
20. Dai, Z.; Dähne, L.; Donath, E.; Möhwald, H. *Langmuir* **2002**, *18*, 4553.
21. Zhang, H.; Rühle, J. *Macromol. Rapid Commun.* **2003**, *24*, 576.
22. Tong, W. J.; Dong, W.-F.; Gao, C. Y.; Möhwald, H. *J. Phys. Chem. B* **2005**, *109*, 13159.
23. (a) Nguyen, M. T.; Diaz, A. F.; Dement'ev, V. V.; Pannell, K. H. *Chem. Mater.* **1993**, *5*, 1389; (b) Pudelski, J. K.; Foucher, D. A.; Honeyman, C. H.; Macdonald, P. M.; Manners, I.; Barlow, S.; O'Hare, D. *Macromolecules* **1996**, *29*, 1894; (c) Rulkens, R.; Resendes, R.; Verma, A.; Manners, I.; Murti, K.; Fossum, E.; Miller, P.; Matyjaszewski, K. *Macromolecules* **1997**, *30*, 8165; (d) Arsenault, A. C.; Míguez, H.; Kitaev, V.; Ozin, G. A.; Manners, I. *Adv. Mater.* **2003**, *15*, 503; (e) Giannotti, M. I.; Lv, H.; Ma, Y.; Steenvoorden, M. P.; Overweg, A. R.; Roerdink, M.; Hempenius, M. A.; Vancso, G. J. *J. Inorg. Organomet. Polym. Mater.* **2005**, *15*, 527.
24. Since the oxidant was on-site added to the capsule sample during the CLSM imaging, the recorded induction period varies with the monitoring location.
25. Tong, W.; Gao, C.; Möhwald, H. *Chem. Mater.* **2005**, *17*, 4610.
26. The PSS<sup>-</sup>/PAH<sup>+</sup> bilayer thickness on the (PSS<sup>-</sup>/PAH<sup>+</sup>)<sub>2</sub>(PFS<sup>-</sup>/PFS<sup>+</sup>)<sub>3</sub> capsules prepared from MF cores as presented in Chapter 5.2.1 was measured by AFM to be around 3.2 nm.
27. (a) Foucher, D. A.; Tang, B. Z.; Manners, I. *J. Am. Chem. Soc.* **1992**, *114*, 6246; (b) Foucher, D.; Ziembinski, R.; Petersen, R.; Pudelski, J.; Edwards, M.; Ni, Y.; Massey, J.; Jaeger, C. R.; Vancso, G. J.; Manners, I. *Macromolecules* **1994**, *27*, 3992; (c) Rulkens, R.; Lough, A. J.; Manners, I.; Lovelace, S. R.; Grant, C.; Geiger, W. E. *J. Am. Chem. Soc.* **1996**, *118*, 12683.
28. Hodak, J.; Etchenique, R.; Calvo, E. J.; Singhal, K.; Bartlett, P. N. *Langmuir* **1997**, *13*, 2708.
29. Gossner, D. K. *Cyclic Voltammetry: Simulation and Analysis of Reaction Mechanisms* VCH, **1993**, 75 - 77.
30. It has been observed that when the molar masses of the polycations and polyanions do not match, the growth profile and the capsule permeability dependence on the bilayer numbers will change as well. For example, when PSS with a molar mass of  $1.3 \times 10^4$

g/mol was assembled with  $5.3 \times 10^4$  g/mol PFS, a majority of impermeable capsules could only be obtained when the number of deposited bilayers was higher than 7.

31. Petrov, A. I.; Antipov, A. A.; Sukhorukov, G. B. *Macromolecules* **2003**, *36*, 10079.
32. Péter, M.; Hempenius, M. A.; Kooij, E. S.; Jenkins, T. A.; Roser S. J.; Knoll, W.; Vancso, G. J. *Langmuir* **2004**, *20*, 891.
33. (a) Zou, S.; Ma, Y.; Hempenius, M. A.; Schönherr, H.; Vancso, G. J. *Langmuir* **2004**, *20*, 6278; (b) Zou, S.; Hempenius, M. A.; Schönherr, H., Vancso, G. J. *Macromol. Rapid Commun.* **2006**, *27*, 103; (c) Zou, S.; Korczagin, I.; Hempenius, M. A.; Schönherr, H.; Vancso, G. J. *Polymer* **2006**, *47*, 2483.
34. Mauser, T.; Déjugnat, C; Möhwald, H.; Sukhorukov, G. B. *Langmuir* **2006**, *22*, 5888.
35. Hoogeveen, N. G.; Cohen Stuart, M. A.; Fleer, G. J.; Böhmer, M. R. *Langmuir* **1996**, *12*, 3675.
36. Bertrand, P.; Jonas, A.; Laschewsky, A.; Legras, R. *Macromol. Rapid. Commun.* **2000**, *21*, 319.



# Chapter 6

## Electrostatic Assembly of Poly(ferrocenylsilane) Polyelectrolytes with DNA\*

*In this Chapter the electrostatic assembly of poly(ferrocenylsilane) polyelectrolytes with DNA is discussed. Following the successful layer-by-layer supramolecular assembly of double-stranded, high molar mass DNA and poly(ferrocenylsilane) polycations, redox-responsive macroporous thin films and free-standing microcapsules with excellent permeability were obtained. In order to clarify the mechanism of the macroporous structure formation, PFS and DNA with varying molar masses were assembled and the surface morphologies of the corresponding multilayers were compared.*

### 6.1 Introduction

The development of bio-compatible and responsive molecular platforms that can be applied to deliver and release functional species represents, if realized, frontiers in materials science. Many biological molecules such as DNA, proteins and polysaccharides are polyelectrolytes. Making use of their charged nature, biomacromolecular polyelectrolytes could be incorporated into the electrostatic self-assembly process to give material structures that may possess desired bio-compatibility. Moreover, the combination of biomacromolecules with a synthetic redox-responsive polyelectrolyte provides added value of directed functions such as controlled release.

The electrostatic layer-by-layer assembly technique offers the great advantage of compatibility with functional species without loss of their specific functions.<sup>1, 2</sup> Functional polyelectrolyte multilayers (PEMs) have shown potential applications in tuneable surface wettability, controlled drug release, and switchable permeability.<sup>3</sup> DNA is a semi-flexible anionic biological polyelectrolyte that can be incorporated into the layer-by-layer supramolecular assembly process.<sup>4</sup> Besides the redox-responsive properties of poly(ferrocenylsilane) (PFS) polyelectrolytes described in the previous Chapters, another important structural characteristic of PFS is its highly hydrophobic and flexible polymer main chain (see molecular structures in Chapter 3). In this Chapter, a new PEM system built up

---

\* Part of the work described in this Chapter has been published: Ma, Y.; Dong, W.-F.; Hempenius, M. A.; Möhwald, H.; Vancso, G. J. *Angew. Chem. Int. Ed. Eng.* **2007**, *46*, 1702 and inside cover of the same issue.

from the above two functional components, *i.e.* semi-flexible double-stranded DNA (ds-DNA) and poly(ferrocenylsilane) polycations will be discussed. In this one-step “bottom-up” self-assembly of high molar mass ds-DNA and PFS, a unique macroporous architecture featuring bio-compatible and redox-active components was obtained. A mechanism of the macropore formation will be proposed based on the macromolecular characteristics of the two components, with supporting evidence from the layer-by-layer deposition of PFS and DNA with varying molar masses.

## **6.2 LBL assembly of poly(ferrocenylsilane) polycations and high molar mass ds-DNA**

In the first experiments, high molar mass, double-stranded DNA was incorporated into the layer-by-layer supramolecular assembly with poly(ferrocenylsilane) polycations to form planar thin films and free-standing microcapsules. Due to the interplay of their specific molecular characteristics, the first layer-by-layer constructed macroporous architectures without using any post treatment following fabrication<sup>5</sup> will be demonstrated here. A main advantage of this strategy is that it could offer a universal and facile route to the spontaneous fabrication of porous thin films containing other semi-flexible polyelectrolytes, such as polysaccharides and liquid-crystalline (LC) materials. Moreover, the unique redox-active component PFS<sup>6</sup> allows us to further study the responsiveness of the as-formed thin films to *e.g.* chemical oxidation.<sup>2</sup>

### **6.2.1 Macroporous multilayers**

The electrostatic layer-by-layer self-assembly process of high molar mass ds-DNA and PFS polycation **4** on quartz slides was first monitored by UV/Vis spectroscopy. In Figure 6.1, the two dominant absorbances at 216 nm and 260 nm in the UV/Vis spectra recorded on the obtained multilayers correspond to the characteristic absorbances of PFS and DNA, respectively. The film appeared to grow in a “true” layer-by-layer fashion, since a linear increase of DNA absorbance at 260 nm was observed after peak deconvolution (Figure 6.1A). However, the increase of PFS absorbance at 216 nm was found to be not entirely linear (Figure 6.1B).



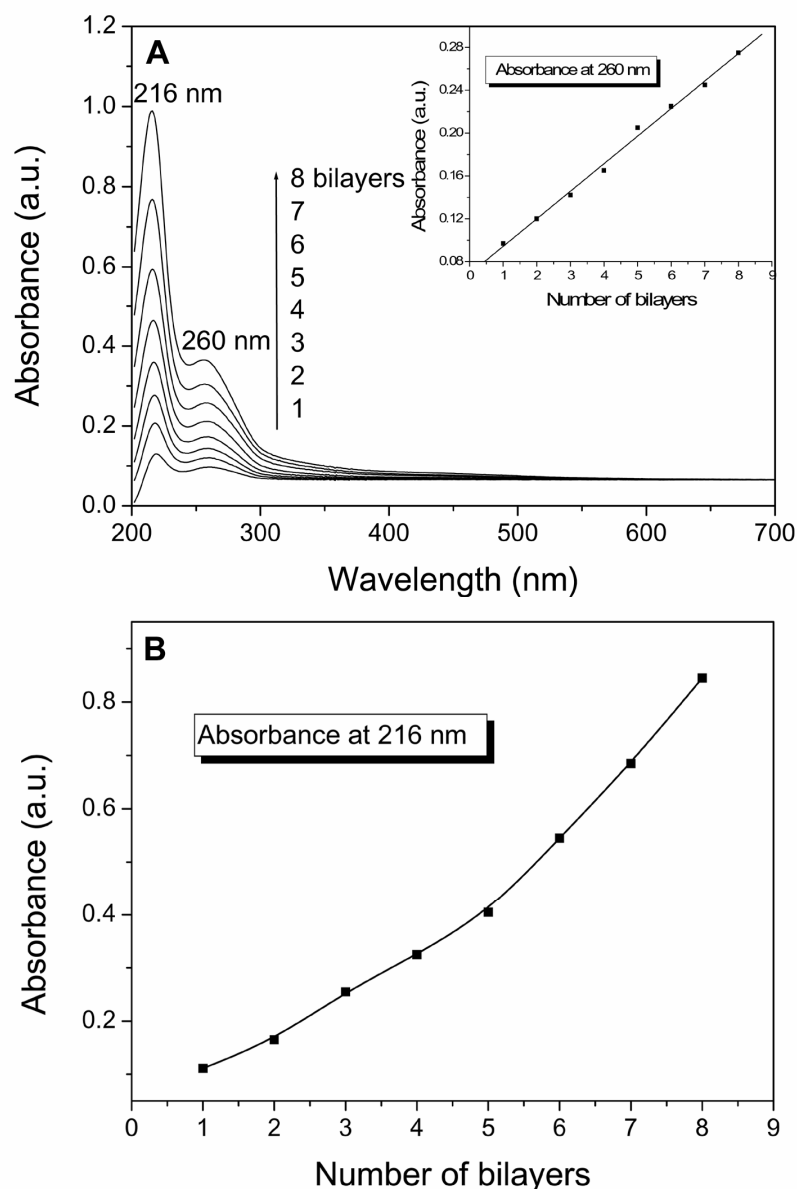


**Figure 6.1** (A) UV/Vis spectra of sequentially absorbed layers of DNA/PFS from aqueous solutions (2 mg/mL, 0.5 M NaCl) on quartz with a pre-deposited layer of PEI. After peak deconvolution, a linear-growth was observed for DNA at 260 nm. (B) A non-linear growth profile was observed for PFS at 216 nm.

This somewhat non-regular film growth was further studied using quartz crystal microbalance (QCM) after each bilayer deposition (Figure 6.2). Since the QCM frequency shift ( $\Delta F$ ) is related linearly to the mass change on the electrode (Chapter 4), the apparent non-linear decrease of the QCM frequency confirmed a non-linear film growth.

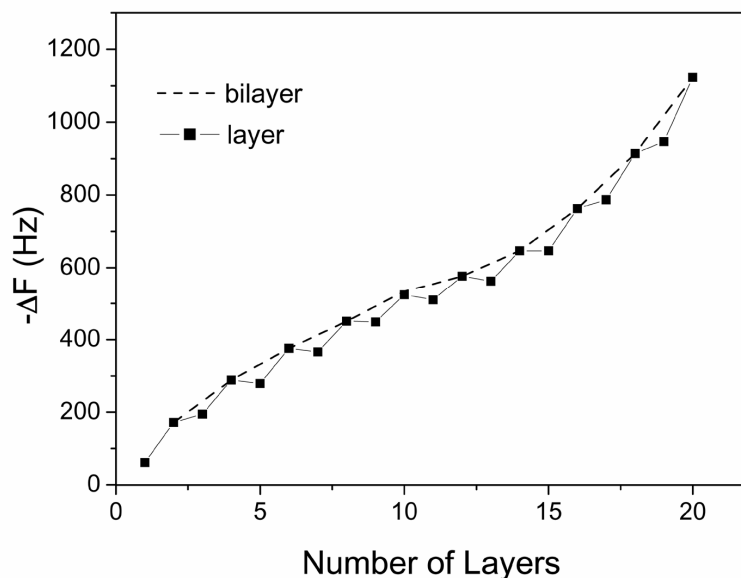


**Figure 6.2** Change in QCM frequency with the layer-by-layer adsorption of DNA/PFS to a QCM electrode with predeposited PEI layer.

The thin film morphology following the LBL self-assembly process was monitored by atomic force microscopy (AFM) used in the tapping mode. As shown in Figure 6.3, after the deposition of a smooth, positively-charged polyethyleneimine (PEI) layer (Figure 6.3A), the first DNA/PFS bilayer transforms the flat, featureless silicon surface to exhibit an irregular, web-like morphology (Figure 6.3B). This is consistent with former reports on DNA network formation from DNA solutions of relatively high concentrations.<sup>7</sup> The 2-dimensional DNA network evolves with increasing the number of deposited polyelectrolyte layers into a 3-dimensional hierarchical structure (Figure 6.3C and D). It is clearly observed from the AFM images that the average pore size of the observed porous structure is also increasing with the number of bilayers, accompanied by an increase of the height of the ridges. Sectional analysis of the film consisting of ten bilayers of DNA/PFS (Figure 6.3D) shows sizes of the largest pores around 350 nm. These features make the as-formed structures macroporous.<sup>8</sup> In this process, the surface roughness of the thin film increases with an increasing number of polyelectrolyte bilayers (Figure 6.4).

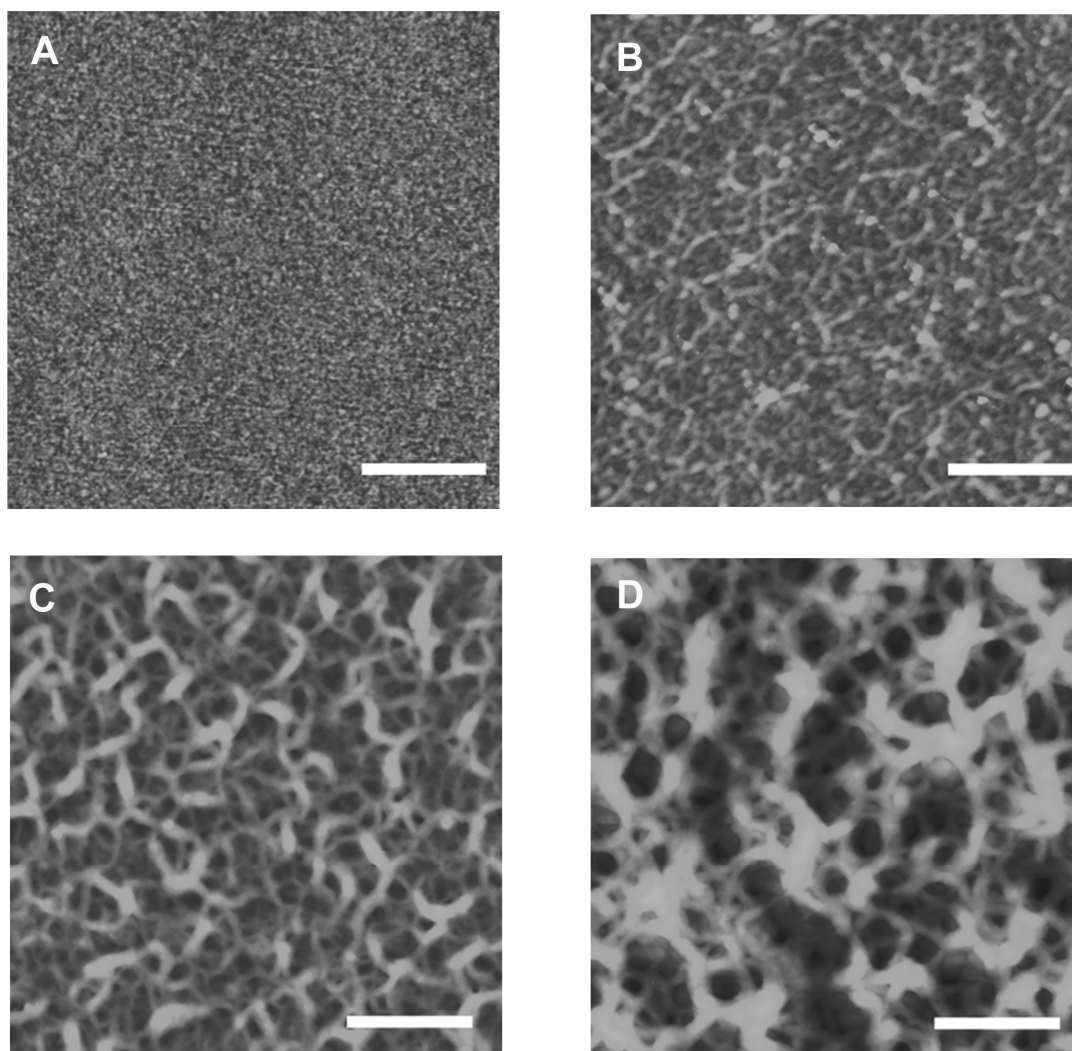


**Figure 6.3** Tapping mode AFM height images of silicon wafers with (A) PEI layer; (B) PEI + (DNA/PFS)<sub>1</sub>; (C) PEI + (DNA/PFS)<sub>5</sub>; (D) PEI + (DNA/PFS)<sub>10</sub>. Z range: (A) 3.0 nm; (B) 20 nm; (C) 80 nm; (D) 100 nm. Scale bar is 500 nm.

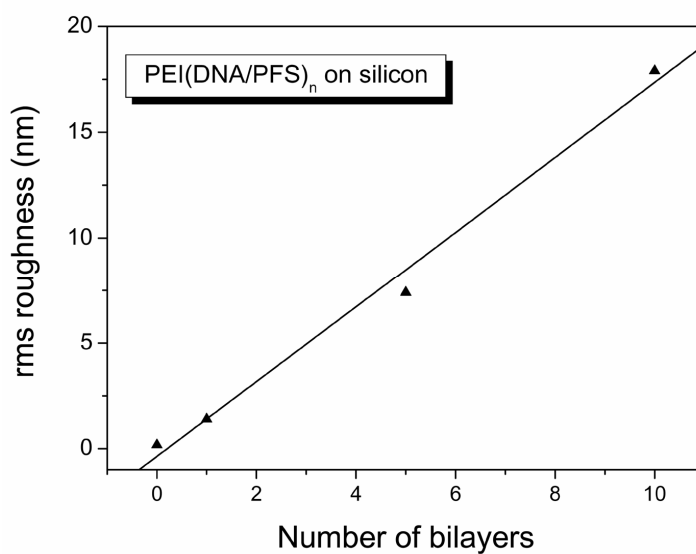


**Figure 6.4** rms roughnesses of PEI+ (DNA/PFS)<sub>n</sub> films on silicon wafers measured by TM-AFM as a function of the number of bilayers.

The large-scale macroporous surface morphology was confirmed by scanning electron microscopy (SEM) imaging on the same type of samples (Figure 6.5), and the pore size observed by SEM and AFM were similar. In order to preserve the features of the surface morphology no conductive layer was applied in SEM imaging, which limited the focal depth. Hence the in-depth information about the macroporous morphology, which could be clearly observed in the AFM images, was compromised.

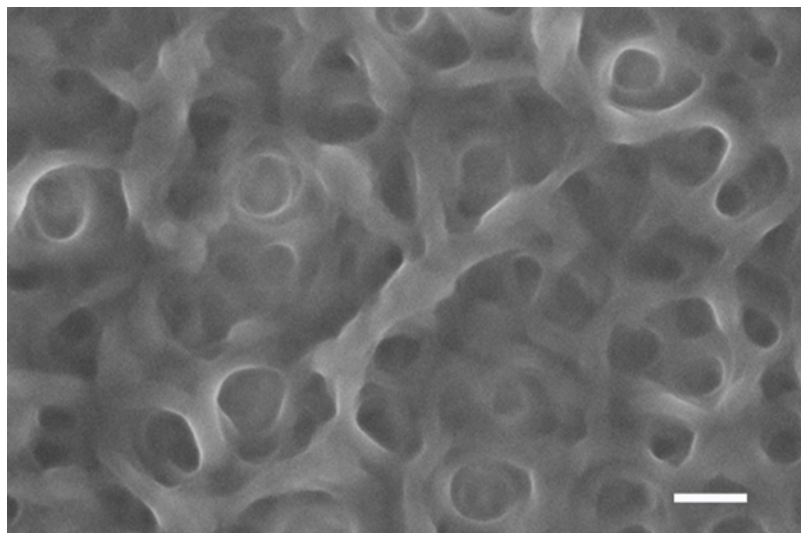


**Figure 6.5** Top view scanning electron microscopy (SEM) images of a PEI + (DNA/PFS)<sub>10</sub> film on a silicon surface. Scale bar = 200 nm.

This observed morphology peculiarly remains porous regardless of the choice of the last layer (DNA or PFS). This observation is in clear contrast with the layer-by-layer system consisting of DNA and other types of cationic polyelectrolytes, for example poly(allylamine hydrochloride) (PAH).<sup>4f, 4g</sup> SEM images show a somewhat different appearance of surface morphology of (DNA/PAH) thin films with varying polyelectrolyte species in the outmost layer (Figure 6.6). The difference in surface morphology when using PFS or PAH as the cationic polyelectrolyte species in the layer-by-layer process was considered to be the consequence of different hydrophobicity of the polycation backbone.

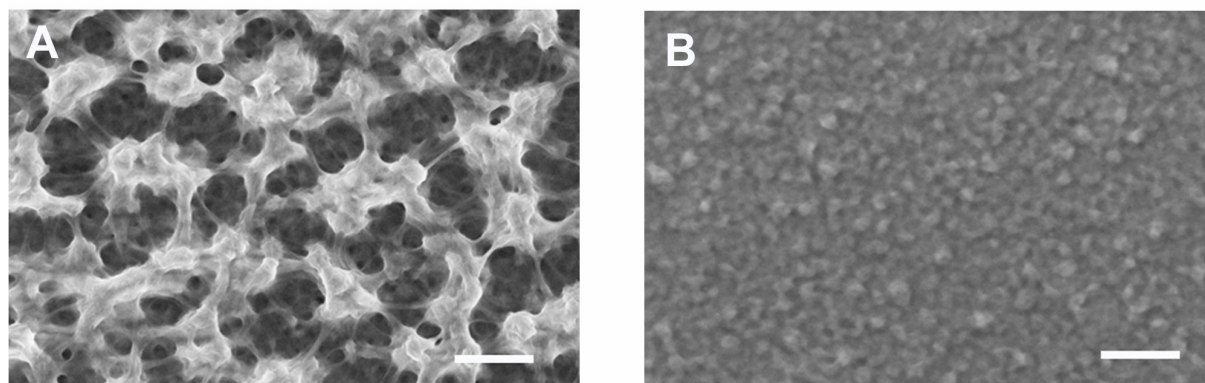
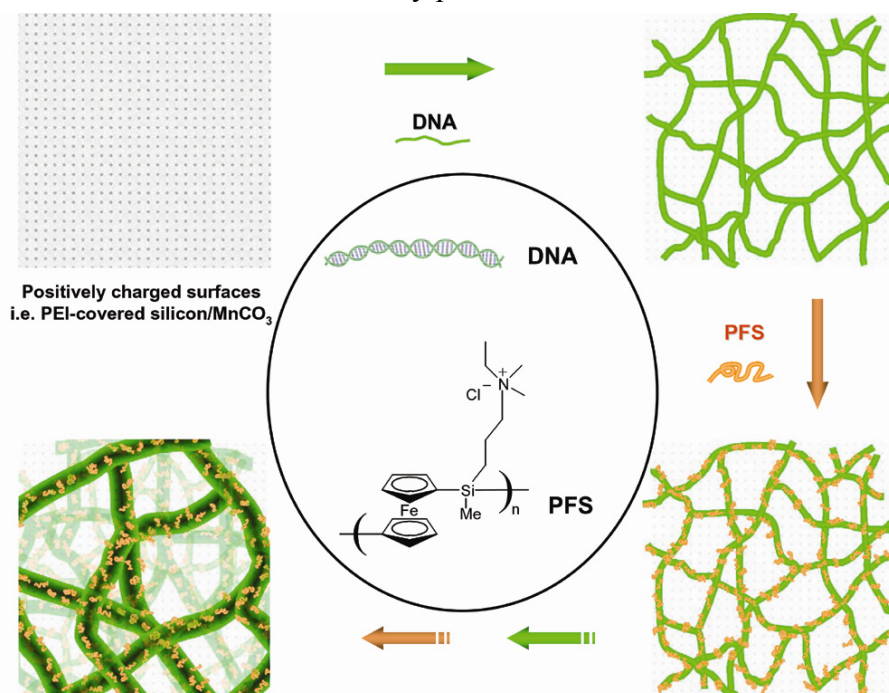


**Figure 6.6** Top view scanning electron microscopy (SEM) images of (A) PEI + (DNA/PAH)<sub>9</sub> + DNA and (B) PEI + (DNA/PAH)<sub>9</sub> thin films on silicon surfaces. Scale bar = 1  $\mu$ m for both images.

The formation of the peculiar porous structure is considered to be the result of an interplay of the persistence length mismatch, chain length/molar mass mismatch and the hydrophobic/hydrophilic nature of the two components. DNA molecules are hydrophobic-hydrophilic in nature due to the existence of hydrophobic bases and hydrophilic backbones that consist of repeating sugar molecules and phosphate groups. The polycation we employed, PFS, has a very hydrophobic backbone and ionic hydrophilic side groups. The strongly hydrophobic PFS backbone is likely the cause of a stable coordination with the DNA molecules. On the other hand, the DNA we used had a molar mass of about one million g/mol, which is much higher than that of PFS ( $5.3 \times 10^4$  g/mol). The molecular weight mismatch will in turn represent a difference in the size of the polymer coils upon their layer-by-layer deposition onto the substrates. Moreover, under the relatively high salt concentration (0.5 M) of our experimental conditions, the charges on the flexible PFS (persistence length,  $L_p \sim 1$  nm<sup>9</sup>) polycations will be completely shielded, forcing them to adopt a collapsed coiled conformation. In contrast, DNA is an extended anionic polyelectrolyte, with an  $L_p$  of about 50 nm, which is relatively insensitive to ionic strength.<sup>10</sup> The large persistence length of DNA will tend to “direct” subsequent bilayer depositions, giving rise to a somewhat “aligned” layer-by-layer structure. The whole assembly process is illustrated in Scheme 6.1.



**Scheme 6.1** Schematic of the preparation of macroporous DNA/PFS architectures by electrostatic layer-by-layer assembly. The semiflexible polyelectrolyte (DNA) forms a network onto which shorter and flexible PFS adsorbs, then the process is repeated to obtain a multilayer network. Chain lengths of PFS and DNA fiber diameters are approximately to scale.

In order to further explain the formation and stability of the macroporous structures, the same type of thin films (DNA/PFS)<sub>n</sub> ( $n$  represents the number of bilayers) was also fabricated without any drying steps in between the LBL depositions. In situ AFM showed

similar porous structures (Figure 6.7), when the samples were immersed in aqueous medium. The morphology observed did not depend on the choice of the last layer as shown in Figure 6.7 (Figure 6.7A: DNA terminating; Figure 6.7B: PFS terminating). These results indicate that the macropore formation may only marginally depend on the drying process, and a drying-induced phase separation was not the main driving force of structure formation. Thus the as-formed hierarchical structures must originate from a spontaneous assembly process. When aqueous solutions (NaCl, 0.5 M) of the two components were mixed, immediate formation of a water insoluble complex was observed, giving further support of the above explanation.

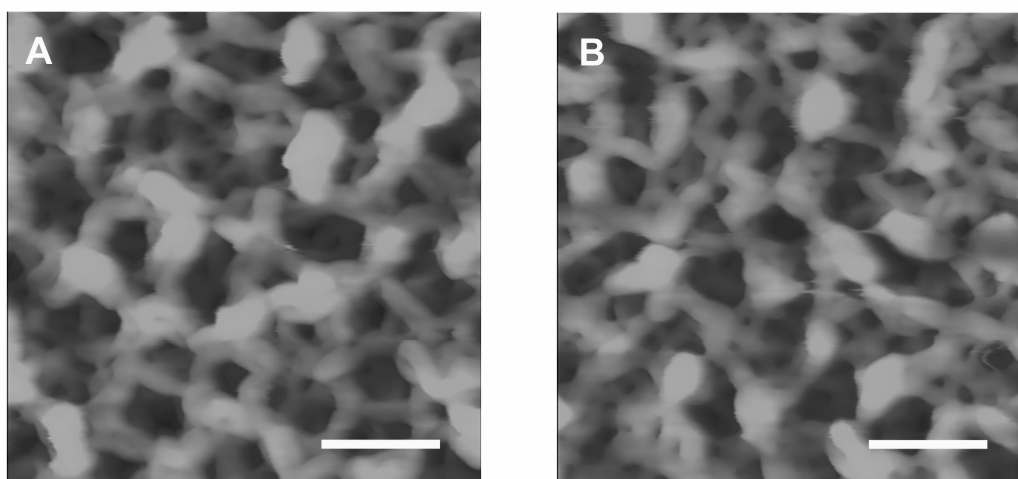


**Figure 6.7** In situ TM-AFM images of a (A) PEI + (DNA/PFS)<sub>9</sub> + DNA and (B) PEI + (DNA/PFS)<sub>10</sub> thin film on silicon substrates. Scale bar and z-range is 500 nm for both images.

The pore formation mechanism described above can be further confirmed and understood by studying the assembly, structure and permeability of DNA/PFS microcapsules. (DNA/PFS)<sub>5</sub> microcapsules were fabricated by alternating layer-by-layer assembly of the two components onto positively charged manganese carbonate (MnCO<sub>3</sub>) colloidal particles followed by template removal. The assembly process was accompanied by severe aggregation, which was usually not observed when making similar coatings using common polyion pairs (see also Chapter 5). Aggregation has been observed before during the fabrication of other DNA-containing multilayer microcapsules, yet no clear explanation was proposed.<sup>4f, 4g</sup> When SEM was used to visualize the dried templates with the layer-by-layer coatings, thick bundles acting as “bridges” between the coated templates were observed (Figure 6.8). These bundles, likely to be mainly composed of DNA, were probably formed due to the very large length of the DNA molecules used (several  $\mu\text{m}$ ). As shown in Figure 6.8B, the macroporous thin film morphology exhibited similar pore sizes on these spherical templates as on planar substrates (Figure 6.5). Apart from the apparent “bridging” of the particles, the cause of aggregation should also come from the electrostatic adhesion between the uncovered (*i.e.* exposed)

positively charged  $\text{MnCO}_3$  surface and negatively charged DNA molecules, as a result of the macroporous thin film structures formed.

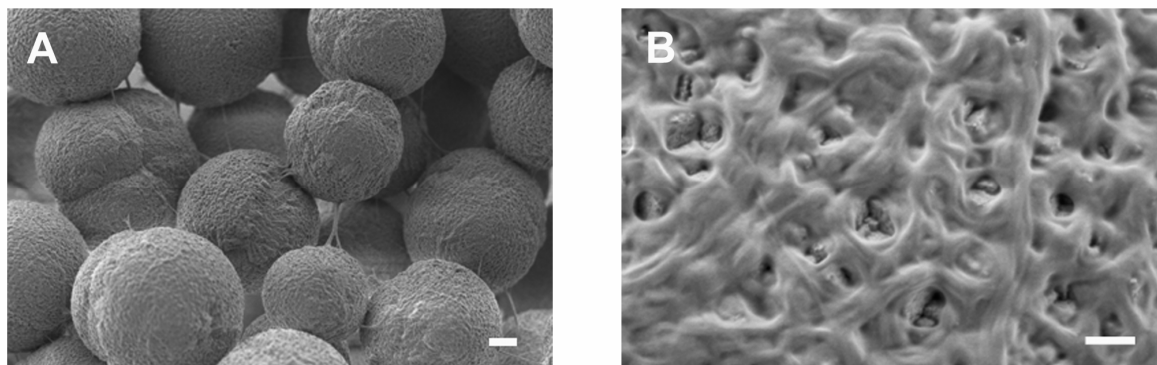


**Figure 6.8** SEM images of  $\text{MnCO}_3$  microspheres coated with  $(\text{DNA/PFS})_5$ : (A) an overview, scale bar = 2  $\mu\text{m}$ ; (B) a zoom-in on the surface of an individual particle, scale bar = 200 nm. Acceleration voltage = 0.6 kV.

$(\text{DNA/PFS})_5$  microcapsules were obtained after removal of the templates using EDTA (0.2 M, pH = 7). SEM images of air-dried capsules show their intact and porous structures (Figure 6.9).

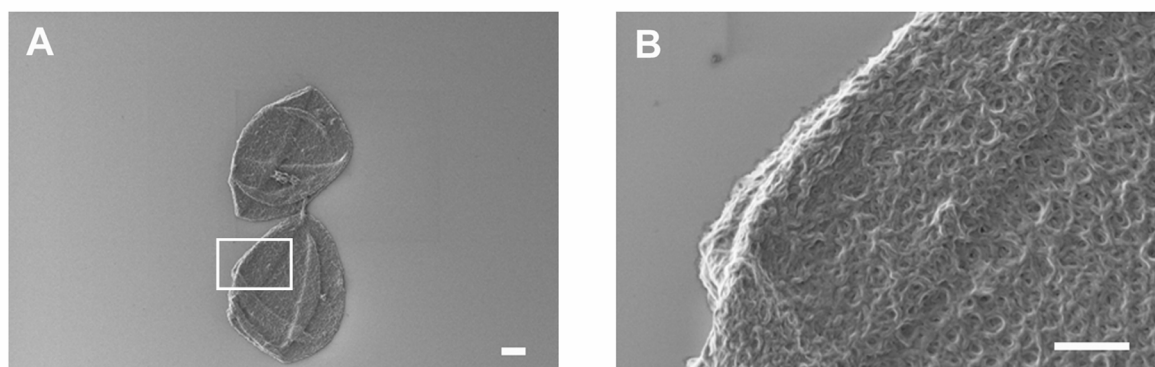


**Figure 6.9**  $(\text{DNA/PFS})_5$  microcapsules: SEM images of (A) collapsed air-dried  $(\text{DNA/PFS})_5$  microcapsules, scale bar = 2  $\mu\text{m}$  and (B) porous capsule wall at a high magnification from the square zone in (A), scale bar = 1  $\mu\text{m}$ .

Confocal laser scanning microscopy (CLSM) images (Figure 6.10) show that unlike conventional  $\text{PSS/PAH}^{11}$  and the previously studied  $\text{PFS}^-/\text{PFS}^+$  capsules, these DNA/PFS microcapsules display complete permeability to large molecules (Figure 6.10A,  $6.6 \times 10^4$  g/mol dextran, hydrodynamic radius = 9 nm<sup>11</sup>) and macromolecules (Figure 6.10B, MRho-PSS,  $1.2 \times 10^5$  g/mol<sup>12</sup>). The unusual permeability behaviour is believed to originate from the unique macroporous structures of the as-prepared thin films.

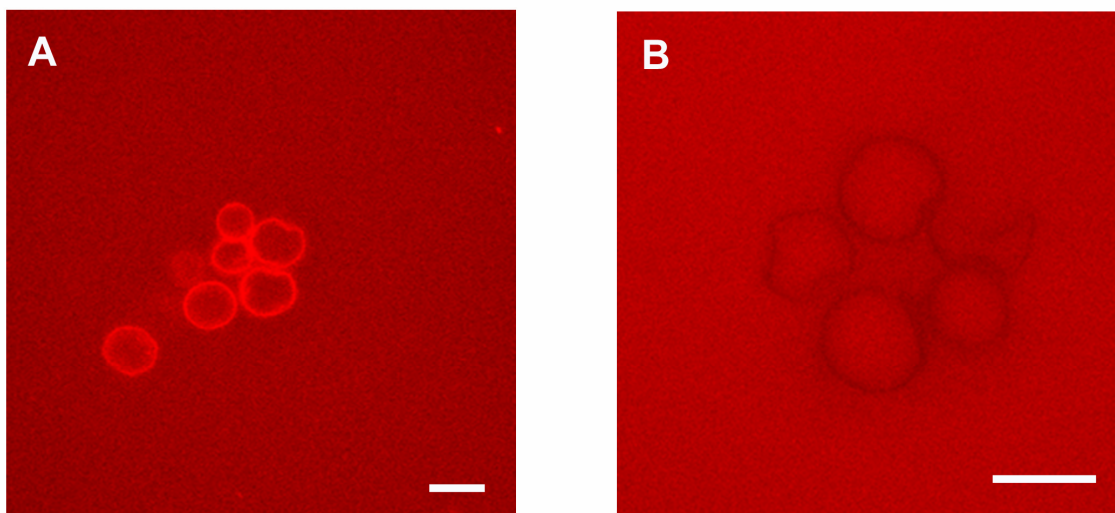


**Figure 6.10** Confocal laser scanning micrographs (CLSM) of (DNA/PFS)<sub>5</sub> microcapsules in the presence of (A) TRITC-dextran ( $6.6 \times 10^4$  g/mol, hydrodynamic radius  $9 \text{ nm}^{11}$ ) and (B) methacroyloxyethylthiocarbamoyl rhodamine B (MRho) labelled PSS ( $1.2 \times 10^5$  g/mol).<sup>12</sup> Scale bar =  $10 \mu\text{m}$  for both images. All capsules display severe aggregation and excellent permeability to the probe molecules. Due to the different nature of the probe molecules, accumulation of TRITC-dextran and expulsion of anionic MRho-PSS were observed, respectively, on the capsule wall.

## 6.2.2 Redox properties

As mentioned earlier, the redox-active component PFS makes the obtained DNA/PFS macroporous structures responsive to chemical oxidation. A quartz crystal microbalance (QCM) was used to follow the thin film oxidation process upon exposure to aqueous ferric chloride ( $\text{FeCl}_3$ ) solutions. The recorded QCM frequency changes with time were converted to mass loss and are presented in Figure 6.11. In contrast to other PFS-containing multilayer systems that bear a continuous thin film morphology, DNA/PFS thin films did not disintegrate completely upon oxidation. However, a fast material loss of up to 35% of the total mass of the as-prepared thin film was obtained. We speculate this to be the result of a partial release of the PFS species in order to maintain charge neutrality of the network structure, as PFS becomes more positively charged after oxidation. Since an estimated total weight loss of 45% was expected for the full oxidation of PFS, the result shown in Figure 6.11 suggests incomplete oxidation. Although material loss happened during chemical oxidation, the surface morphology of these films sustained their unique macroporous architecture (Figure 6.12). A certain degree of material loss was also demonstrated from the AFM topography images where the height of the ridges relative to the voids, which could also be interpreted as the effective film thickness, decreased to  $\sim 3/4$  of its original value. Similarly, (DNA/PFS)<sub>5</sub> microcapsules exhibited a high resistance to chemical oxidation. They kept their integrity in the presence of  $\text{FeCl}_3$  (1 mM) for a rather long period (more than 24 hours), while (PFS<sup>-</sup>/PFS<sup>+</sup>)<sub>5</sub> microcapsules disintegrated within 30 min under the same experimental conditions (see Chapter 5).<sup>2</sup>



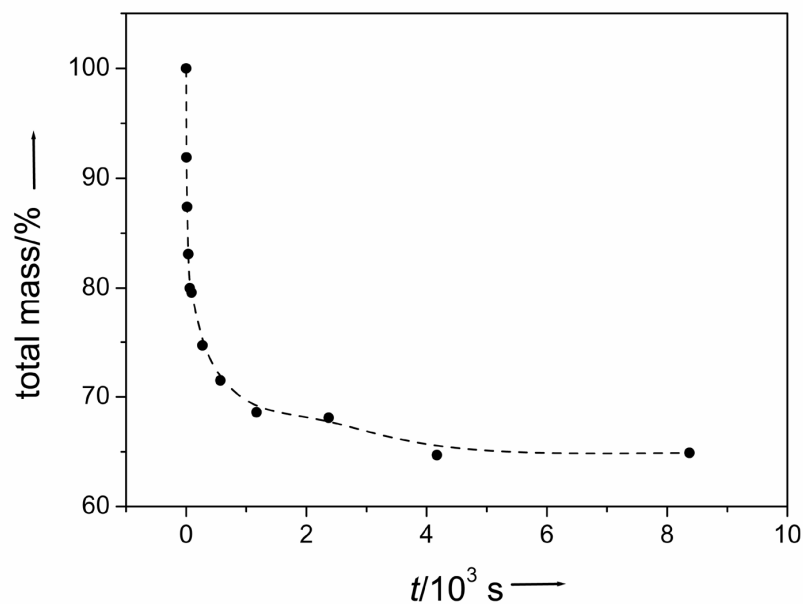


**Figure 6.11** Oxidation of PEI(DNA/PFS)<sub>10</sub> thin films: change in QCM frequency converted to mass loss with time by exposure to FeCl<sub>3</sub> aqueous solutions (1 mM) on a QCM electrode.

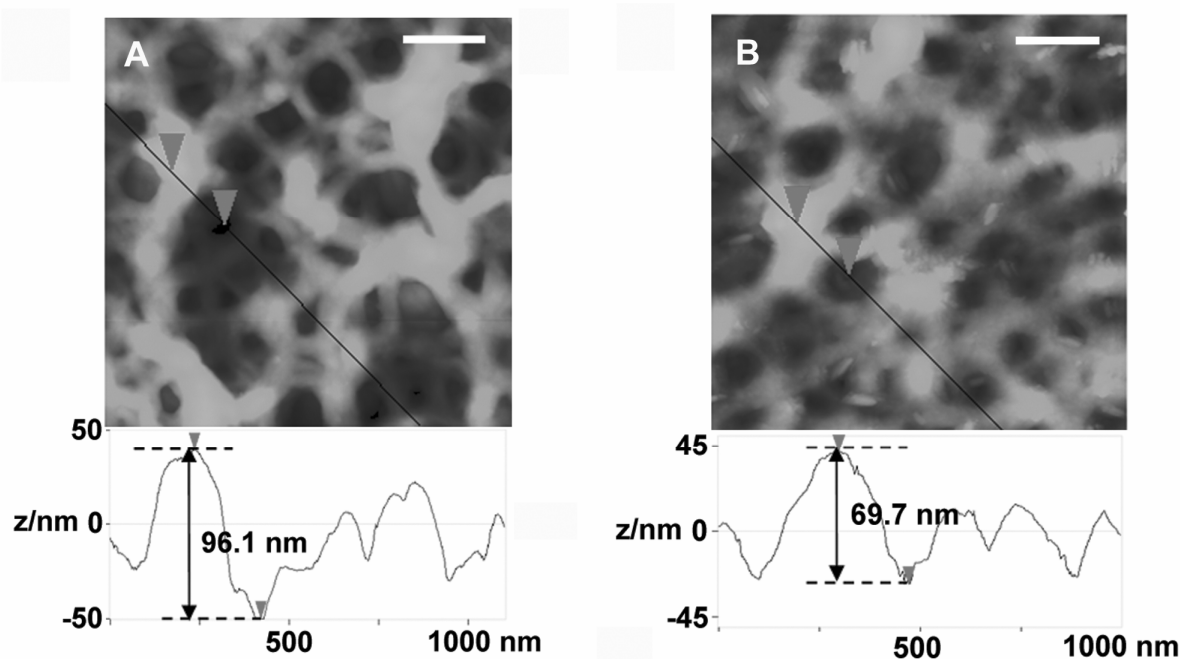


**Figure 6.12** Sectional analyses of TM-AFM height images of PEI(DNA/PFS)<sub>10</sub> on silicon: (A) as prepared, and (B) after oxidation for five minutes by FeCl<sub>3</sub> (3 mM). Z range = 100 nm, scale bar = 200 nm for both images. A decrease in height of the ridges relative to the voids was observed.

### 6.3 Molar mass effect

In Section 6.2, the LBL assembly of low molar mass PFS polycations (LM<sub>w</sub>-PFS) with high molar mass double-stranded DNA (HM<sub>w</sub>-DNA) resulted in a peculiar macroporous thin

film structure. In order to prove the macropore formation mechanism proposed in the previous section (Scheme 6.1), the electrostatic LBL assembly of PFS polycations and DNA with varying degrees of molar mass matching was also studied. The influence of polyelectrolyte molar mass on multilayer formation was investigated by the introduction of two new polyelectrolyte species: high molar mass PFS (HM<sub>w</sub>-PFS, M<sub>w</sub> = 2.9 × 10<sup>5</sup> g/mol) and low molar mass DNA (LM<sub>w</sub>-DNA, M<sub>w</sub> = 5.0 × 10<sup>4</sup> ~ 1.0 × 10<sup>5</sup> g/mol). Varying the molar masses of the polycation and polyanion species in the LBL assembly process is expected to alter the molar mass mismatch while maintaining the persistence length mismatch between these two components.

When HM<sub>w</sub>-PFS was assembled with HM<sub>w</sub>-DNA under the same experimental conditions (0.5 M NaCl), the multilayer surface morphology evolved in a similar manner as the above studied LM<sub>w</sub>-PFS/HM<sub>w</sub>-DNA system. This is demonstrated by the TM-AFM images in Figure 6.13.

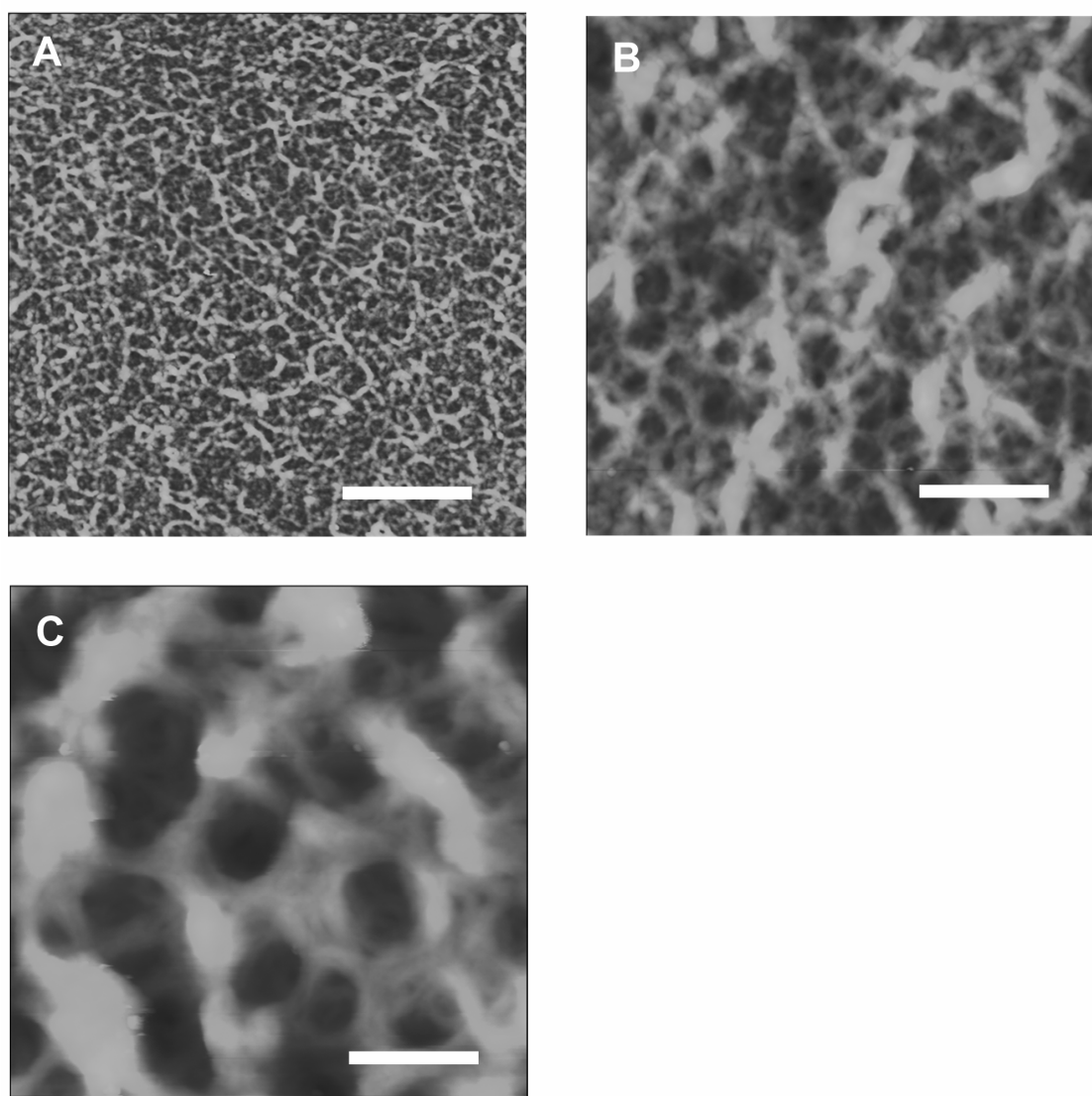


**Figure 6.13** Tapping mode AFM height images of silicon wafers with (A) PEI + (HM<sub>w</sub>-DNA/HM<sub>w</sub>-PFS)<sub>1</sub>; (B) PEI + (HM<sub>w</sub>-DNA/HM<sub>w</sub>-PFS)<sub>5</sub>; (C) PEI + (HM<sub>w</sub>-DNA/HM<sub>w</sub>-PFS)<sub>10</sub>. Z range: (A) 15 nm; (B) 80 nm; (C) 250 nm. Scale bar is 500 nm for all images.

It was observed that the macroporous structures as well as the largest pore size of a ten bilayer  $\text{HM}_w\text{-DNA}/\text{HM}_w\text{-PFS}$  thin film displayed very similar characteristics as the multilayers assembled from  $\text{HM}_w\text{-DNA}/\text{LM}_w\text{-PFS}$ . The surface morphology became completely different when  $\text{LM}_w\text{-PFS}$  was assembled with  $\text{LM}_w\text{-DNA}$  from aqueous solutions with similar ionic strength. As shown in Figure 6.14, the porous features and the certain regularity of the previously observed multilayer structure could not be found in the current system. Moreover, the obtained  $\text{LM}_w\text{-DNA}/\text{LM}_w\text{-PFS}$  multilayers appeared to be very thin, with the thickness of a ten bilayer film below 20 nm.<sup>15</sup>

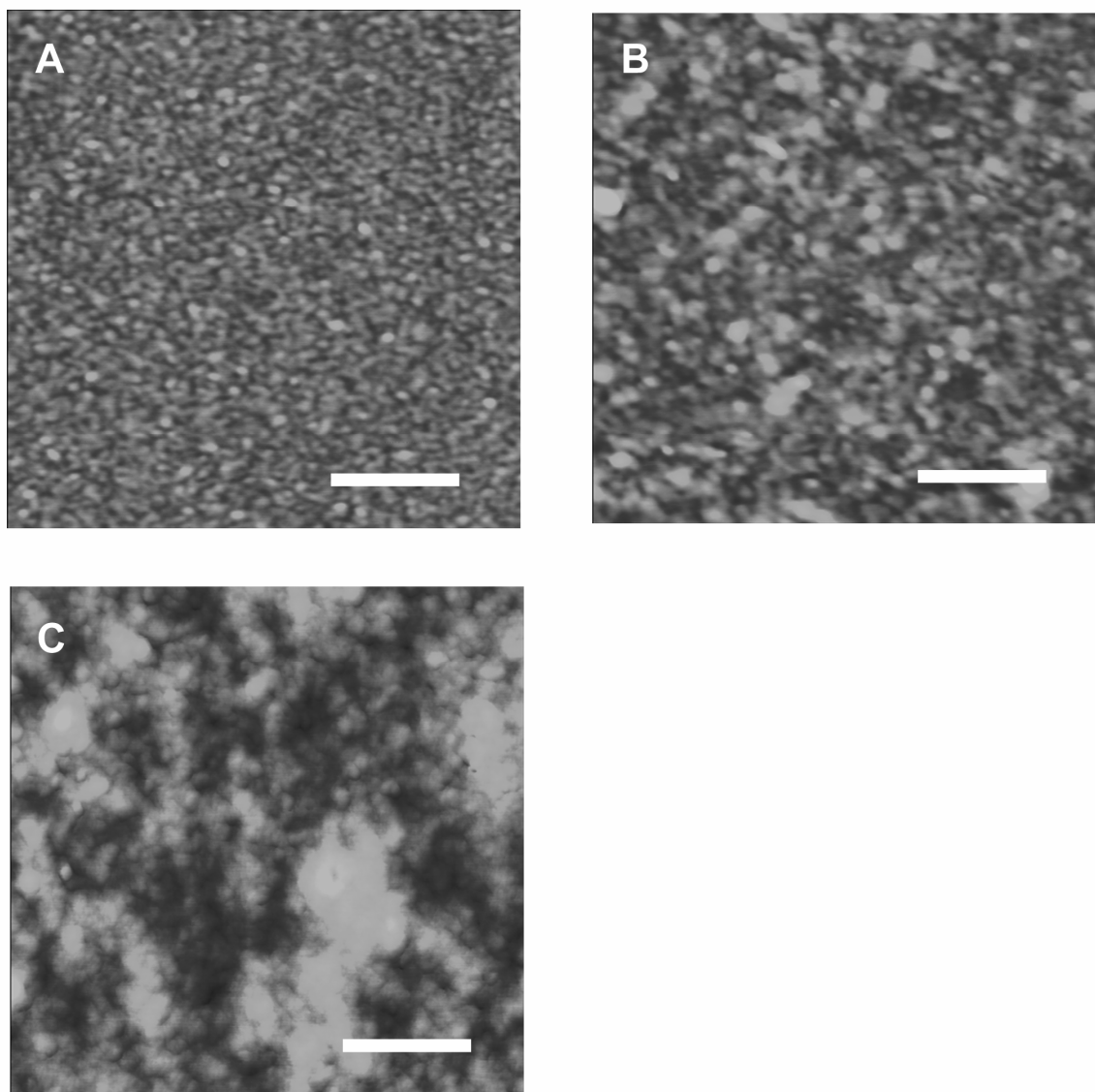


**Figure 6.14** Tapping mode AFM height images of silicon wafers with (A)  $\text{PEI} + (\text{LM}_w\text{-DNA}/\text{LM}_w\text{-PFS})_1$ ; (B)  $\text{PEI} + (\text{LM}_w\text{-DNA}/\text{LM}_w\text{-PFS})_5$ ; (C)  $\text{PEI} + (\text{LM}_w\text{-DNA}/\text{LM}_w\text{-PFS})_{10}$ . Z range: (A) 8 nm; (B) 12 nm; (C) 15 nm. Scale bar is 250 nm for all images.

The results from the above molar mass manipulation experiments of the DNA/PFS multilayer system consolidate the theory that the unique macroporous structure originates from a combination of persistence length and molar mass mismatch of the two components.

The degree of molar mass mismatch in the three studied molecular systems decreased in the sequence of  $HM_w\text{-DNA}/LM_w\text{-PFS} > HM_w\text{-DNA}/HM_w\text{-PFS} > LM_w\text{-DNA}/LM_w\text{-PFS}$ . There appeared to be a critical degree of chain length mismatch, below which the macroporous structure could not be formed any more. In the final case of a short DNA with molecular dimensions almost identical to those of PFS, any pores that might be formed in the early stage of the assembly would possibly be filled-up in the subsequent deposition process to create more compact structures. This could be the reason for the apparently much thinner multilayers<sup>15</sup> obtained in the  $LM_w\text{-DNA}/LM_w\text{-PFS}$  system.

## 6.4 Conclusions

In summary, we have demonstrated the successful electrostatic layer-by-layer assembly of high molar mass double-stranded DNA and poly(ferrocenylsilane) (PFS) polycations into thin films and microcapsules bearing 3-dimensional macroporous structures without any post-treatment. It is proposed that the formation of the highly porous architectures largely originates in the persistence length and chain length mismatch of the two components, as well as the extraordinary hydrophobicity of the macromolecular backbone of PFS. The molecular characteristics of these two components in turn cause aggregation of the as-formed microcapsules and make them highly permeable to macromolecules. The redox-active PFS components render the thin films susceptible to chemical oxidation, while their unique macroporous architectures are maintained. The LBL assembly of PFS and DNA with varying molar masses suggested the existence of a critical molar mass mismatch below which the peculiar macroporous structure could no longer be formed. In conclusion, we have developed a new method for the fabrication of bio-compatible porous structures, which may imply many potential applications, such as their use in new cell scaffold materials, gene therapy, biocompatible surfaces, and controlled, active, molecular release systems.

## 6.5 Experimental

**Materials** Poly(ethyleneimine) (PEI,  $M_w = 2.5 \times 10^4$  g/mol), deoxyribonucleic acid sodium salt from salmon testes (DNA,  $M_w = 1.3 \times 10^6$  g/mol, approximately 2000 bp), low molar mass double-stranded deoxyribonucleic acid salmon sperm (DNA,  $M_w = 5.0 \times 10^4 \sim 1.0 \times 10^5$  g/mol,  $\leq 150$  bp), manganese sulphate ( $MnSO_4$ ), ammonium bicarbonate ( $NH_4HCO_3$ ), ethylenediaminetetraacetic acid trisodium salt (EDTA), ferric chloride ( $FeCl_3$ ) were obtained from Sigma Aldrich and used as received. The fabrication of regular (low)  $M_w$  PFS was described in Chapter 3. The high  $M_w$  PFS ( $M_w = 2.9 \times 10^5$  g/mol) was synthesized as

described in reference 13. Manganese carbonate ( $\text{MnCO}_3$ ) particles were prepared according to the reported method,<sup>14</sup> by using ethanol (concentration 2.5% v/v in the final mixture) as the poor solvent in the crystallization process.

**Layer-by-layer thin film fabrication** After standard cleaning procedure (see Chapter 4), quartz slides, silicon wafers, or quartz crystal microbalance (QCM) electrode substrates were first dipped into a PEI aqueous solution ( $\sim 10$  mM) for 30 minutes to impart positively charged surfaces. Then the modified substrates were alternatively dipped in the PFS polycation and DNA aqueous solutions (2 mg/mL, 0.5 M NaCl) for 10 minutes, with rinsing, dipping into pure MilliQ (2 min), second rinsing and drying with a stream of nitrogen between each deposition step.

**Layer-by-layer microcapsule fabrication** Alternating adsorption of polyelectrolytes (1 mg/mL) onto  $\text{MnCO}_3$  microparticles (average diameter 10  $\mu\text{m}$ ,  $\sim 10\%$  w/w in suspension) was carried out in 0.5 M NaCl solution for 10 min followed by centrifugation (1000 rpm, 2 min) and three MilliQ washing/centrifugation steps. After depositing the desired number of polyelectrolyte bilayers, the coated particles were subjected to core dissolution using 0.2 M EDTA (pH = 7) solution. The resultant capsules were washed thoroughly with and re-suspended in MilliQ.

**Thin film oxidation** Thin films were oxidized by immersion into  $\text{FeCl}_3$  solution (1-3 mM) for desired time intervals, then rinsed thoroughly with MilliQ (2 min) and dried under a stream of nitrogen.

**Characterization** UV/Vis spectra were recorded using a Varian Cary 300 Bio UV/Visible spectrophotometer. Atomic Force Microscopy (AFM) experiments were performed using a NanoScope IIIa multimode AFM (Veeco-Digital Instruments, Santa Barbara, CA) in tapping mode using silicon cantilevers (Nanosensors, Wetzlar, Germany) at room temperature in air or in a liquid cell. Scanning Electron Microscopy (SEM) images of thin film or air-dried capsule samples were taken with a high resolution LEO 1550 FEG SEM at acceleration voltages of 2.5 kV (unless indicated otherwise). Confocal Laser Scanning Microscopy (CLSM) images were taken with a Zeiss LSM 510 (63 x oil immersion objective) confocal scanning system. Equal volumes of capsule suspension and fluorescence probe were mixed before observation.

## 6.6 References and notes

1. Yoo, P. J.; Nam, K. T.; Qi, J. F.; Lee, S.-K.; Park, J.; Belcher, A. M.; Hammond, P. T. *Nat. Mater.* **2006**, *5*, 234.
2. Ma, Y.; Dong, W. F.; Hempenius, M. A.; Möhwald, H.; Vancso, G. J. *Nat. Mater.* **2006**, *5*, 724.

3. (a) Decher, G.; Schlenoff, J. B. (Eds.) *Multilayer Thin Films, Sequential Assembly of Nanocomposite Materials*, Wiley-VCH, Weinheim, Germany, 2003; (b) Donath, E.; Sukhorukov, G. B.; Caruso, F.; Davis, S. A.; Möhwald, H. *Angew. Chem. Int. Ed.* **1998**, *37*, 2202; (c) Hiller, J.; Mendelsohn, J. D.; Rubner, M. F. *Nat. Mater.* **2002**, *1*, 59; (d) Tang, Z. Y.; Kotov, N. A.; Magonov, S.; Ozturk, B. *Nat. Mater.* **2003**, *2*, 413. (e) Shi, X.; Shen, M.; Möhwald, H. *Prog. Polym. Sci.* **2004**, *29*, 987; (f) Hammond, P. T. *Adv. Mater.* **2004**, *16*, 1271; (g) Jiang, C.; Tsukruk, V. V. *Adv. Mater.* **2006**, *18*, 829; (h) Tang, Z.; Wang, Y.; Podsiadlo, P.; Kotov, N. A. *Adv. Mater.* **2006**, *18*, 3203.
4. (a) Lvov, Y.; Decher, G.; Sukhorukov, G. *Macromolecules* **1993**, *26*, 5396; (b) Schuler, C.; Caruso, F. *Biomacromolecules* **2001**, *2*, 921; (c) Serizawa, T.; Yamaguchi, M.; Akashi, M. *Angew. Chem. Int. Ed.* **2003**, *42*, 1115; (d) Zhang, J.; Chua, L. S.; Lynn, D. M. *Langmuir* **2004**, *20*, 8015; (e) Johnston, A. P. R.; Read, E. S.; Caruso, F. *Nano Lett.* **2005**, *5*, 953; (f) Vinogradova, O. I.; Lebedeva, O. V.; Vasilev, K.; Gong, H.; Garcia-Turiel, J.; Kim, B.-S. *Biomacromolecules* **2005**, *6*, 1495; (g) Gong, H.; Garcia-Turiel, J.; Vasilev, K.; Vinogradova, O. I. *Langmuir* **2005**, *21*, 7545.
5. (a) Mendelsohn, J. D.; Barrett, C. J.; Chan, V. V.; Pal, A. J.; Mayes, A. M.; Rubner, M. F. *Langmuir* **2000**, *16*, 5017; (b) Berg, M. C.; Zhai, L.; Cohen, R. E.; Rubner, M. F. *Biomacromolecules* **2006**, *7*, 357.
6. (a) Foucher, D.; Ziembinski, R.; Petersen, R.; Pudelski, J.; Edwards, M.; Ni, Y.; Massey, J.; Jaeger, C. R.; Vancso, G. J.; Manners, I. *Macromolecules* **1994**, *27*, 3992; (b) Rulkens, R.; Lough, A. J.; Manners, I.; Lovelace, S. R.; Grant, C.; Geiger, W. E. *J. Am. Chem. Soc.* **1996**, *118*, 12683; (c) Péter, M.; Hempenius, M. A.; Kooij, E. S.; Jenkins, T. A.; Roser, S. J.; Knoll, W.; Vancso, G. J. *Langmuir* **2004**, *20*, 891.
7. (a) Kanno, T.; Tanaka, H.; Miyoshi, N.; Kawai, T. *Appl. Phys. Lett.* **2000**, *77*, 3848. (b) Xiao, Z.; Xu, M.; Sagisaka, K.; Fujita, D. *Thin Solid Films* **2003**, *438-439*, 114.
8. (a) Mikos, A. G.; Thorsen, A. J.; Czerwonka, L. A.; Bao, Y.; Langer, R.; Winslow, D. N.; Vacanti, J. P. *Polymer* **1994**, *35*, 1068; (b) Imhof, A.; Pine, D. J. *Nature* **1997**, *389*, 948; (c) Holland, B. T.; Blanford, C. F.; Do, T. Stein, A. *Chem. Mater.* **1999**, *11*, 795; (d) Nishikawa, T.; Ookura, R.; Nishida, J.; Arai, K.; Hayashi, J.; Kurono, N.; Sawadaishi, T.; Hara, M.; Shimomura, M. *Langmuir* **2002**, *18*, 5734; (e) Blin, J. L.; Leonard, A.; Yuan, Z. Y.; Gigot, L.; Vantomme, A.; Cheetham, A. K.; Su, B. L. *Angew. Chem. Int. Ed.* **2003**, *42*, 2872; (f) Collins, A.; Carriazo, D.; Davis, S. A.; Mann, S. *Chem. Comm.* **2004**, 568; (g) Chen, V. J.; Ma, P. X. *Biomaterials* **2004**, *25*, 2065; (h) Liu, Y. F.; Wang, S. P.; Lee, J. W.; Kotov, N. A. *Chem. Mater.* **2005**, *17*, 4918; (i) Roy, X.; Sarazin, P.; Favis, B. D. *Adv. Mater.* **2006**, *18*, 1015.
9. Rulkens, R.; Lough, A. J.; Manners, I.; Lovelace, S. R.; Grant, C.; Geiger, W. E.; *J. Am. Chem. Soc.* **1996**, *118*, 12683. The persistence length was estimated from the molecular structure and X-ray diffraction studies of the polymer.

10. (a) Maurstad, G.; Danielsen, S.; Stokke, B. T. *J. Phys. Chem. B* **2003**, *107*, 8172; (b) Baumann, C. G.; Smith, S. B.; Bloomfield, V. A.; Bustamante, C. *Proc. Natl. Acad. Sci.* **1997**, *94*, 6185; (c) Wenner, J. R.; Williams, M. C.; Rouzina, I.; Bloomfield, V. A. *Biophys. J.* **2002**, *82*, 3160.
11. Dong, W.-F.; Ferri, J. K.; Adalsteinsson, T.; Schönhoff, M.; Sukhorukov, G. B.; Möhwald, H. *Chem. Mater.* **2005**, *17*, 2603.
12. Dähne, L.; Leporatti, S.; Donath, E.; Möhwald, H. *J. Am. Chem. Soc.* **2001**, *123*, 5431.
13. Hempenius, M. A.; Brito, F. F.; Vancso, G. J. *Macromolecules* **2003**, *36*, 6683.
14. Antipov, A. A.; Shchukin, D.; Fedutik, Y.; Petrov, A. I.; Sukhorukov, G. B.; Möhwald, H. *Coll. Surf. A: Physicochem. Eng. Asp.* **2003**, *224*, 175.
15. As indicated by AFM topography imaging and independent ellipsometry measurements.





# Chapter 7

## Applications of Poly(ferrocenylsilane) Polyelectrolytes

*Apart from acting as a functional component in the electrostatic layer-by-layer assembly, the charged nature of water-soluble poly(ferrocenylsilanes) also presents many other interesting application potentials. As a first example, cationic poly(ferrocenylsilane) polyelectrolytes were used in plasmid DNA condensation to form polymer-DNA complexes, whose gene transfer properties were studied in vitro. In the second part of this Chapter, the self-assembly of monodisperse polymer-virus nanoparticles based on anionic poly(ferrocenylsilane) polyelectrolytes and cowpea chlorotic mottle virus (CCMV) proteins is discussed.*

### 7.1 Cationic poly(ferrocenylsilane) as DNA condensation and transfection agent\*

#### 7.1.1 Introduction

Many diseases or disorders originate from defected genes. In order to replace those defected genes, an approach called “gene therapy (or gene transfer)” has been introduced.<sup>1</sup> Gene transfer is defined as the transfer of genetic information to specific cells to direct the synthesis of specific proteins. The genetic information (“genes”) is typically encoded with plasmid DNA, although other forms of DNA as well as RNA can also be used.<sup>1</sup> Gene therapy requires DNA to be condensed before it is transported across the cell membrane.<sup>2</sup> DNA condensation refers to the electrostatic attraction between negatively charged DNA and cationic species which leads to partial collapse of the DNA chains as the charge is neutralized and counterions are released. Learning from Nature where viruses have been selected as efficient gene delivery mediators, much of the research in gene therapy is directed at developing synthetic materials that can imitate the assembly function but overcome the immunological concerns of viruses. One group of these synthetic counterparts is cationic polymers.<sup>1-3</sup> In the presence of multivalent polycations, high molar mass DNA undergoes a

---

\* This work was carried out in collaboration with Chao Lin, Dr. Zhi Yuan Zhong and Prof. Jan Feijen from the group of Polymer chemistry and BioMaterials of the University of Twente and has been published: Zhong, Z. Y.; Lin, C.; Ma, Y.; Hempenius, M. A.; Lok, M. C.; Fretz, M. M.; Engbersen, J. F. J.; Vancso, G. J.; Hennink, W. E.; Feijen, J. J. *Control. Rel.* **2006**, *116*, e81.

dramatic condensation to compact nanoparticles called “polyplexes” through polyelectrolyte complex formation (see also Chapter 2.4).

In the past decade, there has been significant progress in the development of cationic polymer-based non-viral gene delivery systems. Polymers such as poly(ethylenimine) (PEI), polylysine (PLL), poly(ethylene glycol) (PEG) based block and graft copolymers poly(2-(dimethylamino)ethyl methacrylate) (PDMAEMA), and polyamidoamine (PAMAM) dendrimers<sup>2</sup> have been evaluated for DNA delivery. However, their utility is rather limited due to cytotoxicity and delivery efficiency reasons. The relatively low transfection activity of these polymers *in vivo* has been shown to remain orders of magnitude below viral vectors.<sup>4</sup>

In addition to effectively package DNA to facilitate its transportation through the cell membrane, it was reported that DNA transfection efficiency could also be increased by unpacking the DNA/polymer polyplexes inside the cell.<sup>5, 6</sup> The cationic and stimuli-responsive nature of organometallic polycations makes it interesting to explore their gene delivery potentials. Here, the use of a poly(ferrocenylsilane) polycation as a new candidate for DNA condensation and *in vitro* transfection is studied.

### 7.1.2 Results and discussion

Polymer/DNA complexes were prepared at the same molar ratios of PFS nitrogen to DNA phosphate (N/P), as originally used for PEI/DNA complexes.<sup>7</sup> PFS polycation **4** (see molecular structure in Chapter 3) was used here. The size and surface charge of the PFS/DNA polyplexes were first studied by dynamic light scattering (DLS) and zeta ( $\zeta$ ) potential measurements. Figure 7.1A shows the relatively small hydrodynamic radius (90 – 140 nm) of PFS polyplexes formed at N/P ratios  $\geq 2/1$  compared to that of the original plasmid DNA. The constant positive surface charges (+ 45 – 50 mV) at the same N/P ratio range indicated the formation of a stable complex. DLS measurements also revealed the gradual evolution of the polyplexes into larger aggregates in the presence of 150 mM NaCl (Figure 7.1B), in a similar manner as observed before for linear PEI/DNA complexes.<sup>7</sup>

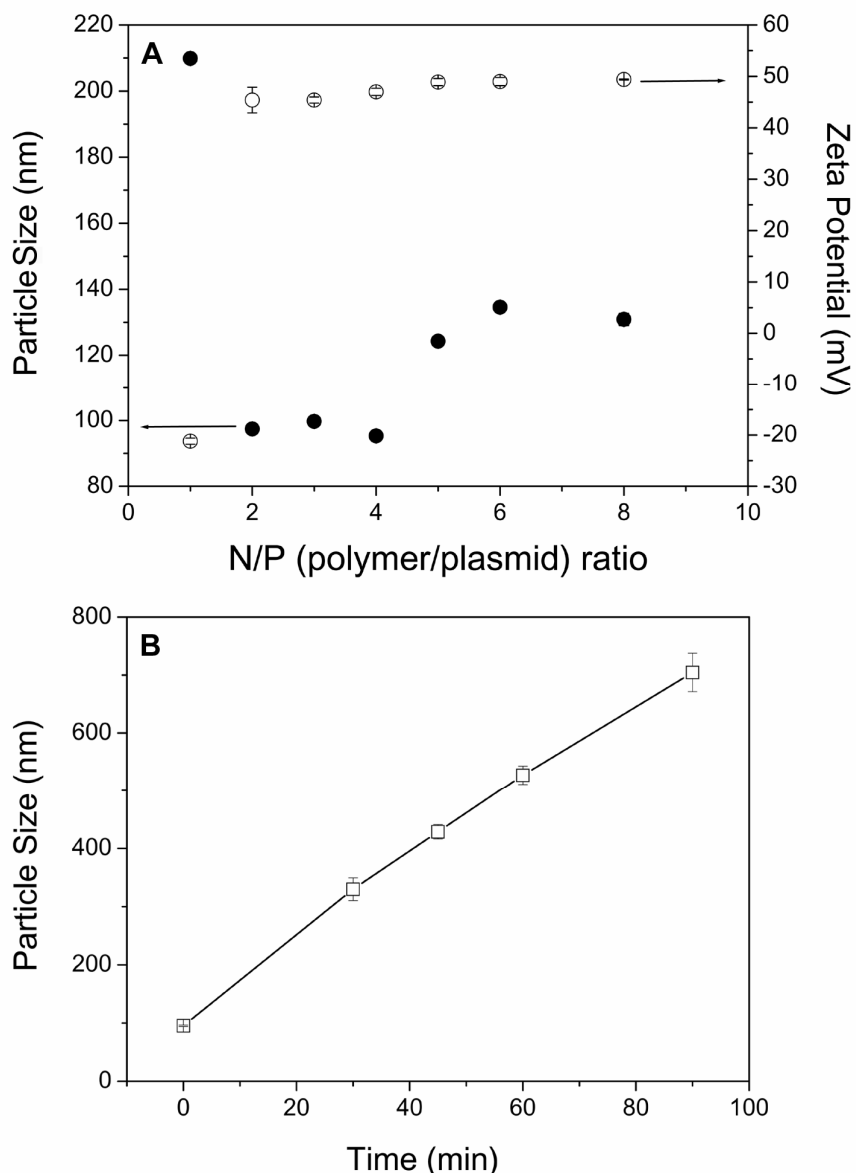


**Figure 7.1** (A) The average diameter (●) and zeta-potential (○) of PFS polyplexes as a function of the polymer/plasmid ratio. (B) The size of PFS/DNA complexes (N/P ratio: 4/1) incubated in 150 mM NaCl as a function of time. The line is drawn as a guide for the eye.

The binding of PFS polycations to DNA was also studied by gel retardation assay. In Figure 7.2, the result of the agarose gel electrophoresis of PFS/plasmid DNA complexes prepared at different N/P ratios is presented. It was observed that the migration of negatively charged DNA was retarded by positively charged PFS at an N/P ratio of 2/1 or higher due to the reversal of its surface potential.<sup>5</sup> This result is in agreement with the above dynamic light scattering results where stable complex formation was detected at the same N/P ratio under the same experimental conditions.

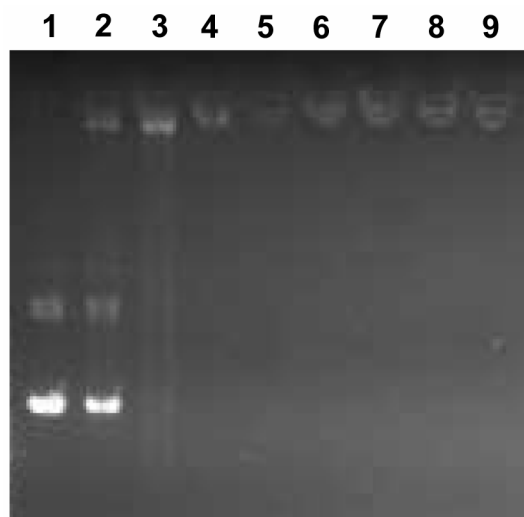


**Figure 7.2** Agarose gel electrophoresis of PFS/plasmid complexes prepared at different polymer/plasmid ratios. Lane 1 contains naked DNA; lanes 2-9 contain DNA condensed with PFS at N/P ratios of 0.5, 1, 2, 3, 4, 5, 6, and 8, respectively.

The formation of nano-sized polyplexes was further confirmed by AFM. In Figure 7.3, tapping mode AFM height images of the original plasmid DNA as well as the DNA/PFS complexes at an N/P ratio of 4:1 deposited on mica surfaces are presented. As expected, the condensation reaction transformed the highly stretched DNA molecules into compact spherical complexes. The lateral size of the complexes is around 100-120 nm, in accordance with the particle size obtained by dynamic light scattering measurement at the same N/P ratio (Figure 7.1).

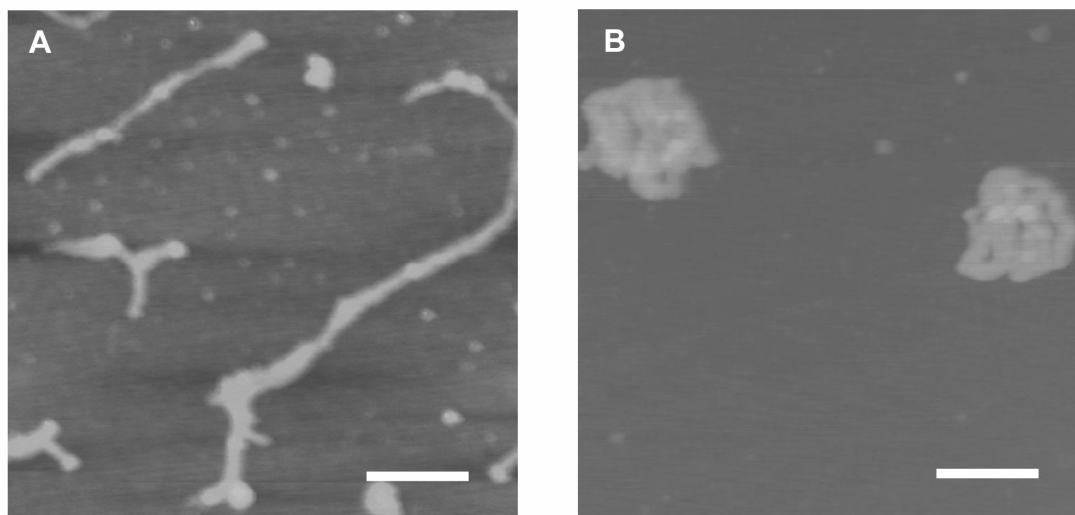


**Figure 7.3** TM-AFM images of plasmid DNA on mica substrates: (A) original shape (scale bar is 200 nm and z range is 10 nm); (B) condensed shape after complexation with PFS polycations at an N/P ratio of 4:1 (scale bar is 100 nm and z range is 20 nm).

Following the successful complex formation, the transfection activity of PFS/plasmid pCMV-LacZ complexes expressing  $\beta$ -galactosidase was studied *in vitro* using COS-7 cells. The transfection was carried out in the presence of endosome disruptive INF7 peptide (1.5

$\mu\text{g/well}$ ), and the cells were incubated with polyplexes for 30 min.<sup>5</sup> In Figure 7.4, relative polyplex transfection efficiencies as normalized to those of the reference poly(2-(dimethylamino)ethyl methacrylate) (PDMAEMA)/DNA polyplexes are demonstrated. For comparison purposes, the transfection efficiencies of polyethylenimine (PEI)/DNA polyplexes are also presented. As shown in the Figure, most of the prepared PFS polyplexes ( $3 \leq \text{N/P} \leq 6$ ) displayed higher transfection activity than the reference. In the absence of serum, the optimum transfection was achieved at an N/P ratio of 4/1, which was more than two fold that of the reference polyplexes. The relative transfection efficiency decreased to 1.3 at the same N/P ratio when serum proteins were present in the transfection medium. The lower transfection efficiency in the presence of serum is a well-known phenomenon since serum often causes the aggregation of polyplexes.<sup>8</sup> Notably, at similar N/P ratios ( $\leq 5$ ), polyplexes of linear PEI/DNA showed significantly lower transfection efficiency.

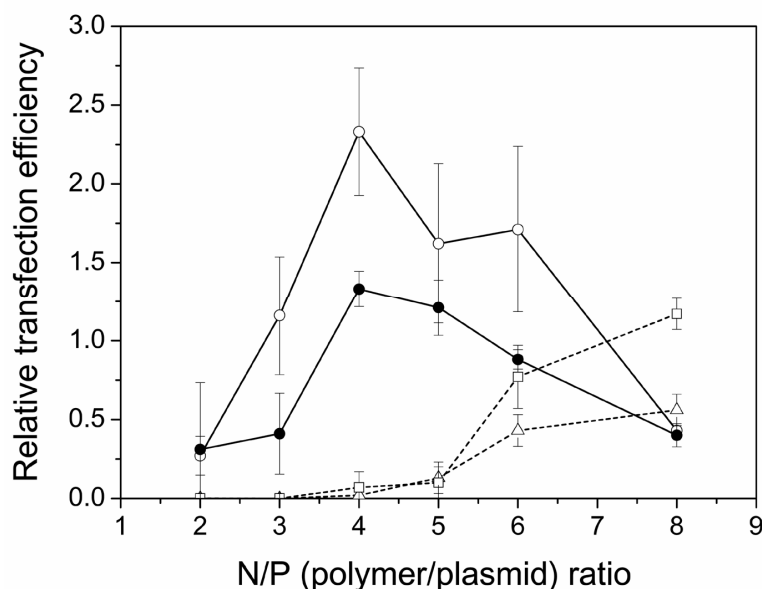


**Figure 7.4** Transfection activity of PFS/DNA polyplexes at varying N/P ratios. (○): no serum; (●): 5% serum. For comparison, the transfection efficiencies of linear PEI/DNA polyplexes in the absence of serum with incubation time of 1 hour (△) or 2 hours (□) are also shown. Transfection efficiency was normalized to that of PDMAEMA/DNA (w/w: 3/1) complexes in the absence of serum.

The cell viability was evaluated by XTT (2,3-bis(2-methoxy-4-nitro-5-sulfo-phenyl)-5-[(phenylamino) carbonyl]-2H-tetrazolium hydroxide) assay. As shown in Figure 7.5, PFS polyplexes do not give pronounced cytotoxicity at N/P ratios  $\leq 6/1$ . The PFS/DNA polyplexes were essentially non-toxic with close to 100% cell viability at the N/P ratio with the highest transfection efficiency (N/P = 4/1).

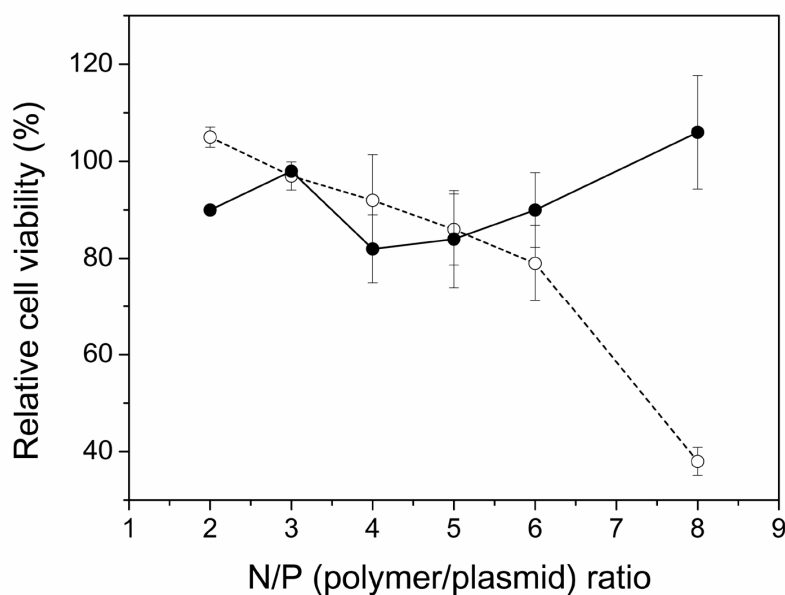


**Figure 7.5** The viability of COS-7 cells incubated with polyplexes prepared at different N/P ratios measured by the XTT assay. (○): In the absence of serum; (●) in the presence of 5% serum.

### 7.1.3 Conclusions

Cationic poly(ferrocenylsilane) can effectively condense plasmid DNA to give stable nano-sized complexes at polymer/plasmid ratios  $\geq 2$ . These PFS/DNA polyplexes can act as non-toxic gene carriers and efficiently transfer COS-7 cells with the highest transfection efficiency at the N/P ratio of 4. This is the first demonstration of the use of organometallic polymers for potential gene delivery applications.

### 7.1.4 Experimental

**Materials** The synthesis and characterization of cationic poly(ferrocenylsilane) **4** (PFS,  $M_w = 5.3 \times 10^4$  g/mol) is described in Chapter 3, PDMAEMA ( $M_w = 1.94 \times 10^5$  g/mol),<sup>9</sup> and INF7 peptide<sup>10</sup> were prepared as described previously. Linear polyethylenimine (PEI,  $M_w = 2.5 \times 10^4$  g/mol) was purchased from Polysciences. The plasmid pCMVLacZ, containing a bacterial LacZ gene preceded by a nuclear localization signal under control of a CMV promoter, was purchased from PlasmidFactory (Bielefeld, Germany).

**Polyplexes preparation** The preparation of polyplexes and the polyplex size and zeta-potential measurements were carried out as reported previously.<sup>11</sup> Atomic Force Microscopy (AFM) experiments were performed using a NanoScope IIIa multimode AFM (Veeco-Digital Instruments, Santa Barbara, CA) with a D-scanner in tapping mode equipped using silicon cantilevers (Nanosensors, Wetzlar, Germany) at room temperature in air. For gel retardation assay, polyplexes were prepared at varying N/P ratios ranging from 0.5 to 8 in HEPES buffered saline (HBS) and incubated for 30 min at room temperature, the samples were

electrophoresed through a 0.7 % agarose gel containing ethidium bromide (0.5 µg/mL), and then DNA was visualized on a UV transilluminator (GelDoc system, Imago).

**In vitro transfection and cell viability assay** Transfection experiments were performed with COS-7 cells using the plasmid pCMV-LacZ as reporter gene. Two parallel transfection series, one for the determination of reporter gene expression ( $\beta$ -galactosidase) using an ONPG assay and the other for the evaluation of cell viability by the XTT assay, were carried out in separate 96 well plates (*ca.*  $1.0 \times 10^4$  cells per well). Different charge ratios ranging from 2 to 8 were used to prepare polyplexes. In the transfection experiments with INF7 peptide, prior to the incubation of cells with the polyplexes, 1.5 µg INF (in 20 µL HBS) was added to the polyplex dispersion. A PDMAEMA/DNA formulation prepared at an optimal polymer/DNA ratio of 3:1 (w/w) was used as a reference.

## 7.2 Monodisperse polymer-virus hybrid nanoparticles<sup>†</sup>

### 7.2.1 Introduction

Nanometer-sized cage structures can be used as nano-reactors or constrained environments to encapsulate guest molecules for delivery purposes.<sup>12, 13</sup> In recent years, many different types of such containers have been introduced, including block copolymer vesicles (or polymersomes),<sup>14</sup> dendrimers,<sup>15</sup> and polyelectrolyte multilayer capsules discussed in the previous Chapters.<sup>16, 17</sup> In synthetic systems, many of the drawbacks are related to their low biocompatibility and broad polydispersity. In this respect, viruses in their native state have the intrinsic advantage in that they are precise protein assemblies which act as host containers for nucleic acid storage and transport.<sup>1, 12</sup>

The well-defined virus cowpea chlorotic mottle virus (CCMV) consists of 180 identical coat protein (CP) subunits (in the form of 90 dimers) arranged in an icosahedral lattice with encapsulated central RNA strand, yielding a highly defined 28 nm virion with an inner cavity of ~ 18 nm in diameter.<sup>18</sup> Each CP subunit contains at least nine basic residues (arginine and lysine) in the interior of the virion, creating a positively charged interior cavity surface.<sup>12</sup> CCMV undergoes a reversible pH-dependent swelling, resulting in a 10% increase of the virus dimension. Structural analysis has revealed that the swelling was caused by the formation of 60 separate openings (2 nm in diameter) in the protein shell (Figure 7.6). Through a pH-gated reversible opening and closing of the shell, selective molecular exchange between the virus cavity and the bulk medium can be realized.<sup>12</sup>

---

<sup>†</sup> This work was carried out in collaboration with Inge Minten, Dr. Jeroen J. L. M. Cornelissen and Prof. Roeland J. M. Nolte at the Institute of Molecules and Materials of the Radboud Universiteit Nijmegen.

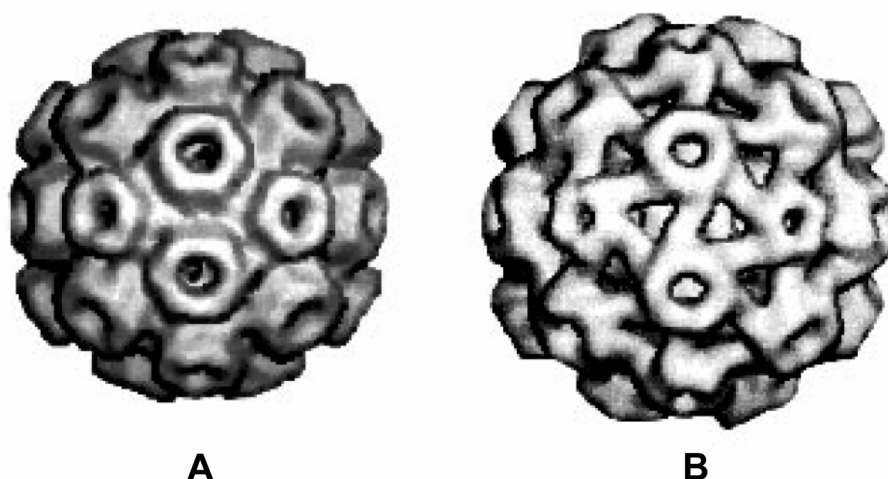


**Figure 7.6** Cryo electron microscopy and image reconstruction of the cowpea chlorotic mottle virus (CCMV). (A) In an unswollen condition induced by low pH ( $\text{pH} < 6.5$ ); (B) in a swollen condition induced by high pH ( $\text{pH} > 6.5$ ). Swelling at the pseudo-three-fold axis results in the formation of sixty 2 nm pores. Reprinted with permission from [12a]. Copyright 1998 Macmillan Publishers Ltd: [Nature].

The icosahedral shape of the virus could be described using the Caspar-Klug T number.<sup>19</sup> In its natural form, the 90 dimeric CP subunits give rise to a  $T = 3$  particle. Removal of the RNA from the interior of the virus at high pH can result in free CP subunits, which could be re-assembled to empty  $T = 3$  (28 nm) capsid by lowering the pH value to  $\sim 5$ . Previous studies have revealed that the assembly of CCMV CP at higher pH values (*e.g.* 7.5) is only possible in the presence of certain anionic polyelectrolyte species (natural or synthetic, such as DNA or poly(styrene sulfonate), PSS).<sup>20</sup> This implies that at lower pH value, interactions between CP subunits dominate capsid formation, while at higher pH the interactions between protein subunits and polyelectrolytes prevail. It has been reported that by using PSS, monodisperse  $T = 1$  nanoparticles with a size of 16 nm could be obtained.<sup>20</sup> Calculations show that the  $T = 1$  particle is an icosahedron with 12 pentameric faces, which is made up from 60 subunits.<sup>21</sup>

Here, a study on the self-assembly of poly(ferrocenylsilane) polyanions with CCMV CP is described. Since PFS is also a functional redox-responsive polyelectrolyte, studies on the stability and responsive behaviour of PFS/CP assembly are currently under way.

## 7.2.2 Results and discussion

Fast protein liquid chromatography (FPLC) was used to characterize the assembly of the capsid protein. Similar to other column chromatography methods, FPLC is often used to separate proteins from complex mixtures based on size differences. The intrinsic characteristic UV absorbance of PFS at  $\lambda = 216$  nm and 450 nm makes it extremely convenient to follow the composition of the elution from FPLC. After incubation of PFS polyanions with CP at pH 7.5 with a PFS/CP ratio of 40,<sup>20</sup> FPLC elution curves were recorded



(Figure 7.7) for three different wavelengths at 216, 280 (characteristic absorbance of protein) and 450 nm.

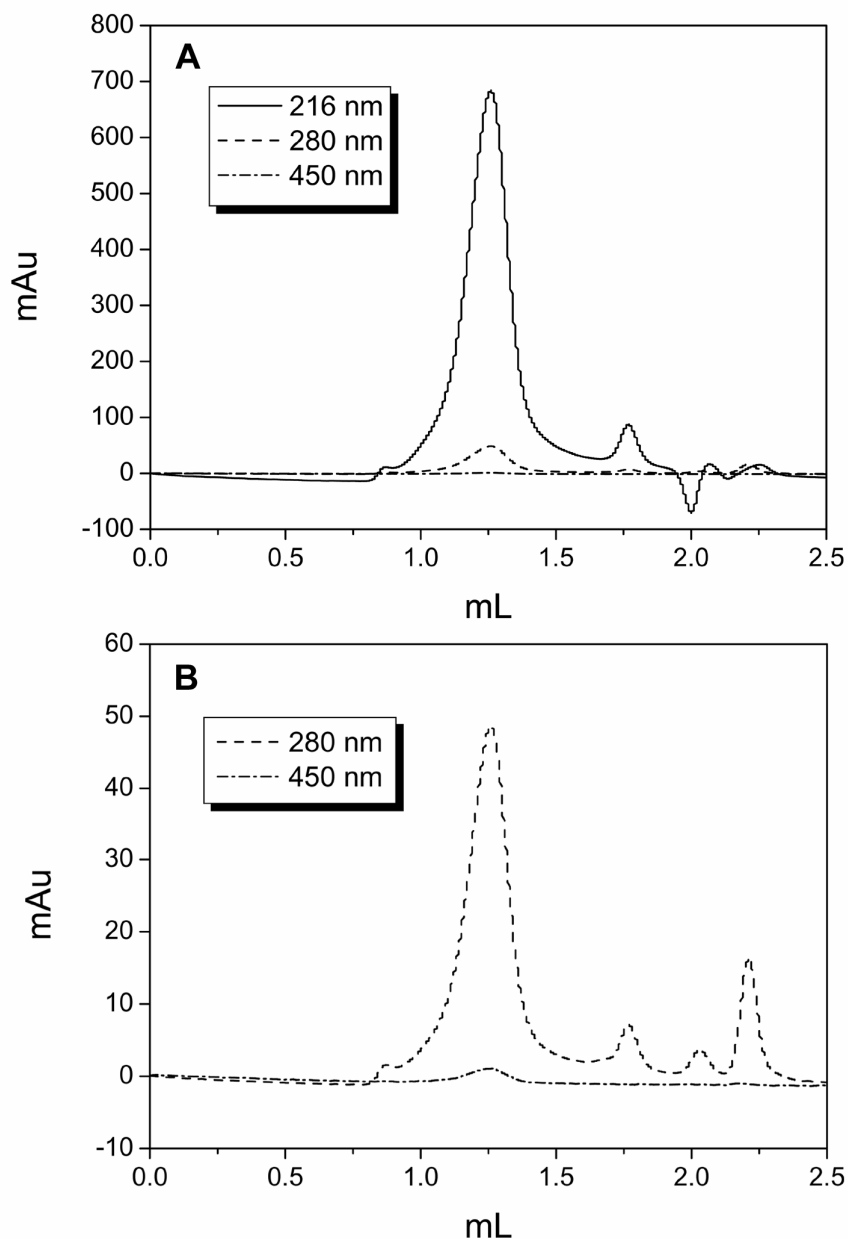


**Figure 7.7** FPLC traces of PFS and capsid protein mixtures containing a PFS/CP ratio of 40. The traces were recorded for three different wavelengths (PFS: 216 nm and 450 nm; protein: 280 nm). The peaks at the elution volume of 1.26 mL indicate the presence of T = 1 protein aggregates, the absence of peaks at the elution volume of 1.0 mL indicate the absence of T = 3 particles.

The curves presented in Figure 7.7 showed the typical elution volume (1.3 mL) for T = 1 particles. No peak was observed at the elution volume of 1.0 mL, indicating the absence of T = 3 particles. Moreover, the absence of peaks for the polymer suggested that all PFS was encapsulated within the particles at the current polymer/CP ratio.

TEM images were taken from the fraction collected at the elution volume of 1.3 mL. In Figure 7.8 and 7.9, TEM images of CP-PFS particles assembled at pH 7.5 and pH 5 are presented.

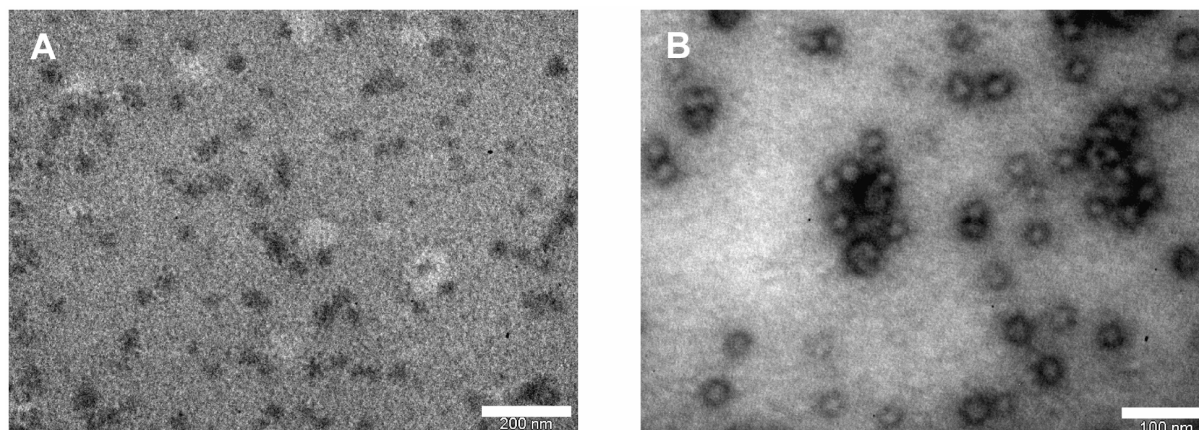


**Figure 7.8** TEM images of CP-PFS nanoparticles at pH 7.5. (A): unstained (scale bar is 200 nm); (B): stained (scale bar is 100 nm).

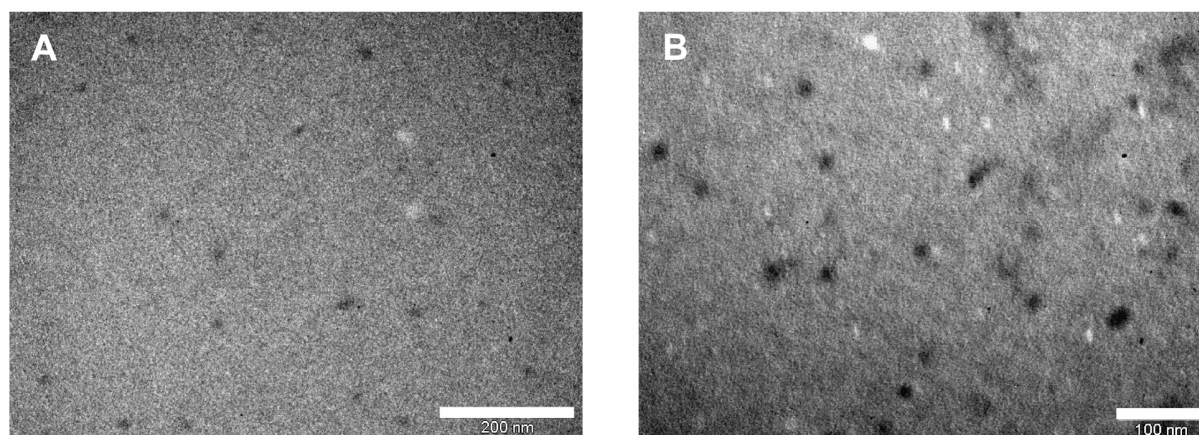


**Figure 7.9** TEM images of CP-PFS nanoparticles at pH 5. (A): unstained (scale bar is 200 nm); (B): stained (scale bar is 100 nm).

As expected, stable nanoparticles with similar sizes were formed at both pH's. The average diameter of the particles (18 nm) resembles that of previously studied CP-PSS nanoparticles (16 nm).<sup>20</sup> The larger size of the CP-PFS nanoparticles could originate from the significantly higher molar mass of PFS ( $M_w \sim 5.3 \times 10^4$  g/mol) compared to that of PSS ( $M_w \sim 9.9 \times 10^3$  g/mol). The slight difference in the particle appearance at different pH is assumed to originate from focussing variations during TEM imaging.

### 7.2.3 Conclusions and outlook

Poly(ferrocenylsilane) polyanions were successfully utilized to assemble CCMV CP by electrostatic interactions to give monodisperse 18 nm  $T = 1$  nanoparticles at pH 7.5 (Figure 7.10). Studies on the responsive characteristics of these nanoparticles under chemical and electrochemical redox stimuli are currently under way. As all the effective PFS oxidation

agents were found to be harmful for the capsid proteins, so far no successful attempts have been made to chemically oxidize PFS-CP nanoparticles. However, electrochemical methods may be promising to manipulate the redox-state of PFS-CP nanoparticles, which may imply some potential applications in drug targeting and transportation areas.

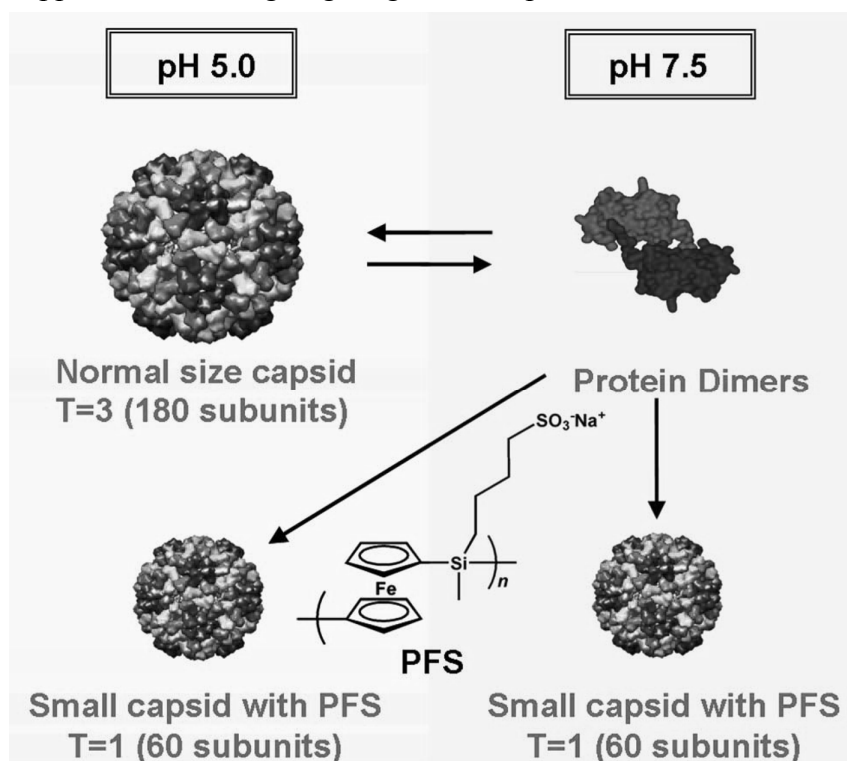


**Figure 7.10** Schematic of the formation of  $T = 1$  nanoparticles by the introduction of PFS polyanions. At pH 7.5, free CP dimers were favoured over the  $T = 3$  particle in the absence of the polymer.

#### 7.2.4 Experimental

**Materials** CP was prepared according to a literature procedure.<sup>22</sup> The synthesis and characterization of poly(ferrocenylsilane) polyanion **5** has been described in Chapter 3.

**Sample preparation** For all the experiments a buffer solution containing 0.05 M Tris-HCl, 0.01 M  $\text{MgCl}_2$ , 0.001 M EDTA and 0.4 M NaCl was used. Based on the fact that there are 72 negative charges on each capsid subunit, the polymer was mixed with CP at a molar ratio of 72:1.

**Characterization** Fast protein liquid chromatography (FPLC) was performed on an Ettan LC, equipped with Superose 6 PC 3.2/30 column from Amersham Biosciences. The injection volume for FPLC experiments was 20  $\mu\text{L}$ , with a flow rate of 0.04 mL/min. Transmission electron microscopy (TEM) images of nanoparticles were taken with a JEOL JEM-1010 TEM (JEOL, Japan). TEM samples were prepared by placing 5  $\mu\text{L}$  of particle solution onto glow-discharge treated TEM grids. Stained samples were made by adding another 5  $\mu\text{L}$  2% uranylacetate aqueous solution. The samples were studied at 60 kV.

### 7.3 Closing remarks

The processability of water-soluble polymers promises a wide range of application potentials of poly(ferrocenylsilane) polyelectrolytes. The lack of pronounced cytotoxicity of DNA/PFS polyplexes *in vitro* implies possible biomedical applications of these materials. For future studies smart strategies need to be developed in order to achieve efficient gene release and explore the stimuli-responsive properties of the nanometer sized self-assembled PFS/CCMV CP cage structures.

### 7.4 References

1. Putnam, D. *Nat. Mater.* **2006**, *5*, 439.
2. Hamley, I. W.; Castelletto, V. *Angew. Chem. Int. Ed.* **2007**, *46*, 4442.
3. (a) Bloomfield, V. A. *Biopoly.* **1997**, *44*, 269; (b) De Smedt, S. C.; Demeester, J.; Hennink, W. E. *Pharm. Res.* **2000**, *17*, 113; (b) Vijayanathan, V.; Thomas, T.; Thomas, T. J. *Biochemistry* **2002**, *41*, 14085.
4. Anwer, K.; Rhee, B. G.; Mendiratta, S. K.; *Crit. Rev. Ther. Drug. Carr. Syst.* **2003**, *20*, 249.
5. Lin, C.; Zhong, Z.; Lok, M. C.; Jiang, X.; Hennink, W. E.; Feijen, J.; Engbersen, J. F. J. *Bioconjugate Chem.* **2007**, *18*, 138.
6. Schaffer, D. V.; Fidelman, N. A.; Dan, N.; Lauffenburger, D. A. *Biotechnol. Bioeng.* **2000**, *67*, 598.
7. Wightman, L.; Kircheis, R.; Rossler, V.; Carotta, S.; Ruzicka, R.; Kursu, M.; Wagner, E. *J. Gene. Med.* **2001**, *3*, 362.
8. Audouy, S.; Molema, G.; de Leij, L.; Hoekstra, D. *J. Gene. Med.* **2000**, *2*, 465.
9. Cherng, J. Y.; van de Wetering, P.; Talsma, P. H.; Crommelin, D. J. A.; Hennink W. E. *Pharm. Res.* **1996**, *13*, 1038.
10. Plank, C.; Oberhauser, B.; Mechtler, K.; Koch, C.; Wagner, E. *J. Bio. Chem.* **1994**, *269*, 12918.
11. Zhong, Z. Y.; Feijen, J.; Lok, M. C.; Hennink, W. E.; Christensen, L. V.; Yockman, J. W.; Kim, Y. H.; Kim, S. W. *Biomacromolecules* **2005**, *6*, 3440.
12. (a) Douglas, T.; Young, M. *Nature* **1998**, *393*, 152; (b) Comellas-Aragonès, M.; Engelkamp, H.; Claessen, V. I.; Sommerdijk, N. A. J. M.; Rowan, A. E.; Christianen, P. C. M.; Maan, J. C.; Verduin, B. J. M.; Cornelissen, J. J. L. M.; Nolte, R. J. M. *Nat. Nanotechnol.* **2007**, *2*, 635.

13. (a) Rebek, J. J. *Chem. Soc. Rev.* **1996**, 25, 255; (b) Vriezema, D. M.; Aragonès, M. C.; Elemans, J. A. A. W.; Cornelissen, J. J. L. M.; Rowan, A. E.; Nolte, R. J. M. *Chem. Rev.* **2005**, 105, 1445.
14. Discher, D. E.; Eisenberg, A. *Science* **2002**, 297, 967.
15. Jansen, J. F. G. A.; de Brabander-van den Berg, E. M. M.; Meijer, E. W. *Science* **1994**, 266, 1226.
16. Donath, E.; Sukhorukov, G. B.; Caruso, F.; Davis, S. A.; Möhwald, H. *Angew. Chem. Int. Ed.* **1998**, 37, 2201.
17. Dähne, L.; Leporatti, S.; Donath, E.; Möhwald, H. *J. Am. Chem. Soc.* **2001**, 123, 5431.
18. Zhao, X.; Fox, J. M.; Olson, N. H.; Baker, T.S.; Young, M. *J. Virology* **1995**, 207, 486.
19. Liepold, L. O.; Revis, J.; Allen, M.; Oltrogge, L.; Young, M.; Douglas, T. *Phys. Bio.* **2005**, 2, S166.
20. Sikkema, F. D.; Comellas-Aragonès, M.; Fokkink, R. G.; Verduin, B. J. M.; Cornelissen, J. J. L. M.; Nolte, R. J. M. *Org. Biomol. Chem.* **2007**, 5, 54.
21. Tang, J.; Johnson, J. M.; Dryden, K. A.; Young, M. J.; Zlotnick, A.; Johnson, J. E. *J. Struct. Biol.* **2006**, 154, 59.
22. (a) Bancroft, J. B.; Hiebert, E.; Rees, M. W.; Markham, R. *Virology* **1968**, 34, 224; (b) Davies, J. W.; Verduin, B. J. M. *J. Gen. Virol.* **1979**, 44, 545; (c) Verduin, B. J. M. *FEBS Lett.* **1974**, 45, 50.



# Chapter 8

## Outlook: Bringing New Shapes and Functions to Redox-Responsive Multilayer Structures

*New shapes may bring new functions. In this Chapter the fabrication of multilayer structures based on the deposition of poly(ferrocenylsilane) polyelectrolytes onto substrates of various shapes and forms is discussed. Material design focuses here on the utilization of a combination of the unique redox-responsive properties of poly(ferrocenylsilanes) with new substrate geometries to fulfil specific requirements. Moreover, some application oriented follow-up studies based on the results from previous Chapters are also discussed.*

### 8.1 Introduction

One of the most attractive assets of layer-by-layer electrostatic self-assembly is its compatibility with various interfaces. Essentially substrates of any material with any shape are potentially useful for multilayer fabrication. The introduction of free-standing multilayer micro and nanocapsules stimulated the design and fabrication of new forms of free-standing multilayer structures, such as multilayer thin films and nanotubes. On the other hand, growing research attention is also focused on the utilization of polyelectrolyte multilayers as functional thin film coatings. In this context, the incorporation of functional polyelectrolyte species into multilayer systems adds a new dimension in broadening their potential applications.

The successful incorporation of poly(ferrocenylsilane) polyions into layer-by-layer deposited planar films and microcapsules described in the previous Chapters opens numerous possibilities for the design and fabrication of other functional structures. In this Chapter, various new forms of poly(ferrocenylsilane) multilayers are discussed, including multilayer nanotubes, membranes and functional surface coatings. Specific emphasis is placed on making use of the characteristic redox-responsive properties of poly(ferrocenylsilane) multilayers.

### 8.2 Multilayer nanotubes

The discovery of carbon nanotubes (CNTs) in 1991<sup>1</sup> has stimulated broad research interests in one-dimensional nanostructured materials.<sup>2</sup> Nanotubular structures could be

fabricated with defined length and diameters through templated synthesis methods using porous membranes.<sup>3</sup> In the same way, polyelectrolyte multilayer nanotubes have been successfully prepared through the layer-by-layer electrostatic assembly of polyelectrolytes onto the porous membranes followed by template removal.<sup>2,4</sup> Moreover, the successful layer-by-layer deposition of polyelectrolyte multilayers onto electrospun nanofibres<sup>5</sup> as well as individual carbon nanotubes<sup>6</sup> has opened up new opportunities for the facile synthesis of composite tubular nanostructures. NTs of various materials are considered to be important building blocks for numerous applications in the fields of nanoelectronics,<sup>7</sup> photonics,<sup>8</sup> catalysis and controlled release.<sup>9</sup>

In the following section, membrane templated synthesis of poly(ferrocenylsilane) multilayer nanotubes is described. The layer-by-layer deposition of poly(ferrocenylsilane) polyelectrolytes onto two types of template materials, *i.e.* porous anodic alumina and polycarbonate (PC) membranes, was studied followed by attempted template dissolution. Since nanoporous alumina can also act as a planar optical waveguide,<sup>10, 11</sup> poly(ferrocenylsilane) multilayer modified alumina templates may also be potentially used as highly sensitive detectors.

### 8.2.1 Porous alumina as templates\*

Planar optical waveguides such as porous anodic alumina are widely used for sensor applications.<sup>11</sup> When a porous alumina film is placed on a substrate, the pores are open to the external environment at the top and the effective refractive index ( $n$ ) can be tuned by filling the pores with different media.<sup>12</sup> A conformal film deposition onto the pore surfaces will lead to a change in the optical characteristics, which constitutes the working principle of a waveguide sensor.<sup>10</sup> Here, the deposition of PFS polyelectrolytes onto the porous alumina templates allows us to fabricate PFS multilayer nanotubes. On the other hand, the electrochemically active poly(ferrocenylsilanes) could be potentially applied to manipulate the optical properties of the waveguide through a redox stimulus.

PFS<sup>-</sup>/PFS<sup>+</sup> multilayers were deposited from aqueous solutions (1 mg/mL, 0.5 M NaCl) onto aminopropyltrimethylethoxysilane treated porous alumina substrates<sup>4a</sup> (average pore size 400 nm, pore depth 100  $\mu$ m). The originally white alumina substrates turned yellow (characteristic colour of PFS, see also Chapter 3) after multilayer deposition (Figure 8.1), giving evidence for the successful layer-by-layer self-assembly. The SEM images of the original and multilayer coated alumina substrates are presented in Figure 8.2. The different morphology of blank and multilayer-covered alumina indicated the successful layer-by-layer deposition. The pore size of (PFS<sup>-</sup>/PFS<sup>+</sup>)<sub>8</sub> coated alumina was around 340 nm, corresponded

---

\* This work was carried out in collaboration with Dr. Chuan Liang Feng and Prof. Wolfgang Knoll at the Max-Planck Institute for Polymer Research in Mainz, Germany, and will be published separately.



well with the multilayer thickness value predicted under the current experimental conditions (3.6 nm).<sup>13</sup>

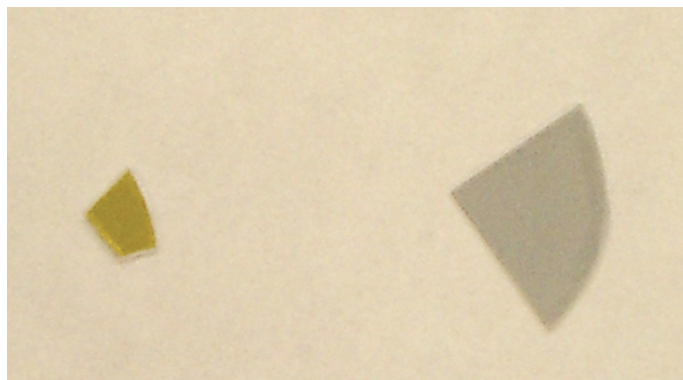


**Figure 8.1** The original white porous alumina substrate (right) turned yellow (left) after the deposition of a multilayer containing  $(\text{PFS}^-/\text{PFS}^+)_8$ .

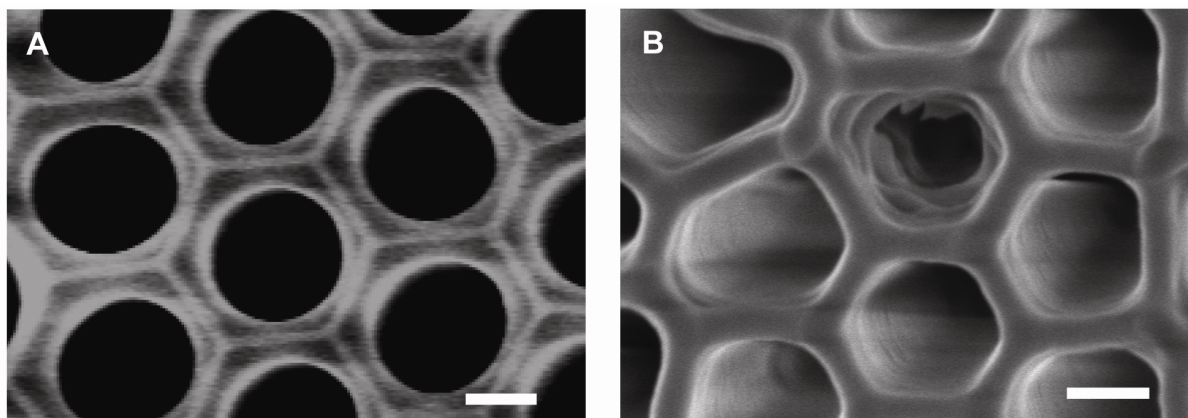


**Figure 8.2** Top view SEM images of (A) a blank porous alumina substrate and (B) a  $(\text{PFS}^-/\text{PFS}^+)_8$  coated alumina substrate. Scale bar = 200 nm for both images.

Following the deposition of PFS multilayers, the alumina templates were removed using KOH aqueous solutions (30%).<sup>4</sup> After several centrifugation/washing steps, an aqueous dispersion containing some yellow precipitants was obtained. The yellow colour suggested the existence of PFS in the material structure. Figure 8.3 shows the SEM images recorded on the PFS nanotubes obtained from the eight bilayer  $\text{PFS}^-/\text{PFS}^+$  coatings. Due to partial collapse, the largest inner diameter of the obtained nanotubes was around 300 nm, slightly lower than the pore size of the coated alumina membrane. The length of these tubes was at least several  $\mu\text{m}$ . Besides these tubular structures, many fibrils, possibly some alumina residues, were also detected by SEM. The composition of these nanotubes will be subjected to further characterization by energy dispersive X-ray (EDX) measurements.

Similar self-standing nanotubes could not be obtained from multilayers containing five bilayers of  $\text{PFS}^-/\text{PFS}^+$ . The tubes made of  $(\text{PFS}^-/\text{PFS}^+)_5$  were shown to display completely collapsed structures after template removal (data not shown). This is probably due to the insufficient mechanical strength relative to the corresponding wall thickness and aspect ratio of the nanotubes.

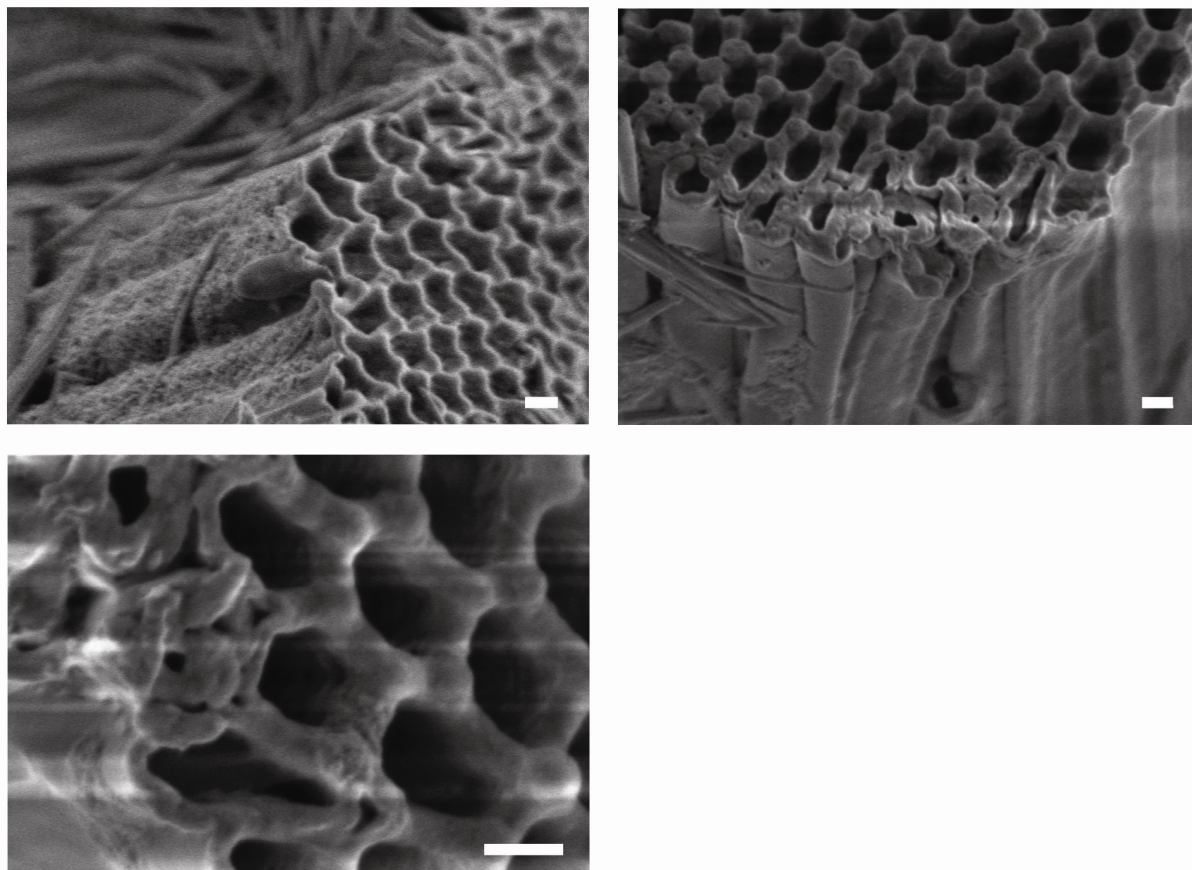


**Figure 8.3** Top view SEM images of PFS nanotubes containing  $(\text{PFS}^-/\text{PFS}^+)_8$  obtained after alumina template removal using KOH. Scale bar = 200 nm for all images.

### 8.2.2 Polycarbonate membranes as templates

The same  $\text{PFS}^-/\text{PFS}^+$  multilayers were successfully deposited onto polycarbonate (PC) membranes (average pore size 400 nm) from 1 mg/mL polyelectrolyte solutions containing 0.5 M NaCl. A similar colour change of the templates from white to yellow was observed after the layer-by-layer deposition (Figure 8.4).

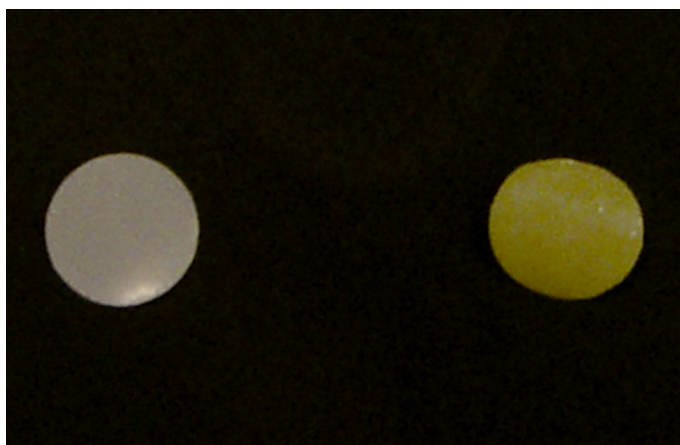


**Figure 8.4** The original white polycarbonate membrane (left) turned yellow after the deposition of a  $(\text{PFS}^-/\text{PFS}^+)_8$  multilayer (right).

Top view SEM images showed decreased pore sizes after PFS<sup>-</sup>/PFS<sup>+</sup> multilayer deposition (Figure 8.5). The pore diameter decreased to 290-310 nm. The decrease by 100 nm ( $\pm 10\%$ ) is higher than double the multilayer thickness predicted from the bilayer thickness value (around 3.5 nm) obtained under the same experimental conditions. This could be partially explained by the nature of the substrate material.<sup>14</sup>

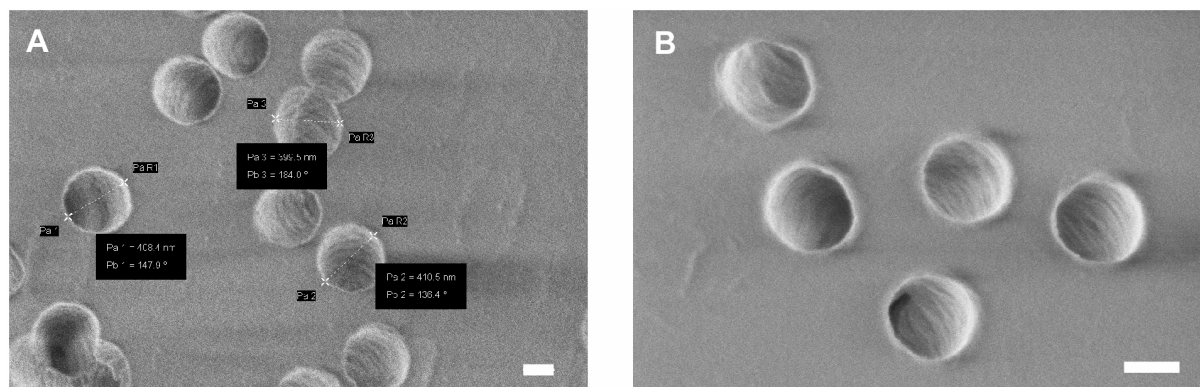


**Figure 8.5** Top view SEM images of (A) blank polycarbonate membranes (uniform pore size 400 nm) and (B) after coated with (PFS<sup>-</sup>/PFS<sup>+</sup>)<sub>8</sub> multilayers (average pore size 290-310 nm). Scale bar = 200 nm for both images.

It is reported that the PC template could be removed by dissolution using dichloromethane (CH<sub>2</sub>Cl<sub>2</sub>).<sup>2</sup> In this way, free-standing polyelectrolyte multilayer nanotubes should also be obtained.

### 8.2.3 Experimental

**Materials** Aminopropyltrimethoxysilane and potassium hydroxide (KOH) was obtained from Sigma Aldrich and used as received. The synthesis and characterization of PFS polyelectrolytes were described in Chapter 3. Porous alumina templates with average pore size of 400 nm and pore depth of 100  $\mu$ m were obtained from Dr. Martin Steinhart, Max Planck Institute of Microstructure Physics, Weinberg 2, 06120 Halle, Germany. Polycarbonate (PC) membranes with an average pore size of 400 nm were obtained from Nuclepore and Whatman.

**Layer-by-layer deposition** Porous alumina substrates were treated with aminopropyltrimethoxysilane at 135°C in a vacuum oven for three hours to impart positively charged surfaces. For the same purpose, the PC membranes were first dipped into a PEI solution ( $\sim 10$  mM) for 30 minutes. The modified substrates were alternatively dipped in the PFS polyelectrolyte aqueous solutions (1 mg/mL, 0.5 M NaCl) for 10 minutes, with rinsing, dipping into pure MilliQ (2 min), second rinsing and drying with a stream of nitrogen between each deposition step.

**Template removal** After a desired number of polyelectrolyte bilayers, the coated porous alumina templates were immersed into KOH aqueous solutions (30%), with constant shaking

for 5-10 min. The solution was removed following a centrifugation step (6000 rpm, 1 min). The resultant yellow precipitants were washed with MilliQ for three times and finally re-dispersed in fresh MilliQ.

**Characterization** Scanning electron microscopy (SEM) images were taken with a LEO1530 or LEO 1550 FEG SEM at acceleration voltages of 0.5 – 3 kV. The sample was prepared by placing a drop of aqueous nanotube dispersion on top of carbon glue followed by vacuum drying.

## 8.3 Separation membranes

### 8.3.1 Multilayer membranes

The idea of making free-standing planar thin films was introduced by Kotov *et al.* in the year 2000.<sup>15</sup> The process resembles that of making multilayer microcapsules: multilayers were assembled onto a solid support with or without a sacrificial layer followed by dissolving the substrate with the aid of certain solvents or by employing a simple “lift-off” process.<sup>16</sup> A successful material for use as the sacrificial layer is cellulose acetate (CA), which possesses some negative charge and is insoluble in water but readily dissolves in acetone. However, making use of hydrophobic surfaces such as Teflon or polypropylene without any sacrificial layers, hydrogen-bonded multilayers could be directly lift-off simply by tweezers.<sup>16</sup> As a promising type of novel structural material, free-standing multilayer thin films prepared by these procedures have been tested for their mechanical strength<sup>17</sup> and thermal characteristics such as glass transition temperature.<sup>16</sup>

In Chapter 6, the formation of a peculiar macroporous multilayer structure with pore sizes as large as 350-400 nm using PFS polycations and double-stranded, high molar mass DNA has been demonstrated. If this type of multilayer could be assembled successfully onto the above mentioned sacrificial or hydrophobic substrates, it would be possible to obtain a free-standing multilayer separation membrane material. Since fully organometallic multilayers composed of strong PFS polyelectrolytes possess the peculiar removable property (Chapter 4), they are also excellent candidates as the sacrificial layer for making free-standing thin films. In this way, bio-compatible scaffold material containing DNA molecules could be prepared with controlled thickness and pore size.

### 8.3.2 Responsive gating

Responsive membranes that could alter their permeation properties under environmental stimuli have drawn continuous attention during the last two decades.<sup>18-25</sup> By the grafting or adsorption of certain materials onto the surface of membrane pores, various

gating systems that could specifically respond to pH,<sup>18-20</sup> light,<sup>21</sup> temperature,<sup>22</sup> redox,<sup>23</sup> electric field<sup>24</sup> and specific interactions<sup>25</sup> have been introduced. Although polymeric coatings have constantly been used for membrane surface modification,<sup>18, 20-22, 23, 25</sup> studies on responsive polyelectrolyte multilayer thin films started only very recently.<sup>20</sup> In the first example of such coatings presented by Rubner *et al.*, the pH-induced swelling/deswelling behaviour of poly(allylamine hydrochloride) (PAH)/poly(styrenesulfonate) (PSS) multilayers in the confined geometry of track-etched polycarbonate membranes has been demonstrated.<sup>20</sup>

The unique redox-responsive characteristics of poly(ferrocenylsilane) multilayers (Chapter 4-6) make them excellent candidates to act as membrane coatings leading to functional membranes with chemically or electrochemically controlled gating properties. In Chapter 8.2 the successful layer-by-layer deposition of PFS multilayers onto PC membranes was shown. The advantage of easily controllable film thickness in layer-by-layer self-assembly provides great potential of realizing tailor-made size-discriminating gating, even with simple “open” and “closed” responsive states.

#### 8.4 Poly(ferrocenylsilane)/polysaccharide multilayers

Hyaluronan (HA) (see molecular structure in Figure 8.6) is a linear polysaccharide, which is also a naturally occurring polyanion (solution pKa  $\approx$  3.0) with a persistence length of  $\sim$  6 nm in the fully ionized state.<sup>26</sup>

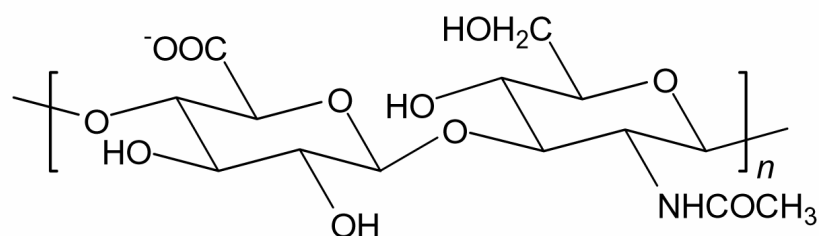


**Figure 8.6** Molecular structure of hyaluronan (HA).

HA is one of the chief components of the extracellular matrix, contributes significantly to cell proliferation and migration and plays an important structural and mechanical role in various tissues. Apart from its apparent medical applications, HA is also a common ingredient in cosmetic products. In the previous Chapters, multilayers and free-standing microcapsules fabricated by the layer-by-layer deposition of PFS polyelectrolytes have shown unique redox-responsive disintegration phenomena, which were attributed to oxidation-induced changes in the charge density and solubility of PFS polyions.<sup>27</sup> Making use of the anionic nature of HA, it is possible to fabricate polyelectrolyte multilayers based on the electrostatic interactions of HA and PFS polycations. Since the persistence length of HA is just in between that of PFS and the high molar mass ds-DNA used in the study described in Chapter 6, it is of great

interest to study the PFS/HA multilayer morphology. Moreover, HA with different molar masses are commercially available, which may constitute another control parameter for structure formation. When oxidized, PFS polycations will adopt increased positive charge density and water solubility, which forms the basis for disrupting the as-prepared HA/PFS multilayers leading to the release of HA molecules.

## 8.5 Superhydrophobic coatings

It is well-known that increasing the roughness of a hydrophobic surface can increase its hydrophobicity.<sup>28,29</sup> Rubner *et al.* have created a stable superhydrophobic coating from a honeycomb-like polyelectrolyte multilayer.<sup>28</sup> The idea originated from the discovery that by simple acid treatments weak polyelectrolyte multilayers would undergo a surface morphology transition from nanoporous to macroporous.<sup>30</sup> Subsequent application of a layer of silica nanoparticles followed by a final coating of a semifluorinated silane on top of the stabilized macroporous multilayer finally rendered superhydrophobicity to the surface.<sup>29</sup>

It has been described in Chapter 6 that a unique macroporous multilayer could be fabricated by the self-assembly of PFS and ds-DNA. The surface roughness of the obtained thin films scales with the film thickness. Making use of the above mentioned principle, the one-step fabricated PFS/DNA multilayers are excellent candidates for the development of new types of superhydrophobic coatings that are also potentially biocompatible.

## 8.6 Follow-up study on the redox-response of poly(ferrocenylsilane) multilayers and microcapsules

As discussed in Chapter 3, potassium hexacyanoferrate ( $K_3Fe(CN)_6$ ) is also a PFS oxidation agent. However, the degree of oxidation as judged from the solubility change of PFS polyanions is very limited. In other words,  $K_3Fe(CN)_6$  is a relatively mild oxidation agent for PFS. Since neither dramatic solubility increases of the PFS polyelectrolytes nor charge density changes are expected to take place upon oxidation by  $K_3Fe(CN)_6$ ,  $K_3Fe(CN)_6$  could be a potentially good oxidation agent for manipulating the permeability of PFS multilayer microcapsules.

For many applications, electrochemical responsive material systems are extremely promising in that electrochemical stimulus possesses the unique possibility in realizing a localized trigger. The electrochemical controlled release of PFS multilayers from ITO substrates by applying a small oxidation potential has been demonstrated in Chapter 4. It has been shown that the rate of material release can be varied by changing the potential. The

stepwise electrochemical oxidation and reduction of PFS provides a relatively broad scope for manipulating the rate of material release. Thus, a more systematic study could be carried out to determine the relationship between the applied potential and the rate and degree of material loss. Moreover, complementary characterizations should be performed in order to gain more insight into the mechanism of the multilayer release process. This fundamental information based on the release of PFS polyelectrolytes from PFS multilayers would later on form a platform leading to application oriented studies. For example, it would be interesting and promising to study the loading and electrochemically controlled release of drugs or DNA into and out of the redox-responsive PFS multilayer thin film structures.

As shown in Chapter 5, PFS multilayer microcapsules could be reversibly oxidized and reduced electrochemically. Actually the hollow micro- or nano-meter sized capsule structure is ideal for the encapsulation of active species. Generally there are two ways to incorporate various substances, such as drugs, proteins and DNA into the interior of the capsules: 1. used directly as core material by aggregation or co-precipitation during the core formation,<sup>31</sup> and 2. adsorption onto the cores before the layer-by-layer deposition of the polymeric shell.<sup>32</sup> For controlled molecular release purposes it would be very interesting to study the encapsulation and controlled, electrochemically-triggered release of materials from inside the poly(ferrocenylsilane) micro- or nano-capsules.

The controlled release of functional materials from porous polymeric thin films is also of great importance.<sup>33</sup> Drugs could be incorporated, for example, into the interior of PFS/ds-DNA macroporous multilayers and microcapsules according to similar methods as described above. Since the pore sizes could be manipulated by varying the number of deposited layers (Chapter 6), in principle the release rate may also be efficiently controlled.

## 8.7 References and notes

1. Iijima, S. *Nature* **1991**, *354*, 56.
2. (a) Liang, Z.; Susha, A. S.; Yu, A.; Caruso, F. *Adv. Mater.* **2003**, *15*, 1849; (b) Ai, S.; He, Q.; Tao, C.; Zheng, S.; Li, J. *Macromol. Rapid Commun.* **2005**, *26*, 1965; (c) Tian, Y.; He, Q.; Cui, Y.; Tao, C.; Li, J. *Chem. Eur. J.* **2006**, *12*, 4808.
3. (a) Martin, C. R. *Science* **1994**, *266*, 1961; (b) Steinhart, M.; Wendorff, J. H.; Greiner, A.; Wehrspohn, R. B.; Neilsch, K.; Schilling, J.; Choi, J.; Gösele, U. *Science* **2002**, *296*, 1997.
4. (a) Kim, D. H.; Karan, P.; Göring, P.; Leclair, J.; Caminade, A.-M.; Majoral, J.-P.; Gösele, U.; Steinhart, M.; Knoll, W. *Small* **2005**, *1*, 99; (b) Hou, S.; Wang, J.; Martin, C. R. *Nano Lett.* **2005**, *5*, 231.
5. Ding, B.; Gong, J.; Kim, J.; Shiratori, S. *Nanotechnology* **2005**, *16*, 785.
6. Artyukhin, A. B.; Bakajin, O.; Stroeve, P.; Noy, A. *Langmuir* **2004**, *20*, 1442.
7. Bradley, K.; Gabriel, J. C. P.; Gruner, G. *Nano Lett.* **2003**, *3*, 1353.

8. Cioslowski, J.; Rao, N.; Moncrieff, D. *J. Am. Chem. Soc.* **2002**, *124*, 8485.
9. de Leeuw, N. H.; Du, Z.; Li, J.; Yip, S.; Zhu, T. *Nano Lett.* **2003**, *3*, 1347.
10. Lau, K. H. A.; Tan, L.-S.; Tamada, K.; Sander, M. S.; Knoll, W. *J. Phys. Chem. B* **2004**, *108*, 10812.
11. Horvath, R.; Pedersen, H. C.; Cuisinier, F. J. G. *Appl. Phys. Lett.* **2006**, *88*, 111102.
12. Saito, M.; Shibasaki, M.; Nakamura, S.; Miyagi, M. *Opt. Lett.* **1994**, *19*, 710.
13. Ma, Y.; Kooij, E. S. unpublished data. When the PFS multilayers were deposited from 1 mg/mL polymer solutions containing 0.5 M NaCl onto planar silicon substrates, the average bilayer thickness was around 3.6 nm.
14. Decher, G.; Schlenoff, J. B. (Eds.) *Multilayer Thin Films, Sequential Assembly of Nanocomposite Materials*, Wiley-VCH, Weinheim, Germany, **2003**.
15. Mamedov, A. A.; Kotov, N. A. *Langmuir* **2000**, *16*, 5530.
16. Lutkenhaus, J. L.; Hrabak, K. D.; McEnnis, K.; Hammond, P. T. *J. Am. Chem. Soc.* **2005**, *127*, 17228.
17. Podsiadlo, P.; Liu, Z.; Paterson, D.; Messersmith, P. B.; Kotov, N. A. *Adv. Mater.* **2007**, *19*, 949.
18. (a) Ito, Y.; Ochiai, Y.; Park, Y. S.; Imanishi, Y. *J. Am. Chem. Soc.* **1997**, *119*, 1619; (b) Ito, Y.; Park, Y. S.; Imanishi, Y. *J. Am. Chem. Soc.* **1997**, *119*, 2739.
19. Lee, S. B.; Martin, C. R. *Anal. Chem.* **2001**, *73*, 768.
20. Lee, D.; Nolte, A. J.; Kunz, A. L.; Rubner, M. F.; Cohen, R. E. *J. Am. Chem. Soc.* **2006**, *128*, 8521.
21. Chung, D.-J.; Ito, Y.; Imanishi, Y. *J. Appl. Polym. Sci.* **1994**, *51*, 2027.
22. Chu, L.-Y.; Li, Y.; Zhu, J.-H.; Chen, W.-M. *Angew. Chem. Int. Ed.* **2005**, *44*, 2124.
23. Ito, Y.; Nishi, S.; Park, Y. S.; Imanishi, Y. *Macromolecules* **1997**, *30*, 5856.
24. Lee, S. B.; Martin, C. R. *J. Am. Chem. Soc.* **2002**, *124*, 11850.
25. Ito, T.; Hioki, T.; Yamaguchi, T.; Shinbo, T.; Nakao, S.-C.; Kimura, S. *J. Am. Chem. Soc.* **2002**, *124*, 7840.
26. Kujawa, P.; Moraille, P.; Sanchez, J.; Badia, A.; Winnik, F. M. *J. Am. Chem. Soc.* **2005**, *127*, 9224.
27. Ma, Y.; Dong, W.-F.; Hempenius, M. A.; Möhwald, H.; Vancso, G. J. *Nat. Mater.* **2006**, *5*, 724.
28. (a) Wenzel, R. N. *Ind. Eng. Chem.* **1936**, *28*, 988; (b) Wenzel, R. N. *J. Phys. Colloid Chem.* **1949**, *53*, 1466.
29. (a) Zhai, L.; Cebeci, F. Ç.; Cohen, R. E.; Rubner, M. F. *Nano Lett.* **2004**, *4*, 1349; (b) Bravo, J.; Zhai, L.; Wu, Z.; Cohen, R. E.; Rubner, M. F. *Langmuir* **2007**, *23*, 7293; (c) Li, X.-M.; Reinhoudt, D.; Crego-Calama, M. *Chem. Soc. Rev.* **2007**, *36*, 1350.
30. (a) Mendelsohn, J. D.; Barrett, C. J.; Chan, V. V.; Pal, A. J.; Mayes, A. M.; Rubner, M. F. *Langmuir* **2000**, *16*, 5017; (b) Hiller, J.; Mendelsohn, J. D.; Rubner, M. F. *Nat. Mater.* **2002**, *1*, 59.



- 
31. (a) Dai, Z.; Voigt, A.; Donath, E.; Möhwald, H. *Macromol. Rapid Commun.* **2001**, *22*, 756; (b) Balabushevitch, N. G.; Sukhorukov, G. B.; Moroz, N. A.; Volodkin, D. V.; Larionova, N. I.; Donath, E.; Möhwald, H. *Biotech. & Bioeng.* **2001**, *76*, 207; (c) Antipov, A. A.; Sukhorukov, G. B.; Donath, E.; Möhwald, H. *J. Phys. Chem. B.* **2001**, *105*, 2281; (d) Dudnik, V.; Sukhorukov, G. B.; Radtchenko, I. L.; Möhwald, H. *Macromolecules* **2001**, *34*, 2329; (e) Pargaonkar, N.; Lvov, Y. M.; Li, N.; Steenekamp, J. H.; de Villier, M. M. *Pharmaceutical Research* **2005**, *22*, 826.
32. (a) Radtchenko, I. L.; Sukhorukov, G. B.; Möhwald, H. *Int. J. Pharm.* **2002**, *242*, 219; (b) Yu, A.; Wang, Y.; Barlow, E.; Caruso, F. *Adv. Mater.* **2005**, *17*, 1737.
33. Berg, M. C.; Zhai, L.; Cohen, R. E.; Rubner, M. F. *Biomacromolecules* **2006**, *7*, 357.



## Summary

This thesis describes the synthesis and electrostatic assembly of organometallic poly(ferrocenylsilane) (PFS) strong polyelectrolytes. The distinctive structural features of poly(ferrocenylsilanes) come from the silicon and iron atoms in the main chain. The presence of redox-active ferrocene units in the polymer backbone provides unique redox-responsive properties to PFS. The charged nature and redox-responsiveness of these organometallic polyelectrolytes makes them particularly useful in the electrostatic self-assembly process for the fabrication of novel functional supramolecular nanostructures. A major part of the research described in the thesis (Chapter 4-6) is focused on the electrostatic layer-by-layer assembly featuring poly(ferrocenylsilane) polyelectrolytes.

Chapter 1 gives a short introduction on the thesis and in Chapter 2 a literature overview is given on the electrostatic assembly of polyelectrolytes. Following introductions on the general characteristics of polyelectrolytes, two dominant molecular interactions that are acting between oppositely charged polyelectrolytes are discussed. Electrostatic and hydrophobic interactions often lead to the complexation of oppositely charged polyelectrolytes. As a special case of polyelectrolyte complexation, discussions are mainly focused on the “template-assisted” layer-by-layer sequential assembly of polyelectrolytes. The fabrication, characterization, properties and applications of planar substrate-supported and spherical free-standing polyelectrolyte multilayers are described.

As the first part of the thesis, Chapter 3 deals with the synthesis and redox properties of PFS strong polyelectrolytes used throughout the study. Poly(ferrocenylsilane) polyions and fluorescence labelled polycations were obtained from side group modifications on the precursor polymer poly(ferrocenyl(3-chloropropyl)methylsilane) synthesized with controlled molar mass in the presence of  $\text{Et}_3\text{SiH}$ . Fully reversible redox chemistry of these polyelectrolytes was demonstrated following the discovery of several water soluble redox agents. UV/Vis spectroscopy confirmed that poly(ferrocenylsilane) polyelectrolytes could be effectively oxidized by ferric chloride ( $\text{FeCl}_3$ ) and potassium ferricyanide ( $\text{K}_3\text{Fe}(\text{CN})_6$ ). Subsequent complete reduction of the oxidized water-soluble polymers was achieved using ascorbic acid (vitamin C) or dithiothreitol (DTT).

Chapter 4 describes the fabrication, characterization and properties of fully organometallic poly(ferrocenylsilane) planar multilayers. Water-soluble poly(ferrocenylsilane) strong polyelectrolytes have been employed in the electrostatic layer-by-layer supramolecular assembly process to give full organometallic polyion multilayer structures on various planar supports. The multilayer film growth was found to follow a linear profile, monitored by UV/Vis spectroscopy, spectroscopic ellipsometry and quartz crystal microgravimetry. Additional ellipsometric studies showed a square root dependence of the film thickness on polyelectrolyte solution salt (NaCl) concentration. On studying the redox properties of PFS

multilayers, we found that both burst release and controlled release of PFS polyelectrolytes from their multilayer thin film structures are possible by the choice of different types of stimuli. The redox-responsive nature of the ferrocene-containing polymer backbone renders the multilayers removable by chemical oxidation. UV/Vis spectroscopy and ellipsometry measurements showed fast and complete PFS multilayer removal by exposure to  $\text{FeCl}_3$  solutions. This oxidation induced dissolution was used to create PFS multilayer patterns by a “reactive” soft lithography procedure using hydrophilic PDMS stamps and  $\text{FeCl}_3$  solutions as ink. The release of PFS polyelectrolytes from PFS multilayers can also be realized electrochemically by prolonged exposure to a small potential ( $\leq 0.4$  V). The quantity and rate of material release can be precisely manipulated by the on-off switching of the electrical potential and the application of different oxidation potentials. Some successful attempts were made to selectively deposit poly(ferrocenylsilane) multilayers on patterned gold and silicon substrates.

The successful fabrication procedure for preparing planar poly(ferrocenylsilane) multilayers was extended to the fabrication of free-standing multilayer microcapsules, whose structure and properties are described in Chapter 5. Free-standing microcapsules were fabricated from the electrostatic layer-by-layer self-assembly of poly(ferrocenylsilane) polyelectrolytes onto curved substrates followed by core dissolution. Optimum preparation conditions were established in order to obtain microcapsules with desired properties. Manganese carbonate ( $\text{MnCO}_3$ ) microparticles were chosen as the optimum core material. It was shown that the stability and integrity of the capsules obtained depend mainly on the wall thickness, which is tuned by varying the number of deposited polyelectrolyte bilayers. We demonstrated that by using fluorescence-labelled  $4.4 \times 10^3$  g/mol dextran as the reference probe molecule, stable and impermeable PFS capsules with an average size of around  $10 \mu\text{m}$  were obtained when the bilayer number was higher than four. The stable and impermeable capsules were very well suited for the subsequent responsive permeability studies.

The permeability of stable PFS capsules can be tuned via chemical oxidation. The oxidation agents iodine ( $\text{I}_2$ ) and iron chloride ( $\text{FeCl}_3$ ) are both effective in oxidizing water-soluble PFS based multilayer capsules.  $\text{FeCl}_3$  was found to be an effective oxidation agent in that a very dilute solution (in the sub-mM range) was sufficient to cause a fast increase in the capsule permeability. Permeability change was believed to result from increased pore size due to the multilayer expansion along the chain direction and in the multilayer growth direction, which was caused by oxidation-introduced additional positive charges along the polymer backbone. In the later stages of chemical oxidation by  $\text{FeCl}_3$ , capsules made solely from PFS showed a continuous expansion towards their final disintegration. The rate of expansion could be easily tuned by varying the number of deposited polyelectrolyte bilayers and the concentration of the oxidants used. The mechanism of redox-induced capsule expansion and disintegration was studied in detail by the comparison of the responsive behaviour of fully PFS capsules and PFS/organic polyelectrolyte hybrid capsules. The cause of capsule

disintegration is likely an alteration of the charge densities of the polyanion and polycation species upon oxidation, leading to a loss of the original charge compensated multilayer structure.

The deposition of additional redox-insensitive polyelectrolyte species PSS<sup>-</sup>/PAH<sup>+</sup> as capsule capping layers ensured the shape and integrity of PFS capsules after chemical oxidation. By varying the number of PSS<sup>-</sup>/PAH<sup>+</sup> bilayers, the permeability changing rate could be further manipulated. However, collapsed capsules still showed a decreased capsule wall thickness upon chemical oxidation, indicating some material loss. The electrochemical oxidation and reduction of these composite-wall microcapsules featuring PFS polyelectrolytes was realized by immobilizing them onto gold electrodes. Cyclic voltammograms exhibited redox waves typical for PFS, verifying the reversible electrochemical addressability of these redox-responsive microcapsules.

Chapter 6 describes the hybrid electrostatic assembly of poly(ferrocenylsilane) polycations with the natural anionic polyelectrolyte DNA. Multilayer assembly using double-stranded, high molar mass DNA resulted in unique redox-responsive macroporous thin films and aggregated, free-standing microcapsules with excellent molecular permeability. The redox-active PFS components render the thin films susceptible to chemical oxidation, while their unique macroporous architectures are maintained. The formation mechanism of the peculiar macroporous architectures was proposed as originating in the persistence length and chain length mismatch of the two components, as well as in the extraordinary hydrophobicity of the macromolecular backbone of PFS. The LBL assembly of PFS and DNA with varying molecular weights suggested the existence of a critical molar mass mismatch below which the peculiar macroporous structure could no longer be formed.

Going beyond the above fundamental studies, Chapter 7 describes various applications of organometallic poly(ferrocenylsilane) polyelectrolytes. As a first example, cationic poly(ferrocenylsilane) polyelectrolytes were used in plasmid DNA condensation to give stable nano-sized polymer-DNA complexes with high efficiency. Acting as non-toxic gene carriers, these PFS/DNA polyplexes displayed promising gene transfer properties. In a second approach, poly(ferrocenylsilane) polyanions were self-assembled with positively charged cowpea chlorotic mottle virus (CCMV) capsid proteins. Electrostatic interactions between poly(ferrocenylsilane) polyanions and CCMV capsid proteins resulted in monodisperse polymer-virus nanoparticles with sizes around 18 nm. These particles are potentially useful as nanometer-sized compartments in drug targeting and transportation applications.

In the final part (Chapter 8), an outlook was given on some of the possible future research directions. The fabrication of various other forms of multilayer structures based on poly(ferrocenylsilane) polyelectrolytes, such as multilayer nanotubes and free-standing planar films are discussed. The necessity of follow-up studies on the functional structural platforms presented throughout the thesis was described. Many new functions are envisaged by a

combination of the unique redox-responsive properties of poly(ferrocenylsilane) as well as these new shapes.

## Samenvatting

Dit proefschrift beschrijft de synthese en electrostatische zelforganisatie van organometaal poly(ferrocenylsilaan) (PFS) sterke polyelectrolieten. De bijzondere eigenschappen van poly(ferrocenylsilanen) vinden hun oorsprong in de silicium- en ijzeratomen in de PFS hoofdketen. De aanwezigheid van redox-actieve ferrocen eenheden in de polymeer hoofdketen geeft PFS unieke redox-responsieve eigenschappen. De geladen zijgroepen en redox eigenschappen maken deze polyelectrolieten zeer geschikt voor fabricage van nieuwe functionele supramoleculaire nanostructuren door electrostatische zelf-assemblage. Een groot deel van het onderzoek beschreven in het proefschrift (Hoofdstuk 4-6) is gericht op de electrostatische laag-op-laag zelforganisatie van poly(ferrocenylsilaan) polyelectrolieten.

Hoofdstuk 1 geeft een korte inleiding van het proefschrift. In Hoofdstuk 2 wordt een literatuuroverzicht gegeven van de electrostatische zelforganisatie van polyelectrolieten. Na een inleiding over de algemene eigenschappen van polyelectrolieten worden twee belangrijke moleculaire interacties tussen tegengesteld geladen polyelectrolieten behandeld. Electrostatische en hydrofobe interacties leiden vaak tot aggregatie van tegengesteld geladen polyelectrolieten. Een bijzonder geval van polyelectroliet complexering, de template-assisted laag-op-laag assemblage van polyelectrolieten, wordt met name bediscussieerd. Fabricage, karakterisering, eigenschappen en toepassingen van vlakke substraat-gedragen en bolvormige substraat-vrije polyelectroliet multilagen worden beschreven.

Als eerste experimentele hoofdstuk van het proefschrift beschrijft Hoofdstuk 3 de synthese en redox eigenschappen van de PFS sterke polyelectrolieten die voor de gehele studie zijn gebruikt. Poly(ferrocenylsilaan) polyionen en fluorescentie-gelabelde polykationen werden verkregen door zijgroepmodificatie van het precursorpolymeer poly(ferrocenyl(3-chloropropyl)methylsilaan), gesynthetiseerd met een gecontroleerd molecuulgewicht in aanwezigheid van  $\text{Et}_3\text{SiH}$ . Volledig reversibele redoxchemie van deze polyelectrolieten werd gedemonstreerd na de ontdekking van enkele wateroplosbare redox agentia. UV/Vis spectroscopie bevestigde dat poly(ferrocenylsilaan) polyelectrolieten effectief geoxideerd konden worden door ijzerchloride ( $\text{FeCl}_3$ ) en kalium ferricyanide ( $\text{K}_3\text{Fe}(\text{CN})_6$ ). Daaropvolgende volledige reductie van de geoxideerde wateroplosbare polymeren werd bereikt door middel van ascorbinezuur (Vitamine C) of dithiothreitol (DTT).

Hoofdstuk 4 beschrijft de fabricage, karakterisering en eigenschappen van volledig organometaal poly(ferrocenylsilaan) vlakke multilagen. Wateroplosbare poly(ferrocenylsilaan) sterke polyelectrolieten werden gebruikt in het electrostatische laag-op-laag supramoleculaire assemblageproces voor de vorming van volledig-organometaal polyion multilaagstructuren op diverse vlakke substraten. De multilaag filmgroei bleek lineair te verlopen zoals bleek uit UV/Vis spectroscopie, spectroscopische ellipsometrie en quartz

crystal microgravimetry. Verdere ellipsometriestudies toonden aan dat de filmdikte toenam met de wortel van de zoutconcentratie (NaCl) van de polyelectrolietoplossing. Bij het bestuderen van de redoxeigenschappen van PFS multilagen vonden we dat zowel directe afgifte als gecontroleerde afgifte van PFS polyelectrolieten uit hun multilaagstructuren mogelijk zijn en bepaald worden door de keuze van de stimulus. De redox-responsieve eigenschappen van de ferroceenbevattende polymeer hoofdketen maken verwijdering van de multilagen door chemische of electrochemische oxidatie mogelijk. UV/Vis spectroscopie en ellipsometriemetingen toonden een snelle en volledige verwijdering van PFS multilagen aan bij blootstelling aan FeCl<sub>3</sub> oplossingen. Dit oxidatie-geïnduceerd oplossingsproces werd gebruikt om PFS multilaagpatronen te creëren door middel van een reactieve soft lithography procedure, met hydrofiele PDMS stempels en FeCl<sub>3</sub> oplossingen als inkt. De afgifte van PFS polyelectrolieten uit PFS multilagen kan ook electrochemisch worden gerealiseerd door het aanleggen van een klein elektrisch spanningsverschil ( $\leq 0.4$  V). De hoeveelheid en snelheid van materiaalafgifte kan nauwkeurig gemanipuleerd worden door het aan/uitschakelen van de elektrische potentiaal en het aanleggen van verschillende oxidatiepotentialen. Enkele succesvolle pogingen leidden tot selectieve poly(ferrocenylsilaan) multilaaggroei op gepatroneerde goud en siliciumsubstraten.

De succesvolle procedure voor het opbouwen van vlakke poly(ferrocenylsilaan) multilagen werd uitgebreid naar de fabricage van vrije, niet substraatgebonden multilaag microcapsules, waarvan de structuur en eigenschappen beschreven zijn in Hoofdstuk 5. Vrije microcapsules werden gefabriceerd door de electrostatische laag-op-laag zelf-assemblage van poly(ferrocenylsilaan) polyelectrolieten op bolvormige substraten gevolgd door oplossen van het substraat. Optimale fabricageomstandigheden werden vastgesteld teneinde microcapsules met gewenste eigenschappen te verkrijgen. Mangaancarbonaat (MnCO<sub>3</sub>) microdeeltjes werden geselecteerd als ideale, oplosbare kernen. Aangetoond werd dat stabiliteit en defectvrijheid van de verkregen capsules voornamelijk afhankelijk was van de wanddikte, die wordt bepaald door het aantal aangebrachte bilagen. We toonden aan dat door gebruik van fluorescentie-gelabelde  $4.4 \times 10^3$  g/mol dextran als referentiemolecuul voor permeabiliteitsstudies, stabiele en ondoordringbare PFS capsules met een gemiddelde grootte van 10  $\mu\text{m}$  verkregen werden wanneer het aantal bilagen groter was dan vier. De stabiele en ondoordringbare capsules waren zeer geschikt voor vervolgstudies naar schakelbare permeabiliteit.

De permeabiliteit van stabiele PFS capsules kan worden gestuurd door chemische oxidatie. De oxidatiemiddelen jodium (I<sub>2</sub>) en ijzerchloride zijn beide in staat om op wateroplosbaar PFS gebaseerde multilaagcapsules te oxideren. FeCl<sub>3</sub> bleek het meest effectieve oxidatiemiddel. Zeer lage FeCl<sub>3</sub> concentraties (sub-mM gebied) bleken al voldoende om een snelle toename in capsule permeabiliteit te bewerkstelligen. De permeabiliteitstoename is waarschijnlijk het gevolg van een toegenomen poriegrootte door multilaagexpansie in de ketenrichting en in de richting van de multilaaggroei, veroorzaakt



door de door oxidatie geïntroduceerde extra positieve ladingen in de polymeer hoofdketen. In de latere stadia van chemische oxidatie door  $\text{FeCl}_3$  vertoonden alleen uit PFS bestaande capsules een continue expansie tot aan hun uiteindelijke desintegratie. De expansiesnelheid kon makkelijk worden gestuurd door variëren van het aantal aangebrachte polyelectrolyet bilagen en de concentratie van de gebruikte oxidanten. Het mechanisme van redox-geïnduceerde capsule expansie en desintegratie werd in detail bestudeerd door vergelijking van het responsieve gedrag van volledig-PFS capsules en PFS/organische polyelectrolyet hybride capsules. De oorzaak van capsule desintegratie is waarschijnlijk de verandering van de ladingsdichtheid van de polyanionen en polykationen door oxidatie, waardoor de oorspronkelijke ladingscompensatie in de multilaag is verdwenen.

De depositie van additionele, redox-ongevoelige polyelectrolyeten  $\text{PSS}^-/\text{PAH}^+$  als capsule buitenlagen verzekerde het behoud van vorm en intactheid van PFS capsules na chemische oxidatie. Door variëren van het aantal  $\text{PSS}^-/\text{PAH}^+$  bilagen kon de snelheid van permeabiliteitsverandering verder worden beïnvloed. Capsules in gedroogde toestand vertoonden echter nog steeds een verminderde wanddikte na oxidatie, wat duidt op enig materiaalverlies. Electrochemische oxidatie en reductie van deze composite-wall microcapsules werd gerealiseerd door immobilisatie van de capsules op goud electrodes. Cyclische voltammogrammen vertoonden redox pieken typisch voor PFS en bevestigden daarmee de reversibele electrochemie van deze redox-gevoelige microcapsules.

Hoofdstuk 6 beschrijft de hybride electrostatische assemblage van poly(ferrocenylsilaan) polykationen met het natuurlijke anionische polyelectrolyet DNA. Multilaagvorming gebruikmakend van dubbelstrengs DNA met een hoog molecuulgewicht resulteerde in unieke redox-responsieve macroporeuze dunne films en geaggregeerde, vrije microcapsules met een uitstekende moleculaire permeabiliteit. De redox-actieve PFS componenten maken de dunne films gevoelig voor chemische oxidatie, terwijl hun unieke macroporeuze architectuur behouden blijft. De vorming van de bijzondere macroporeuze architecturen werd voorgesteld als een gevolg van het grote verschil in persistentielengte en ketenlengte van de twee componenten, en de hydrofobiciteit van de PFS hoofdketen. De laag-op-laag assemblage van PFS, en DNA van verschillend molecuulgewicht suggereert het bestaan van een kritisch verschil in molecuulgewicht waaronder de bijzondere macroporeuze structuur niet langer kan worden gevormd.

Hoofdstuk 7 beschrijft diverse toepassingen van poly(ferrocenylsilaan) polyelectrolyeten. Als eerste voorbeeld werden kationische poly(ferrocenylsilaan) polyelectrolyeten gebruikt in plasmide DNA condensatie wat leidde tot de vorming van stabiele, nanometer-grootte polymeer-DNA complexen met hoge efficiëntie. Dienend als niet-giftige gene-carriers, vertoonden deze PFS/DNA polyplexen veelbelovende gene transfer eigenschappen. Poly(ferrocenylsilaan) polyanionen konden worden gecomplexeerd met positief geladen cowpea chlorotic mottle virus (CCMV) capside eiwitten. Electrostatische interacties tussen poly(ferrocenylsilaan) polyanionen en CCMV capside eiwitten resulteerde

in monodisperse polymeer-virus nanodeeltjes met afmetingen rond 18 nm. Deze deeltjes zijn mogelijk bruikbaar als nanometer-groote containers voor medicijnopname en -transport toepassingen.

In Hoofdstuk 8 wordt een overzicht gegeven van mogelijk toekomstig onderzoek. De fabricage van verschillende andere vormen van multilaagstructuren gebaseerd op poly(ferrocenylsilaan) polyelectrolieten, zoals multilaag nanotubes en vrije, niet-substraatgedragen vlakke films, wordt besproken. De noodzaak van vervolgstudies aan de functionele multilaagstructuren die in dit proefschrift zijn gepresenteerd wordt bediscussieerd. Nieuwe functionaliteiten worden voorzien door het combineren van de unieke redox-responsieve eigenschappen van poly(ferrocenylsilaan) met nieuwe multilaagstructuren.

## Acknowledgements

The research described in this thesis would not be possible without the help of many people, to whom I owe many thanks. During these four years, I cannot help but feeling lucky from time to time for the great opportunities I had to work with such a group of smart and stimulating people. I would like to express my gratitude to some of them in particular.

First and foremost, I have to start with my promoter, Prof. Julius Vancso, for giving me the opportunity to carry out a master project, and later on to become a Ph.D. student in the MTP group. Before coming to the Netherlands, I had little idea about what macromolecule has to do with nanotechnology. Being a member in the MESA<sup>+</sup> institute really helped in shaping up my scientific perspective. Thanks to Julius, I had many efficient and encouraging scientific discussions during my research. Julius, you may not know how grateful I felt to have collaborated with so many excellent research groups during these four years! I treasure so much the “personal touch” you’ve given me concerning my personal interests and future career.

I sincerely thank Dr. Mark Hempenius, my assistant promoter. Mark, you are such a good scientist and nice person to work with! Being a nervous person myself, I would not succeed without your patience and care. Your guidance and help during the polymer synthesis are simply irreplaceable! On the one hand, you gave me a lot of freedom to do my work; on the other hand, you were always there for discussions. I truly appreciate your meticulous corrections on all my scientific outputs and your translation of the English summary into Dutch.

Many work described in this thesis resulted from some excellent collaborations. I am deeply grateful to Prof. Helmuth Möhwald (Max-Planck Institute of Colloids and Interfaces, Golm, Germany), with whom I shared many inspirational discussions. Thanks to my working partner Dr. Wenfei Dong, I spent so much memorable time in Golm. Wenfei, like a big brother, you are not only my teacher but also a great friend. I often recollect all those talks we had about life, which were so beyond having a successful career. I would like to also express my thanks to Prof. Wolfgang Knoll and Dr. Chuanliang Feng (Max-Planck Institute for Polymer Research, Mainz, Germany) for their help and support in the polyelectrolyte nanotube project described in Chapter 8. I enjoyed the nice atmosphere in Nijmegen and hospitality from Prof. Roeland Nolte, Dr. Jeroen Cornelissen and Inge Minten (Radboud Universiteit Nijmegen) through the virus capsid project as presented in Chapter 7. Dr. Stefan Kooij (SSP group) is appreciated for providing me with the great privilege to use their spectroscopic ellipsometer and helping in analyzing the data. I wish to thank Dr. Zhi Yuan Zhong and Chao Lin (PBM group) for their initiative and collaborative work to use our polymer as DNA packaging material (Chapter 7).

I am very grateful to Dr. Holger Schönherr, who taught me how to use AFM. Many thanks to our great technician Clemens Padberg! Clemens, I could not imagine how much longer things will get delayed without your dexterous hands. Geneviève, thank you so much for always helping me with the (Dutch) paperwork and your professional opinions on some of the figure illustrations! Cindy, Thelma, Karin are all acknowledged for their help in making the group function efficiently. Zlata and Anika, thank you for taking care of the ordering. I would like to also extend my gratitude to several people who have helped me with the experimental work: Dr. Henk-Jan van Manen (BPE group), Mark Smithers (SEM), Jing Song (in-situ AFM), Anneliese Heilig and Annegret Praast (Max-Planck Institute of Colloids and Interfaces, Golm, Germany).

I had a wonderful time working with many great colleagues. It would be impossible to mention all the names of the people who have helped me one way or another. I wish to express my special thanks to my officemates: Dr. Shan Zou, Dr. Szczepan Zapotoczny for creating such a relaxing working atmosphere; and Jing Song and Joost Duvigneau for accepting to be my paranimfen. I am thankful to all the past and present MTP members during my stay here at the University of Twente. I also extend my gratitude to the help from members of other research groups (SMCT, PBM, BPE, SSP).

The support and company of my friends have contributed to making my life here in Twente an unforgettable experience: Shan Zou, Yuguo Tao, Jing Song, Wei Cheng, Huaping Xu, Shuying Gu, Boon-Hua Tan, AiLing Tang, Hui Lv, Rui Guo, Hongmei Zhang, Zheng Zhang, Xiao Li, Fenghua Meng, Weiqing Shi, Lanti Yang, Hao Gu, Tian Gang, Xin Wan, Chao Lin, Rong Jin, Ivan Vera. I thank my friends in Golm and Mainz who made my stay there really colourful: Wenfei Dong, Dahui Yu, Weijun Tong, Haijun Niu, Wei Li, Xinliang Feng, Wei Cheng. Thank you so much for all those great dinner parties and wonderful times we had!

Finally and most importantly, I owe my family my deepest gratitude for giving me their unconditional support all through these years! Mum, Dad and Qi, thank you so much for your listening, sharing and advising. I dedicate this thesis to all of you.

Yujie

Enschede, 2008

## Curriculum Vitae

Yujie Ma was born on April 18, 1979 in Wuhan, China. After graduating from the No.1 Middle School in Wuhan, she continued her study at the Shanghai Jiao Tong University. During her undergraduate study, she won two prestigious excellent student awards (top 5%) of Shanghai Jiao Tong University. In 2001, she obtained her BE degree in Polymer Materials and Engineering. In the same year, she started her master's studies at the same university, graduating in 2004 with an MSc degree in Polymer Chemistry and Physics. In the mean time, during 2002-2003, she was an exchange student between Shanghai Jiao Tong University and Twente University in the Netherlands for an international master programme. Her master research was carried out in the group of Materials Science and Technology of Polymers (MTP) headed by Prof. Dr. Julius Vancso. With a master thesis entitled "*Grafting of Isolated Poly(ferrocenylsilane) Molecules to Surfaces: Model Systems for the Investigation of Stimuli-Responsive Polymers on A Single Molecule Level*", she obtained her second MSc degree in Chemical Engineering from the University of Twente in 2003. From January 2004, she re-joined the same group at the University of Twente as a Ph.D. student, working on the synthesis and self-assembly of iron-containing organometallic polyelectrolytes. Part of her Ph.D. research was carried out in close collaboration with the group of Prof. Dr. Helmuth Möhwald at the Max-Planck Institute of Colloids and Interfaces in Germany. The results of this four-year research are presented in this thesis. In 2007, she received the Chinese Government Award for Outstanding Self-Financed Students Abroad.

